UNIVERSITY OF CALIFORNIA, SAN DIEGO

An Integrated Genetic and Biochemical Analysis of the Yeast Telomerase Complex

A dissertation submitted in partial satisfaction of the requirements for the degree

Doctor of Philosophy

in

Biology

by

Timothy Michael Tucey

Committee in charge:

Professor Vicki Lundblad, Chair
Professor Randolph Hampton
Professor James Kadonaga
Professor Lorraine Pillus
Professor Huilin Zhou

2013

The Dissertation of Timothy Michael Tucey is approved, and it is acceptable in quality and form for publication on microfilm and electronically:

_____

_____

_____

_____

_____

Chair

University of California, San Diego

2013

DEDICATION

Completing this dissertation has been a feat of endurance, much like running in a marathon – a journey full of challenges and meticulous deliberations, patience and perseverance, which ultimately yields an incredible sense of exhilaration – and I wouldn't have wanted it any other way.

First and foremost, I would like to thank my parents, Richard and Mary, for instilling in me the value of education, not only in the institutional sense of the word, but also for supporting my curiosity-driven, and often times eccentric ventures: collecting insect species in the backyard, cross-country camping trips during the summers, ornithological fascinations, piano lessons and soccer practices, as well as teaching me to do what is genuinely best for society despite the fact that it often goes against widely held conventions. This intellectual upbringing surely contributed to my ability and willingness to undertake such a challenging dissertation.

I would also like to thank the people who have been part of this chapter of my life – Emily Chan ; Yang Yang (and Mochi the Bichon Frisé who was an excellent companion when smuggled into the campus apartment) ; the ultimate frisbee group ; running partners Horng Ou, Zohreh Akhavan, Mark Huising, and Melissa Wei ; my high school friend Benedikt Siegler who I am extremely grateful to have stayed in touch with over the years ; my brother Nick and sister-in-law Cindy for some excellent hiking trips, as well as their amazing nature photography to remind me of the incredible "other" world that exists outside of the lab bench. I will always cherish the memories we had during this time, which currently constitutes nearly 1/4 of my life!

TABLE OF CONTENTS

LIST OF FIGURES

Chapter 2

Chapter 3

Chapter 7

Appendix A

Appendix B

LIST OF TABLES

ACKNOWLEDGMENTS

I would like to thank my advisor, Vicki Lundblad, for bringing out more in me than I could have ever imagined being capable of, for being available for questions and discussions in a manner that seemed humanly impossible, and from a non-scientific standpoint, for introducing me to my favourite varietal of white wine – Viognier. Her guidance has been invaluable to my scientific development, and I look forward to applying what I have learned to the next chapter of my life.

Many thanks to my committee members – Randy Hampton, Jim Kadonaga, Lorraine Pillus, and Huilin Zhou – for their scientific advice and career assistance, and for somehow managing to find an overlap in their schedules to make the arduous journey from UCSD to the Salk for each committee meeting. I would also like to acknowledge Vicki's husband, Lou Zumstein, for providing some helpful technical advice regarding the biochemistry experiments shown in the later chapters of this dissertation.

Lastly, I would like to thank the lab members past and present, who created an intellectually stimulating environment that was an honor to be a part of. I would particularly like to acknowledge the collaborating lab members in this dissertation. Jaesung Lee, Ed Mandell, and Danna Morris were co-authors for the work presented in Chapter 2, John Lubin was a co-author for the work presented in Chapters 4 and 6, and Lisa Nguyen was a collaborator for the preliminary data presented in Appendix B.

A portion of Chapter 2 is a modified reprint of the material as it appears in Lee, J., Mandell, E.K., Tucey, T.M., Morris, D.K., and Lundblad, V. (2008). The Est3

protein associates with yeast telomerase through an OB-fold domain. Nat Struct Mol Biol *15*, 990-997. The dissertation author was a co-author for this publication. Reprinted with premission from Nature Publishing Group, copyright, 2008.

A portion of Chapter 3 a modified reprint of the material as it appears in Tucey, T.M., and Lundblad, V. (2013). A yeast telomerase complex containing the Est1 recruitment protein is assembled early in the cell cycle. Biochemistry *52*, 1131-1133. The dissertation author was the primary researcher for this publication. Reprinted with permission from American Chemical Society, copyright, 2013.

Chapter 4 is a formatted reprint of the material as it appears in Lubin, J.W., Tucey, T.M., and Lundblad, V. (2012). The interaction between the yeast telomerase RNA and the Est1 protein requires three structural elements. RNA *18*, 1597-1604. The dissertation author was a co-first author for this publication. Reprinted with premission from RNA Society, copyright, 2012.

Chapter 5 is a formatted reprint of the material as it appears in Tucey, T.M., and Lundblad, V. (2013). A yeast telomerase complex containing the Est1 recruitment protein is assembled early in the cell cycle. Biochemistry *52*, 1131-1133. The dissertation author was the primary researcher of this paper. Reprinted with permission from American Chemical Society, copyright, 2013.

Chapter 6 contains material from a manuscript that is being prepared for publication: Tucey, T.M., Lubin, J.W., and Lundblad, V. (2013). Identification of four functionally distinct interfaces on Est1.

VITA

2013	University of California, San Diego, La Jolla, CA Doctor of Philosophy in Biology
2008-2010	University of California, San Diego, La Jolla, CA Teaching Assistant, Department of Biological Sciences
2004	Cornell University, Ithaca, NY Bachelor of Science in Biological Sciences

RESEARCH

2007-2013	Salk Institute for Biological Studies, La Jolla, CA Telomere Maintenance Professor Vicki Lundblad
2004-2006	Massachusetts General Hospital, Boston, MA Molecular Neuroscience Professor Anne Hart

ABSTRACT OF THE DISSERTATION

An Integrated Genetic and Biochemical Analysis of the Yeast Telomerase Complex

by

Timothy Michael Tucey

Doctor of Philosophy in Biology

University of California, San Diego 2013

Professor Vicki Lundblad, Chair

In the budding yeast *S. cerevisiae*, the telomerase enzyme is composed of a 1.3 kb TLC1 RNA, which forms a complex with Est2 (the catalytic subunit) and two regulatory proteins, Est1 and Est3. Telomerase acts at a particular period of the cell cycle, late S phase, to sufficiently counteract chromosome erosion and cellular senescence. However, the telomerase complex is very limiting in expression, which argues for a highly regulated process for getting telomerase to where it needs to act.

Although yeast telomerase has been the subject of intense investigation by numerous laboratories, a high-resolution view of the precise mechanistic contributions

by each subunit to telomere homeostasis has not yet been achieved. To address this, I have employed a biochemical method that provides a detailed view of the stoichiometry of the telomerase holoenzyme combined with a genetic strategy intended to characterize the functional surface of telomerase.

First, I developed a genetic strategy that targets functionally important residues on the surface of a protein. This identified dominant negative mutations in *EST3* that confer a telomere replication defect when over-expressed in a wild-type yeast strain. This approach was continued by other members of the lab and has resulted in a large collection of separation-of-function alleles in each of the three *EST* genes.

The biochemical method relies on a yeast strain designed to allow quantitative immunoprecipitation of the limiting subunit of the holoenzyme (Est2), followed by equivalent detection of each protein subunit by western blotting. I used this stoichiometry assay to evaluate how Est1 associates with a long helical arm on the TLC1 RNA. I also show that an enzyme complex containing Est1 assembles early in the cell cycle, well before telomere elongation occurs, in accordance with prior genetic observations, whereas the Est3 subunit associates much later in the cell cycle. Integrating the mutations from the genetic strategy with the biochemical method has identified four functionally distinct interfaces on Est1, as well as additional interfaces on Est2 and Est3. Finally, I have uncovered evidence that telomerase exists as two separate complexes with different stoichiometries, arguing for yet an additional level of telomerase regulation.

Chapter 1: Introduction

Telomeres

Telomeres are vital structures found at the ends of virtually all eukaryotic chromosomes (Blackburn, 2000). They are composed of tandem repeats of guanine-rich DNA, and this forms a molecular platform for telomeric protein complexes to associate (Laroche et al., 2000). These complexes play a vital role in end protection, a process that maintains the integrity of the genome and distinguishes normal chromosome ends from DNA breaks.

In the 1930s, Barbara McClintock and Hermann Muller were the first to observe that normal chromosome ends possess a protective ability that prevents them from being recognized and processed as DNA double-strand breaks. In maize, Barbara McClintock demonstrated that a broken chromosome induced by x-ray irradiation could fuse with its sister chromatid creating a breakage-fusion-bridge cycle (McClintock, 1941). However, under certain conditions a broken end would permanently heal during the reproductive cycle of the chromosome and lose its tendency to fuse with other chromosome ends (McClintock, 1942). In *Drosophila melanogaster*, Hermann Muller observed that deletions or inversions at the terminal ends of chromosomes could not be recovered after x-ray irradiation (Muller, 1938). He coined the term telomere from the Greek words “telos” (end) and “meros” (part) to describe the specialized structures he reasoned must exist at the ends of chromosomes.

McClintock and Muller’s research suggested that there must be an important mechanism for generating and maintaining the ends of chromosomes, but it was not until the late 1970s that the true nature of the telomere structure began to emerge.

Using the ciliated protozoan *Tetrahymena thermophila*, Elizabeth Blackburn first identified that the molecular sequence of telomeric DNA consists of a repeated series of nucleotides (Blackburn and Gall, 1978). Jack Szostak and Blackburn introduced into budding yeast a linear plasmid that carries *Tetrahymena* telomere sequence at the ends. Strikingly, the linear plasmid was stable in yeast, and sequencing of the ends indicated that a new type of telomeric sequence had been added (Szostak and Blackburn, 1982). Later under the guidance of Blackburn, Carol Greider identified and characterized the telomerase enzyme, which functions to maintain telomere length (Greider and Blackburn, 1985).

In virtually all eukaryotes that have been examined, the chromosome ends are composed of small tandem arrays of repeated DNA sequences. The strand running 5' to 3' from the centromere towards the telomere is guanine-rich (G-strand) and extends beyond its complementary C-rich strand to form a single-stranded G-rich overhang. The telomeric repeat unit, length of the G-rich overhang, and overall telomere lengths vary from species to species, and there can also be considerable variation among individuals of the same species. In the best-characterized system, the budding yeast *Saccharomyces cerevisiae*, telomeres contain approximately 300 bp of heterogeneous 5'-$[TG_{1\text{-}3}]_n$-3' double-stranded repeats and a 3' overhang of 12-14 nt (Larrivee et al., 2004). The fission yeast *Schizosaccharomyces pombe* also measures approximately 300 bps, while the ciliate *Oxytricha nova* has a fixed 4.5 repeats of G_4T_4 (Nandakumar and Cech, 2013). The telomeres of the laboratory mouse *Mus musculus* are 20-50 kb, and humans measure 10-15 kb (Hastie et al., 1990; Zijlmans et al., 1997). In contrast

to *S. cerevisiae*, the telomeric DNA sequence of *S. pombe* is degenerate with the most frequently occurring motif being GGTTACA, while vertebrate telomeres have a strict consensus sequence of GGTTAG.

While G-rich telomeric sequence is conserved in most eukaryotes, there are exceptions that exist. In *Drosophila*, telomeres are composed of retrotransposable elements, with spontaneous addition of new transposons fully compensating for the terminal loss that occurs at the ends of chromosomes (Mason and Biessmann, 1995). Therefore, *Drosophila* telomere maintenance and protection involves an entirely different set of telomere-related proteins.

Due to the concentration of guanine residues at the telomere of most species, the telomere has been proposed to form higher order structures that may have functional relevance. The G-quadruplex is a configuration with high thermal stability due to the stacking of quartets of coplanar guanines and is an example of a non-Watson-Crick base paired secondary structure. *In vitro* intra- and intermolecular G-quadruplex structures have been demonstrated to form in G-rich single-stranded telomeric DNA (Maizels, 2006). Furthermore, these structures have been demonstrated to form *in vivo* at the telomeres of ciliates, and their thermal stability may be influenced by telomere binding proteins (Paeschke et al., 2008; Paeschke et al., 2005).

An additional higher-order structure called t-loops was observed by electron microscopy (Griffith et al., 1999) and has been detected at the telomeres of humans, mice, trypanosomes, ciliates, and nematodes. T-loops are a duplex lariat structure

formed by the looping and incorporation of the 3' single stranded G-rich overhang into the double stranded region of the same chromosome. T-loops are thought sequester the chromosome end and protect telomeres from nucleolytic attack and chromosome end-to-end fusions (Palm and de Lange, 2008), but it is unclear how they are regulated during the cell cycle to allow for replication of the telomere. It is also possible that t-loops are recombination intermediates as opposed to capping structures. Furthermore, *S. cerevisiae* telomeres do not form t-loops, perhaps on account of the telomere sequences being more degenerate than other eukaryotes, or the length of the 3' overhang being shorter. However, a different type of fold-back structure has been proposed at budding yeast telomeres (de Bruin et al., 2001). A major challenge in investigating the functional significance of G-quadruplex and t-loop structures is that it is difficult to genetically modify the telomeric DNA in order to directly assess the phenotypic consequence of altered telomeric structures, without also affecting the binding of telomeric proteins.

Telomere-associated proteins

A series of proteins have been characterized that can bind directly to the double-stranded or single-stranded telomeric DNA in a sequence-specific manner, while other proteins associate with the chromosome termini via protein-protein interactions. Well-characterized double-stranded telomeric DNA binding proteins include Rap1 in *S. cerevisiae* (Conrad et al., 1990), Taz1 in *S. pombe* (Cooper et al., 1997), and TRF1 and TRF2 in mammals (Broccoli et al., 1997). These proteins

recognize and bind double-stranded telomeric DNA via Myb-like DNA binding motifs.

The single-stranded telomeric binding proteins include TEBP from the ciliate *Oxytricha nova* (Gottschling and Zakian, 1986), Cdc13 in *S. cerevisiae* (Garvik et al., 1995), and Pot1 from *S. pombe* and vertebrates (Baumann and Cech, 2001). These proteins bind the G-rich overhang, and are characterized by one or more predicted oligo-saccharide/oligo-nucleotide binding folds (OB-folds). The OB-fold is a common protein domain, consisting of a five stranded beta-sheet coiled to form a closed beta-barrel. OB-fold containing proteins are often involved in the recognition of single-stranded nucleic acids, including rRNA (ribosomal proteins), tRNA (ex. aspartyl-tRNA synthetases), single-stranded DNA (ex. Replication Protein A), and the telomere single-stranded G-rich overhang (ex. Cdc13, Pot1) (Theobald et al., 2003). In addition to the proteins that directly bind at the telomere, there are telomere-associated proteins that are recruited to the telomeres via protein-protein interactions. Such proteins include Rif1 and Rif2 in budding yeast, and RAP1/TIN2/TPP1 in vertebrates.

These telomere-associated proteins provide two main functions. First, they modulate telomere length by regulating access of telomerase and other enzymes at the telomere. Second, they play essential roles in chromosome end protection, which is often referred to as "telomere capping." The overall complex formed by these proteins, which is inclusive of proteins at both the double-stranded and single-stranded sides of the telomere, is known as the shelterin complex.

In *S. cerevisiae*, Cdc13 serves a multi-functional role at the telomere. Cdc13 binds the G-rich single-stranded overhang through a single OB-fold (Nugent et al., 1996) and serves as the platform to deliver multiple complexes to the telomere: Stn1 and Ten1, to protect chromosome ends, and recruitment of telomerase to maintain telomere length (Pennock et al., 2001). Like Cdc13, Stn1 and Ten1 are also OB-fold containing proteins. It is proposed that Cdc13/Stn1/Ten1 form a heterotrimeric complex (called the CST complex) in an analogous manner to the replication protein A complex (Gao et al., 2007). CST is essential for cell viability and end protection, and loss-of-function of any of the CST components results in extremely long single-stranded G-rich telomeric DNA accompanied by cell cycle arrest. Cdc13 also interacts with the catalytic subunit of polymerase α (Pol 1) for C-strand telomere synthesis (Qi and Zakian, 2000), so it may be involved in coordinating the G- and C-strand telomere synthesis during late S phase of the cell cycle.

End replication problem

In the absence of telomere maintenance, linear chromosomes will shorten progressively with every round of DNA replication, a phenomenon referred to as the end replication problem and first theoretically described by Alexy Olovnikov and James Watson in the early 1970s. The end replication problem refers to the difficulty posed by conventional DNA polymerases to completely replicate linear chromosomes (Olovnikov, 1971; Watson, 1972). All known DNA polymerases require a polynucleotide primer, which gets removed after synthesis has been primed.

Consequently, in each S phase of the cell cycle, semi-conservative replication of a linear chromosome results in an 8-12 bp gap in the lagging strand due to the removal of a terminal 8-12 bp RNA primer. In addition to incomplete DNA replication, nucleolytic attack also contributes to telomere attrition.

Due to incomplete DNA replication and nucleolytic degradation, the telomeres will shorten with each cell division and thereby reduce the amount of binding sites for end protection proteins (Harley et al., 1990), eventually reaching a crucially short length that results in cellular senescence or apoptosis. Therefore, there is a limit for the number of times that a cell can divide – this is known as the Hayflick limit, named after Leonard Hayflick who discovered that cultured normal human cells have a limited capacity to divide (Hayflick and Moorhead, 1961). Abnormal cancer cells circumvent this problem in order to divide indefinitely by taking advantage of a natural cellular mechanism to maintain telomere length via the telomerase enzyme (as described in the next section), or more rarely, through recombination-mediated telomere lengthening.

In the absence of telomerase, homologous recombination offers an alternative pathway (ALT) for the maintenance of telomeric DNA. There are two ALT pathways in yeast, called type I and type II recombination, that differ in the substrates and proteins that catalyse the reaction. In *S. cerevisiae*, type I survivors carry short telomeric DNA tracts, but their subtelomeric repeats (called Y' elements) are extensively amplified (Lundblad and Blackburn, 1993), while type II survivors maintain long and heterogeneous telomeric repeats where one telomere uses another

telomere as a template for extension (Teng and Zakian, 1999). Both types of survivors are found to be dependent on Rad52, a key component of homologous recombination. In the absence of telomerase, *S. pombe* cells maintain telomeres by recombination or chromosome circularization (Nakamura et al., 1998). Telomere recombination may also contribute to telomere length regulation in telomerase positive cells. For example, an intrachromatid recombination process called telomere rapid deletion (TRD) can reduce a very long telomere to wild-type length in a single cell cycle.

Telomerase

Despite species-to-species differences in telomere length and composition, most eukaryotes employ the enzyme telomerase to counteract the end replication problem. Telomerase is a specialized reverse transcriptase that aligns to and uses the G-rich single-stranded overhang at the chromosome terminus as a primer to copy a short template sequence residing within telomerase RNA. Each nucleotide in the telomere repeat is sequentially added, one at a time, and after the last nucleotide in the RNA template is copied, a translocation step is required for telomerase to further elongate the substrate (Greider and Blackburn, 1985). Thus, telomerase exhibits two types of processivity – nucleotide addition and repeat addition processivity – and both are potential nodes of regulation for telomere length homeostasis. Repeated alignment and extension of the G-rich strand by telomerase creates the typical arrays of direct telomeric repeats found at the chromosome ends, and there is a lot of heterogeneity in telomerase activity when assaying from cell extracts of different organisms. *S.*

cerevisiae has especially poor telomerase activity, in terms of both nucleotide addition and repeat addition processivity, and product synthesis *in vitro* is severely limited by slow turnover of the product-template hybrid (Prescott and Blackburn, 1997).

The catalytic core of telomerase consists of the reverse transcriptase-like protein subunit (TERT in mammals, Est2 in *S. cerevisiae*, Trt1 in *S. pombe*) and an essential telomerase RNA component (TR in mammals, TLC1 in *S. cerevisiae*, TER1 in *S. pombe*). The carboxyl-terminal half of the telomerase catalytic protein subunit shares sequence homology with reverse transcriptases (RTs) of retro-elements and retroviruses, with seven defined active site motifs in this conserved region (Nakamura et al., 1997). The amino terminal half contains several conserved sequence motifs, including the domain for binding the RNA. Telomerase RNA components are highly divergent in size and sequence among eukaryotes, although these molecules assume conserved secondary structures (Chen et al., 2000). The size of telomerase RNAs varies from ≈150 nucleotides in ciliates, to ≈500 nucleotides in vertebrates, to ≈1300 nucleotides in budding yeast.

The prevailing model for telomerase action originated from studies in two types of single-celled eukaryotes: ciliates and yeast. Telomerase activity was first discovered in the ciliate *Tetrahymena* (Greider and Blackburn, 1985), and identification of protein subunits of telomerase came from two sources: biochemical purification of telomerase from another ciliate, *Euplotes* (Lingner and Cech, 1996), and genetic analysis in the budding yeast *Saccharomyces cerevisiae* (Lendvay et al., 1996). The catalytic subunit of telomerase was discovered through the identification

of conserved reverse transcriptase sequence motifs in a protein common to both *Euplotes* and yeast (Lingner et al., 1997b). These studies in model organisms have subsequently resulted in the identification of key aspects of human telomerase.

Although there are distinct differences from species to species, the overall structures of the telomere sequence and the protein complexes, as well as the mechanism for telomere elongation, are generally thought to be conserved. Telomerase loss-of-function mutants in single-celled eukaryotes display a senescence phenotype - characterized by progressive telomere shortening and a decreased growth rate and viability (Lendvay et al., 1996; Lundblad and Szostak, 1989). Dysregulation of telomerase in human cells is also deleterious (Mitchell et al., 1999), and mice lacking telomerase can survive up to six generations, displaying progressive shortening of telomeres (≈2 to 7 kb per generation), and eventually, late generations of mouse mutants exhibit defective reproductive organs and cells with severe genomic instability, including aneuploidy and end-to-end fusions (Blasco et al., 1997).

Unlike single-celled eukaryotes like ciliates and yeast, most somatic cells of the human body lack telomerase activity (Shay and Wright, 2005). In those cells, senescence induced by short telomeres may serve an important tumor suppressor mechanism, with most cells undergoing growth arrest before multiple genetic mutations are incurred that could cause the cell to become cancerous. In contrast, greater than 85% of human cancer cells are able to maintain stable telomeres by up-regulating telomerase activity (Kim et al., 1994). In these tumor cells, elongation of the telomere promotes cell proliferation and immortality, and therefore, telomerase has

become an attractive target for cancer therapeutics. Potential treatment methods exist that display high specificity and low toxic side effects (Shay and Wright, 2002), and several anti-telomerase drugs are in clinical trials. Telomerase inhibitors are also being studied in combination with other conventional cancer treatments.

Even in the proliferative tissues where telomerase is expressed (including fetal liver, lung, and spleen cells, stem cells, and adult germ cells), it is very nonabundant, with only ≈6 molecules of telomerase per cell (Cohen et al., 2007). Moreover, telomerase does not extend every telomere in a cell cycle, but tends to preferentially extend short telomeres in mammalian cells (Hemann et al., 2001). Similar phenomena have also been reported in plants and yeast (Shakirov et al., 2005; Teixeira et al., 2004), and it has been proposed that telomeres switch between telomerase-extendable (short telomere) and non-extendable (long telomere) states, allowing establishment of telomere length homeostasis.

A genetic deficiency in telomerase function leads to limited renewal capacity in highly proliferative cells, progressive bone marrow failure, and premature aging – hallmarks of the diseases dyskeratosis congenita, aplastic anemia, and idiopathic pulmonary fibrosis (Armanios, 2009; Heiss et al., 1998). Even a slight reduction in gene dosage has severe clinical consequences, underscoring the importance in understanding precisely how telomerase is regulated.

Telomerase beyond the minimal components: associated factors

In addition to the catalytic core, a variety of telomerase-associated factors are involved in the biogenesis, regulation, and recruitment of telomerase to the telomere. Some of these factors are conserved, but there is a lot of variation from species to species. In the ciliate *Tetrahymena*, there are at least four telomerase associated proteins: p75, p65, p45, and p20. Of the two proteins whose functions have been determined, p65 mediates proper RNA folding and nuclear retention of telomerase, while p20 is a component of SCF ubiquitin ligases and negatively regulates TERT stability (Witkin and Collins, 2004; Witkin et al., 2007).

In *S. cerevisiae*, telomerase activity *in vivo* requires the association of Est1 and Est3 with the TLC1/Est2 catalytic core (as described in detail in the next section). Associations with the budding yeast telomerase holoenzyme also include the Ku70/80 heterodimer, Sm proteins, Gno1, p23, and Ies3. Ku70/80 plays a role in telomere protection and nuclear recruitment (Fisher et al., 2004), Sm proteins function in telomerase RNA maturity and stability (Seto et al., 1999), Gno1 is the yeast orthologue of PinX1 and has been suggested to inhibit biogenesis by sequestering Est2 in the nucleolus in an inactive complex lacking TLC1 (Lin and Blackburn, 2004), p23 is a molecular chaperone implicated in telomerase assembly (Toogun et al., 2007), and Ies3 is a subunit of the INO80 chromatin remodelling complex that interacts with Est1 (Yu et al., 2007). For all of these proteins, it is unclear exactly how they associate and to what extent they regulate telomerase activity through the cell cycle.

In *S. pombe*, telomerase-associated proteins include an Est1 homologue, SpEst1 that functions in telomere elongation and telomere capping (Yu et al., 2007),

Sm proteins that function in TER1 RNA processing and maturation (Leonardi et al., 2008), and Ccq1 interacts with SpEst1 and functions in the recruitment of telomerase to telomeres (Webb and Zakian, 2012).

In humans, there is a long list of telomerase associated proteins that includes multiple Est1 homologues, molecular chaperones, as well as PinX1, 14-3-3, MKRN1, and the dyskerin protein complex. The molecular chaperone proteins function in telomerase assembly, with hsp90 and p23 stably associating with the active complex (Holt et al., 1999). PinX1 has been suggested to repress telomerase activity by binding to hTERT and hTR (Holt et al., 1999). Protein 14-3-3 is involved in nuclear shuttling and localization of hTERT (Seimiya et al., 2000). MKRN1 E3 ligase mediates ubiquitination of hTERT (Kim et al., 2005). The dyskerin protein complex binds a Box H/ACA motif of human TR for regulation of RNA processing and maturation (Gu et al., 2009). Mutations have been identified in both the human TR and dyskerin that result in dyskeratosis congenita, indicating that telomerase-associated proteins have a profound effect on telomerase and telomere regulation.

Budding yeast telomerase: 3 proteins and the RNA

In the budding yeast, telomerase is composed of three proteins, Est1, Est2, and Est3, in a complex with the templating TLC1 RNA, which provides a flexible scaffold on which telomerase associates (Zappulla and Cech, 2004). Est2 and TLC1 constitute the catalytic core of the enzyme.

Est2 contains distinctive motifs common to all reverse transcriptases as well as motifs that are specific to telomerase. Est2 is related to canonical viral reverse transcriptases. Mutations in residues conserved between Est2 and HIV-RT, located in the putative palm, thumb, and finger subdomains, are critical for telomerase activity (Lingner et al., 1997b). Furthermore, Est2 interacts with TLC1 at a stem-loop adjacent to the Est1-interacting stem-loop (Chappell and Lundblad, 2004). An N-terminal TEN domain in Est2 helps to mediate this RNA interaction. Atomic-resolution structure has been determined for the TEN domain of the *Tetrahymena thermophila* homologue, revealing a surface groove with features suggestive of a channel for binding single-stranded DNA (Jacobs et al., 2006). Using this structure as a guide, mutations at surface residues strongly reduced recombinant telomerase activity. To date, this is the only high-resolution structure of any portion of a telomerase subunit in any organism (soluble, stable domains of telomere proteins have been notoriously difficult to express in *E. coli*). Interestingly, mutations in three clusters of residues in Est2 can cause telomeres to over-elongate. Mutations in motif E of the reverse transcriptase domain increase nucleotide addition processivity *in vitro* (Peng et al., 2001). *est2-up* mutations in the finger subdomain allow telomerase to escape inhibition by Pif1p helicase (Eugster et al., 2006). *est2-LT* mutations in the N-terminal TEN domain cause decreased association of a negative regulator Rap1 at the telomere (Ji et al., 2008).

TLC1 encodes the 1.3 kb RNA subunit which contains a template region for the elongation of telomeric DNA. Est2 and TLC1 are necessary and sufficient for

extension of an oligo primer *in vitro* (Lingner et al., 1997a). However, additional factors are required for *in vivo* telomerase action: Est1, Est3, and Cdc13.

Est1 is responsible for recruiting telomerase to the telomere through an electrostatic interaction with the single-stranded DNA binding protein Cdc13. Studies of different alleles of *CDC13* reveal that Cdc13 is involved in both telomere end protection and telomerase recruitment (Pennock et al., 2001). Recruitment defective alleles of Cdc13 have a senescence phenotype comparable to the phenotype of telomerase null mutants. Est1 expression is cell cycle regulated, peaking in late S phase, and this correlates with the timing of telomere elongation (Taggart et al., 2002).

Est3 is the smallest subunit of telomerase. *EST3* encodes two forms of protein: one is a truncated protein resulting from translation of only the first open reading frame and the other is the full-length Est3 protein which has been translated through a frame-shift site (Morris and Lundblad, 1997). Only the full-length Est3 (181 amino acids) with a molecular weight of 20.5 kDa is required for telomere maintenance function *in vivo*. Est3 is poorly conserved, but has been shown to contain a predicted OB-fold (Lee et al., 2008). To date, the mechanism for the function of Est3 in telomere replication is still poorly understood.

Yeast telomerase biogenesis and cell cycle regulation

In *S. cerevisiae*, telomere structure and elongation are closely interrelated with DNA replication during each cell cycle, and there is accumulating evidence that telomerase biogenesis, intracellular trafficking of telomerase components, telomerase

complex stoichiometry, as well as the structure of the telomere itself, all affect the homeostasis of telomeres *in vivo*.

In *S. cerevisiae*, the TLC1 RNA undergoes several steps of maturation before being assembled with telomerase proteins to form the active holoenzyme. TLC1 is transcribed by RNA polymerase II, polyadenylated, capped on its 5' end with a 2,2,7-trimethyl guanosine cap structure, and processed to remove the 3' polyadenosine tail (Collins, 2006). In *S. cerevisiae*, the shuttling of TLC1 between the nucleus and cytoplasm appears to play a critical role in telomerase biogenesis that is not well understood (Gallardo et al., 2008; Teixeira et al., 2002). This shuttling occurs via association of TLC1 with the nuclear exportin Crm1, and importins Mtr10-Kap122 (Ferrezuelo et al., 2002). Interestingly, the absence of the telomerase holoenzyme protein components Est1 or Est2, as well as the absence of telomere associated proteins Ku70, Tel1, or the MRX complex, all result in the cytoplasmic accumulation of *S. cerevisiae* TLC1 (Gallardo et al., 2008).

In budding yeast, telomerase is very limiting in expression and only elongates a subset of telomeres during each cell cycle (Teixeira et al., 2004). Therefore, there must be some regulatory mechanism to allow this limiting complex to sufficiently elongate telomeres. Although an active form of *S. cerevisiae* telomerase is present in various stages of the cell cycle, telomere replication, telomerase activity, and synthesis of the complementary C-rich strand all occur during late S phase in a series of tightly coupled steps. The timing of telomere elongation correlates with the telomere binding of many proteins involved in telomere elongation. The shortest telomeres are

preferentially elongated, while telomerase activity is repressed at over-elongated telomeres. Because Est1 expression peaks in late S phase, and Est1 is recruited to the telomere (based on chromatin immunoprecipitation) in late S phase (Taggart et al., 2002), it has been assumed that Est1 joins the complex in late S phase, thus recruiting the complex to its site of action so that it can extend telomeres.

Challenges in understanding yeast telomerase

The details of telomerase complex stoichiometry and the mechanisms of telomerase regulation are lacking because there have been numerous biochemical challenges in yeast. To date, there has not been a successful purification of yeast telomerase (telomerase has only been purified in the ciliates *Tetrahymena* and *Euplotes*), and there are no working antibodies against Est1, Est2, and Est3. Telomerase is in very low expression (only ≈29 molecules of TLC1 per haploid cell) (Mozdy and Cech, 2006), so detecting a low abundance complex in cell extracts has been problematic. Early attempts to tag the proteins at their endogenous loci have been challenging because many epitope tags adversely affect the function of telomerase. In many cases, the tagged proteins could only be detected by immunoprecipitation, but not in cell extracts.

As a consequence, experiments that have monitored association of Est proteins with each other or with the telomere have certain limitations. Chromatin immunoprecipitation experiments have looked at recruitment of Est1 and Est2 at the telomere during the cell cycle, but each protein was tagged in a separate strain, making

it difficult to make cross comparisons of the subunits. Multiple labs have examined complex formation in co-immunoprecipitation experiments, using strains with different tags on each Est protein, but therefore the relative proportions of each protein in the complex could not be determined. Est3 has been subject to even less scrutiny, and it is still very unclear how it assembles into the complex and whether it is regulated through the cell cycle.

The difficulties in studying telomerase are not just limited to yeast. One of the outstanding problems in the telomerase field is that different species have considerable variation in terms of enzymatic activity and expression levels, as well as the composition and stoichiometry of proteins in the complex. For example, ciliates express large volumes of telomerase, but are not amenable to genetics. Budding yeast, for reasons that are unfortunate and still unclear, have poor enzyme activity, yet the genetics is excellent. Structural information is severely lacking in all systems, but particularly in yeast. What is really needed is a single system that combines the ability to monitor each subunit of the holoenzyme, facile genetics that is structure-driven, and robust enzyme activity.

Dissertation overview

In this dissertation, I take a multi-disciplinary approach combining genetics with biochemistry that improves on the limitations in yeast, resulting in the identification of several unexpected aspects of telomerase assembly and regulation.

First, I developed a reverse mutagenesis approach designed to target functionally important residues on the surface of the telomerase protein subunits, even in the absence of structural information. This was used to identify key surface residues in Est3 as described in Chapter 2, and this approach was continued by other members of the Lundblad lab, John Lubin and Lisa Nguyen, to obtain a collection of separation-of-function alleles in each of the three *EST* genes.

In order to overcome limitations in detecting telomerase and monitoring the subunits in the complex, I developed a biochemical assay that allows simultaneous detection of the relative levels of Est1, Est2, and Est3 from extracts and following immunoprecipitation of any one of the subunits. Tagged versions were introduced into the genome in place of the untagged *EST* genes, so that each tagged protein is expressed from its native promoter and with minimal disruption of telomere length control. This biochemical assay is described in Chapter 3.

Chapters 4 – 7 integrate genetics with the biochemical assay described in Chapter 3. Chapter 4 provides a detailed analysis of three elements on a long helical arm of TLC1 that are required for Est1 association. Chapter 5 tests two contradictory models regarding Est1 function and finds that an Est1-containing complex is assembled much earlier in the cell cycle than previously reported, with a biochemical interaction between Est1 and Cdc13 that recapitulates their genetic relationship. Chapter 6 contains a detailed analysis of Est1 and identifies four functionally distinct interfaces on the protein: two in the N-terminus (one of which maps to Domain A and is required for binding the TLC1 RNA) and two in the C-terminus (involved in Est3

and Cdc13 association). Chapter 7 describes two unexpected observations about the association of Est3 with the telomerase complex that suggest that telomerase exists in multiple complexes.

Finally, the Appendix contains an additional body of data that was obtained during the course of my graduate studies. Appendix A examines a series of candidate factors for association with telomerase, and Appendix B includes some preliminary biochemistry data on the catalytic subunit Est2.

Chapter 2: Development of a protocol for identification of separation-of-function mutations

Introduction

As a starting point for this dissertation, I was interested in obtaining an extensive collection of separation-of-function alleles in each of the three *EST* genes. Such mutations would be instrumental for examining assembly and regulation of telomerase, given that the telomerase complex has multiple protein-protein and protein-nucleic acid interactions. For example, although Est2 has residues that are critical for catalysis (Lingner et al., 1997b), it also binds to a stem-loop on the TLC1 RNA (Chappell and Lundblad, 2004), makes contact with single-stranded telomeric DNA (Jacobs et al., 2006) and potentially mediates a direct interaction with Est3 (Hughes et al., 2000; Talley et al., 2011) and potentially other yet-to-be-identified factors. Therefore, separation-of-function mutations would be valuable for delineating specific biochemical activities that can potentially dictate sites of interaction with other molecules.

Separation-of-function mutants have been difficult to obtain, and generally represent a small sub-class of mutations that can be identified in a gene. The work on *cdc13-2* underscores the potential use of separation-of-function mutations in determining a surface of direct protein-protein interaction (Evans and Lundblad, 1999), but this allele was fortuitously isolated in a labor intensive, four-tiered forward mutagenesis screen (Lendvay et al., 1996). An easier method for obtaining similar types of alleles is needed. With the rapid development of bioinformatics and high-throughput genome sequencing technologies, reverse genetics has become a viable option. However, with traditional loss-of-function approaches, it is difficult to

determine whether a mutant phenotype is a consequence of general protein misfolding or if a single function on that protein has been impacted (Alber, 1989). My goal was to develop a method that is both rapid and sufficiently comprehensive in acquiring separation-of-function mutations that affect every biochemical function on the telomerase proteins.

Since yeast telomerase is a multi-subunit complex that is limiting in expression, there is potential for uncovering dominant negative alleles. Indeed, a limited number of dominant negative alleles have been isolated in all four of the yeast telomerase components (Evans and Lundblad, 2002; Lee et al., 2008; Lingner et al., 1997b; Singer and Gottschling, 1994; Virta-Pearlman et al., 1996). These mutants, when over-expressed in otherwise wild-type cells, confer a telomere shortening phenotype, presumably by titrating away other components responsible for telomere replication. Dominant negative proteins are particularly useful because they suggest that (1) the protein is stably expressed and (2) at least one biochemical activity of the protein is still intact. Therefore, dominant negative mutations are also good candidates for being separation-of-function mutations. In contrast, residues in the internal core of a protein are not likely to be involved in surface interactions with other proteins. These mutants will not confer a dominant negative phenotype because they will not interfere with the endogenous telomerase complex.

To test the effectiveness of a dominant negative reverse genetics approach for identifying separation-of-function alleles, I started with Est3 for the following reasons: (1) A structure prediction had been determined by Ed Mandell in the lab at the start of

this project (Lee et al., 2008); (2) there was already a large collection of *est3*$^{-}$ mutations that had been generated, some of which had been tested in loss-of-function assays; (3) Some *est3*$^{-}$ alanine scan mutations had previously been shown by Danna Morris to be dominant negative when over-expressed (Morris, 2000), suggesting that this method has potential for surveying the entire surface of the protein. Residues of high interest were chosen based on the structure prediction and conservation with related yeast species, with particular emphasis in mutating charged residues likely to be at the surface and mediating interaction with another factor (Figure 2.1). The expected outcome was that if a mutant is dominant negative, there would be a telomere replication defect in a wild-type yeast strain when it is over-expressed. If a mutation destabilizes the protein, no dominant negative phenotype would be expected since that protein would be unable to interfere with any biological processes. Finally, if the mutation produces stable protein but with minimal perturbation of a biochemical activity, then the defect on telomere replication would be expected to be modest and no different than when wild-type Est3 is over-expressed.

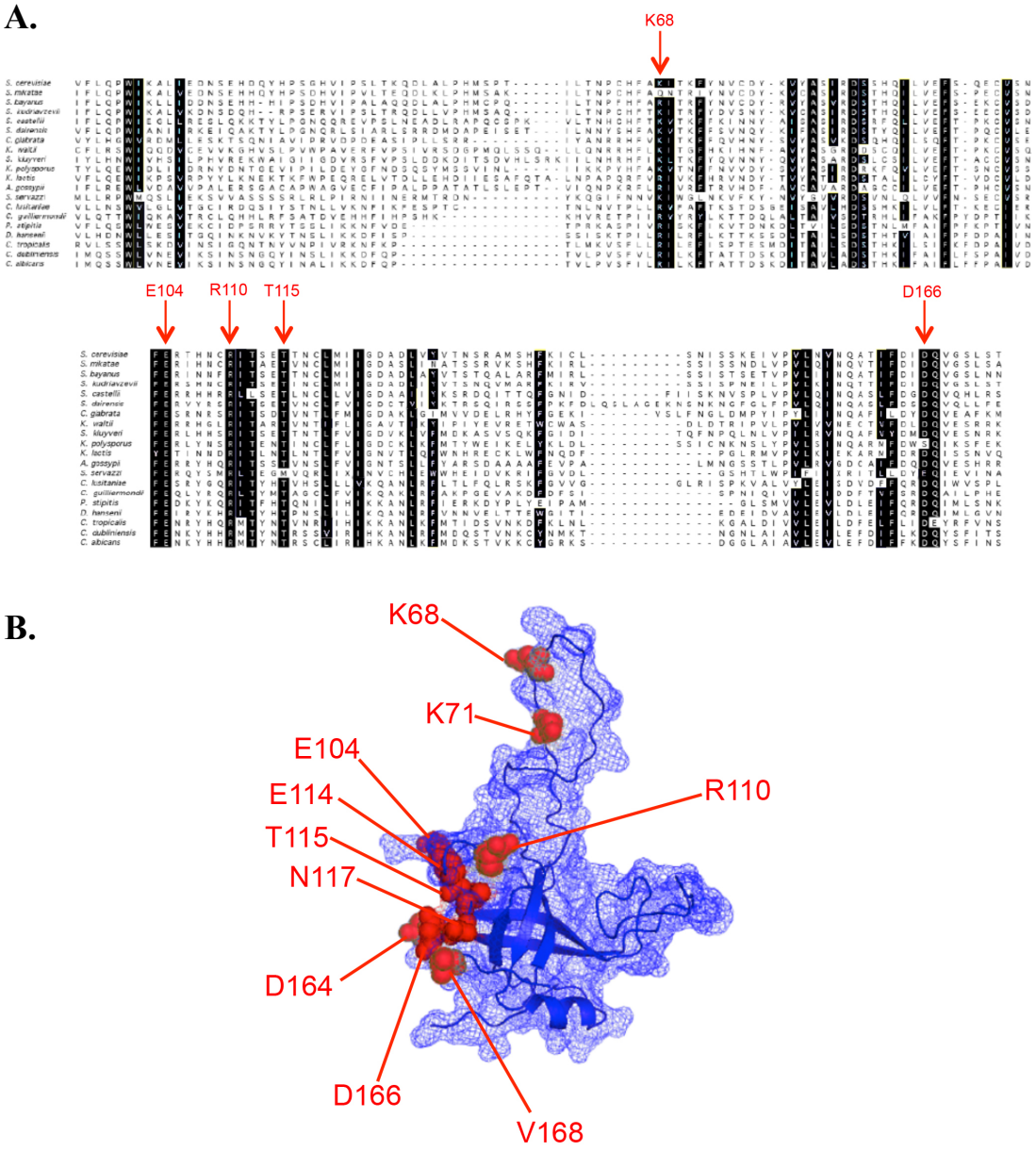

Figure 2.1 Rationale for how Est3 residues were selected for reverse mutagenesis. A) Alignment of 20 Est3 protein sequences. Residues highlighted in black exhibit a high degree of conservation; red arrows point to select residues that are highly conserved and predicted to be located at the surface of the protein. B) Wire mesh model of the predicted structure of Est3; indicated in red are a subset of the candidate surface residues that were mutated and tested for an over-expression dominant negative phenotype. This figure was adapted from (Lee et al., 2008), Figure 1.

Results

Identification of dominant negative Est3 mutants

To test for an over-expression dominant negative phenotype, a wild-type *EST3* strain was transformed with a high-copy (2μ) plasmid expressing wild-type or mutant Est3 proteins under control of an *ADH* promoter. In total, 37 mutations were tested that surveyed 20 residues (multiple mutations were tested for some residues – for example, *est3-Q167R*, *Q167A*, and *Q167V*). I also included Danna Morris's alanine scan mutations and two Est2 catalytically inactive mutants as positive controls.

Genomic DNA was prepared after ~75 generations of growth, and a southern blot was probed for a telomere-specific sequence. Figures 2.2 and 2.5a contain a subset of the mutations that were tested for telomere length. Increased expression of wild-type Est3 had a very modest effect, with a telomere length decline of ≤ 50 bp; in contrast, over-expression of a predicted internal mutant, Est3-W21A, had no effect on telomere length, consistent with western blot data indicating that this protein had unfolded and destabilized (see Figure 2.7b). Over-expression of mutants in functionally important surface residues, like Est3-R110A and Est3-D164A, showed a substantial decrease in telomere length, indicative of a severe dominant negative phenotype. In fact, the dominant negative phenotypes of Est3-R110A and Est3-R110E were even more pronounced than the Est2 catalytically dead mutants. In all, 25 out of the 37 mutations examined had some degree of a dominant negative phenotype.

Figure 2.3 demonstrates that the dominant negative phenotype is affected by the dosage of over-expression. When dominant negative mutants were over-expressed behind an *ADH* promoter on a *CEN* plasmid (typically 1 copy / cell) instead of a 2μ plasmid (≈50-100 copies per cell, Romanos et al., 1992), the telomere replication defect was less pronounced. This provides strong support that the dominant negative phenotype is due to dosage dependent titration of a telomere replication factor away from the endogenous complex. For Est3-R110E, the dominant negative phenotype was so pronounced that it was even detectable under native expression conditions (i.e. in the same *EST3* strain but with Est3-R110E expressed from a *CEN* plasmid behind the native promoter instead of *ADH* ; unpublished observation).

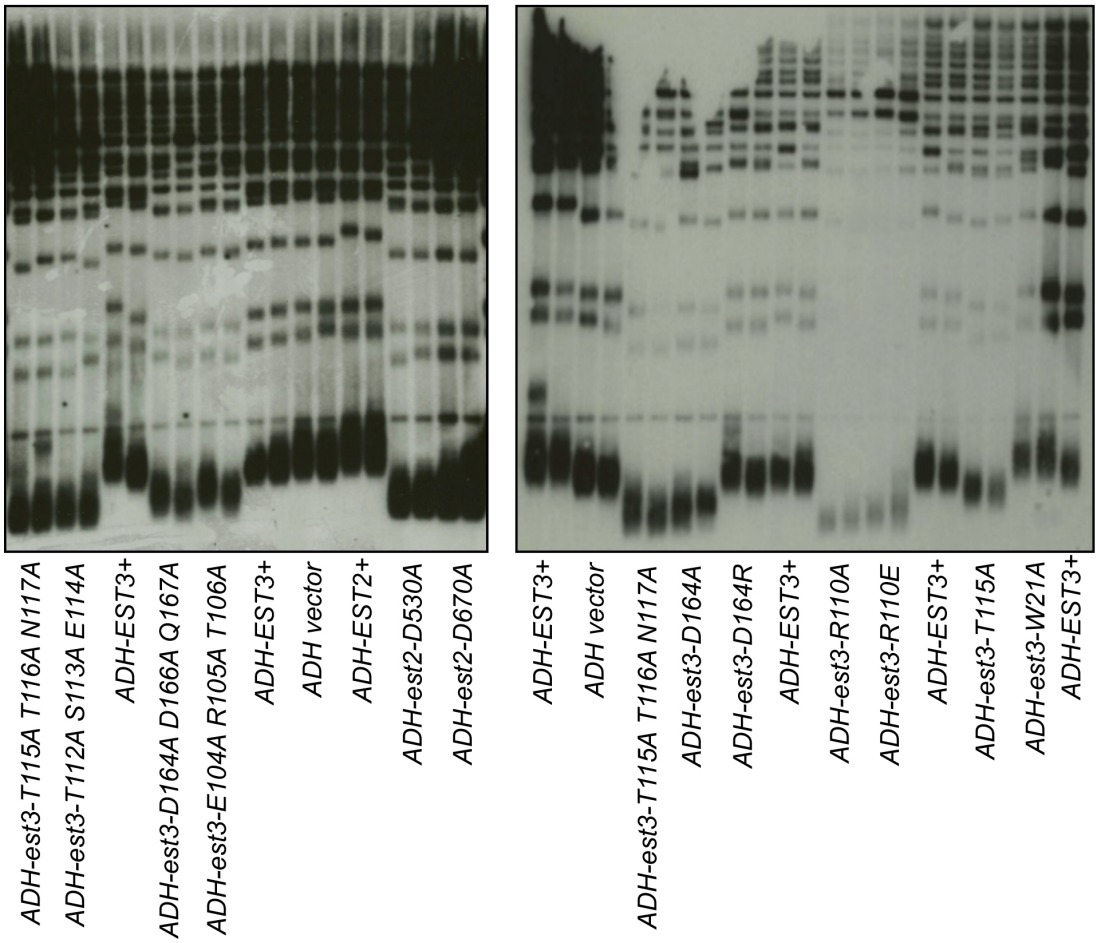

Figure 2.2 The dominant negative effect on telomere length for a subset of mutations in *EST3*. An *EST3* wild-type strain was transformed with 2μ plasmids over-expressing either wild-type or mutant alleles of *EST3* and examined for telomere length after ~75 generations of propagation. Catalytically dead alleles of *EST2 (est2-D530A* and *est2-D670A*) were included as positive controls on the left panel. Right panel was adapted from (Lee et al., 2008), Figure S3.

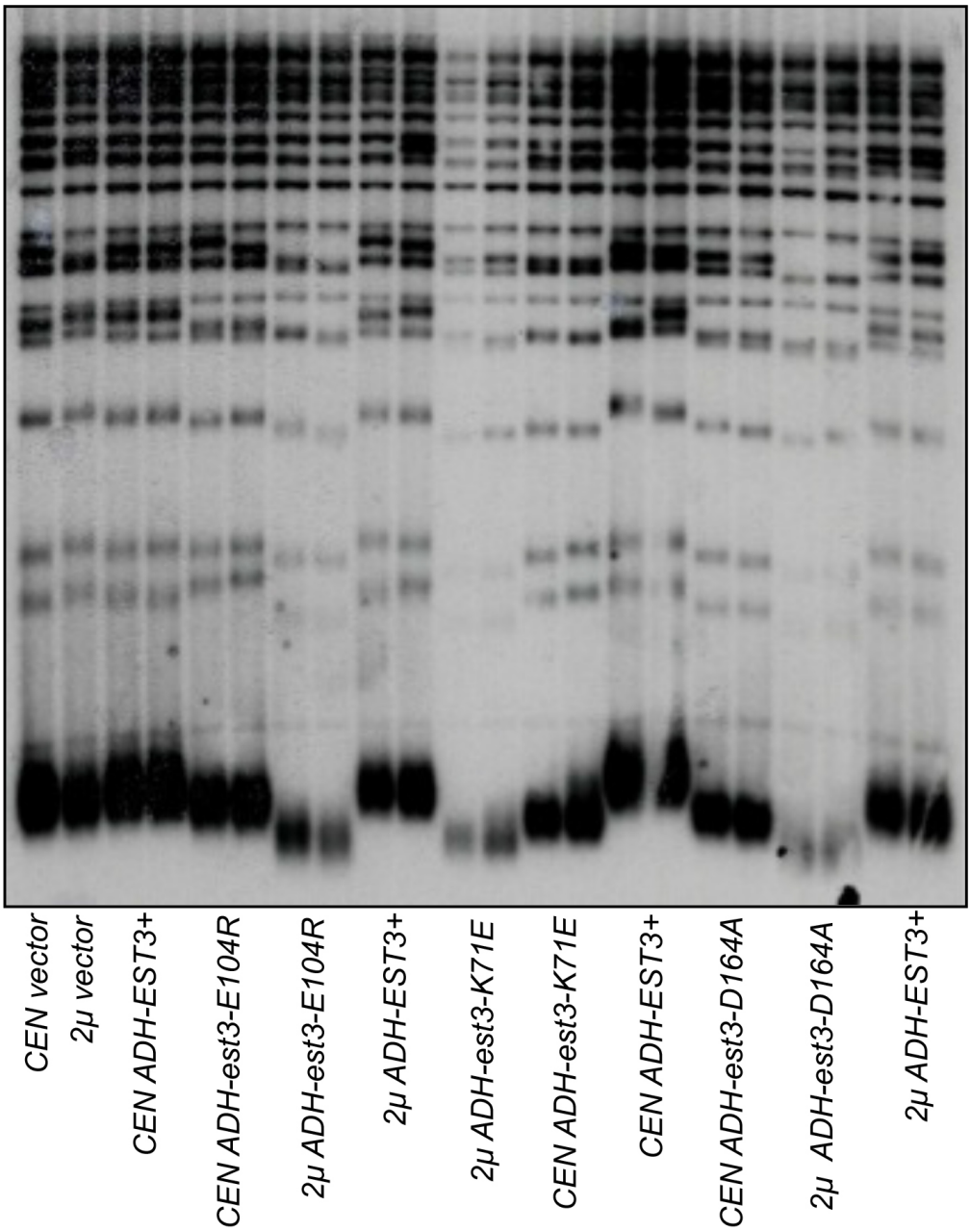

Figure 2.3 The dominant negative effect on telomere length is dependent on the dosage of over-expression. An *EST3* wild-type strain was transformed with 2μ or *CEN* plasmids bearing wild-type or mutant alleles of *EST3* behind an *ADH* promoter. When expressed from a *CEN* plasmid, the dominant negative phenotype is less pronounced for each mutant tested.

Using a synthetic growth assay to monitor the dominant negative phenotype

The telomere length phenotype shown in Figures 2.2 and 2.3 is useful for demonstrating that over-expression of select *est3*$^{-}$ mutations has a direct impact on telomere maintenance. However, the ultimate goal is to survey the entire protein surfaces of telomerase and obtain a comprehensive collection of dominant negative alleles in Est1, Est2, and Est3. Surveying all the mutations by southern blot has limitations in terms of the time it takes to complete a single assay, as well as the volume of mutations that can be tested in a single experiment.

To improve on this, I tested the Est3 mutants in a synthetic assay that allows for a more rapid yet similarly sensitive read-out of the dominant negative phenotype. This assay is based on prior observations demonstrating that a *yku80-Δ* strain is sensitized to defects in telomerase, such that even modest reductions in telomerase function can confer severe growth defects or even lethality when combined with a null mutation in *YKU70* or *YKU80* (Evans and Lundblad, 2002). Furthermore, the synthetic growth defects displayed by *yku80-Δ* strains can be enhanced by increases in temperature. Therefore, this strain provides a highly sensitive assay for monitoring the potential dominant negative phenotypes displayed by a panel of *est3*$^{-}$ mutations.

The same over-expression plasmids used for the telomere length assay were transformed into an *EST3 yku80-Δ* strain and subsequently examined for growth by plating 5-fold serial dilutions of equivalent numbers of cells. The growth was examined at 30° and 32° and Figure 2.4 contains a subset of the mutations tested in this assay. Underscoring how sensitive this assay is to slight differences in

temperature, the dominant negative phenotype is clearly more pronounced at 32°, although severe mutants like Est3-R110E maintain a substantial growth defect at 30°. Higher temperatures were also tested (34° and 36°) but resulted in considerably greater variation in the assay, indicating the *YKU80* disruption alone was having an impact on viability (*yku80-Δ* is unable to form colonies when incubated at 37° - Boulton and Jackson, 1996).

Figure 2.5 compares the *EST3 yku80-Δ* synthetic assay with a southern blot where the same plasmids were transformed in the *EST3 YKU80* strain. The mutant Est3 dominant negative phenotypes in each assay were quantified and are displayed in Figure 2.6. With the exception of *est3-K68E* and *est3-E104R*, there is a strong correlation between the degree of telomere shortening in the *EST3 YKU80* strain and the synthetic growth defect in *EST3 yku80-Δ*. This indicates that the synthetic growth assay is valid for testing a large volume of mutants for dominant negative phenotypes, although synthetic growth candidates should still be subjected to telomere length analysis to confirm that the phenotype is telomere specific.

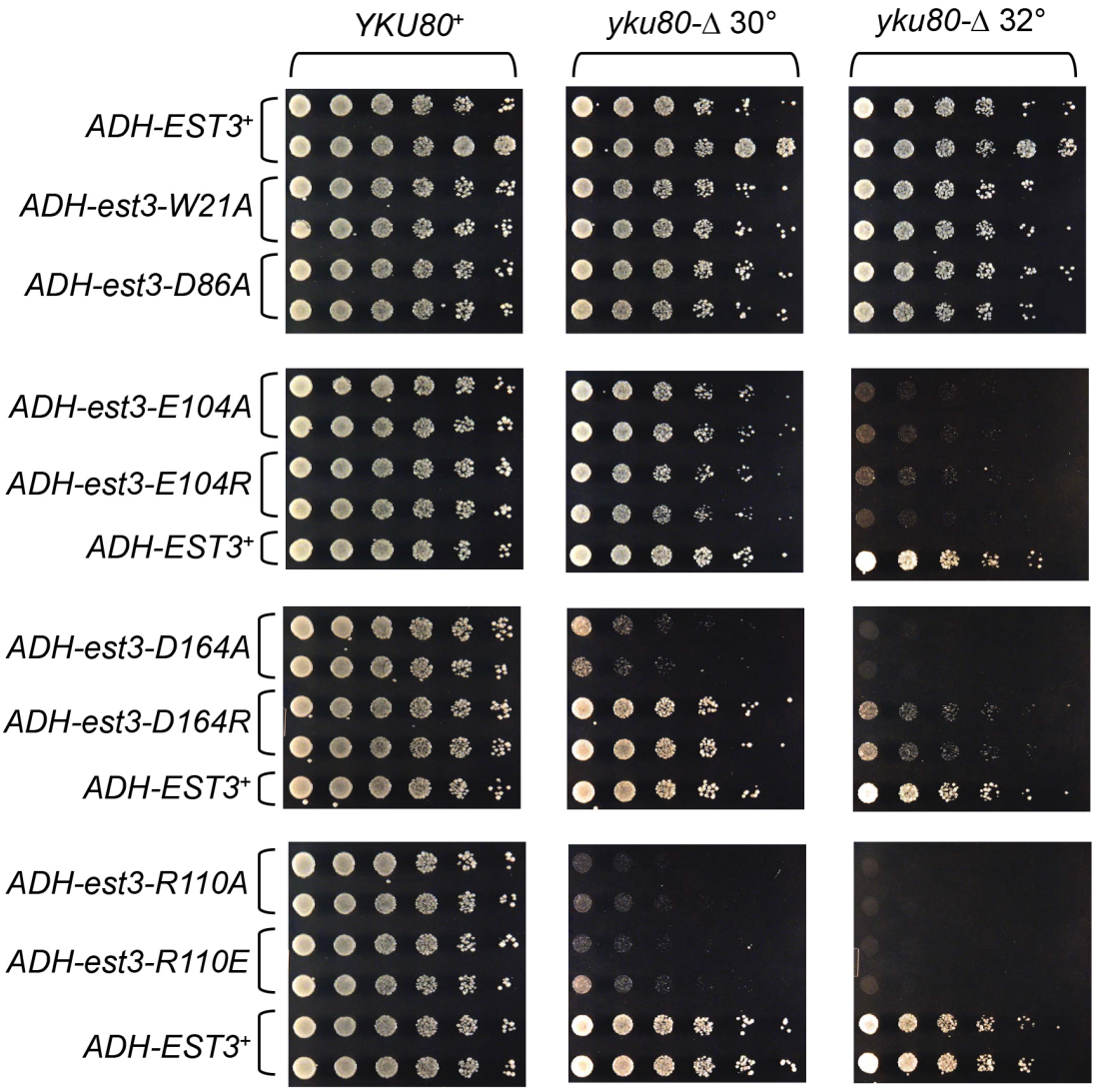

Figure 2.4 Dominant negative synthetic growth phenotype of a subset of *est3*⁻ mutant alleles. High copy (2μ) plasmids expressing wild-type and mutant alleles of *EST3*, under control of the *ADH* promoter, were transformed into a *yku80*-Δ/p *YKU80 URA3* strain and subsequently examined for growth by plating 5-fold serial dilutions of equivalent numbers of cells on media that retains *YKU80* (leftmost panel) or selects for loss of the *YKU80* plasmid (*yku80*-Δ). Growth of the *yku80*-Δ/p *ADH-est3*⁻ strains was examined at both 30° and 32°.

Figure 2.5 Comparison of the dominant negative phenotype in the telomere shortening and synthetic growth assays. The exact same 2μ plasmids expressing wild-type and mutant alleles of *EST3*, under control of the *ADH* promoter, were transformed into the *EST3 YKU80* wild-type strain in A) and the *EST3 yku80*-Δ strain in B) for a direct comparison of the dominant negative phenotype in each assay.

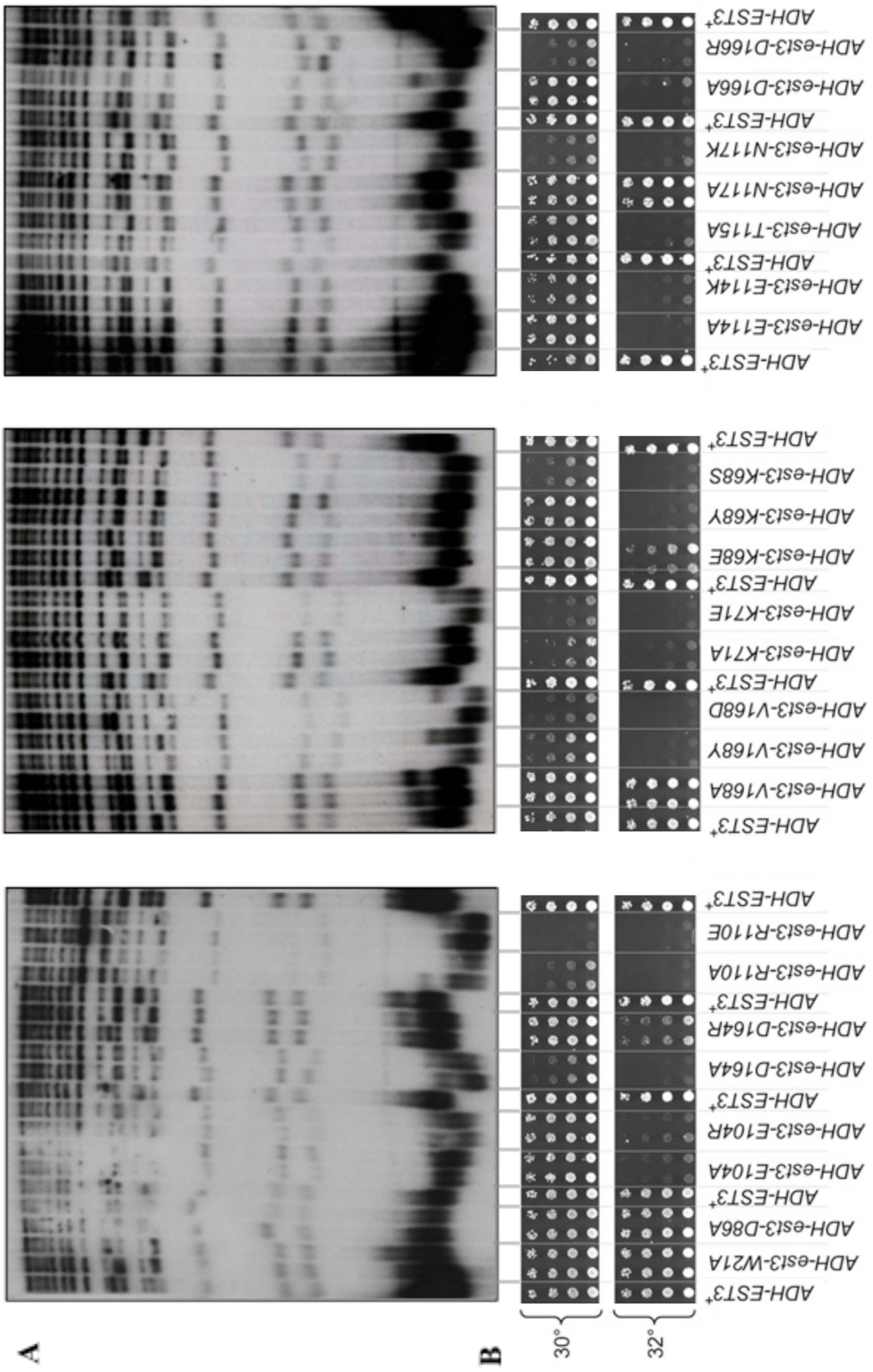
A
B
30°
32°
ADH-EST3+
ADH-esl3-W214A
ADH-esl3-D86A
ADH-EST3+
ADH-esl3-E104A
ADH-esl3-E104R
ADH-EST3+
ADH-esl3-D164A
ADH-esl3-D164R
ADH-EST3+
ADH-esl3-R110A
ADH-esl3-R110E
ADH-EST3+
ADH-esl3-V168A
ADH-esl3-V168Y
ADH-esl3-V168D
ADH-EST3+
ADH-esl3-K71A
ADH-esl3-K71E
ADH-EST3+
ADH-esl3-K68E
ADH-esl3-K68Y
ADH-esl3-K68S
ADH-EST3+
ADH-EST3+
ADH-esl3-E114A
ADH-esl3-E114K
ADH-EST3+
ADH-esl3-T115A
ADH-esl3-N117A
ADH-esl3-N117K
ADH-EST3+
ADH-esl3-D166A
ADH-esl3-D166R
ADH-EST3+

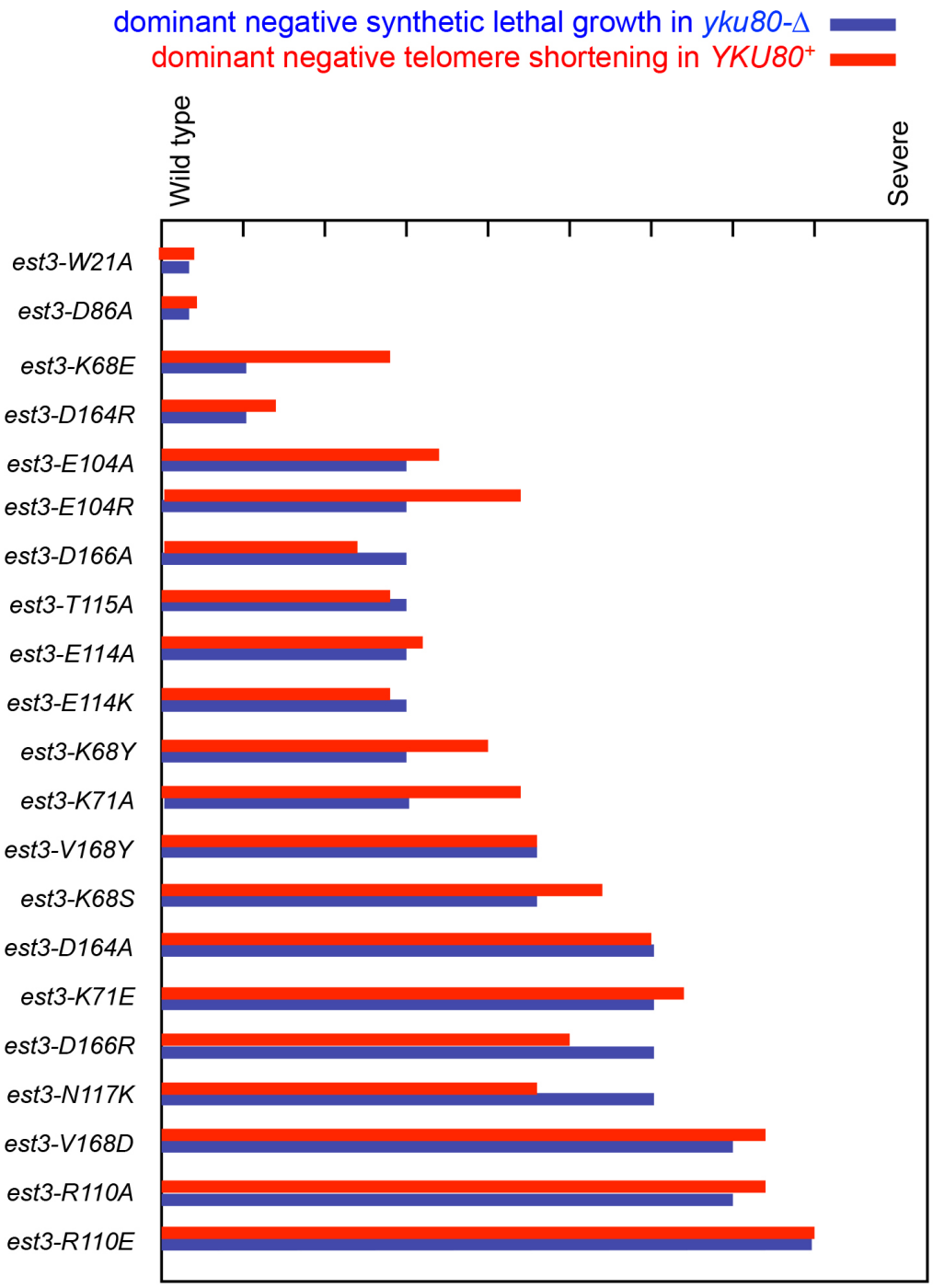

Figure 2.6 Correlating the dominant negative phenotype in the telomere shortening and synthetic growth assays. Quantitation of the telomere shortening phenotype (shown in red) is based on telomere length measurements of the data shown in Figure 2.5a. Evaluation of the synthetic growth phenotype (shown in blue) is based on quantification of the growth shown in Figure 2.5b.

The dominant negative phenotype is a reliable indicator of protein stability

In collaboration with Jaesung Lee and Ed Mandell, the *est3*$^{-}$ mutations were also tested in a loss-of-function assay, and for protein expression on a western blot (Lee et al., 2008). The results in Figure 2.7a and 2.7c indicate that this panel of *est3*$^{-}$ mutations could be classified on the basis of their relative behavior in the loss-of-function and dominant negative assays. Mutations in internal residues, such as *est3-W21A* and *est3-D86A*, were at one extreme end of the spectrum, with no dominant negative phenotype despite a severe loss-of-function defect, whereas mutations such as *est3-R110A* and *est3-R110E* were at the opposite end, with a strong defect in both assays.

A graphical representation of the relative effect of these mutations in these two assays is shown in Figure 2.8. This demonstrates that for most mutations, there is an excellent correlation between the severity of the defects in the loss-of-function and dominant negative assays. For a small subset of mutations, however, there is a roughly inverse correlation, suggesting that loss of function in these mutant proteins is potentially due to protein destabilization. For example, the *est3-K68E* mutation has a loss-of-function defect roughly comparable to that of *est3-K68Y* but a greatly reduced effect in the dominant negative assay; the Est3-K68E mutant protein also exhibits a modest reduction in protein levels. Furthermore, mutations in the predicted internal residues *est3-W21A* and *est3-D86A* clearly had reductions in protein levels (Figure 2.7b).

Figure 2.7 Detailed phenotypic analysis of mutations in predicted surface residues of Est3. A) Telomere length analysis: an *est3-Δ* strain was transformed with single-copy plasmids expressing either a mutant allele or the wild-type *EST3* gene and propagated for ~80 cell divisions and examined for telomere length, as described previously. B) Steady state levels of wild-type and mutant derivatives of Est3-$(FLAG)_3$ proteins. C) Dominant negative phenotypes of *est3*$^-$ mutant alleles: high copy (2μ) plasmids expressing wild type and mutant alleles of *EST3*, under control of the *ADH* promoter, were transformed into a *yku80-Δ*/p *YKU80 URA3* strain as described in Figure 2.4. This figure is a direct reproduction from (Lee et al., 2008), Figure 3.

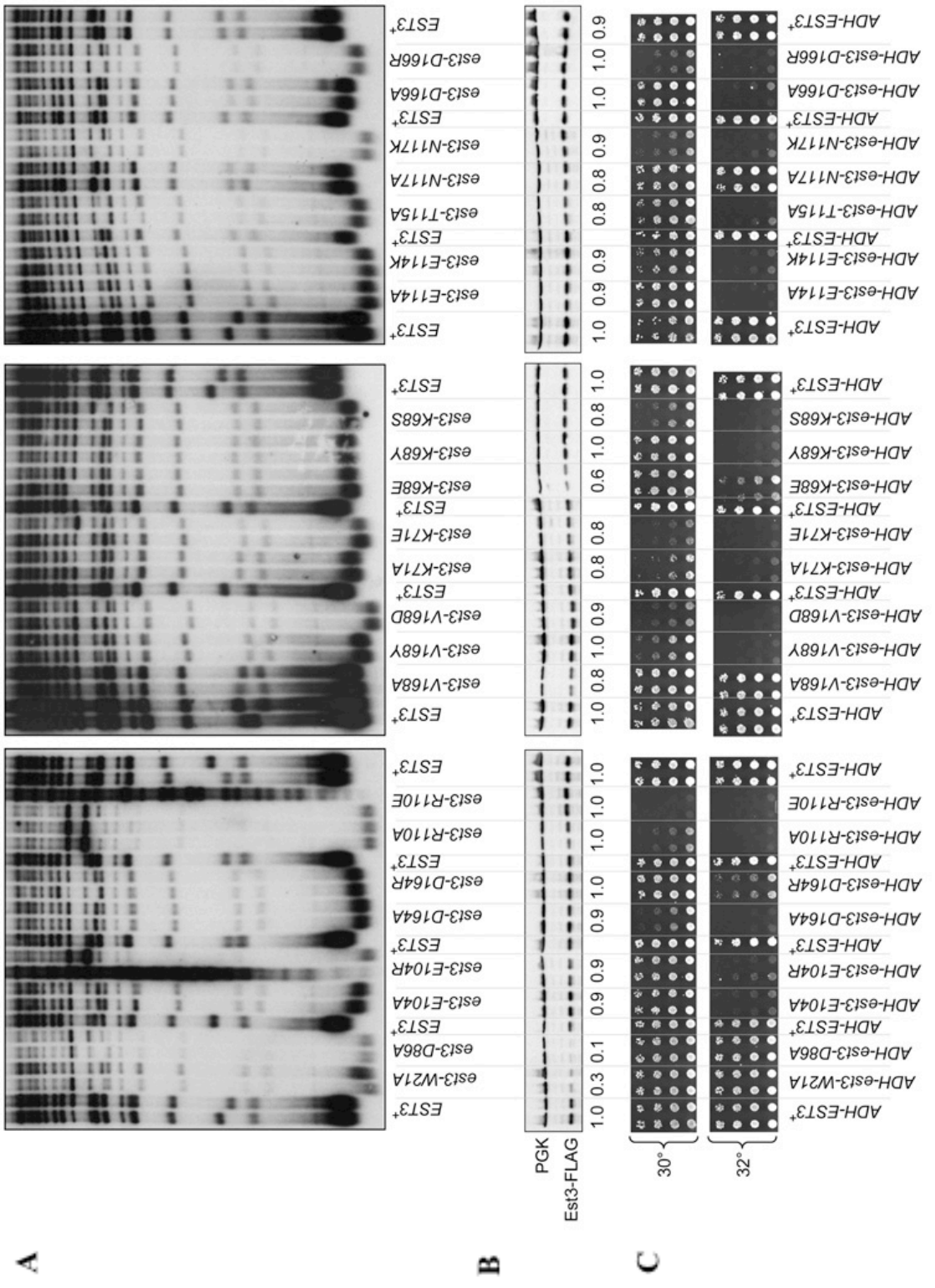
A
B
C
PGK
Est3-FLAG
30°
32°
1.0 0.3 0.1
1.0 0.8 1.0 0.9
1.0 0.9 0.9
1.0 0.8 0.8 0.9
1.0 1.0 0.9
1.0 0.6 1.0 0.8 1.0
1.0 1.0 1.0
1.0 1.0 1.0
ADH-EST3+
ADH-est3-W214A
ADH-est3-D86A
ADH-EST3+
ADH-est3-E104A
ADH-est3-E104R
ADH-EST3+
ADH-est3-D164A
ADH-est3-D164R
ADH-EST3+
ADH-est3-R110A
ADH-est3-R110E
ADH-EST3+
ADH-EST3+
ADH-est3-V168A
ADH-est3-V168Y
ADH-est3-V168D
ADH-EST3+
ADH-est3-K71A
ADH-est3-K71E
ADH-EST3+
ADH-est3-K68E
ADH-est3-K68Y
ADH-est3-K68S
ADH-EST3+
ADH-EST3+
ADH-est3-E114A
ADH-est3-E114K
ADH-EST3+
ADH-est3-T115A
ADH-est3-N117A
ADH-est3-N117K
ADH-EST3+
ADH-est3-D166A
ADH-est3-D166R
ADH-EST3+
EST3+
est3-W214A
est3-D86A
EST3+
est3-E104A
est3-E104R
EST3+
est3-D164A
est3-D164R
EST3+
est3-R110A
est3-R110E
EST3+
EST3+
est3-V168A
est3-V168Y
est3-V168D
EST3+
est3-K71A
est3-K71E
EST3+
est3-K68E
est3-K68Y
est3-K68S
EST3+
EST3+
est3-E114A
est3-E114K
EST3+
est3-T115A
est3-N117A
est3-N117K
EST3+
est3-D166A
est3-D166R
EST3+

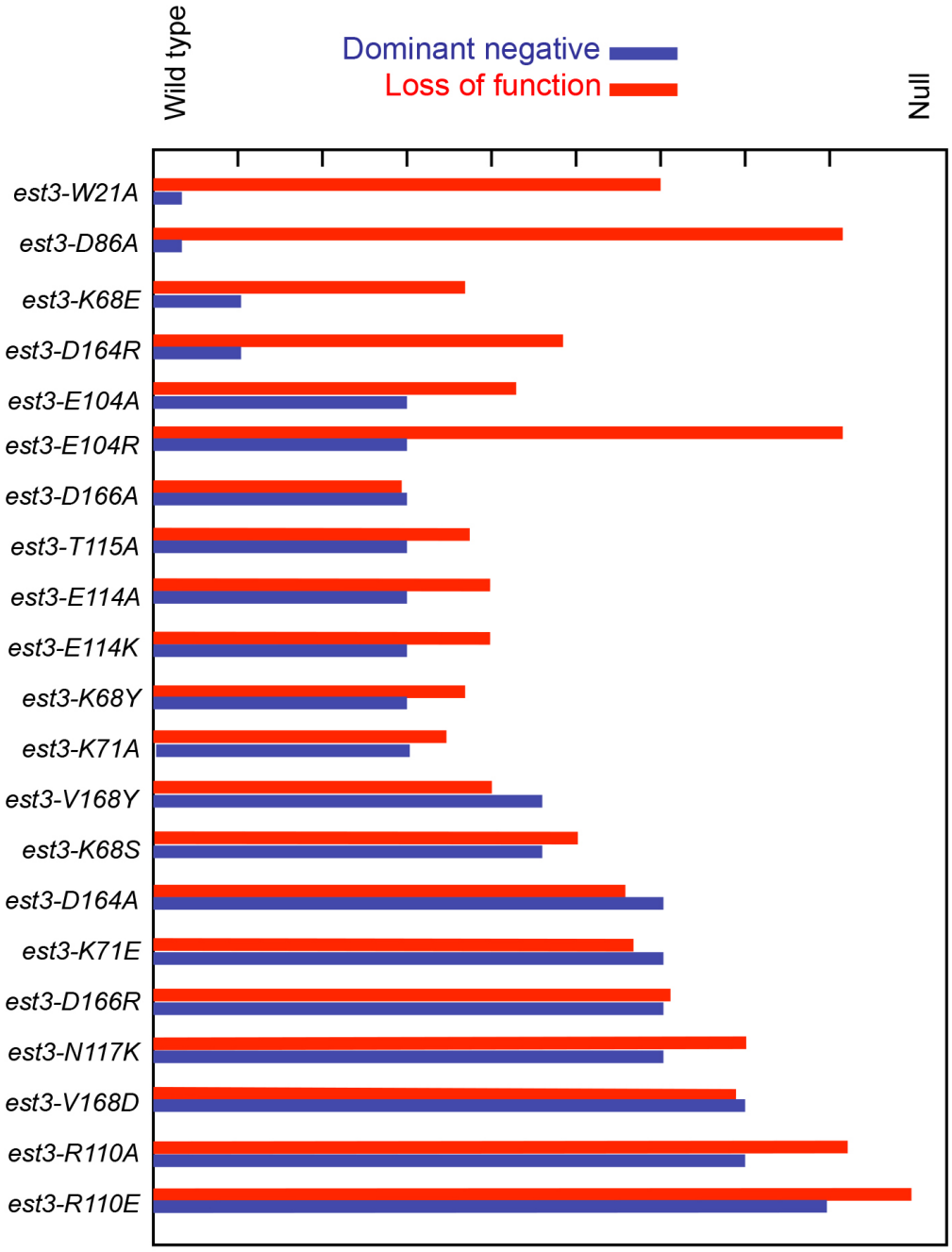

Figure 2.8 Correlating the effect of mutations on loss-of-function versus dominant negative phenotypes. Quantitation of the loss-of-function phenotype (shown in red) is based on telomere length measurements of the data shown in Figure 2.7a. Evaluation of the dominant negative phenotype (shown in blue) is based on the synthetic lethal growth data in Figure 2.7c. This figure was adapted from (Lee et al., 2008), Figure S4.

Defining the biochemical function of the dominant negative alleles

The results above suggest that some subset of the *est3*$^{-}$ dominant negative alleles may be separation-of-function alleles that have specifically lost a single biochemical activity associated with the Est3 telomerase subunit. In collaboration with Jaesung Lee, it was determined that mutations in a subset of residues (E104, E114, T115, N117, and D166) lost association with telomerase as measured by reduced TLC1 co-immunoprecipitation. Strikingly, several of the most defective alleles (K71, R110, V168) still retained association with telomerase when mutated, arguing that a property other than interaction with the telomerase RNP is affected (Lee et al., 2008). It is worth re-emphasizing that mutations in both groups of residues exhibited strong dominant negative phenotypes when over-expressed, indicating that the absence of a dominant negative phenotype was not simply due to a difference in whether the Est3 protein associated with telomerase or not.

I chose a subset of alleles from both classes to see if the dominant negative phenotype could be genetically suppressed by over-expression of Est1 or Est2. This was attempted under conditions where the Est3 mutant was over-expressed from a 2μ plasmid (Figure 2.9), a *CEN* plasmid (Figure 2.10) or under native conditions (data not shown). For the mutants that were tested, I found that no evidence for suppression by either Est1 or Est2.

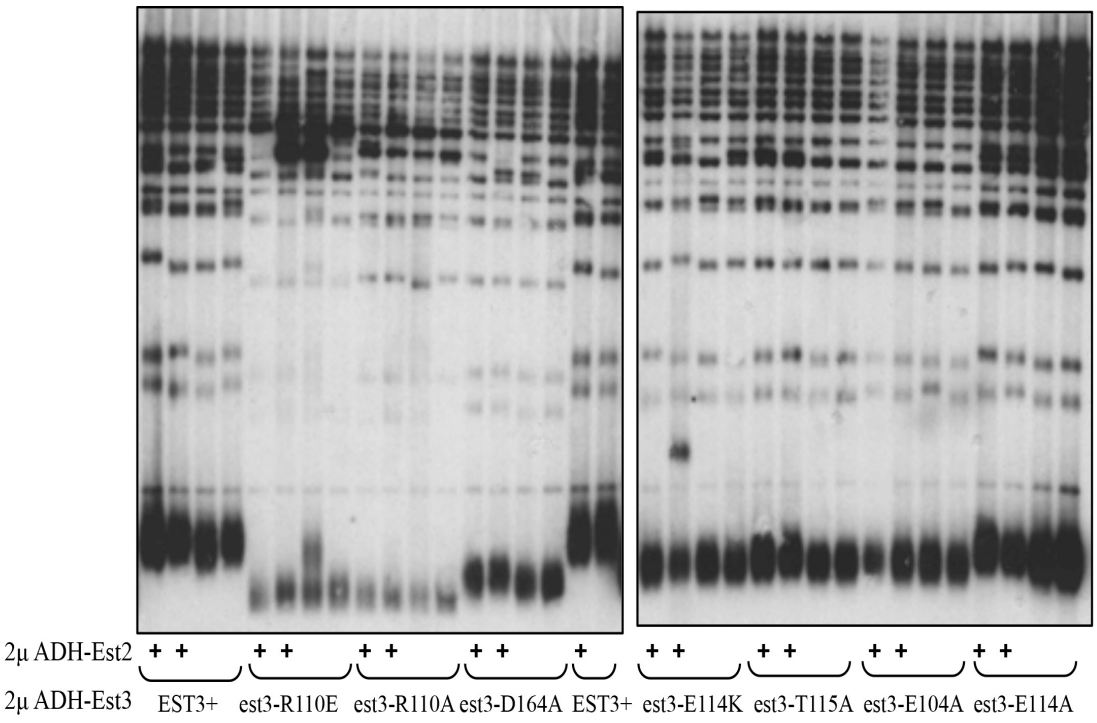

Figure 2.9 *est3*⁻ dominant negative alleles are not suppressed by over-expression of Est2. Telomere length (after propagation for ~75 generations) of the indicated *EST3* / *2μ ADH-est3*⁻ strains transformed with either a 2μ plasmid over-expressing *EST2* (pVL369) or vector (pRL63).

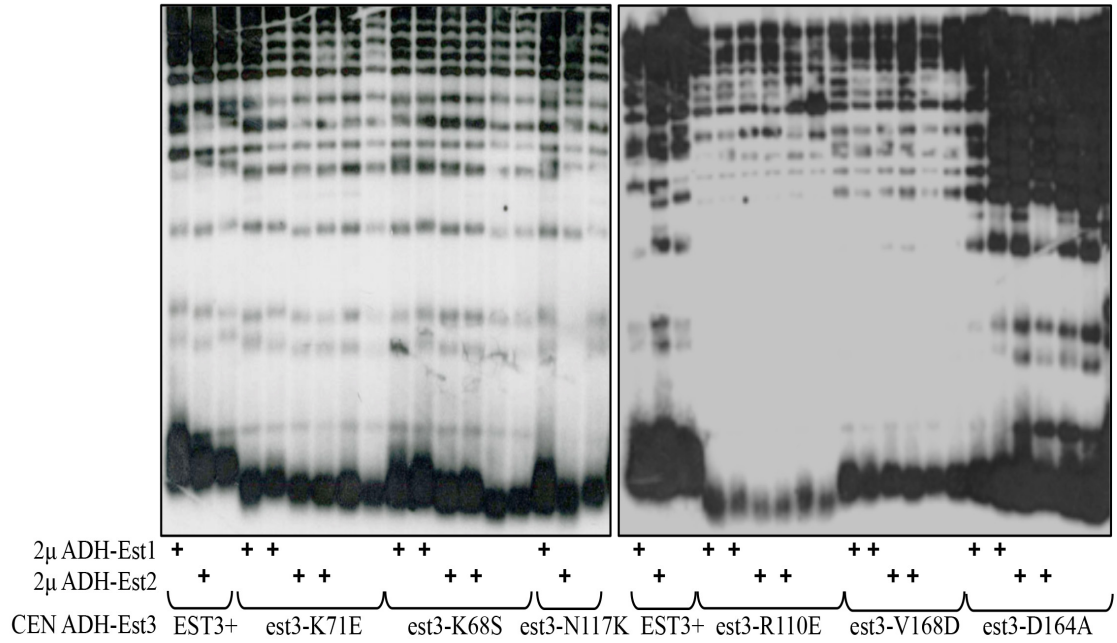

Figure 2.10 *est3*⁻ dominant negative alleles are not suppressed by over-expression of Est1 or Est2. Telomere length (after propagation for ~75 generations) of the indicated *EST3* / *p CEN ADH-est3*⁻ strains transformed with either a 2μ plasmid over-expressing *EST1* (pVL249), *EST2* (pVL4120), or vector (YEplac112).

Discussion

This reverse genetics approach was very successful in identifying dominant negative alleles of *EST3*. Even in the absence of structure information, the *yku80*-Δ synthetic growth assay makes it possible to survey the entire surface of a protein, particularly when including criteria such as sequence conservation and emphasis on charged resides which are expected to have a greater likelihood of mediating direct interactions with other factors. This especially has potential for investigating low expression multi-subunit complexes like telomerase, where titration of critical subunits can have a drastic effect on the phenotype. Theoretically, this approach should be applicable to other protein complexes, although the dominant negative phenotypes might be less pronounced in situations where the endogenous complex is expressed at a higher level. Since over-expression of wild-type Est3 alone causes slight telomere shortening, this suggests that Est3 is unusually sensitive to genetic perturbations.

This approach was continued by John Lubin to extensively mutate surface residues in *EST3* (Lubin et al.) and *EST1* (unpublished data), and by Lisa Nguyen for identifying dominant negative mutations in *EST2* (Nguyen, 2013). The end result is that we now have a large collection of separation-of-function mutations in each of the three *EST* genes. Chapters 6, 7 and Appendix B of my thesis contain some of these mutations that were incorporated into the biochemical system that I describe in Chapter 3.

An advantage to this approach is that it simultaneously provides evidence that a mutant protein has lost a biochemical function, has retained another biochemical function, AND expresses stable protein. In a loss-of-function assay, further tests would have to be done to determine whether the protein is being stably expressed and if it is still proficient for other biochemical activities. Furthermore, monitoring protein expression levels on a western blot is not an accurate means of assessing stability, while other *in vitro* assays for protein stability are time consuming and/or may not be feasible.

One of the limitations of this approach is that the type of the amino acid mutation can make a substantial difference. For example, Est3-N117K had a severe dominant negative phenotype, while Est3-N117A was not dominant negative even though protein levels appeared stable. Est3-K68E had a reduction in protein levels, while Est3-K68Y was stable and dominant negative. Therefore, it is likely that some key surface residues will be overlooked if the wrong mutation is chosen. Furthermore, in some situations, a single mutation might not be sufficient to impact the biochemical activity, so a combinatorial approach might need to be taken. Given that Est3 is a small protein, it might be more amenable to phenotypic consequences from individual missense mutations.

To overcome the inherent biases in reverse genetics approaches, an intriguing study would be to automate this procedure in order to generate every possible missense mutation in *EST3* and assay it for a dominant negative phenotype. Mutating the 180 amino acids of Est3 to each of 19 amino acids would require a total of 3420

mutations to be generated and tested. All steps of the procedure (site-directed mutagenesis, large-scale yeast transformations, serial dilutions of liquid cultures) could potentially be automated as a quick means of surveying the entire protein to complete saturation. Such a large-scale approach would be valuable for determining if any residues were overlooked by the reverse genetics approach, and if certain types of residue changes are most successful in causing separation-of-function.

Another outstanding question is whether this dominant negative assay is effective in isolating mutations that affect every biochemical activity on that protein. As noted in subsequent chapters, there were regions on Est1 and Est2 where no dominant negative alleles could be isolated, despite extensive mutagenesis. Those regions likely correspond to the TLC1-binding domains of Est1 and Est2. This suggests that the current approach might be ineffective in isolating mutants that have lost RNA binding, and in fact, most, if not all, of the dominant negative mutants could be the result of the TLC1 RNA being titrated away, destabilized, or otherwise misregulated.

Finally, it should be pointed out that this method is merely a tool for building a large collection of mutations. The Lee et al. paper provides one example for how the Est3 mutants were separated into classes that lose versus retain association with telomerase. However, it is still unclear exactly how telomerase association is lost (i.e. does Est3 directly interact with Est2 or Est1, or is the interaction more complex?). For the other class of mutants, it is still unknown what biochemical activity is impacted. I attempted some genetic experiments to identify whether Est1 or Est2 could suppress

certain *est3*$^{-}$ mutations, as well as a series of forward mutagenesis, high copy suppression, and two hybrid screens (data not shown). However, no substantial evidence was obtained for any candidate interactors or sites of interaction responsible for those Est3 biochemical activities, so it is still unclear as to exactly how Est3 is functioning in the telomerase complex.

Recently, Debbie Wuttke's lab has obtained a high-resolution structure of Est3. This structure provided direct evidence for one key assumption of the overexpression dominant negative strategy – that it effectively targets surface residues. All 11 of the predicted surface residues identified by the overexpression dominant negative analysis are in fact located on the experimentally determined surface of the Est3 protein. Furthermore, this method was successful in recovering the majority (≈70%) of the functionally important residues on the surface of Est3. Therefore, even though the structures of Est1 and Est2 are not yet available, the structure-based validation of the results with Est3 argues that applying this protocol to the other telomerase proteins will similarly target surface residues.

Materials and methods

Strains and plasmids

The *EST3* wild type strain used in the dominant negative telomere length assay was YVL2967 (*MAT***a** *ura3-52 lys2-801 trp1-*Δ*1 his3-*Δ*200 leu2-*Δ*1*).

The strain used for the *yku80-*Δ synthetic lethality assay was YVL3142 (*MAT***a** *yku80-Δ::KAN ura3-52 lys2-801 trp1-Δ1 his3-Δ200 leu2-Δ1*/p *CEN URA YKU80*).

The deletion of *YKU80* was generated by one-step gene deletion (Longtine et al., 1998) followed by transformation of a covering plasmid (*p CEN URA YKU80)*.

A complete list of plasmids used in this study can be found in Tables 2.1 and 2.2. The frameshift that is present in the genomic version of *EST3* has been corrected in these constructs (Morris and Lundblad, 1997). Missense mutations in *EST3* were derived from pVL1024 (*2μ LEU2 ADH-EST3*) and select mutations were subcloned into vector YCplac111 to generate *CEN LEU2 ADH-EST3* and mutant allele derivatives.

Table 2.1 2μ plasmids used in this chapter.

Plasmid Name	Type	Marker	Promoter	Gene
pVL399	2μ	*LEU2*	*ADH*	empty vector
YEplac112	2μ	*TRP1*	*ADH*	empty vector
pRL63	2μ	*URA3*	*ADH*	empty vector
pVL249	2μ	*TRP1*	*ADH*	*EST1*
pVL369	2μ	*URA3*	*ADH*	*EST2*
pVL4120	2μ	*TRP1*	*ADH*	*EST2*
pVL715	2μ	*URA3*	*ADH*	*EST2*
pVL735	2μ	*URA3*	*ADH*	*est2-D530A*
pVL743	2μ	*URA3*	*ADH*	*est2-D670A*
pVL1024	2μ	*LEU2*	*ADH*	*EST3*
pVL3544	2μ	*LEU2*	*ADH*	*est3-W21A*
pVL3713	2μ	*LEU2*	*ADH*	*est3-K68E*
pVL3712	2μ	*LEU2*	*ADH*	*est3-K68Y*
pVL3708	2μ	*LEU2*	*ADH*	*est3-K68S*
pVL3706	2μ	*LEU2*	*ADH*	*est3-K71A*
pVL3707	2μ	*LEU2*	*ADH*	*est3-K71E*
pVL3766	2μ	*LEU2*	*ADH*	*est3-D86A*
pVL1184	2μ	*LEU2*	*ADH*	*est3-E104A R105A T106A*
pVL3499	2μ	*LEU2*	*ADH*	*est3-E104A*
pVL3495	2μ	*LEU2*	*ADH*	*est3-E104R*
pVL3492	2μ	*LEU2*	*ADH*	*est3-R110A*
pVL3494	2μ	*LEU2*	*ADH*	*est3-R110E*
pVL1186	2μ	*LEU2*	*ADH*	*est3-T112A S113A E114A*
pVL3496	2μ	*LEU2*	*ADH*	*est3-E114A*
pVL3545	2μ	*LEU2*	*ADH*	*est3-E114K*
pVL3493	2μ	*LEU2*	*ADH*	*est3-T115A*
pVL1187	2μ	*LEU2*	*ADH*	*est3-T115A T116A N117A*
pVL3768	2μ	*LEU2*	*ADH*	*est3-N117A*
pVL3714	2μ	*LEU2*	*ADH*	*est3-N117K*
pVL3497	2μ	*LEU2*	*ADH*	*est3-D164A*
pVL3500	2μ	*LEU2*	*ADH*	*est3-D164R*
pVL1188	2μ	*LEU2*	*ADH*	*est3-D164A D166A Q167A*
pVL3715	2μ	*LEU2*	*ADH*	*est3-D166A*
pVL3646	2μ	*LEU2*	*ADH*	*est3-D166R*
pVL3805	2μ	*LEU2*	*ADH*	*est3-V168A*
pVL3710	2μ	*LEU2*	*ADH*	*est3-V168D*
pVL3709	2μ	*LEU2*	ADH	*est3-V168Y*

Table 2.2 *CEN* plasmids used in this chapter.

Plasmid Name	Type	Marker	Promoter	Gene
YCplac111	*CEN*	*LEU2*	ADH	empty vector
pVL4254	*CEN*	*LEU2*	ADH	*EST3*
pVL4257	*CEN*	*LEU2*	ADH	*est3-K68S*
pVL4256	*CEN*	*LEU2*	ADH	*est3-K71E*
pVL4253	*CEN*	*LEU2*	ADH	*est3-E104R*
pVL4255	*CEN*	*LEU2*	ADH	*est3-R110E*
pVL4251	*CEN*	*LEU2*	ADH	*est3-N117K*
pVL4259	*CEN*	*LEU2*	ADH	*est3-D164A*
pVL4250	*CEN*	*LEU2*	ADH	*est3-V168D*

Telomere length assay

Standard genetic methods were used to transform *est3*$^{-}$ mutations (derived from two parental *EST3* vectors: from pVL1024, a 2μ plasmid expressing the Est3 protein under the control of the ADH promoter, and from pVL4254, a *CEN* plasmid expressing the Est3 protein under control of the ADH promoter) into YVL2967. Transformants were propagated for ~70 generations by streaking for single colonies. DNA was isolated from samples using the Wizard Genomic DNA Purification Kit (Promega), with the following modifications: yeast samples were spheroplasted by incubation in 500μL Sorbitol Solution (1M sorbitol, 20mM potassium phosphate pH7.4, 100mM EDTA) with freshly added DTT (50μL of 1M solution) and zymolyase (50μL of 20mg/mL solution) for 1h. Spheroplasts were pelleted by centrifugation at 7000rpm for 3min, and then resuspended in the Wizard Kit's nuclei lysis solution. Telomere length was analysed by southern blot, as previously described (Lendvay et al., 1996).

Synthetic lethal growth assay

Growth phenotypes were analyzed following transformation of *est3*$^{-}$ mutations (derived from pVL1024, a 2μ plasmid expressing the Est3 protein under the control of the ADH promoter) into YVL3142 (*yku80-Δ::KAN* /p *CEN URA YKU80*) at 30°. Transformants were inoculated into a 2-ml culture that maintained selection for the *EST3* plasmid, grown overnight at 30°, then 5-fold serial dilutions were added to prewarmed plates containing -Leu -Ura and -Leu 5-fluoroorotic acid (5-FOA) to

maintain or evict the *YKU80* covering plasmid, respectively. Plates were incubated for 3-4 days at 30° and 32°.

Genetic suppression

Standard genetic methods were used to transform *est3*$^{-}$ mutations (derived from pVL1024, a 2μ plasmid expressing the Est3 protein under the control of the ADH promoter, and mutations derived from pVL4254, a *CEN* plasmid expressing the Est3 protein under control of the ADH promoter) into YVL2967. Transformants were propagated for ~25 generations by streaking for single colonies, then transformed with *2μ ADH-EST1*, *2μ ADH-EST2*, or *2μ ADH* vector control. After propagation of the double transformants for another ~50 generations, telomere length was analysed by southern blot as described in the telomere length assay.

Acknowledgements

A portion of Chapter 2 is a modified reprint of the material as it appears in Lee, J., Mandell, E.K., Tucey, T.M., Morris, D.K., and Lundblad, V. (2008). The Est3 protein associates with yeast telomerase through an OB-fold domain. Nat Struct Mol Biol *15*, 990-997. The dissertation author was a co-author for this publication. Reprinted with premission from Nature Publishing Group, copyright, 2008.

Chapter 3: Development of a yeast telomerase co-immunoprecipitation assay

Introduction

The budding yeast telomerase complex is limiting and only elongates a subset of telomeres during each cell cycle. Telomere replication, telomerase activity, and synthesis of the complementary C-rich strand all occur during late S phase in a series of tightly coupled steps. The shortest telomeres are preferentially elongated, while telomerase activity is repressed at over-elongated telomeres (Chang et al., 2007; Teixeira et al., 2004). Prior to this study, it was also unclear whether the subunits Est1 or Est3 exhibited regulated association with the telomerase complex.

The mechanistic details of these regulatory steps are lacking because there have been numerous biochemical challenges in yeast. To date, there has not been a successful purification of yeast telomerase (telomerase has only been purified in the ciliates *Tetrahymena* and *Euplotes*), and there are no working antibodies against Est1, Est2, and Est3. Telomerase is in very low expression, so detecting a low abundance complex in cell extracts has been problematic. Early attempts to tag the proteins at their endogenous loci have been challenging because many epitope tags adversely affect the function of telomerase. In many cases, the tagged proteins could only be detected by immunoprecipitation, but not in cell extracts.

As a consequence, experiments that have monitored association of Est proteins with each other or with the telomere have certain limitations. Chromatin immunoprecipitation experiments have looked at recruitment of Est1 and Est2 at the telomere during the cell cycle, but each protein was tagged in a separate strain, making it difficult to make cross comparisons of the subunits. Multiple labs have examined

complex formation in co-immunoprecipitation experiments, using strains with different tags on each Est protein – for example, $(HA)_3$-Est1 and $(myc)_9$-Est2 – but because each protein is detected on a different western blot, the relative proportions of each protein in the complex cannot be determined. Est3 has been subject to even less scrutiny, and it is still very unclear how it assembles into the complex and whether it is regulated through the cell cycle.

Because of the caveats discussed above, I have developed a set of strains that allow the subunits in the complex to be rigorously compared from the same starting extract, on the same western blot. In general, my experimental strategy involves constructing the following strain, with all three epitope-tagged versions integrated in the genome and expressed under their respective native promoters:

Est1-TagA Est2-TagA-TagB Est3-TagA

My approach is to immunoprecipitate Est2 via TagB, and then monitor all three Est proteins on the same western blot through detection of TagA. Yeast cells can be arrested in the cell cycle (in G1 by α-factor, and in G2/M by nocodazole), allowing the complex to be monitored at different stages of the cell cycle in order to see how the stoichiometry changes. Furthermore, I have utilized epitope tags that allow me to sufficiently detect each Est protein in extracts, without immunoprecipitation of Est2, in order to analyze protein expression levels. The RNA levels of TLC1 can be monitored by northern blot and there is also a tagging system available that could allow TLC1 to also be detected on western blot by using the MS2 coat protein (Gallardo et al., 2011).

The method I used for the strain constructions is a two step allele replacement method called pop-in / pop-out, which allows integration of tagged versions of the *EST* genes into the genome, without any additional modifications to the genome (Scherer and Davis, 1979). See Figure 3.1 for a conceptual overview of this method. The tag sequence is positioned in-frame with the gene of interest on a *URA3*-based YIp integrating vector and integrated into its chromosomal location by homologous recombination (to facilitate correct integration, the plasmid is linearized with a restriction digest to greatly increase the probability it will target the same site in the genome). The resulting pop-in contains tandem wild-type and tagged copies of the gene separated by the YIp vector sequences. 5-FOA counterselection is then used to screen for spontaneous excision of the vector sequences via a second homologous recombination event. This pop-out recombination will occur throughout the gene and at different locations, and in a proportion of cells that have looped out *URA3*, the tag will remain at the genomic locus. Diagnostic PCR is used to confirm that both the pop-in and pop-out steps occurred in the correct fashion.

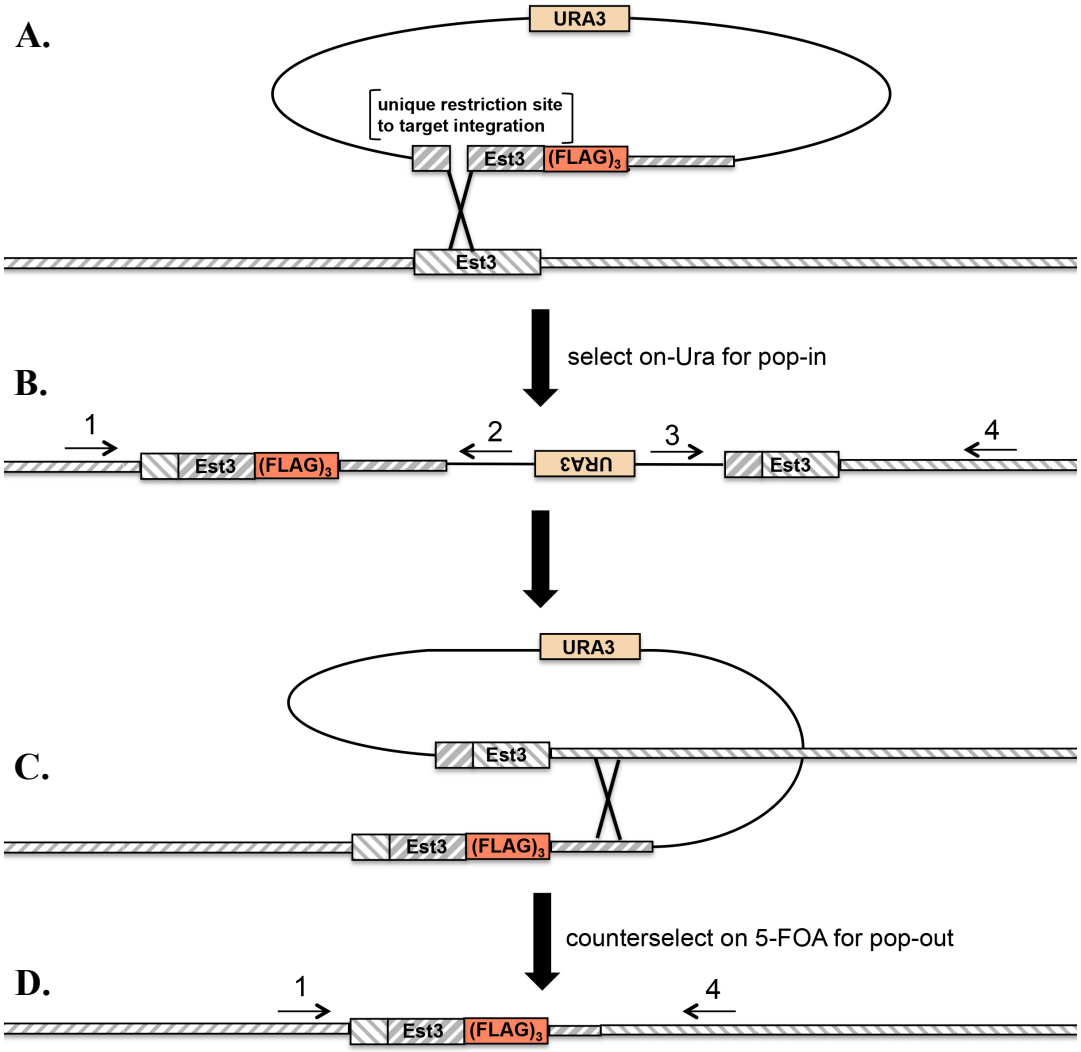

Figure 3.1 Diagram of pop-in / pop-out allele replacement. A) The *EST3-(FLAG)$_3$* gene is subcloned to an integrating vector that contains the *URA3* selectable marker. Note that some downstream genomic sequence must be present in order to generate pop-outs containing the tag. A unique restriction sequence upstream of the tag is used to linearize the plasmid and facilitate targeting of the pop-in to the *EST3* genomic locus. (B) Transformants are plated on –Ura media to select for pop-ins. Correct pop-ins will have tandem copies of *EST3-(FLAG)$_3$* and *EST3* as indicated. Primer sets 1 and 2, and 3 and 4, can be used for diagnosing both junctions of the pop-in. (C) At a rare frequency, recombination will occur at the homologous sequences downstream of *EST3*, resulting in loss of the plasmid sequence. Note that this recombination could also occur upstream of the tag. (D) The recombination events from (C) can be isolated by counterselection on 5-FOA-containing medium. Resulting pop-outs will retain or lose the $(FLAG)_3$ tag and can be diagnosed with primers 1 and 4. The pop-outs that retain the $(FLAG)_3$ tag have the exact same genomic sequence as the starting strain, except for the tag insertion.

The advantage of the pop-in / pop-out method is that it maintains the entire integrity of the yeast genome, except for the desired modification. Thus, the resulting tagged pop-out is isogenic to the original parent strain used for the pop-in, at all regions of the genome except for the inserted tag. This allows for a much more rigorous set of genetic reagents compared to other methods. For example, fluctuations in expression levels can occur when the tagged proteins are expressed from a plasmid, and additionally, the wild-type untagged genomic copy will interfere with the biochemical analysis of complex formation unless it is modified by deletion. There is also a one-step allele replacement method for tagging (Longtine et al., 1998), but this results in modifications to the genome (for example, insertion of a *TRP1* marker downstream of the tag, which can affect gene expression by decreasing mRNA abundance). Using the pop-in / pop-out method, I am able to generate new tagged strains in approximately 10 days, using a rigid set of diagnostics to confirm that the integration is correct, and there is a high likelihood in getting the desired pop-out strains once an integration and diagnostic strategy is developed for a given gene. In addition to tagged insertions, this method can also be used for deletions and single base-pair changes.

Using pop-in / pop-out, several iterations of strain constructions were made, for the following reasons: (1) For each protein, it is important to achieve the most functional tag possible. Placement of the tag (N-terminus vs. C-terminus), type of epitope (FLAG, myc, HA, etc.), number of epitope repeats (for example, $(myc)_9$ vs. $(myc)_{12}$) and inclusion of a flexible glycine linker between the tag and the Est protein,

were some of the variations that were made. This resulted in a combinatorial expansion of strain constructions. (2) I wanted two different Est2 immunoprecipitation options in order to analyse telomerase complex formation in two independently created strains. Therefore, different strain versions contain either a FLAG or HA tag on Est2. This also increases the possibility that at least one of the tags will completely deplete Est2 from extracts, so that I can effectively isolate the entire complex. (3) In case there was a strain glitch along the way, this strategy made it easier to backtrack and correct the issue. It is critical that the strains are generated correctly, since they will be the basis of many experiments for publication. (4) Finally, having a large and carefully organized collection of strains opens up additional experimental avenues that may not have been feasible or immediately accessible. For example, if an intermediate strain is created that contains myc and HA tags on Est3, it might become a useful reagent if a situation were to arise where Est3 needs to be detected or immunoprecipitated using HA or myc.

Results

A biochemical analysis of telomerase using two different tagged strains

An initial strain was constructed to test the effectiveness of this approach:

Est1-$(myc)_{13}$::TRP1 $(myc)_{12}$-$(HA)_3$-Est2 Est3-$(G)_8$-$(myc)_9$-$(FLAG)_3$

This initial strain was made using pre-existing components that were available in the lab, and therefore contains a heterogeneous set of epitope tags on each Est protein. Figure 3.2 summarizes the relevant biochemical properties of this strain. Protein

levels were analysed by western blot (Figure 3.2b, left panel) in asynchronous, α-factor arrested, and nocodazole arrested cells. Both Est1 and Est2 could be detected in extracts, indicating that the tagged proteins are being stably expressed. Interestingly, Est1 shows an apparent greater abundance than Est2 in α-factor arrested cells. This conflicts with published data suggesting that Est1 has lower expression than Est2 during G1 (Taggart et al., 2002). However, this strain allows for a direct comparison of Est1 and Est2, from the same extract and on the same western blot. Est3 is the most abundantly expressed of the three proteins.

The telomerase complex was analysed by immunoprecipitation of Est2, the most limiting of the three proteins, from extracts using HA beads (Figure 3.2b, right panel). Unexpectedly, Est1 is part of the telomerase complex in G1, and it appears to be in ≈1:1 stoichiometry. This conflicts with previous immunoprecipitation data suggesting that Est1 is not in the complex during G1 (Osterhage et al., 2006). Also, Est3 is detected in the complex at a higher stoichiometry in G2/M compared to G1, raising the possibility that Est3's association with the complex is regulated.

To determine whether any of the tags had an impact on telomerase function, telomere length of this strain, as well as the precursor strains, were analysed on southern blots (Figure 3.2e; also see Figures 3.5 and 3.6). The epitope tags on Est1 and Est2 each resulted in a slight reduction in telomere length, which was further reduced when Est3 was also tagged. Therefore, each of the tagged subunits appears to have a modest perturbation of telomerase function, and this has an additive effect when multiple subunits are tagged.

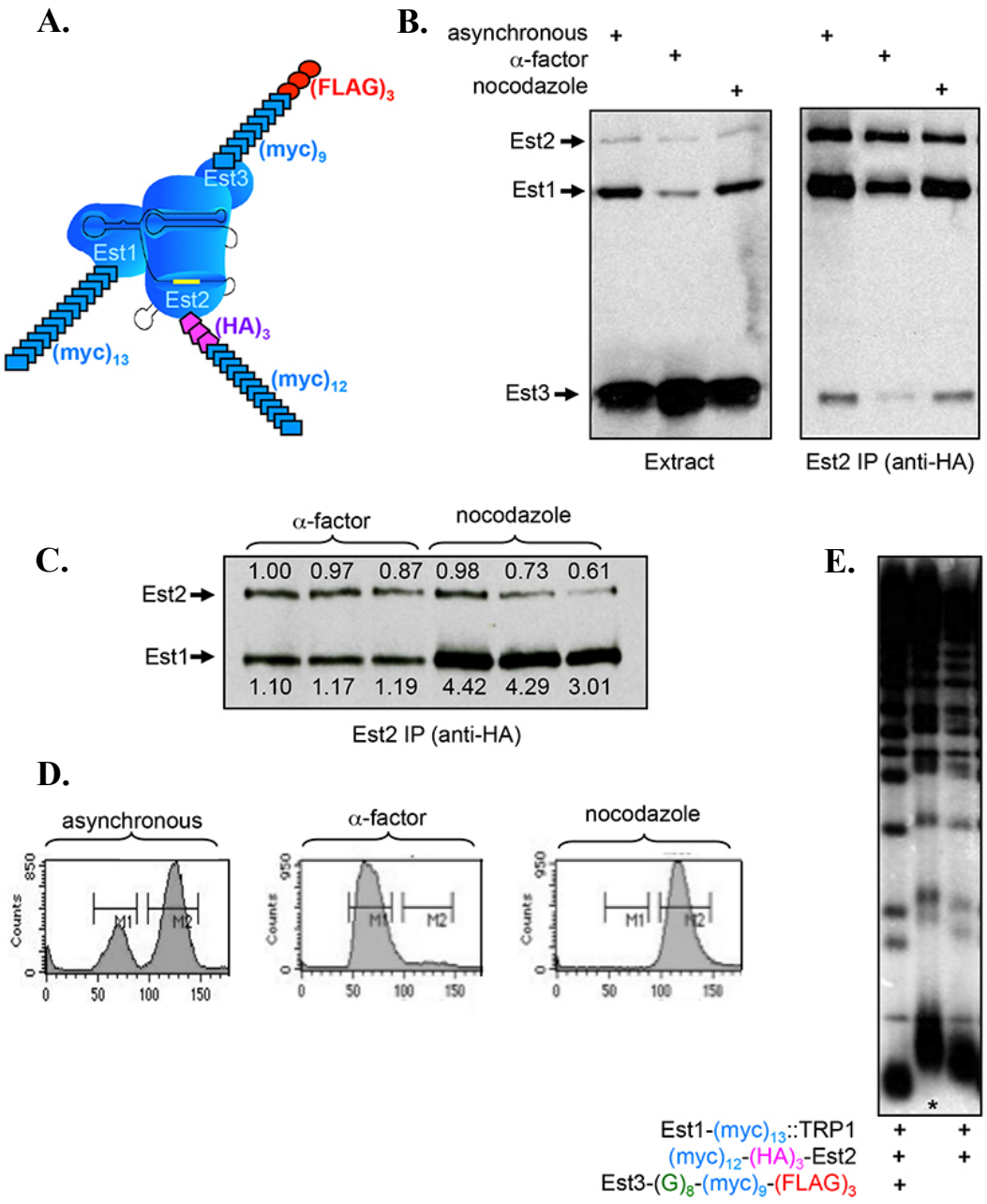

Figure 3.2 Biochemical properties of the initial tagged strain. A) Diagram illustrating the tag placement for this strain. B) Anti-myc western blots of inputs (left side) and anti-HA IPs (right side) from asynchronous, α-factor, and nocodazole arrested cells. C) Anti-myc western of anti-HA IPs from α-factor and nocodazole arrested cells, with quantification of the bands normalized to the Est2 signal in the first lane. D) FACS analysis of the cultures used in panel B. E) Telomere length of strains integrated with the indicated tags compared to the wild-type parental strain (labelled with an *).

This strain provided an initial view of the telomerase complex, with some surprising implications, but it was not an ideal strain for the following reasons: (1) Est1 was tagged using a one-step replacement method, which modifies the genome with a TRP1 marker, thereby potentially influencing gene expression. (2) Est2 was unable to be completely depleted from extracts when using HA beads (data not shown). (3) The $(myc)_{12}$-$(HA)_3$ tag on Est2 was not positioned at the very N-terminus, but rather, after the first 12 amino acids of Est2 and in a manner that altered the primary amino acid sequence. (4) The number of myc tags on each protein is different, and the sequence of several of the myc epitopes also differs slightly, making it more challenging to directly compare protein levels on a single western blot and also raising questions about whether the observed stoichiometries in the immunoprecipitations were correct. (5) Each tagged protein had an effect on telomere length, even in strains where the other proteins were left untagged.

To address these limitations, another strain version was constructed to allow for a more rigorous analysis of the telomerase complex:

$Est1\text{-}(G)_6\text{-}(myc)_{12}$ $(FLAG)_3\text{-}(myc)_{12}\text{-}(G)_6\text{-}Est2$ $Est3\text{-}(G)_6\text{-}(myc)_{12}$

One key difference in this strain, compared to the prior strain, is that I ensured that all three epitope tags contained the exact same amino acid sequence for the $(myc)_{12}$ tag, and I avoided using PCR to integrate the constructs, to further ensure that no differences between the three epitope tags were introduced. Figure 3.3 summarizes the relevant biochemical properties of this strain. Similar to the original strain, expression of Est3 is in excess throughout the cell cycle, and its association with the

complex appears to be regulated. Notably, Est1 is detected in the complex in G1 and G2/M, but to a lesser extent compared to the original strain (compare the quantifications in Figures 3.2c and 3.3c). Thus, each strain exhibits similar trends with regard to cell cycle changes in expression and complex formation, but the apparent stoichiometry of the complexes is different. With regard to telomerase function, the tagged versions of Est1 and Est2 are fully functional in this more rigorously constructed strain; however, Est3-$(G)_6$-$(myc)_{12}$ by itself has a stable but significant reduction in telomere length (Figure 3.3e; see also Figures 3.5 – 3.7).

Both strain versions were subjected to a more rigorous cell cycle analysis by performing α-factor arrest and release experiments. Following release from α-factor, cultures were collected at 15 minute timepoints and the extracts were immunoprecipitated for Est2 using anti-HA beads and anti-FLAG beads for the appropriate strain. Figure 3.4 displays a side-by-side comparison of the telomerase complex in the two strain versions. The overall trend is similar: Est1 association with the complex increases after G1, while Est3 association is only detected at the later stages of the cell cycle. However, at every timepoint, there is a greater Est1 stoichiometry when using the strain where Est1 and Est2 are tagged with a different number of myc tags and contain sequence differences between the $(myc)_{13}$ and $(myc)_{12}$ epitopes. Independent repeats of this α-factor arrest and release experiment were performed and are shown in Chapter 5.

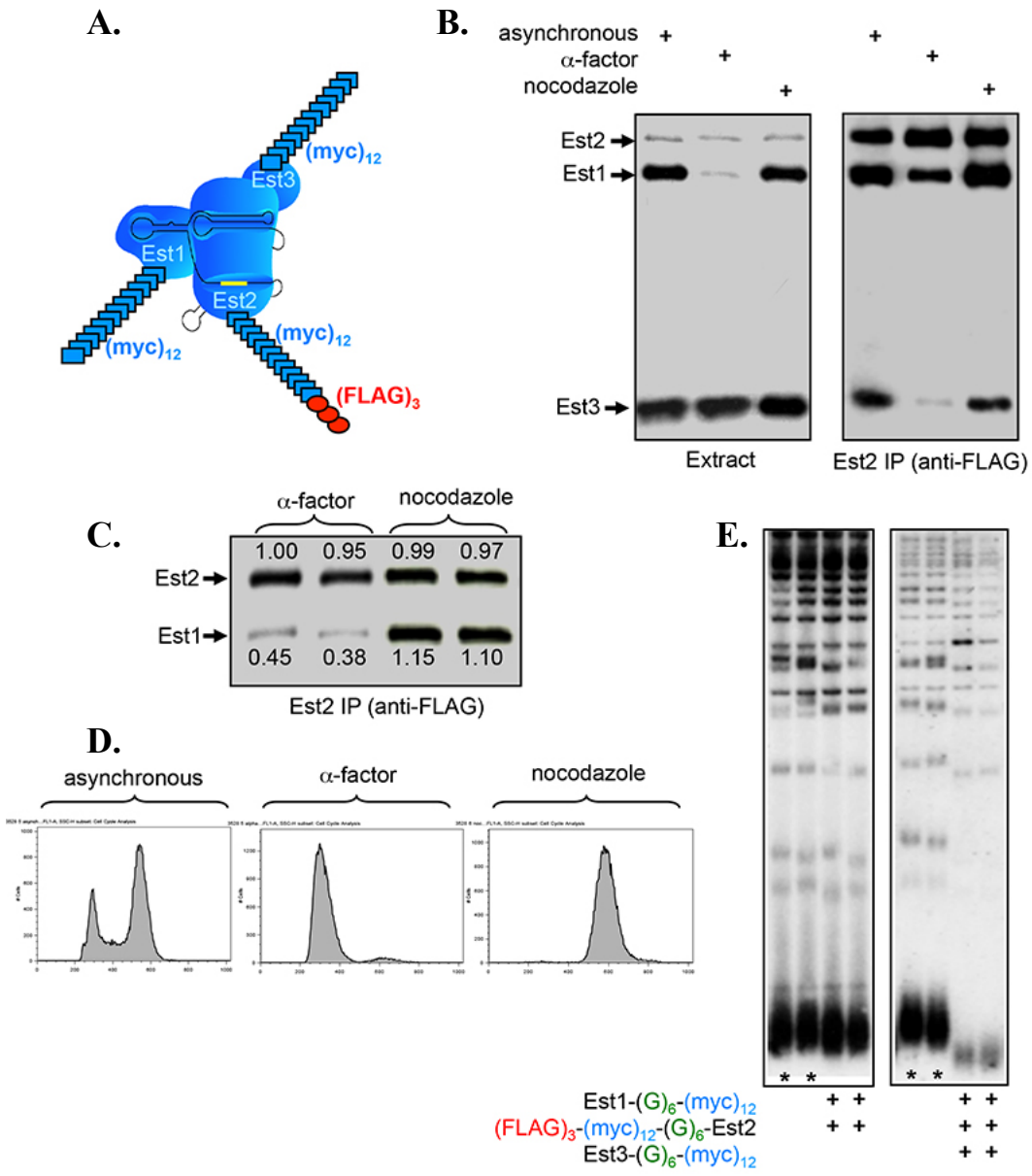

Figure 3.3 Biochemical properties of a second, independently constructed tagged strain. A) Diagram illustrating the tag placement for this strain. B) Anti-myc western blots of inputs (left side) and anti-FLAG IPs (right side) from asynchronous, α-factor, and nocodazole arrested cells. C) Anti-myc western of anti-FLAG IPs from α-factor and nocodazole arrested cells, with quantification of the bands normalized to the Est2 signal in the first lane. D) FACS analysis of the cultures used in panel B. E) Telomere length of strains integrated with the indicated tags compared to the wild-type parental strain (labelled with an *).

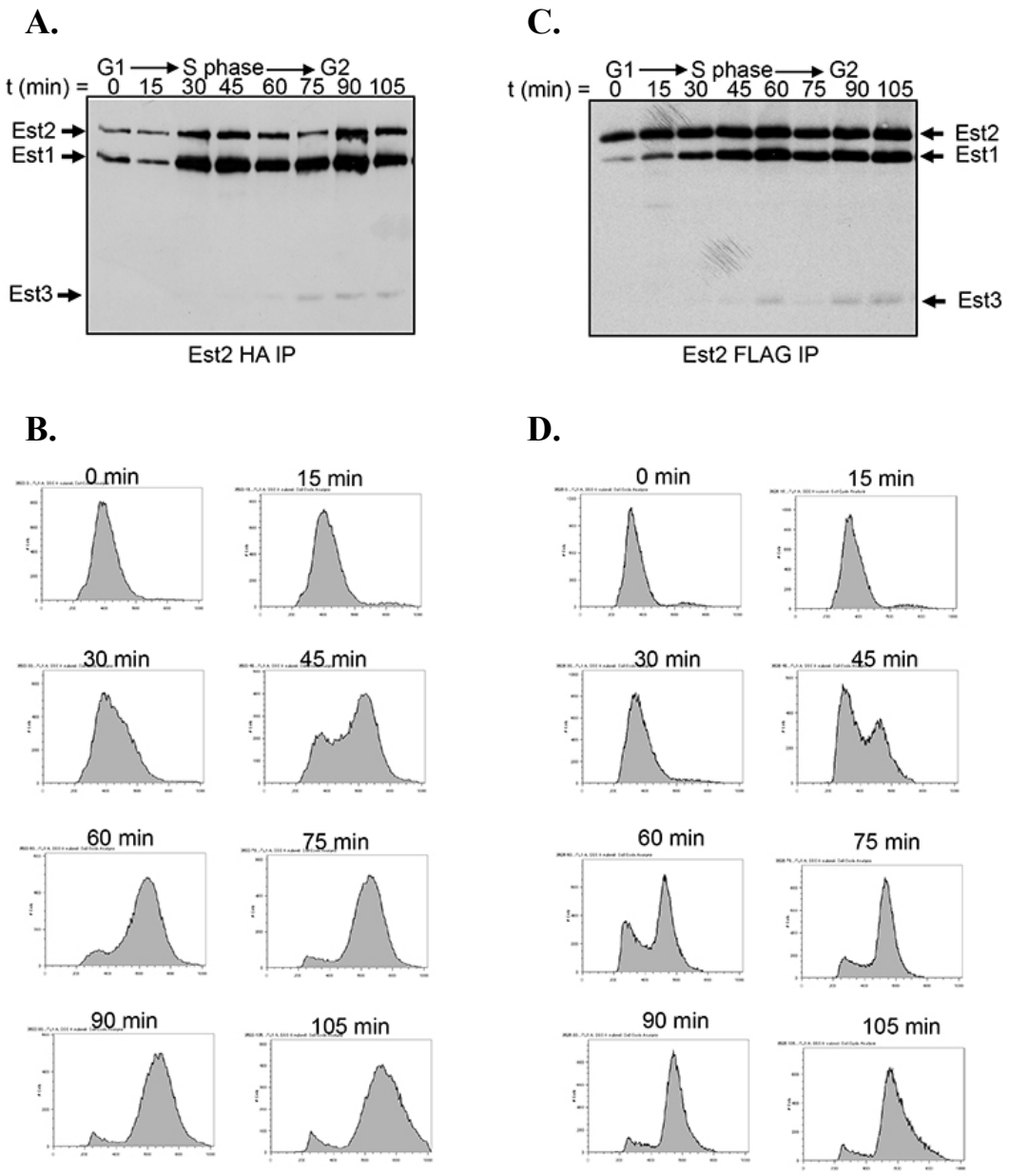

Figure 3.4 Comparison of the two strain versions through the cell cycle. A) An anti-myc western blot of anti-HA immunoprecipitates at the indicated timepoints following a G1 phase arrest of the strain Est1-$(myc)_{13}$::TRP1 ; $(myc)_{12}$-$(HA)_3$-Est2 ; Est3-$(G)_8$-$(myc)_9$-$(FLAG)_3$. B) FACS analysis of the cultures used for panel A. C) An anti-myc western blot of anti-FLAG immunoprecipitates at the indicated timepoints following a G1 phase arrest of the strain Est1-$(G)_6$-$(myc)_{12}$; $(FLAG)_3$-$(myc)_{12}$-$(G)_6$-Est2 ; Est3-$(G)_6$-$(myc)_{12}$. D) FACS analysis of the cultures used for panel C.

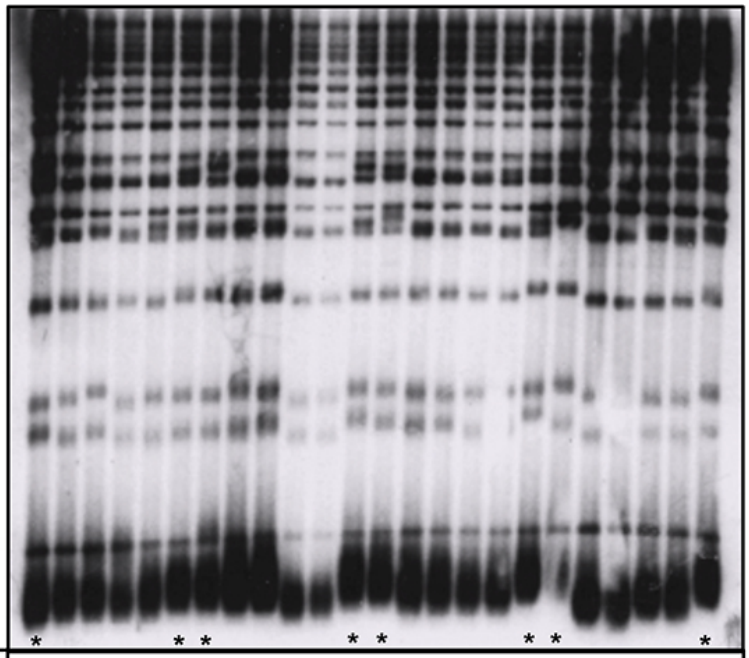

Est1-(myc)$_{13}$::TRP1	+ +
Est1-(G)$_6$-(myc)$_{12}$	+ +
(myc)$_{12}$-Est2	+ +
(myc)$_{12}$-(G)$_6$-Est2	+ +
(myc)$_{12}$-(HA)$_3$-(G)$_6$-Est2	+ +
(FLAG)$_3$-(myc)$_{12}$-(G)$_6$-Est2	+ +
Est3-(FLAG)$_3$	+ +
Est3-(G)$_6$-(myc)$_{12}$	+ +

Figure 3.5 Telomere length of tagged pop-out strains (blot 1 of 4). Telomere length was assessed from two single colonies of the indicated tagged pop-out strains compared to the wild-type parental strain (labelled with an *) following propagation for ≈75 generations.

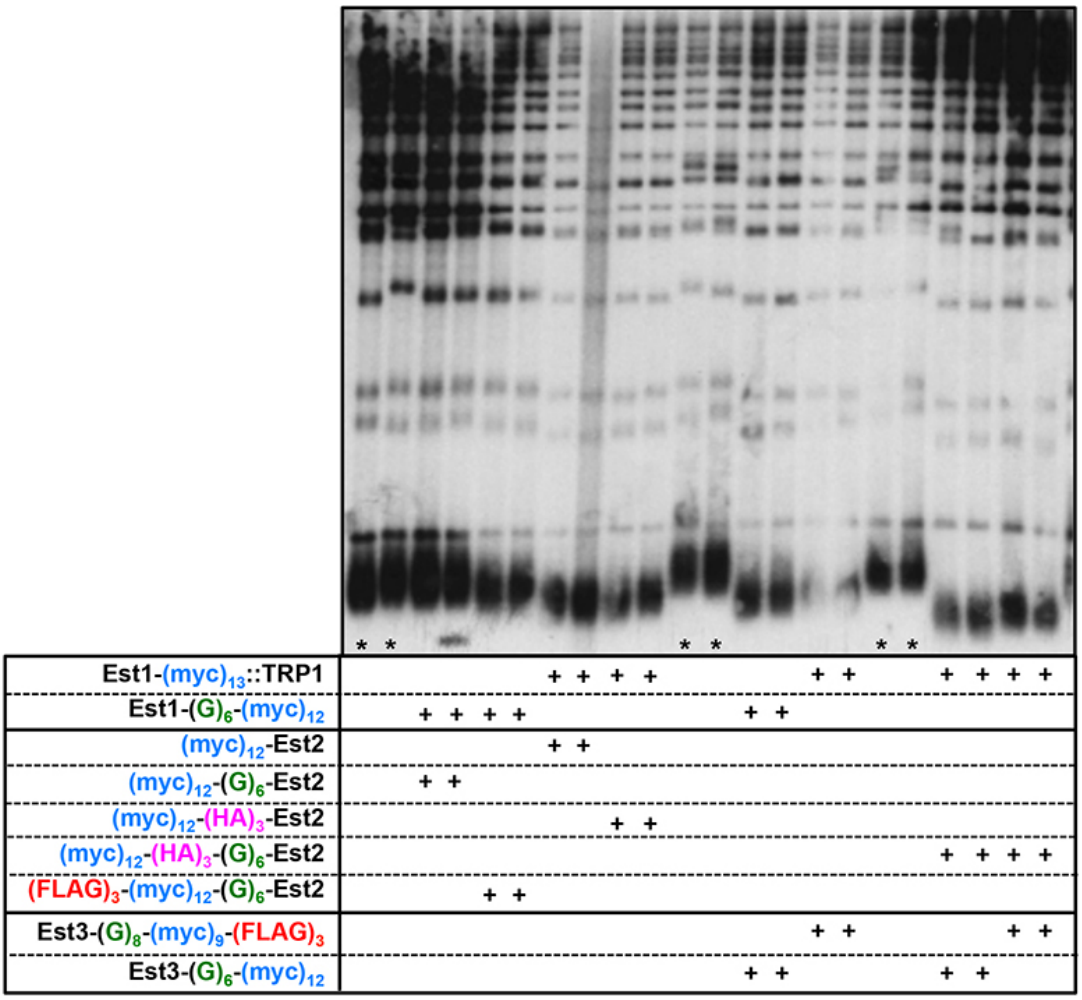

Figure 3.6 Telomere length of tagged pop-out strains (blot 2 of 4). Telomere length was assessed from two single colonies of the indicated tagged pop-out strains compared to the wild-type parental strain (labelled with an *) following propagation for ≈75 generations.

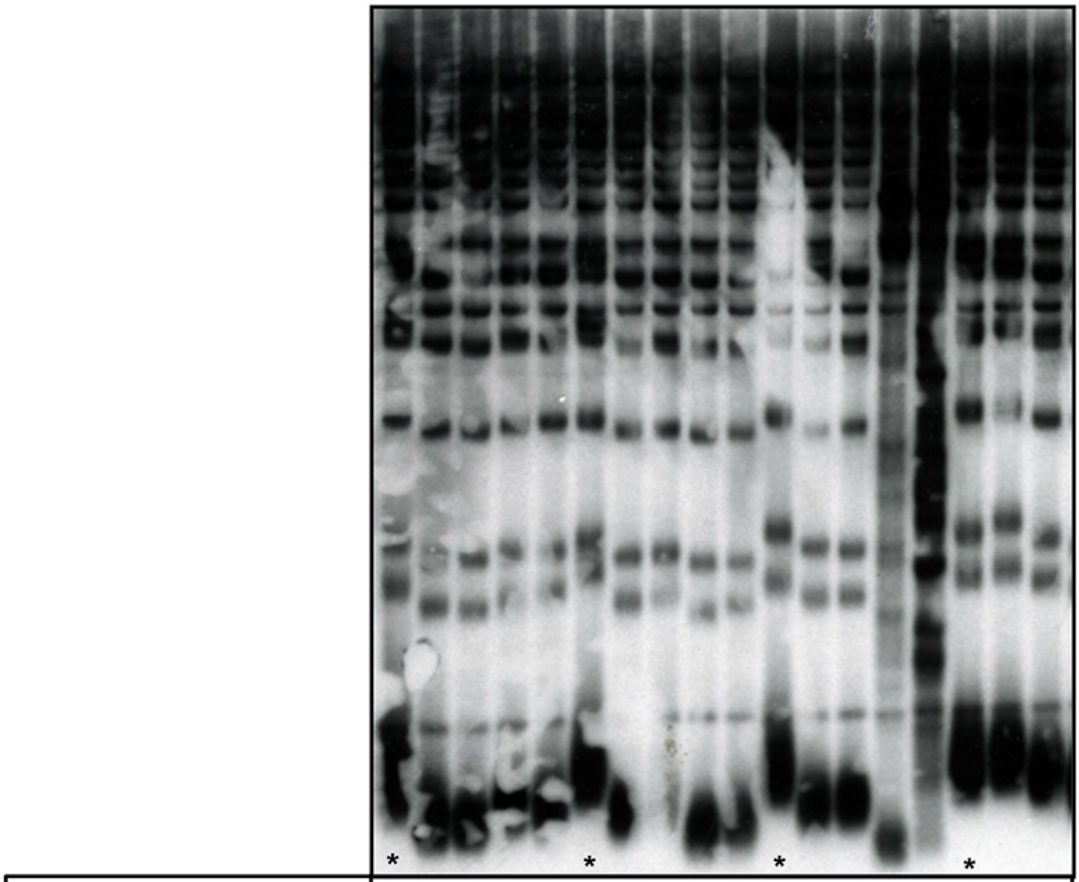

Figure 3.7 Telomere length of tagged pop-out strains (blot 3 of 4). Telomere length was assessed from two single colonies of the indicated tagged pop-out strains compared to the wild-type parental strain (labelled with an *) following propagation for ≈75 generations.

FLAG immunoprecipitation of telomerase quantitatively depletes the catalytic core

Because the strain containing Est1-$(G)_6$-$(myc)_{12}$ and $(FLAG)_3$-$(myc)_{12}$-$(G)_6$-Est2 had wild-type telomere length, several controls were performed with this strain to determine if it should serve as the basis for developing a biochemical assay of the telomerase complex.

First, it was established that an anti-FLAG immunoprecipitation quantitatively depletes Est2 from the extracts. In Figure 3.8, no Est2 can be detected in the supernate recovered from the anti-FLAG immunoprecipitation when it is examined on either an anti-FLAG or anti-myc western blot. Furthermore, when detecting the supernate on an anti-myc western blot, the unbound Est1 can be detected. Given that Est1 is expressed at a higher level than Est2, but associates with the Est2 complex at ≈1:1 stoichiometry, this represents the excess Est1 that did not associate with the Est2 complex.

Secondly, it was determined that the anti-FLAG immunoprecipitation is isolating a complex that consists of the catalytic care – that is, the complex contains Est2, Est1, and the TLC1 RNA. TLC1 RNA levels were determined by northern blot, and the RNA dependence was also confirmed genetically. When *tlc1-47*, a mutation that has previously been shown to decrease Est1 binding to the RNA, was integrated into the Est1-$(G)_6$-$(myc)_{12}$; $(FLAG)_3$-$(myc)_{12}$-$(G)_6$-Est2 strain, Est1 association with the anti-FLAG immunoprecipitates was significantly reduced (Figure 3.9a). This was completely in agreement with previous data suggesting that Est1 associates with the telomerase complex via a direct interaction with the TLC1 RNA (Seto et al., 2002). A

more detailed investigation of the Est1-TLC1 interaction is discussed in Chapter 4. Figure 3.9 also contains an untagged Est2 control, where Est1 and Est2 are only tagged with $(myc)_{12}$, to confirm that neither myc-tagged protein is able to non-specifically bind to the FLAG beads.

Finally, a dilution series of the anti-FLAG immunoprecipitation was quantified to determine the detection range (Figure 3.10). A 20-fold dilution of the Est2 complex was able to be detected, and 2-fold differences in protein levels were able to be quantitatively detected over a ~10- fold range of protein levels. Based on the analyses in Figures 3.8 – 3.10, as well as the meticulous construction and diagnosis to ensure that the epitope tags were completely identical, it was decided that the Est1-$(G)_6$-$(myc)_{12}$; $(FLAG)_3$-$(myc)_{12}$-$(G)_6$-Est2 strain would serve as the basis for most experiments involving the regulatory aspects of those two proteins, as discussed in Chapters 4 – 6.

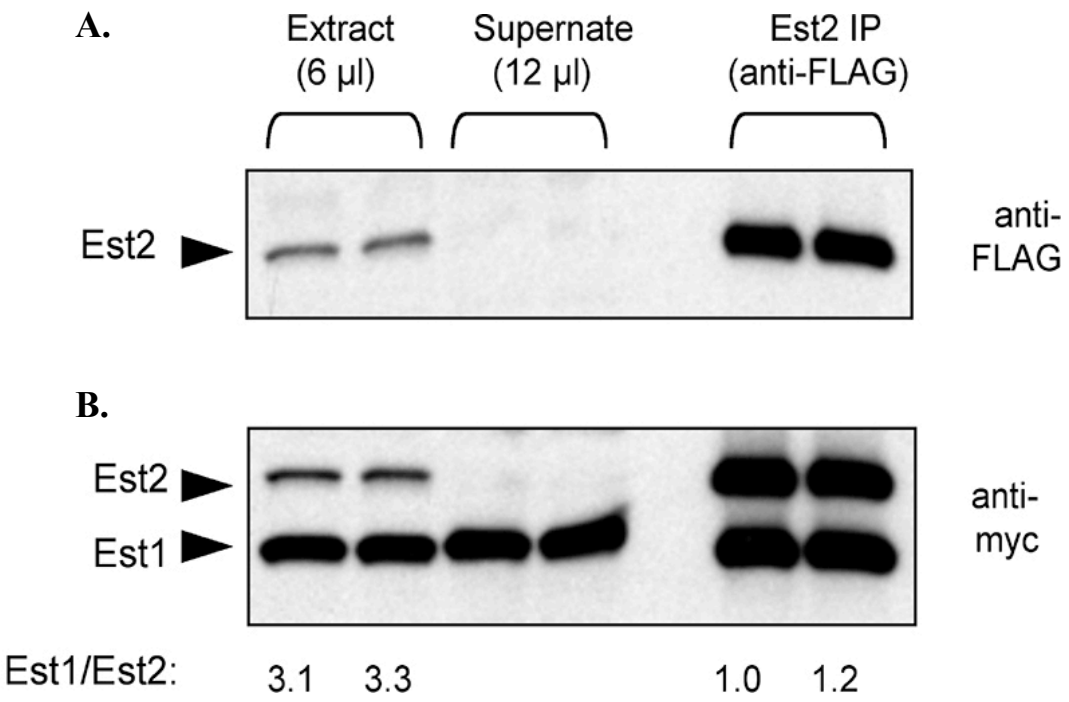

Figure 3.8 Est2 (the limiting protein subunit in the telomerase complex) is depleted from extracts by anti-FLAG immunoprecipitation. A) Anti-FLAG western monitoring the $(FLAG)_3$-$(myc)_{12}$-Est2 protein in extracts, Est2 immunoprecipitates (IP) and the supernate recovered from the IP. Note that 2-fold more supernate than extract was loaded, to ensure that reduced levels of Est2 could be detected. B) The same samples as in part (A) were assessed by anti-myc western to detect the Est1 and Est2 proteins, which bear identical $(myc)_{12}$ epitopes; the relative ratios of the two proteins in extracts (which were prepared from asynchronous cells) and IPs are included. This figure is a direct reproduction from (Tucey and Lundblad, 2013), Figure S1.

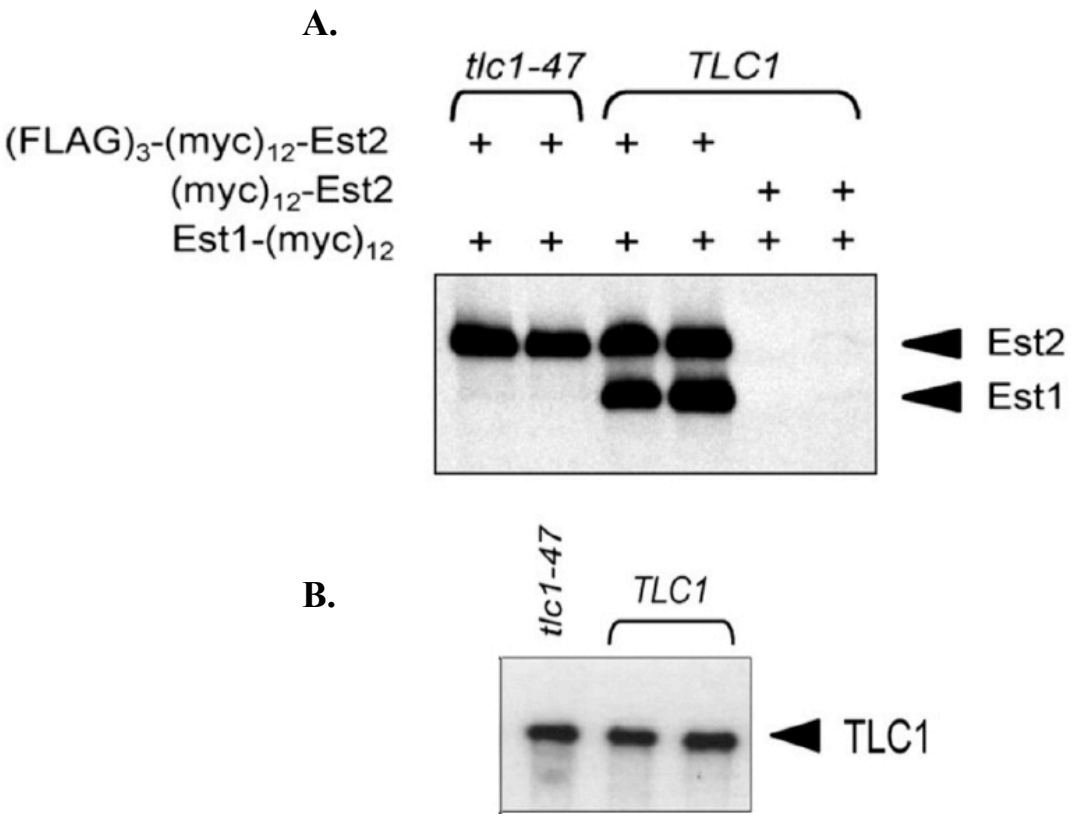

Figure 3.9 Anti-FLAG immunoprecipitation of Est2 is isolating the catalytic core of telomerase. A) Anti-myc western blot of anti-FLAG immunoprecipitates of the indicated tagged strains; for the strain in lanes 1-2, the *tlc1-47* mutation was integrated into the genome and derived from the strain in lanes 3-4. B) Northern analysis monitoring levels of the TLC1 RNA in anti-FLAG immunoprecipitates, for the same strains indicated in panel A, as performed by John Lubin. This figure was adapted from (Lubin et al., 2012), Figures 3c and 3e.

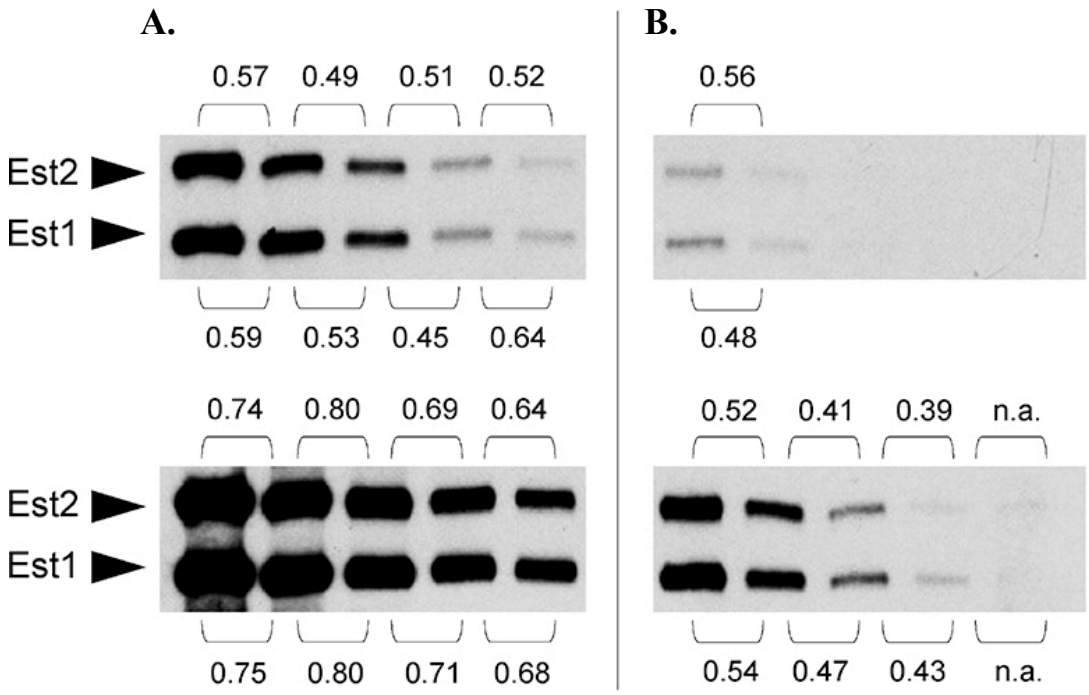

Figure 3.10 Monitoring Est1 and Est2 protein levels in a dilution series of anti-FLAG immunoprecipitates. Anti-myc western of two-fold dilutions of anti-FLAG IPs of extracts prepared from a Est1-$(myc)_{12}$ $(FLAG)_3$-$(myc)_{12}$-Est2 strain. A 10-fold lower amount is loaded in lane 1, part (B). Quantitation of the two exposures for the gels in (A) and (B) demonstrate that 2-fold differences in protein levels can be quantitatively detected over a ≈10- fold range of protein levels for the top exposure in part (A) and the bottom exposure in part (B). This figure is a direct reproduction from (Tucey and Lundblad, 2013), Figure S7.

Every attempt to place an epitope tag on Est3 has affected its function

Numerous attempts were taken to generate a tagged *EST3* construct that would retain complete telomerase function. Tags were placed at the N-terminus, C-terminus, as well as internally along regions of the protein that are less conserved and potentially more amenable to a tag insertion. Different sizes of glycine spacers were included to provide extra separation between Est3 and the tag. However, every tag that has been attempted has resulted in a noticeable decline in telomere length (see Figures 3.5 – 3.7 and Figure 3.11). Of the constructs tested, Est3-$(FLAG)_3$ by far has the least impact on function. Figure 3.12 summarizes the tag locations and resulting phenotypes for the constructs that were tested. Recently, a couple of tags were placed at the N-terminus of Est3, and their functional consequence has not yet been assessed.

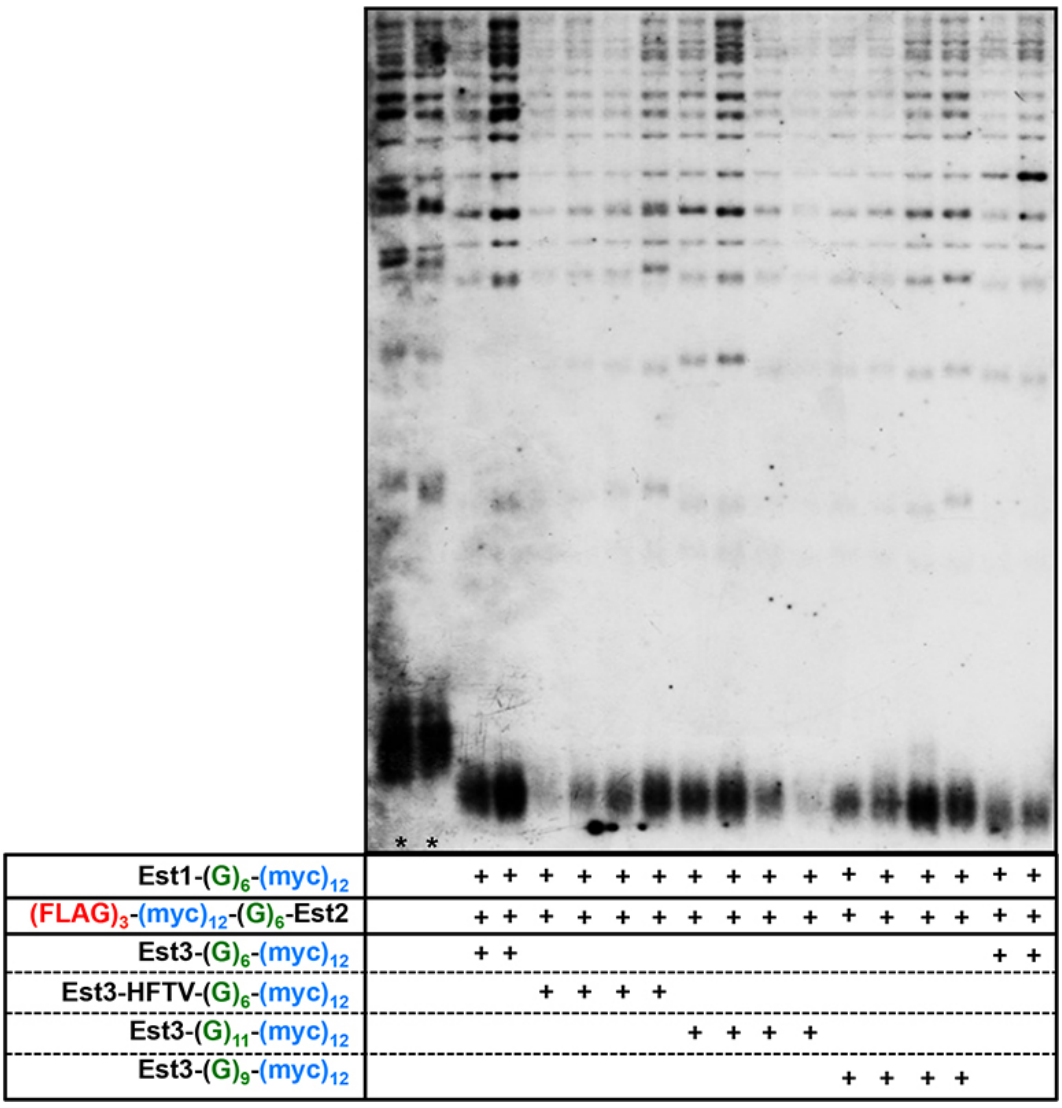

Figure 3.11 Telomere length of tagged pop-out strains (blot 4 of 4). Telomere length was assessed from two single colonies of the indicated tagged pop-out strains compared to the wild-type parental strain (labelled with an *) following propagation for ≈75 generations.

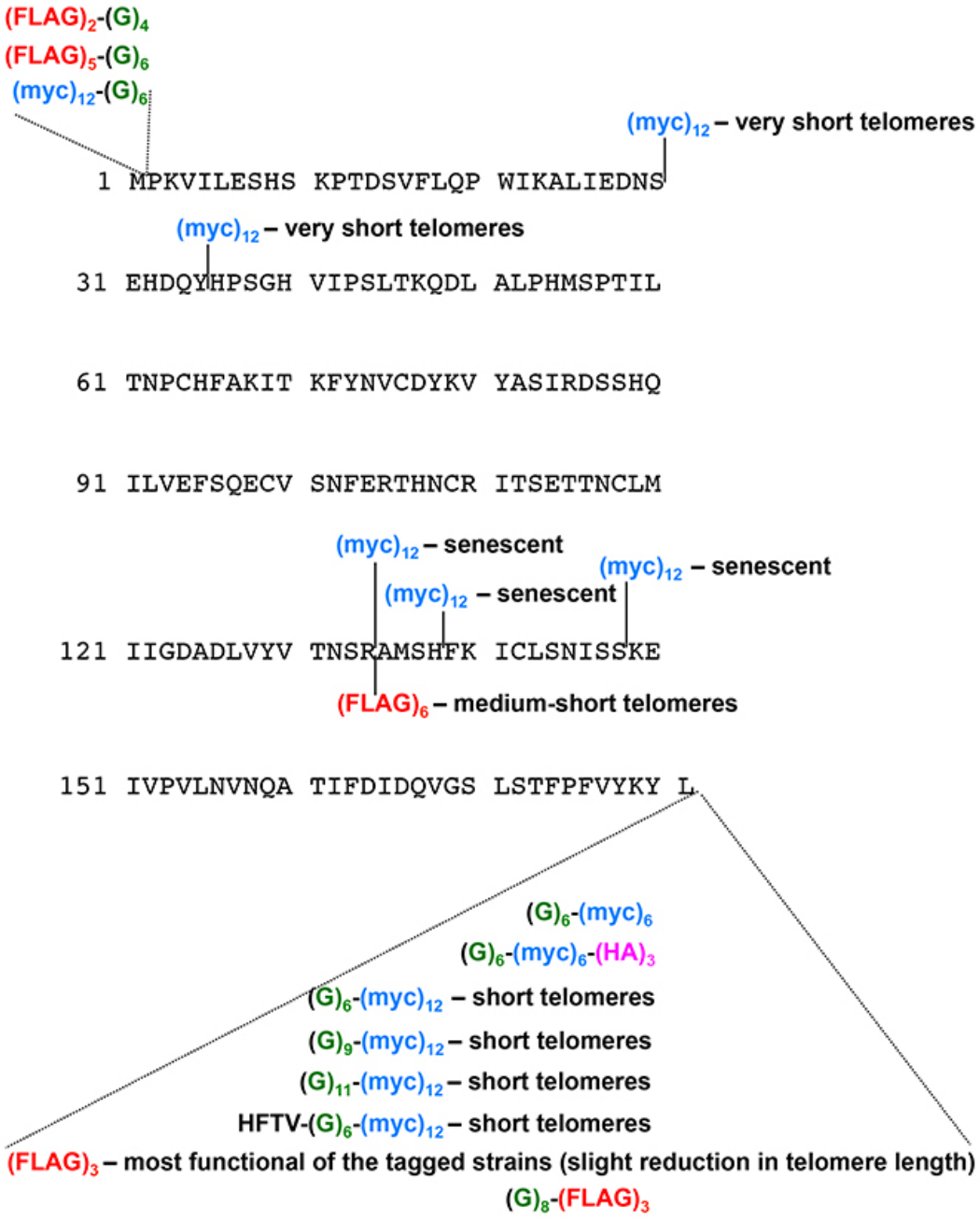

Figure 3.12 Summary of Est3 tagged constructs that were generated. Identity and position of tags are indicated along the primary amino acid sequence of *S. cerevisiae* Est3. The tags at the very N and C-terminus were integrated into the genome, while the internally positioned tags were assessed for functional complementation over an *est3*-Δ strain. For the tags that were not senescent after ~75 generations of propagation, telomere length was analyzed on southern blot as indicated.

Discussion

Understanding the regulation of yeast telomerase has been challenging, in part because the complex is in very low abundance and difficult to detect quantitatively. There are only ≈29 molecules of TLC1 per haploid cell (Mozdy and Cech, 2006), while the abundance of the Est proteins has been reported to be ≈37 molecules of Est2 per cell, 71 molecules of Est1, and 84 molecules of Est3 (Tuzon et al., 2011). In order to overcome this limitation, I have constructed a set of tagged strains that allow simultaneous detection of the relative levels of Est1, Est2, and Est3 from extracts and after immunoprecipitation of the most limiting subunit, Est2. From the set of strains I have created, the relative expression levels of the tagged proteins are in agreement with the reported calculation, with Est2 detection from extracts only achievable after 12 myc epitopes have been attached.

The results from the immunoprecipitation experiments raise the question of what proportion of the pulled down Est2 complex is actually present at the telomere versus other locations in the cell. One model in the field assumes that Est2 is bound to telomeric chromatin throughout the cell cycle, with Est1 not part of this telomere-bound complex until late S phase. Thus, it would be interesting to test how much of the α-factor arrested complex is actually at the telomere, or whether it defines a separate type of complex (with a different stoichiometry) not positioned at the telomere. Various configurations of these tagged strains should serve as excellent reagents for doing chromatin immunoprecipitation experiments for analysing the

complex at the telomere, as well as isolating other cellular fractions for comparing telomerase stoichiometry within other regions of the cell.

In addition to the western blots displayed in this chapter, many others were performed using different iterations of tagged strains. The western blots shown in figures 3.2 – 3.4 are the most representative for illustrating the key similarities and differences between two versions of tagged strains:

version 1 – Est1-$(myc)_{13}$::TRP1 $(myc)_{12}$-$(HA)_3$-Est2

version 2 – Est1-$(G)_6$-$(myc)_{12}$ $(FLAG)_3$-$(myc)_{12}$-$(G)_6$-Est2

The most significant difference between the two versions is the greater apparent stoichiometry of Est1 present in the complex, at all stages of the cell cycle, when Est2 is immunoprecipitated with anti-HA in version 1 compared with anti-FLAG version 2. This difference was consistently seen irrespective of whether Est3 was additionally tagged, so it does not appear to be due to a functional consequence of tagging Est3. The difference is presumably due to the different number of myc epitopes, as well as other differences in amino acid sequences in these two tags (in both the myc epitopes and the linkers between the epitopes) which influences antibody recognition. Moving the myc epitope to the extreme N-terminus of the Est2 protein may also increase its accessibility to recognition by the anti-myc antibody. I also noticed a similar phenomenon when looking at complex stoichiometry of Est3 when using anti-FLAG versus anti-HA to immunoprecipitate Est3-$(FLAG)_3$ and Est3-$(G)_6$-$(myc)_6$-$(HA)_3$, respectively. This is discussed in Chapter 7.

Ultimately, version 2 – Est1-$(G)_6$-$(myc)_{12}$ $(FLAG)_3$-$(myc)_{12}$-$(G)_6$-Est2 – was chosen as the strain to use for biochemical analysis because it has no disruption in telomere length control, the identical tags ensure an accurate representation of relative stoichiometries in the telomerase complex, and the protocol for FLAG immunoprecipitation was highly successful in quantitatively depleting Est2 from extracts, which means that the anti-myc westerns of these Est2 immunoprecipitates provides a highly quantitative means of monitoring the catalytic core of telomerase. Therefore, additional modifications of Est1, Est2 as well as TLC1 and other telomere proteins of interest can be integrated into this strain for directly assessing how they affect the stoichiometry of the catalytic core.

It is unclear why Est3 has been challenging to epitope tag without impacting function, and what biochemical activity or activities on Est3 are being perturbed by the tags. Given that it is a small protein with a single structural motif, an OB-fold, there simply might not be enough space to accommodate a multi-epitope tag without affecting stability or function. Based on the dominant negative mutagenesis in Chapter 2, some portions of the surface on Est3 are required for function, with a significant effect on telomere homeostasis when mutants in those regions are overexpressed. However, based on a recent high-resolution structure of Est3 obtained by Debbie Wuttke's lab, there is still a large area of surface on Est3 that appears to be dispensable for function. Nevertheless, Est3 has been highly sensitive to epitope tag insertions, and so far, positioning a $(FLAG)_3$ tag at the C-terminus has had the least effect on telomere length.

If a property intrinsic to the protein (such as telomerase processivity) is being perturbed by the tag on Est3, with no impact on protein-protein interactions, then the results from the co-immunoprecipitation experiments are completely reflective of how Est3 is associating with the catalytic core. It would be interesting to do a detailed analysis of several of the tagged Est3 proteins that have a range of telomere shortening phenotypes, to see if any difference can be seen with regard to how the tagged Est3 proteins, as well as Est1, associate with the catalytic core through the cell cycle. If there is any pattern of association that correlates with telomere length, then that could provide some inferences as to how untagged wild-type Est3 is normally functioning.

Materials and methods

Strains and plasmids

The parental strain for generating the tagged strains was AVL78 (*MAT***a** *leu2 trp1 ura3-52 prb1 prc1 pep4-3*). Figures 3.14 and 3.15 contain pedigrees that outline the derivation of the first and second set of tagged strains, respectively. In the first set of strains, integration of *EST1-(myc)*$_{13}$*::TRP1* was achieved via one step allele replacement (Longtine et al., 1998). All other integrations were achieved via pop-in / pop-out two step allele replacement. Table 3.1 lists the integrating plasmids that were used for the strain constructions. All were derived from YIplac211, and for the *EST3* constructs, the frameshift that is present in the genomic version of *EST3* was corrected. Pop-in and pop-out integrations were diagnosed by PCR using sets of primers in the regions described in Figure 3.1, and the initial strain constructions for

tagging Est1, Est2, and Est3 were checked by sequencing the entire open reading frame to confirm that no mutations were incorporated and that the tag was positioned correctly.

YVL3057 (*MAT***a** *est3-Δ::LYS2 ura3-52 lys2-801 trp1-Δ1 his3-Δ200 leu2-Δ1*/p *CEN URA EST3*) was used to check for complementation of the *CEN LEU2 EST3* tagged plasmids listed in Table 3.1.

For the α-factor arrest and release experiments, strains were deleted for *BAR1* by integration of *bar1*-Δ*::KAN* via one step allele replacement.

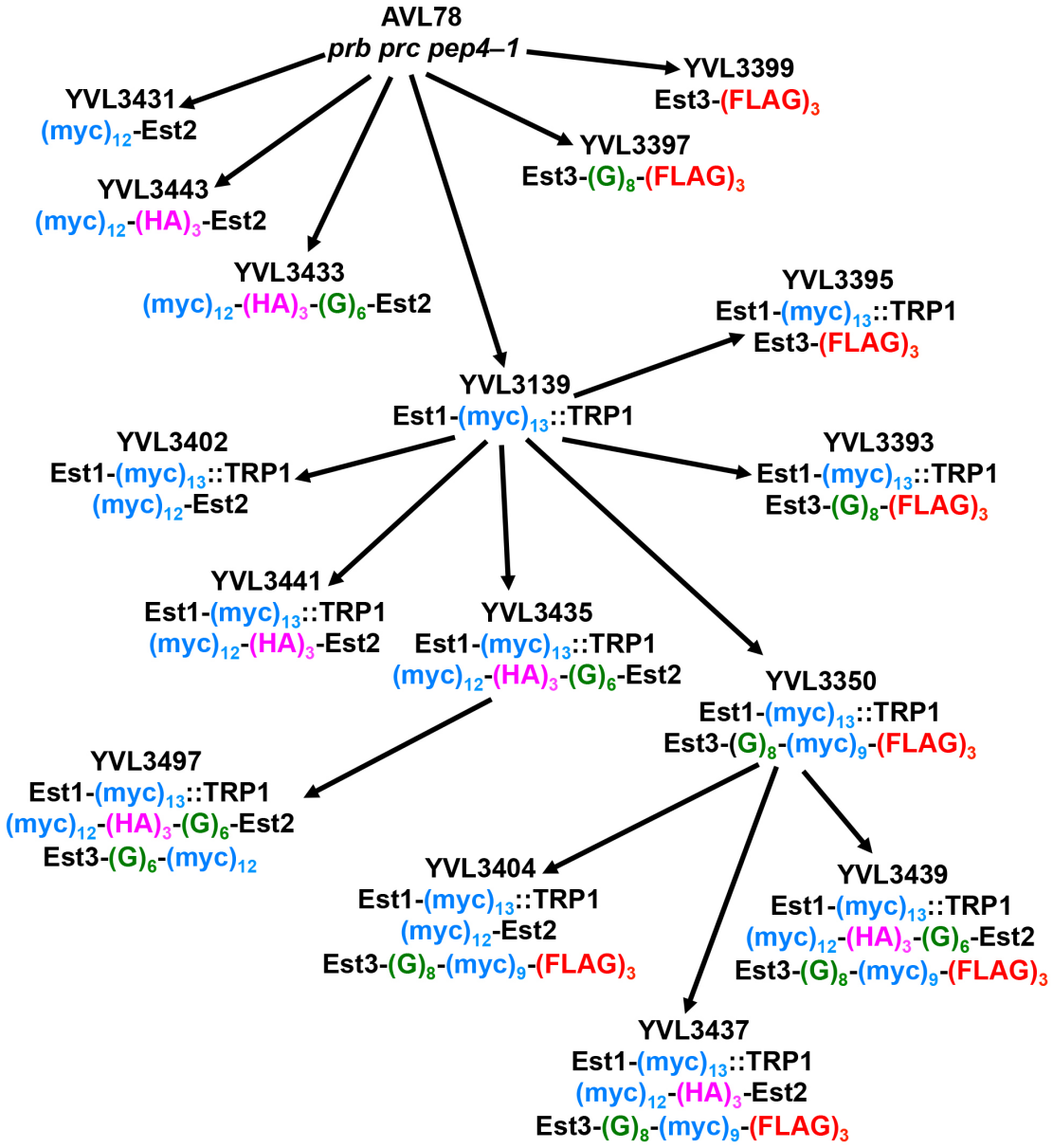

Figure 3.13 Pedigree of the first set of tagged strains that were integrated.

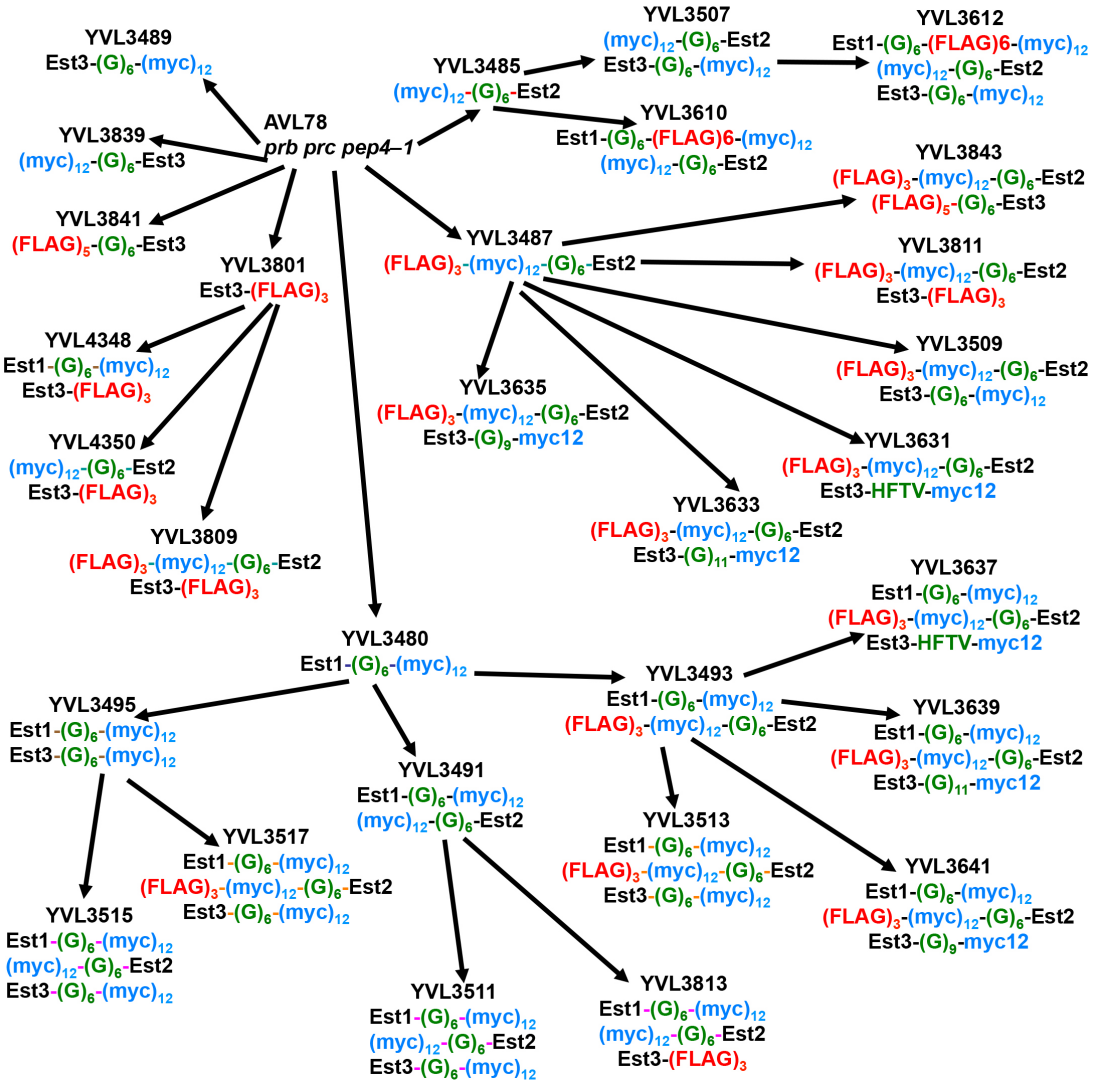

Figure 3.14 Pedigree of the second set of tagged strains that were integrated.

Table 3.1 Plasmids used in this chapter.

Plasmid name	Type	Marker	Promoter	Gene
pVL5187	integrating	*URA3*	native	*EST1-$(G)_6$-$(myc)_{12}$*
pVL5577	integrating	*URA3*	native	*EST1-$(G)_6$-$(FLAG)_6$-$(myc)_{12}$*
pVL4532	integrating	*URA3*	native	*$(myc)_{12}$-EST2*
pVL5272	integrating	*URA3*	native	*$(myc)_{12}$-$(G)_6$-EST2*
pVL4547	integrating	*URA3*	native	*$(myc)_{12}$-$(HA)_3$-EST2*
pVL4664	integrating	*URA3*	native	*$(myc)_{12}$-$(HA)_3$-$(G)_6$-EST2*
pVL5273	integrating	*URA3*	native	*$(FLAG)_3$-$(myc)_{12}$-$(G)_6$-EST2*
pVL4478	integrating	*URA3*	native	*EST3-$(FLAG)_3$*
pVL4205	integrating	*URA3*	native	*EST3-$(G)_8$-$(FLAG)_3$*
pVL5274	integrating	*URA3*	native	*EST3-$(G)_6$-$(myc)_{12}$*
pVL5585	integrating	*URA3*	native	*EST3-$(G)_9$-$(myc)_{12}$*
pVL5584	integrating	*URA3*	native	*EST3-$(G)_{11}$-$(myc)_{12}$*
pVL5583	integrating	*URA3*	native	*EST3-HFTV-$(G)_6$-$(myc)_{12}$*
pVL4206	integrating	*URA3*	native	*EST3-$(G)_8$-$(myc)_9$-$(FLAG)_3$*
pVL5896	integrating	*URA3*	native	*$(FLAG)_2$-$(G)_4$-EST3*
pVL5902	integrating	*URA3*	native	*$(FLAG)_5$-$(G)_6$-EST3*
pVL5895	integrating	*URA3*	native	*$(myc)_{12}$-$(G)_6$-EST3*
pVL5717	*CEN*	*LEU2*	native	*$EST3_{1-30}$-$(myc)_{12}$-$EST3_{31-181}$*
pVL5714	*CEN*	*LEU2*	native	*$EST3_{1-35}$-$(myc)_{12}$-$EST3_{36-181}$*
pVL5715	*CEN*	*LEU2*	native	*$EST3_{1-134}$-$(myc)_{12}$-$EST3_{135-181}$*
pVL5716	*CEN*	*LEU2*	native	*$EST3_{1-138}$-$(myc)_{12}$-$EST3_{139-181}$*
pVL5718	*CEN*	*LEU2*	native	*$EST3_{1-148}$-$(myc)_{12}$-$EST3_{149-181}$*
pVL5707	*CEN*	*LEU2*	native	*$EST3_{1-134}$-$(FLAG)_6$-$EST3_{133-181}$*

Biochemical methods

250mL cultures were grown at 30°C in YPD and harvested at an OD_{600} of 0.8–1.0. All subsequent steps were performed at 4°C. The cell pellet was washed once in water, once in TMG (10mM Tris-HCl pH 8.0, 1mM $MgCl_2$, 5% glycerol) plus 200mM NaCl, and resuspended in 1mL TMG plus 200mM NaCl and cOmplete protease inhibitor tablet (Roche). Cells were frozen in liquid nitrogen and homogenized with a mortar and pestle. After clarifying extracts twice by centrifugation for 15 min at 12,000 rpm, Tween20 (0.1% final concentration) was added. ≈2.5mg of crude extract in 0.5mL was used for the immunoprecipitations.

For HA immunoprecipitation, 25µL settled volume anti-HA affinity matrix (Roche) was added and incubated for 2 hours. After gentle pulse centrifugation, the beads were washed 3 times with 1mL of TMG plus 200mM NaCl, cOmplete protease inhibitor tablet, 0.1% Tween-20, and then beads were resuspended in 40µL Laemelli sample buffer.

For FLAG immunoprecipitation, 5µL settled volume anti-FLAG M2 beads (Sigma) were added and incubated for 2 hours. Washes were performed as described above and then beads were resuspended in 40µL Laemelli sample buffer.

Immunoprecipitates containing myc- and FLAG-tagged proteins were resolved on 6% SDS-PAGE gels and probed with either anti-myc 2272 (Cell Signaling Technology) at 1:1000 or anti-FLAG F7425 (Sigma-Aldrich) at 1:2000 dilution, respectively, followed by anti-rabbit IgG HRP conjugate (Promega) at 1:10,000 and

subsequent ECL (enhanced chemiluminescence) detection with pre-flashed film. Protein signals were quantitated using FUJIFILM Science Lab Image Gauge.

Southern blot analysis of telomere length

To check for complementation of the *CEN LEU2 EST3* tagged plasmids listed in Table 3.1, the plasmids were transformed into YVL3057 (*MAT***a** *est3-Δ::LYS2 ura3-52 lys2-801 trp1-Δ1 his3-Δ200 leu2-Δ1*/p *CEN URA EST3*) following eviction of the *EST3* covering plasmid on 5-fluoroorotic acid (5-FOA). Transformants were propagated by streaking for single colonies for ~75 generations or until senescence was observed. For the transformants that did not senesce, telomere length was analyzed on southern blot as described in Chapter 2.

To assess telomere length of the integrated strains, pop-outs were propagated for ~75 generations and then analysed by southern blot as described above.

Cell cycle arrest

For nocodazole arrest, 250mL cultures were grown to an OD_{600} of 0.35. Nocodazole was added to a concentration of 10μg/mL, incubated for 140 min, then 50% more nocodazole was added and incubated for an additional 70 min followed by harvesting of pellets as described in the biochemical methods section.

For α-factor arrest, strains were deleted for *BAR1* by integration of *bar1-Δ::KAN* via one step allele replacement. 250mL cultures were grown to an OD_{600} of 0.35, then α-factor was added to a final concentration of 10^{-8}M and incubated for 3

hours followed by harvesting of pellets as described in the biochemical methods section.

For α-factor arrest and release experiments, 2L cultures were grown at 30°C in YPD, spiked with 10^{-8}M α-factor at OD_{600} of 0.35, and arrested for 3 hours. To release from α-factor, cells were washed 2x in an equivalent volume of 30°C water, resuspended in 2L of 30°C YPD, and 200mL aliquots were collected at the following timepoints: 0, 15, 30, 45, 60, 75, 90, 105, 120, and 135 min. For each timepoint collection, 1 ml was saved in 4°C 70% ethanol for FACS analysis and the remaining cell pellet was washed in 4°C TMG (10mM Tris-HCl pH 8.0, 1mM $MgCl_2$, 5% glycerol) plus 200mM NaCl and then the pellet saved at -80°C until extract preparation.

Fluorescence-activated cell sorting

To prepare samples for FACS analysis, 2-3 x 10^6 cells were washed in 3mL 50mM sodium citrate. Cells were pelleted and resuspended in 0.5mL 50mM sodium citrate containing 0.1mg/mL RNase A and incubated for 2h at 37°C. Then, cells were stained by the addition of 0.5mL 50mM sodium citrate containing 2μM Sytox Green. Prior to flow cytometric analysis, samples were sonicated for 15s on a Branson sonifier (microtip level 2, 80% output). For each sample, 30,000 gated events were collected using a Becton-Dickinson FACScan. Data was collected and graphed using CellQuest.

Acknowledgements

A portion of Chapter 3 a modified reprint of the material as it appears in Tucey, T.M., and Lundblad, V. (2013). A yeast telomerase complex containing the Est1 recruitment protein is assembled early in the cell cycle. Biochemistry *52*, 1131-1133. The dissertation author was the primary researcher for this publication. Reprinted with permission from American Chemical Society, copyright, 2013.

Chapter 4: Identification of two additional structural elements on TLC1 required for Est1 binding

This chapter contains the first publication that introduces the stoichiometry assay described in Chapter 3.

In collaboration with John Lubin, another member of the Lundblad lab, this study identified two novel structural elements on TLC1 that are critical for Est1 association with the RNA. Previous work had implicated a conserved five-nucleotide bulge, present in a long helical arm of TLC1, for Est1 binding (Seto et al., 2002). Immediately adjacent to this bulge, we identified a conserved single-stranded internal loop that is also required for the Est1-RNA interaction. An additional structural feature consisting of a single-stranded region at the base of this helix also contributes to recognition of TLC1 by Est1, potentially by providing structural flexibility. The identification of three elements of TLC1 that are required for Est1 association provides a detailed view of this particular protein-RNA interaction.

The following is a formatted reprint of the material as it appears in Lubin, J.W.*, Tucey, T.M.*, and Lundblad, V. (2012). The interaction between the yeast telomerase RNA and the Est1 protein requires three structural elements. RNA *18*, 1597-1604. * co-equal contributions

Abstract

In the budding yeast *Saccharomyces cerevisiae*, the telomerase enzyme is composed of a 1.3-kb TLC1 RNA that forms a complex with Est2 (the catalytic subunit) and two regulatory proteins, Est1 and Est3. Previous work has identified a conserved 5-nt bulge, present in a long helical arm of TLC1, which mediates binding of Est1 to TLC1. However, increased expression of Est1 can bypass the consequences of removal of this RNA bulge, indicating that there are additional binding site(s) for Est1 on TLC1. We report here that a conserved single-stranded internal loop immediately adjacent to the bulge is also required for the Est1-RNA interaction; furthermore, a TLC1 variant that lacks this internal loop but retains the bulge cannot be suppressed by Est1 overexpression, arguing that the internal loop may be a more critical element for Est1 binding. An additional structural feature consisting of a single-stranded region at the base of the helix containing the bulge and internal loop also contributes to recognition of TLC1 by Est1, potentially by providing flexibility to this helical arm. Association of Est1 with each of these TLC1 motifs was assessed using a highly sensitive biochemical assay that simultaneously monitors the relative levels of the Est1 and Est2 proteins in the telomerase complex. The identification of three elements of TLC1 that are required for Est1 association provides a detailed view of this particular protein-RNA interaction.

Introduction

In most species, telomerase contributes to the maintenance of chromosome termini using a conserved mechanism for elongation of the G-rich strand of telomeres. The synthesis of telomeric DNA by telomerase relies on a conserved catalytic core composed of a reverse-transcriptase-like subunit and a template-containing RNA, although additional telomerase-associated proteins contribute to holoenzyme function. In humans, telomere erosion in cells that lack telomerase can be a substantial contributing factor to age-dependent limitations on tissue renewal in the lung, liver, pancreas, or bone marrow, resulting in impaired organ maintenance and consequent effects on life span (Armanios, 2009; Garcia, 2011; Guo et al., 2011; Savage and Alter, 2008; von Figura et al., 2011).

The RNA subunit of telomerase provides more than simply a template which dictates the synthesis of telomere repeats. It contributes to the fidelity of the catalytic reaction cycle and also performs crucial roles in localization and accumulation of the enzyme complex (Blackburn and Collins, 2011). Derivation of separate secondary structure models for telomerase RNAs from ciliates, vertebrates, and budding yeasts have revealed several conserved motifs, which include a single-stranded region encompassing the template and a pseudoknot present in a central core domain as well as a 3′ stem-terminus element (Theimer and Feigon, 2006). However, telomerase RNAs display an exceptional degree of evolutionary diversity, with a striking degree of length variation (ranging from 147 nt to >2 kb) (Chakrabarti et al., 2007; Kachouri-Lafond et al., 2009; Ye and Romero, 2002) which is accompanied by sequence

divergence even within the conserved structural motifs. The tolerance to such a high degree of variation might be explained if the RNA subunit does not fold into a compact well-defined three-dimensional structure with fixed orientation of structural elements. Consistent with this premise, the budding yeast telomerase RNA has been proposed to form a flexible scaffold for protein assembly (Zappulla and Cech, 2004), with independent binding domains for the regulatory Est1 protein and the catalytic Est2 subunit (Chappell and Lundblad, 2004; Evans and Lundblad, 2002; Livengood et al., 2002; Seto et al., 2002). This architecture appears to be maintained in the fission yeast telomerase complex as well, where the RNA subunit similarly mediates the indirect association of Est1 with the catalytic subunit (Leonardi et al., 2008; Webb and Zakian, 2008).

In budding yeast, the Est1 subunit of telomerase mediates a key regulatory event, which is recruitment of the telomerase enzyme to its site of action through interaction with the telomere-bound Cdc13 protein (Bianchi et al., 2004; Evans and Lundblad, 1999; Pennock et al., 2001). Both chromatin immunoprecipitation and live-cell imaging of the telomerase RNA subunit have shown that telomerase associates with telomeres in late S phase, with association eliminated by the recruitment-defective *cdc13-2* mutation (Chan et al., 2008; Gallardo et al., 2011). Est1 therefore serves as a bridging protein, by binding both Cdc13 and the telomerase RNA to bring the catalytic core of the enzyme to its substrate. The Est1–TLC1 interaction is localized to a long helical arm (referred to as Helix IV in this study, based on the nomenclature used by Dandjinou et al. 2004), which can be relocated to ectopic

locations within the telomerase RNA (Zappulla and Cech, 2004). One determinant for Est1 has already been described, which is a conserved 5-nt bulge present in sub-helix IVc (Seto et al., 2002). We show here that a second conserved element—a single-stranded internal loop which is immediately adjacent to the pentanucleotide bulge—is also critical for recognition of TLC1 by Est1. These observations argue that the specificity of this interaction relies on two adjacent RNA binding motifs which together generate an interface for RNA recognition by Est1.

Results and Discussion

A conserved internal loop in Helix IV of TLC1 is essential for in vivo function

Previous work has established that a 5-nt bulge (nucleotides 660–664) (Figure 4.1a) mediates Est1 association with the telomerase complex (Seto et al., 2002). To address whether other features of Helix IV are required for TLC1 function, two mutations that deleted sub-helices IVb and IVc to generate *tlc1-201* (Δ559–598) and *tlc1-101* (Δ599–670), respectively (Figure 4.1a), were assessed for effects on telomere length (Figure 4.1b) and senescence (Figure 4.1c and data not shown). Sub-helix IVb appeared to be dispensable for function, as telomere maintenance in the tlc1-201 strain was indistinguishable from a wild-type TLC1 strain, indicating that this sub-helix did not contribute to Est1 association with the RNA. In contrast, the *tlc1-101* strain, bearing a deletion which encompassed the previously characterized Est1-binding bulge, resulted in a severe telomere replication defect. The phenotype of the *tlc1-101* strain was comparable with that displayed by the *tlc1-47* strain, which expressed a

variant of TLC1 which was only deleted for the bulge (Figure 4.1b,c). However, the telomere replication defects of *tlc1-101* and *tlc1-47* strains differed in one key aspect when examined in the presence of increased levels of the Est1 protein. In the presence of a high copy plasmid which expressed Est1 from the constitutive ADH promoter, the senescence defect of the *tlc1-47* strain was reversed (Figure 4.1c) and telomeres were restored back to a length that approximated that of a wild-type strain (see below), as previously observed (Seto et al., 2002). In contrast, the severe growth defect and short telomeres displayed by the *tlc1-101* strain were unaffected by the presence of the ADH-Est1 plasmid (Figure 4.1c and data not shown).

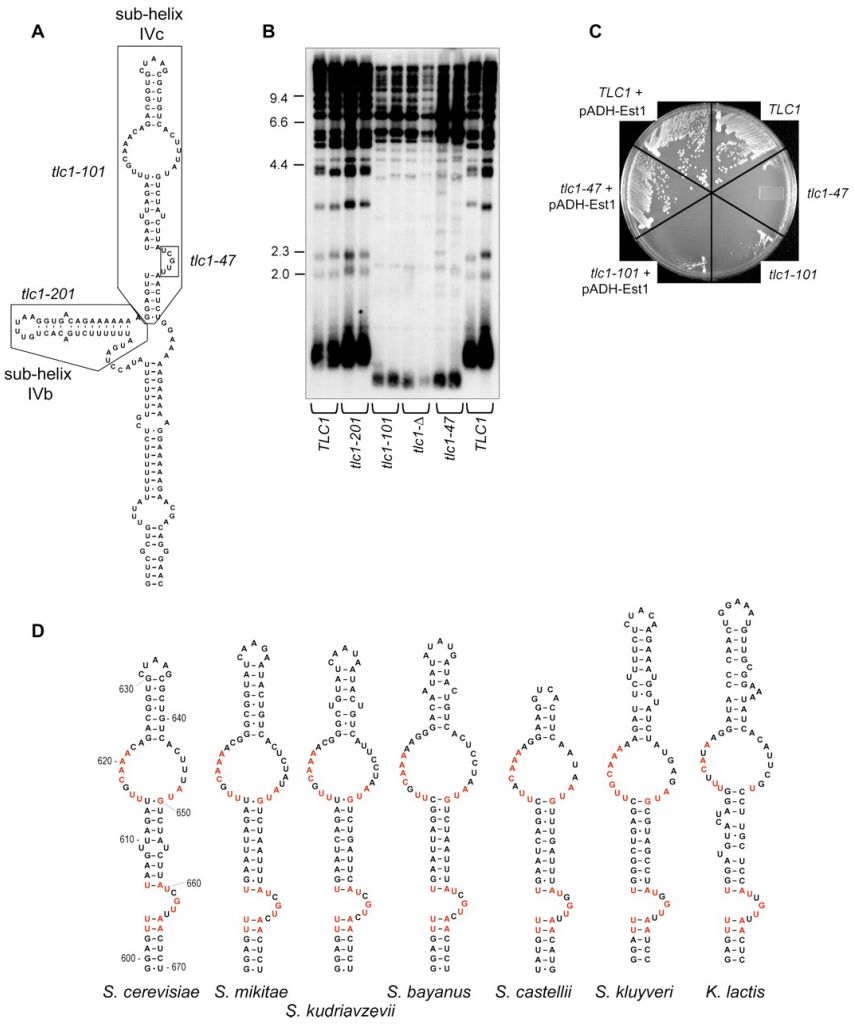

Figure 4.1 Deletion of sub-helix IVc cannot be suppressed by overexpression of Est1. A) Proposed secondary structure of Helix IV of TLC1, with the boundaries indicated for two mutations, *tlc1-101* and *tlc1-201*, which delete sub-helices IVc and IVb, respectively; the previously described Est1-binding bulge (nucleotides 660–664), which is deleted by the *tlc1-47* mutation, is indicated by the smaller box. B) Telomere length of the indicated strains, examined after ~75 generations of growth; size markers (in kb) are indicated. C) Growth characteristics of *TLC1*, *tlc1-47*, and *tlc1-101* strains in the presence (*left*) or absence (*right*) of a high copy plasmid expressing the Est1 telomerase subunit from the constitutive ADH promoter; strains were examined at a point when senescence was most pronounced (~100 generations). D) Proposed secondary structures for sub-helix IVc from TLC1 RNAs from selected isolates from the *Saccharomyces* and *Kluveromyces* clades; the two clusters of sequences indicated in red are invariant in the *Saccharomyces* clade, with partial conservation extending into the *Kluveromyces* clade. Determination of structures was based on sequence alignments to identify conserved elements as well as comparison with previously published proposed secondary structures, aided by RNA Mfold.

The fact that the telomere replication defect displayed by the *tlc1-47* mutant strain could be suppressed by enhanced Est1 expression argued that one or more binding sites for Est1 were still present in the TLC1 RNA bearing the Δ660–664 deletion. Since Est1 overexpression failed to suppress the *tlc1-101* defect, we surmised that an additional binding site for Est1 might exist in sub-helix IVc. As a first step in testing this premise, we reexamined the predicted structure of this helix, based on a phylogenetic comparison of sequences from species from the *Saccharomyces* and *Kluveromyces* clades (Figure 4.1d). Comparison of this region of TLC1 revealed the presence of a conserved internal loop, adjacent to the 660–664 bulge, with two single-stranded sequences (5′-U_{615}UGCAAA_{621}-3′ and 5′-A_{648}UG_{650}-3′; indicated in red in Figure 4.1d) which were highly conserved. Previous work by Tomaska and colleagues analyzing conserved domains in the *Candida* clade telomerase RNAs proposed a similar structure, although with more relaxed pattern of sequence conservation, which may reflect the absence of Est1 homologs in several species in the *Candida* clade (Gunisova et al., 2009).

To test whether this internal loop was required in vivo, a panel of five mutations was constructed (depicted in Figure 4.2a). Two mutations changed the sequence of either strand of the two conserved blocks of sequence in the internal loop, without altering the proposed single-stranded secondary structure (*tlc1-202* and *tlc1-203*). Two additional mutations changed the sequence of either of the two single strands of the loop (*tlc1-204* and *tlc1-205*), creating a structure that would be predicted to form a duplex and thereby eliminate the internal loop. Finally, a mutation which

deleted the predicted terminal hairpin was generated (*tlc1-206*). These five mutations were introduced into a *tlc1-Δ* strain and examined for effects on telomere length and senescence (Figure 4.2b,c). Alteration of one of the two blocks of conserved nucleotides (5′-AUG-3′) resulted in a modest reduction in telomere length (*tlc1-202*), indicating that this region of the internal loop made a minimal contribution to TLC1 function. In contrast, introducing a sequence change into the larger block of conserved nucleotides on the other strand of the internal loop (5′-UUGCAAA-3′) resulted in extremely short telomeres (*tlc1-203*). Furthermore, two mutations which closed the internal loop to generate a predicted duplex (*tlc1-204* and *tlc1-205*) displayed a phenotype indistinguishable from that of a *tlc1-Δ* null strain. Removal of the nonconserved terminal hairpin (*tlc1-206*) also reduced telomere length, although the effect was less pronounced. The telomere replication defects displayed by these strains were not due to reduced levels of TLC1, as quantitation of the levels of the TLC1 RNA (normalized to levels of the U1 RNA) in extracts prepared from strains in which these *tlc1* mutations were integrated into the genome did not reveal any significant differences, relative to wild-type TLC1 (normalized TLC1/U1 ratios for *tlc1*-47, *tlc1*-202, *tlc1*-203, *tlc1*-204, and *tlc1*-206 were 1.0, 1.0, 1.0, 1.1, and 0.9, respectively; data not shown). Collectively, this analysis indicates that the conserved internal loop is a protein binding site which is essential for in vivo TLC1 function, with the 5′-UUGCAAA-3′ and 5′-AUG-3′ sequence motifs on either single strand contributing to binding.

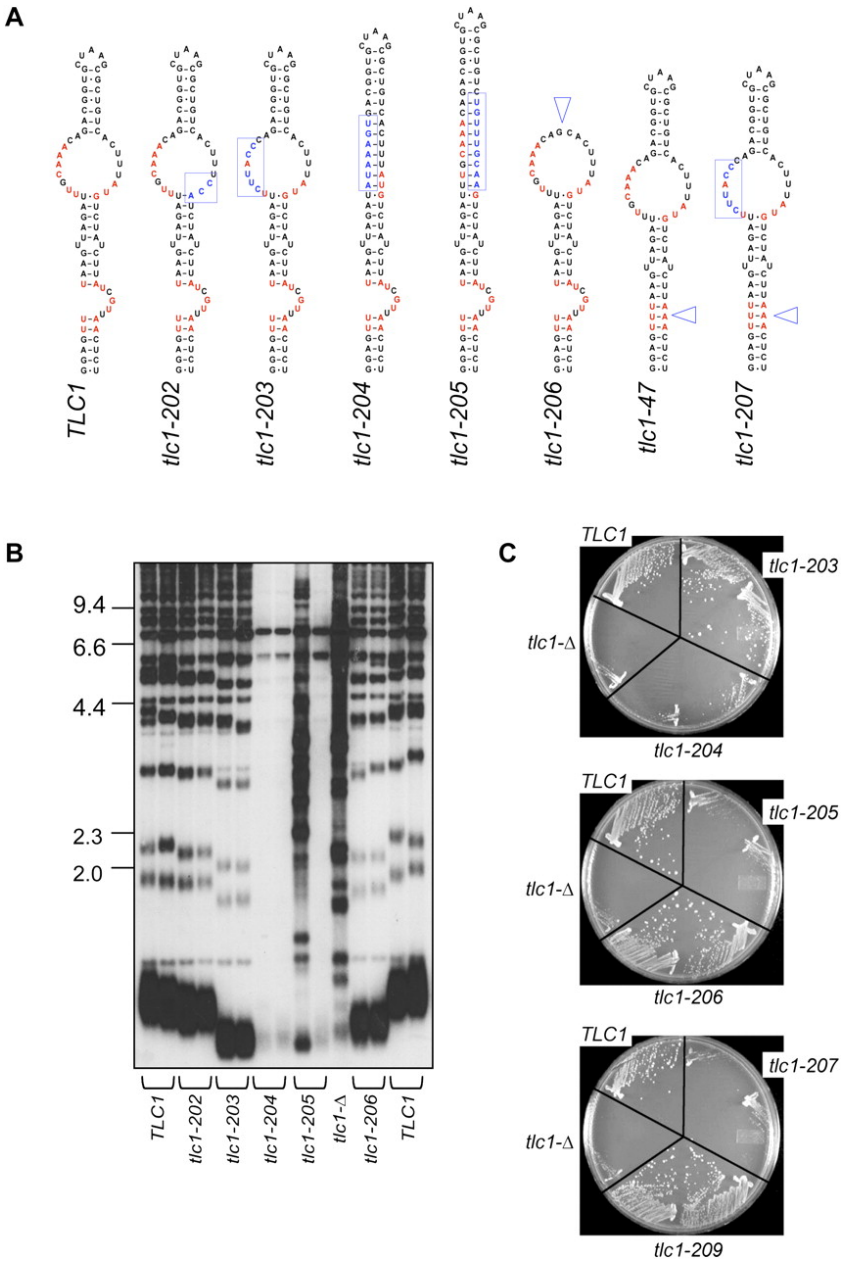

Figure 4.2 A conserved internal loop is required for telomere length maintenance. A) A depiction of mutations introduced into the conserved internal loop of sub-helix IVc, with blue boxes or triangles indicating sequence changes or deleted nucleotides, respectively. B) Telomere length of strains bearing the indicated mutations (expressed from single-copy plasmids introduced into the *tlc1*-Δ strain YVL3554) examined after ~100 generations, at a point when the *tlc1-Δ* null strain (lane *11*) has given rise to recombination-dependent survivors (Lundblad and Blackburn, 1993). C) Growth characteristics of the indicated mutant strains, which have been propagated for ~100 generations.

Mutations in the conserved internal loop are suppressed by Est1 overexpression

The obvious candidate for binding to this internal loop would be Est1, given the close proximity to the previously defined Est1 binding site at nucleotides 660–664. This predicts that increased expression of Est1 might similarly suppress mutations in this second proposed protein binding site. Consistent with this prediction, the severe telomere replication defect displayed by the *tlc1-203* strain, in which the conserved 5′-UUGCAAA-3′ motif was mutated, was reversed by overexpression of Est1. Telomeres were restored to roughly wild-type telomere length, comparable with that previously observed for a *tlc1-47* mutant strain (Figure 4.3a; Seto et al. 2002). Suppression of the *tlc1-47* and *tlc1-203* defects by Est1 overexpression was also specific, as increased expression of either Est2 or Est3 failed to suppress either mutation (data not shown). These observations indicate that in the presence of excess Est1, either of these two structures is sufficient to mediate association of Est1 with the complex. In contrast, a variant of TLC1 (*tlc1-207*), which combined the *tlc1-47* and *tlc1-203* mutations to eliminate both of the proposed binding sites, exhibited a different behavior in response to increased levels of Est1. Like the *tlc1-47* strain, the *tlc1-207* strain displayed a telomere replication defect that was indistinguishable from a *tlc1-Δ* null strain (Figures 4.2c, 4.3a). However, the ADH–Est1 construct was unable to reverse the short telomere length and senescence phenotype of the *tlc1-207* strain (Figure 4.3a and data not shown). Collectively, these overexpression data argue that the main determinants for association of Est1 with the telomerase complex are two adjacent structures on sub-helix IVc.

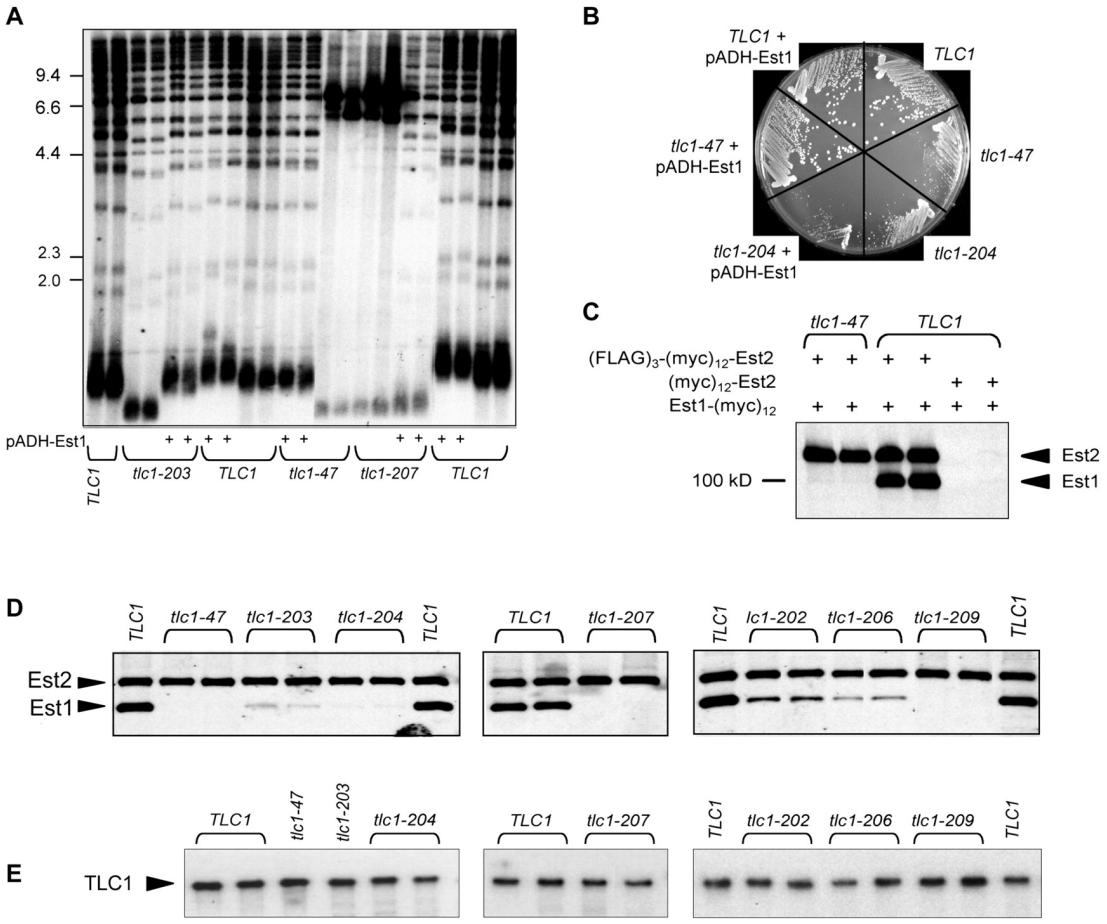

Figure 4.3 Est1 association with telomerase is abolished by mutations in the conserved internal loop. A) Telomere length of the indicated strains was examined after ~100 generations. B) Growth characteristics determined as described in Figure 4.1c, although strains were examined at ~75 generations, when senescence was not as pronounced. C,D) Anti-myc Western analysis of anti-FLAG immunoprecipitates following 6% PAGE of the indicated strains; the *tlc1* mutations were integrated into the genome of YVL3493 (with the exception of *tlc1*-207 and the accompanying *TLC1* control, which were present on single-copy plasmids in the YVL3701 *tlc1-Δ* strain). E) Northern analysis monitoring levels of the TLC1 RNA in the same immunoprecipitates shown in *D*.

In addition to *tlc1-203*, the short telomere phenotypes of strains expressing either *tlc1-202* or *tlc1-206* were also restored to approximately wild-type length by enhanced expression of Est1 (data not shown). However, the *tlc1-204* and *tlc1-205* strains, which expressed mutant derivatives of TLC1 with the internal loop replaced by a duplex structure, could not be suppressed by the ADH–Est1 construct (Figure 4.3b and data not shown). This indicates that, in the complete absence of the internal loop, the bulge at 660–664 nt is not sufficient to sustain association of Est1 with TLC1, arguing that the internal loop may make a more dominant contribution to the Est1–TLC1 interaction.

The internal loop is required for association of Est1 with telomerase

The above genetic observations indicate that both the bulge and the internal loop of Helix IVc are required for Est1 binding to TLC1. To test this premise biochemically, association of a myc-tagged variant of Est1 with the telomerase complex was monitored using an assay that monitored the relative level of the Est1 and Est2 proteins following immunoprecipitation of Est2. To do so, we generated a strain in which both Est1 and Est2 could be detected by identical $(myc)_{12}$ epitopes present at the C-terminus and N-terminus, respectively, of the two Est proteins; in addition, the Est2 protein contained a triple FLAG epitope adjacent to the $(myc)_{12}$ epitope. These tagged versions were introduced into the genome in place of the untagged *EST1* and *EST2* genes, so that each tagged protein was expressed by its native promoter. The $(myc)_{12}$ and $(FLAG)_3$ sequences were also engineered in order to

minimize any disruption of protein function, such that the resulting strain had wild-type telomere length (data not shown).

The design of the Est1–$(myc)_{12}$ $(FLAG)_3$–$(myc)_{12}$–Est2 strain allows quantitative assessment of the degree of association of the Est1 protein with the Est2–TLC1 catalytic core of telomerase, by simultaneously monitoring Est1 and Est2 protein levels with the same antibody (anti-myc) following anti-FLAG immunoprecipitation of the Est2 subunit. Since numerous previous studies have established that Est1 and Est2 independently bind TLC1 (Chappell and Lundblad, 2004; Evans and Lundblad, 2002; Livengood et al., 2002; Seto et al., 2002), this assay provides an alternative means of quantitating the Est1–RNA interaction. This has several advantages relative to approaches used previously by our laboratory and others. For example, one commonly used assay monitored the relative ability of wild-type *TLC1* and a deletion derivative (*TLC1–Δ148–440*) to be co-immunoprecipitated with a telomerase protein subunit (Chappell and Lundblad, 2004; Lee et al., 2008). However, this strategy relies on a strain which expresses twice the normal level of TLC1; given that TLC1 is limiting for telomere length maintenance, altering the dosage of TLC1 may adversely affect the conclusions that stem from this method (Mozdy and Cech, 2006). Furthermore, most strains that employ this assay express at least one of the two TLC1 variants from a plasmid; variations in plasmid copy levels (for example, see input lanes of Fig. 3D in Chappell and Lundblad 2004) can further limit the sensitivity of the *TLC1* vs. *TLC1–Δ148–440* assay. In contrast, in the assay used here, the epitope-tagged Est1 and Est2 subunits of the telomerase complex were

expressed from alleles integrated at their respective genomic loci, as were the mutant *tlc1* RNAs (with one exception).

Examination of anti-FLAG immunoprecipitates prepared from extracts of the Est1–myc)$_{12}$ (FLAG)$_3$–(myc)$_{12}$–Est2 strain demonstrated that Est1 could be co-immunoprecipitated with Est2 with a highly reproducible 1:1 stoichiometry (Figure 4.3c,d). Detection of both Est1 and Est2 in immunoprecipitates was dependent on the presence of the FLAG epitope, and as predicted by prior observations, association of Est1 could not be detected in a strain expressing the *tlc1*-47 mutation, which removed the 5-nt bulge (Figure 4.3c). Similarly, mutations which removed the internal loop (*tlc1-204* and *tlc1*-205) also eliminated interaction with the complex (Figure 4.3d and data not shown), establishing that this conserved internal loop, like the 5-nt bulge, is required for Est1–TLC1 binding.

These three mutations (*tlc1*-47, *tlc1*-204, and *tlc1*-205), which conferred a telomere replication defect comparable with that of a *tlc1*-Δ null strain, reduced the amount of the Est1 protein in the anti-FLAG immunoprecipitates to below detection levels. Thus, although the genetic data implied that the internal loop was more important for binding of Est1 to TLC1, we were unable to detect a difference between mutations in the 5-nt bulge vs. the internal loop in this biochemical assay. Nevertheless, for mutations that did not confer a null phenotype, this biochemical assay was sensitive enough to detect a reduction in Est1 levels in anti-Est2 immunoprecipitates which closely correlated with the severity of the in vivo phenotype. For example, the *tlc1*-203 mutation, which altered the highly conserved 5′-

UUGCAAA-3′ motif of the internal loop, conferred a pronounced telomere replication defect which was slightly less severe than the null phenotype exhibited by the *tlc1*-47, *tlc1*-204, and *tlc1*-205 strains. This slight retention of function was reflected in the ability to detect a very low level of Est1 in the *tlc1*-203 immunoprecipitates (Figure 4.3d, left panel), which was abolished by in the *tlc1*-207 mutant strain which combined the *tlc1*-47 and *tlc1*-203 mutations (Figure 4.3d, middle panel). The relative association of Est1 with telomerase in the *tlc1-202* and *tlc1-206* strains similarly correlated with telomere length. The *tlc1-202* strain, in which the smaller conserved region of the internal loop (5′-AUG-3′) was mutated, exhibited a moderate reduction in the ability of Est1 to associate with telomerase, with Est1 association further reduced in the *tlc1-206* mutant strain which lacked the terminal hairpin (Figure 4.3d, right hand panel). Since the hairpin deleted by the *tcl1*-206 mutation does not exhibit any conserved sequence elements (Figure 4.1d), it might simply provide structural stability for the conserved loop; however, we cannot rule out the possibility of an additional interaction between Est1 and this region of the RNA. For all of these mutations, the interaction between the catalytic Est2 protein and the RNA was unchanged (Figure 4.3d,e). This demonstrates that the altered association of Est1 with the complex was not an indirect consequence of reduced TLC1 levels and also indicates that the in vivo defects displayed by this set of mutant RNAs was not simply due to global misfolding.

An additional single-stranded region of TLC1 is required for Est1 binding

The analysis shown in Figure 4.1 indicated that sub-helix IVb was dispensable for Est1 function, in contrast to the two conserved binding sites for Est1 in sub-helix IVc. However, the deletion of sub-helix IVb to generate the *tlc1-201* mutation still retained an internal single-stranded loop at the base of sub-helix IVc (indicated by the gray box in Figure 4.4a). Furthermore, a prior phylogenetic analysis of Helix IV supported the idea that a discontinuous duplex at the base of sub-helix IVc is conserved (Dandjinou et al., 2004; Zappulla and Cech, 2004). To investigate this further, mutations which eliminated several adjacent secondary structures were constructed (Figure 4.4a) and examined for effects on telomere length maintenance (Figure 4.4b). These results showed that conversion of the *tlc1-201* RNA to a version with a continuous duplex stem (*tlc1-209*) resulted in short telomeres (Figure 4.4b) and reduced association of Est1 with the telomerase complex (Figure 4.3d), which was not due to reduced levels of the Tlc1-209 RNA in either extracts or immunoprecipitates (Figure 4.3e and data not shown). This was also not the consequence of the particular nucleotide changes used to convert *tlc1-201* to *tlc1-209*, as the same mutation had no effect when introduced into the wild-type TLC1 RNA to create *tlc1-208* (Figure 4.4b). Furthermore, increased expression of Est1 reversed the telomere length defect of the *tlc1*-209 mutant strain (Figure 4.4c), similar to effects observed with mutations in the 5-nt bulge and the conserved internal loop. Figure 4.4 further shows that one additional internal loop (at nucleotides 532–535), which was eliminated by *tlc1-210* and *tlc1-211*, was not required for function.

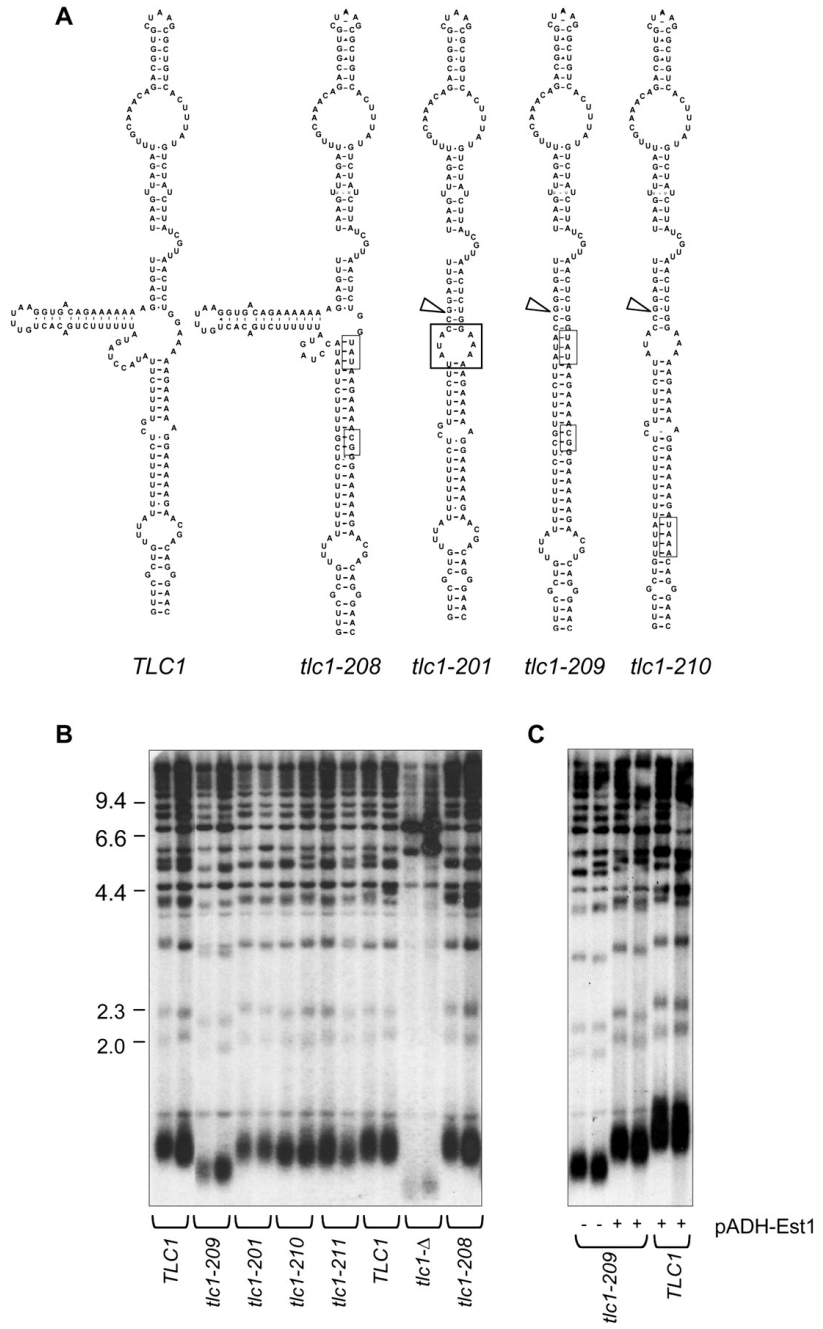

Figure 4.4 A single-stranded region at the base of sub-helix IVc contributes to TLC1–Est1 association. A) Proposed secondary structure of Helix IV, with various mutations indicated as in Figure 4.1d; the *tlc1-209* mutation is a combination of the mutations shown in *tlc1-201* and *tlc1-208*. B) Telomere length of strains expressing the mutations shown in *A*, after 75 generations of growth. C) Telomere length of the *tlc1*-209 strain in the presence or absence of a high copy ADH–Est1 plasmid, compared with a *TLC1* strain with the same plasmid.

The experiments reported here provide a comprehensive analysis of all of the proposed secondary structural elements in Helix IV of TLC1. These results lead us to propose that three discrete features of sub-helix IVc are required for Est1 binding: the previously characterized pentanucleotide bulge, an immediately adjacent internal loop, and a single-stranded region at the base of sub-helix IVc. Both the bulge and internal loop structures exhibit sequence conservation (Figure 4.1d) which presumably mediates specificity for binding by Est1; whether these two motifs collaborate or instead represent two discrete RNA–protein interactions will most likely await a structural determination of the Est1:RNA complex. In contrast, there does not appear to be any sequence specificity at the base of sub-helix IVc, suggesting that this third structural feature simply provides a flexible hinge which may help ensure accessibility of the two Est1 binding motifs. These results also demonstrate that sub-helix IVb is dispensable for in vivo function, at least in a laboratory setting; however, the fact that this sub-helix is conserved at least among the *Saccharomyces* clade (Dandjinou et al., 2004; Zappulla and Cech, 2004) suggests a role for this sub-helix in TLC1 function, which has not yet been elucidated.

Materials and methods

Strains and plasmids

All in vivo observations were performed with derivatives of YVL3554 (*MATα tlc1-Δ::HIS ura3-52 lys2-801 trp-Δ1 his3-Δ200 leu2-Δ1*/p *CEN URA3 TLC1*), which was transformed with single-copy *CEN TRP1* plasmids expressing wild-type or

mutant *TLC1* genes expressed from the native *TLC1* promoter (derived from pVL795, as described below). The *TLC1 URA3* plasmid was subsequently evicted by propagation on 5-FOA-containing media, and strains were grown for ~75–100 generations prior to examination of senescence and/or telomere length, which were monitored as described previously (Chappell and Lundblad, 2004; Lendvay et al., 1996). The parental strains used for the biochemical experiments shown in Figure 4.3e and 4.3d, respectively, were YVL3493 (*MAT***a** *leu2 trp1 ura3-52 prb$^-$ prc$^-$ pep4-3* Est1–Gly_6–myc_{12} $FLAG_3$–myc_{12}–Gly_6–Est2) or YVL3701 (a *tlc1-Δ* derivative of YVL3493 containing a *TLC1 URA3* plasmid). *TLC1* mutations were introduced by Quikchange mutagenesis into pVL795 (*CEN TRP1 TLC1*) (Chappell and Lundblad, 2004) to generate pVL2128 (*tlc1-47*; Δ660–664), pVL2272 (*tlc1-101*; Δ599–670), pVL5385 (*tlc1-201*; Δ559–598), pVL5377 (*tlc1-202*; $A_{648}TG_{650}$→CCA), pVL5379 (*tlc1-203*; $T_{615}TGCAAA_{621}$→TCTTACC), pVL5378 (*tlc1-204*; $T_{615}TGCAAACA_{623}$→ATAAAGT), pVL5602 (*tlc1-205*; $A_{643}CTTTAT_{649}$→TGTTTGCAA), pVL5386 (*tlc1-206*; Δ625–641), pVL5640 (*tlc1-207*; Δ660–664, $T_{615}TGCAAA_{621}$→TCTTACC), pVL5689 (*tlc1-208*; A_{673}→T, A_{675}→T, A_{683}→CG), pVL5599 (*tlc1-209*; Δ559–598, A_{673}→T, A_{675}→T, A_{683}→CG), pVL5600 (*tlc1-210*; Δ559–598, $A_{693}CGT_{696}$→TAAA), and pVL5601 (*tlc1-211*; Δ559–598, $T_{532}TTA_{535}$→ACGT).

Biochemical methods

Whole-cell extracts were prepared from 250-mL cultures grown to O.D. 0.8–1.0, and extract preparation and immunoprecipitations with anti-FLAG M2 beads

(Sigma) were performed as described previously (Evans and Lundblad, 2002). The Est1–$(myc)_{12}$ and $(FLAG)_3$–$(myc)_{12}$–Est2 proteins were detected on 6% SDS-PAGE gels with anti-myc 2272 (Cell Signaling Technology) at 1:1000 dilution and anti-rabbit IgG HRP conjugate (Promega) at 1:10,000. Northern analysis to monitor TLC1 RNA levels was conducted as described in (Lee et al., 2008).

Acknowledgements

We thank Deborah Wuttke and members of the Lundblad laboratory for discussions and helpful comments on the manuscript, and Lou Zumstein for technical advice. This work was supported by the UCSD CMG Training Program T32 GM007240 from the NIH (to T.M.T.), a Rose Hills Foundation Fellowship (to T.M.T.), and by R37 AG011728 from the NIH (to V.L.).

Chapter 4 is a formatted reprint of the material as it appears in Lubin, J.W., Tucey, T.M., and Lundblad, V. (2012). The interaction between the yeast telomerase RNA and the Est1 protein requires three structural elements. RNA *18*, 1597-1604. The dissertation author was a co-first author for this publication. Reprinted with premission from RNA Society, copyright, 2012.

I am grateful to my collaborator, John Lubin, for providing a thorough genetic analysis of the *tlc1* mutations, as well as Northern blots to monitor TLC1 RNA levels. I integrated the *tlc1* mutations into the genome and provided the biochemistry.

Chapter 5: An Est1-containing telomerase complex is assembled early in the cell cycle

Two contradictory models have been proposed for Est1 function: (1) Est1 recruits the catalytic core of telomerase to its site of action; or (2) Est1 associates with an already telomere-bound catalytic core late in S phase, in order to "activate" the catalytic core of the complex. These two models have been based on indirect observations – genetics and chromatin immunoprecipitation experiments – because prior to the development of the high resolution telomerase stoichiometry assay described in Chapter 3, it has not been possible to monitor the relative stoichiometry of individual components of the telomerase through the cell cycle.

In the study presented in this chapter, I show that Est1 associates with the Est2-TLC1 catalytic core by early S phase (well before telomerase elongates telomeres), with Est1 and Est2 at 1:1 stoichiometry. Increasing the expression levels of Est1 by just 2-fold ensures that Est1 associates with the complex at 1:1 stoichiometry throughout the cell cycle. Since telomere length is unchanged by a 2-fold increase in Est1 expression, this shows that association of Est1 with the holoenzyme is not a regulatory step for telomere length maintenance.

I also observed a biochemical interaction between Est1 and the telomere binding protein Cdc13 that recapitulates the previously observed genetic relationship between *EST1* and *CDC13*. This supports a model in which regulated binding of Cdc13 to chromosome termini dictates subsequent interaction of a recruitment-competent telomerase complex with telomeres.

The following is a formatted reprint of the material as it appears in Tucey, T.M., and Lundblad, V. (2013). A yeast telomerase complex containing the Est1 recruitment protein is assembled early in the cell cycle. Biochemistry *52*, 1131-1133.

Introduction

In the budding yeast *Saccharomyces cerevisiae*, telomerase is present in very low abundance, at a level that is ~2-fold lower than the number of chromosome ends (Mozdy and Cech, 2006) during the period of the cell cycle when telomeres are elongated (Marcand et al., 2000). This disparity implies that a high level of regulation is needed to ensure that underelongated telomeres are preferentially targeted by telomerase (Teixeira et al., 2004). One key regulatory node involves the Est1 regulatory subunit of telomerase that is essential for telomere replication in vivo but dispensable for enzyme catalysis in vitro (Cohn and Blackburn, 1995; Lundblad and Szostak, 1989). Two competing models have been proposed for the role of Est1. The first model, driven largely by genetic observations, proposes that recruitment of telomerase to its site of action is driven by an interaction between the telomerase-associated Est1 subunit and the telomere-bound Cdc13 protein (Bianchi et al., 2004; Evans and Lundblad, 1999; Nugent et al., 1996). A second model, which has primarily depended on chromatin immunoprecipitation, proposes that the catalytic core of telomerase is constitutively bound to telomeres in an inactive state and becomes "activated" in the late S phase through regulated association of Est1 with chromosome termini (Chan et al., 2008; Taggart et al., 2002).

Results and Discussion

Absent from these prior studies has been a direct assessment of the relative stoichiometry of telomerase subunits throughout the cell cycle, as these two models make different predictions regarding the timing of association of Est1 with the telomerase complex. This omission has been caused by the low abundance of telomerase, combined with the difficulty in introducing high-affinity epitope tags that do not impair function (Sabourin et al., 2007; Tuzon et al., 2011). We have addressed this using an assay that assesses the relative stoichiometry of the Est1 regulatory subunit with the Est2 catalytic subunit. This relies on a strain in which Est1 and Est2 contain identical $(myc)_{12}$ epitopes as well as a $(FLAG)_3$ epitope on Est2, thereby permitting levels of the two proteins to be simultaneously monitored following anti-FLAG immunoprecipitation (IP). Examination of Est1 and Est2 protein levels in extracts prepared from this strain indicated that Est1 was in excess relative to Est2 throughout most of the cell cycle (see Figure 3.8 and Figure 5.5). Thus, this strategy targets the limiting factor in the telomerase complex (Est2), which could be quantitatively depleted from extracts by anti-FLAG IP (see Figure 3.8). The epitope-tagged versions of each protein were integrated into the genome in place of the endogenous *EST1* and *EST2* genes, ensuring protein levels comparable to that of a wild-type strain. These modifications also had no effect on telomerase function (in contrast to the behavior of previously constructed strains with epitope tags on telomerase subunits (Taggart et al., 2002; Tuzon et al., 2011), as evidenced by the wild-type telomere length displayed by this strain (Figure 5.1a).

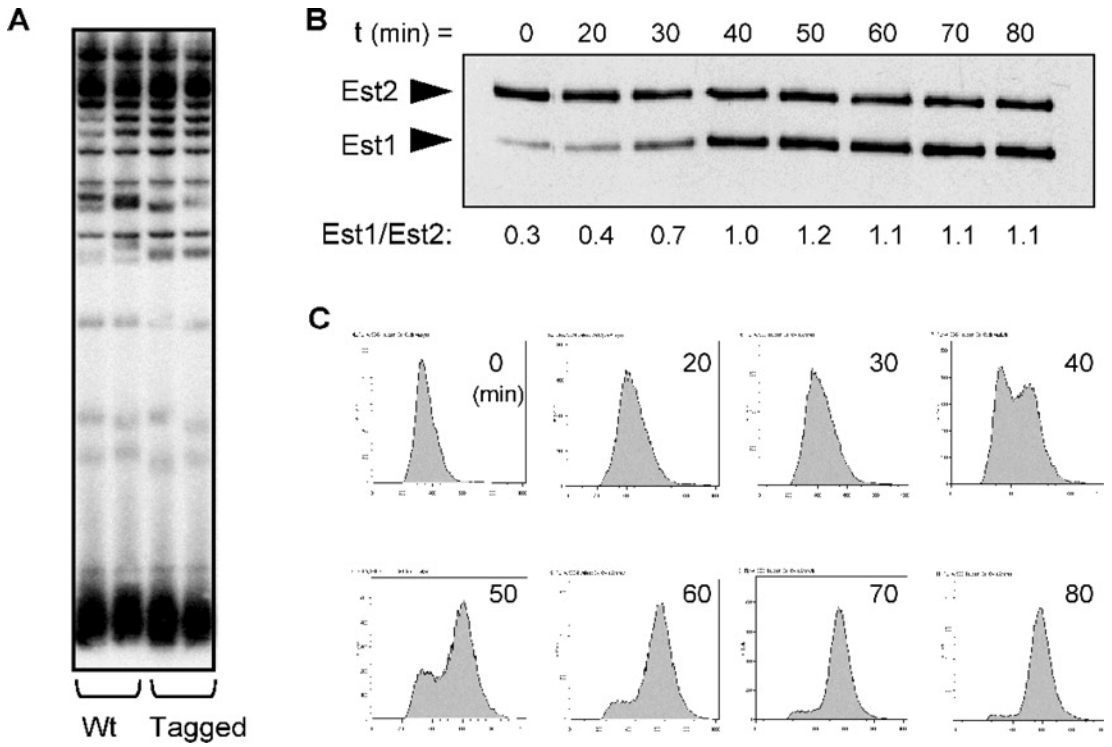

Figure 5.1 Est1:Est2 stoichiometry through the cell cycle. A) Telomere length of a wild-type strain (lanes 1 and 2) compared to an Est1-$(myc)_{12}$ $(FLAG)_3$-$(myc)_{12}$-Est2 strain (lanes 3 and 4). B) An anti-myc Western blot of anti-FLAG immunoprecipitates prepared from cultures released from a G1 phase arrest. C) FACS analysis of the cultures used for panel B. An independent repeat is shown in Figure 5.5.

We recently used this assay to demonstrate that Est1 interacts with the telomerase complex in a 1:1 stoichiometry relative to Est2 (Lubin et al., 2012). This previous experiment monitored telomerase in an asynchronous culture, which might miss transient perturbations in the Est1:Est2 ratio. To address this, Est1 and Est2 protein levels in Est2 IPs were examined through the cell cycle. Cells were arrested in the G1 phase by treatment with α-factor; aliquots were collected every 10 min after release into the cell cycle, and anti-FLAG IPs were examined for the presence of the Est1 and Est2 proteins by anti-myc Western blots. In cells arrested in the G1 phase, the level of Est1 in the complex was ~3-fold below that of Est2 (Figure 5.1b). However, following release into the cell cycle, the amount of Est1 protein in Est2 IPs began to increase. By the second time point after release, the ratio of Est1 to Est2 was already 0.7:1, and by 40 min, when a large percentage of cells were still progressing through the S phase (Figure 5.1c), the ratio was 1:1, which was maintained as cells continued into the G2/M phase (Figures 5.1 and 5.5). These results show that a telomerase complex containing Est1 and Est2 is assembled early in the S phase, well before the period when telomerase elongates telomeres (Marcand et al., 2000).

Although Est1 protein levels in extracts were in excess throughout most of the cell cycle, Est1 and Est2 were roughly equivalent in the G1 phase (Figure 5.5). As pointed out previously (Osterhage et al., 2006), lower Est1 protein levels could account for the reduced amount of Est1 in the telomerase complex at the start of the cell cycle. To test this, a strain was created with a tandem duplication of Est1-$(myc)_{12}$, thereby increasing the dosage of Est1 by 2-fold. When the telomerase stoichiometry

from this tandem duplication strain was examined, the ratio of Est1 to Est2 was 1:1 even in Est2 IPs from cells arrested in the G1 phase (Figure 5.2a). This ratio was constant throughout the cell cycle (Figures 5.2 and 5.6), indicating that when Est1 protein levels were no longer limiting, the Est1:Est2 ratio in the telomerase complex was continuously maintained at 1:1.

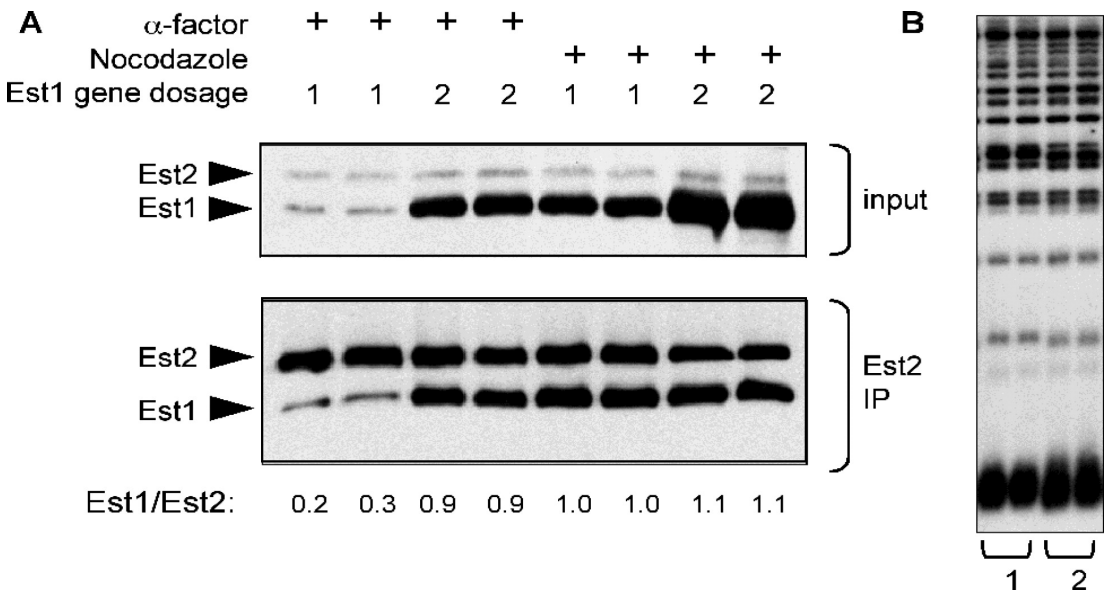

Figure 5.2 Constitutive association of Est1 with telomerase does not impact telomere length. A) Anti-myc Western blots of inputs and anti-FLAG IPs from isogenic strains bearing one or two copies of Est1-$(myc)_{12}$, arrested in the G1 (α-factor) or G2/M (nocodazole) phase. B) Telomere length of wild-type and tandem duplication strains (indicated by 1 or 2, respectively, equivalent to one or two copies of *EST1*).

However, even though Est1 was constitutively associated with the complex, there was no impact on telomere length. The effects of a 2-fold increase in Est1 gene dosage on telomere length were examined in the strain bearing the tandem duplication of Est1-$(myc)_{12}$ (Figure 5.2b) and also in a strain with a tandem duplication of Est1 in an otherwise completely wild-type strain (data not shown). These observations establish that regulated association of Est1 with the telomerase complex does not contribute to telomere homeostasis, in contrast to previous proposals (Osterhage et al., 2006; Taggart et al., 2002).

An alternative source of telomere length regulation stems from the interaction between Est1 and the telomere-bound Cdc13 protein, which led us to propose that Cdc13 recruits telomerase to its site of action by binding the Est1 telomerase subunit (Evans and Lundblad, 1999; Nugent et al., 1996). This model was further supported by a genetic relationship between *CDC13* and *EST1*, as revealed by the behavior of reciprocal cosuppressing mutations in these genes (Pennock et al., 2001). Whereas *cdc13-2* and *est1-60* single-mutant strains each exhibit a severe telomere replication defect, telomeres are restored to near wild-type length in the *cdc13-2 est1-60* double-mutant strain (Pennock et al., 2001). These two alleles are "charge swap" mutations (*cdc13-2* and *est1-60* correspond to E → K and K → E mutations, respectively), indicating that this genetic relationship had uncovered a salt bridge that contributes to the binding between Est1 and Cdc13.

This was recently challenged by an in vitro assessment of the potential interaction between recombinant Est1 and Cdc13 proteins expressed in *Escherichia*

coli, as the association between these two proteins was not abolished by mutations in either protein in this in vitro binding assay (Wu and Zakian, 2011). However, expression of soluble, nonaggregated versions of full-length Cdc13 and Est1 proteins has been a substantial technical hurdle for multiple laboratories (Anderson et al., 2002 and personal communication of D. Wuttke). Thus, the inability to recapitulate the genetic observations in this prior study (Wu and Zakian, 2011) might simply reflect an inability to obtain structurally well-behaved recombinant Est1 and Cdc13 proteins from *E. coli*.

This potential caveat prompted us to examine the association between the Est1 and Cdc13 proteins in yeast extracts, using a strain with $(myc)_{12}$ and $(FLAG)_3$ epitopes on Est1 and Cdc13, respectively, with each tagged protein expressed from its endogenous promoter. Following anti-FLAG IP from extracts, an interaction between Cdc13 and Est1 could be detected, albeit at low levels (Figure 5.3a). The weak binding of Est1 to Cdc13 was consistent with past challenges in observing this interaction from yeast extracts using proteins expressed at endogenous levels (Li et al., 2009). Nevertheless, the signal was clearly above background, as assessed by a control anti-FLAG IP from a strain lacking the $(FLAG)_3$ epitope on Cdc13 (lanes 5 and 6 of Figure 5.3a). Additional controls further support the specificity of this interaction (Figure 5.8) and also demonstrate that it is not mediated by a DNA bridge (Figure 5.9).

The ability to detect binding between Est1 and Cdc13 allowed us to ask about the impact of defects in either protein on this association. As predicted, the recruitment-defective Cdc13-2 mutant protein had lost the ability to IP the Est1

protein (Figure 5.3b). Strikingly, binding between the mutant Cdc13-2 and Est1-60 proteins was restored to a degree that was comparable to that of the wild-type Cdc13–Est1 interaction. This result was highly reproducible, as it was observed in three independent experiments. These biochemical results therefore recapitulate our prior genetic observations (Pennock et al., 2001), supporting the conclusion that these two proteins interact in vivo through surfaces defined by the location of these two mutations.

We also exploited the increased levels of Est1 protein in the strain bearing a tandem duplication of *EST1* to ask if the Est1–Cdc13 association could be observed in the G1 phase of the cell cycle. An additional copy of the $(myc)_{12}$-tagged *EST1* gene was introduced into the Cdc13-$(FLAG)_3$ strain, and anti-FLAG IPs from α-factor-arrested cells were examined on anti-myc Western blots. Notably, an interaction was observed between Est1 and Cdc13, in a *cdc13-2*-dependent manner (Figure 5.3c), in a phase of the cell cycle when telomerase does not elongate telomeres (Marcand et al., 2000). This argues that the physical interaction between Est1 and Cdc13 is not dependent on cell cycle-specific regulatory event(s) and does not require prior binding of Cdc13 to telomeres.

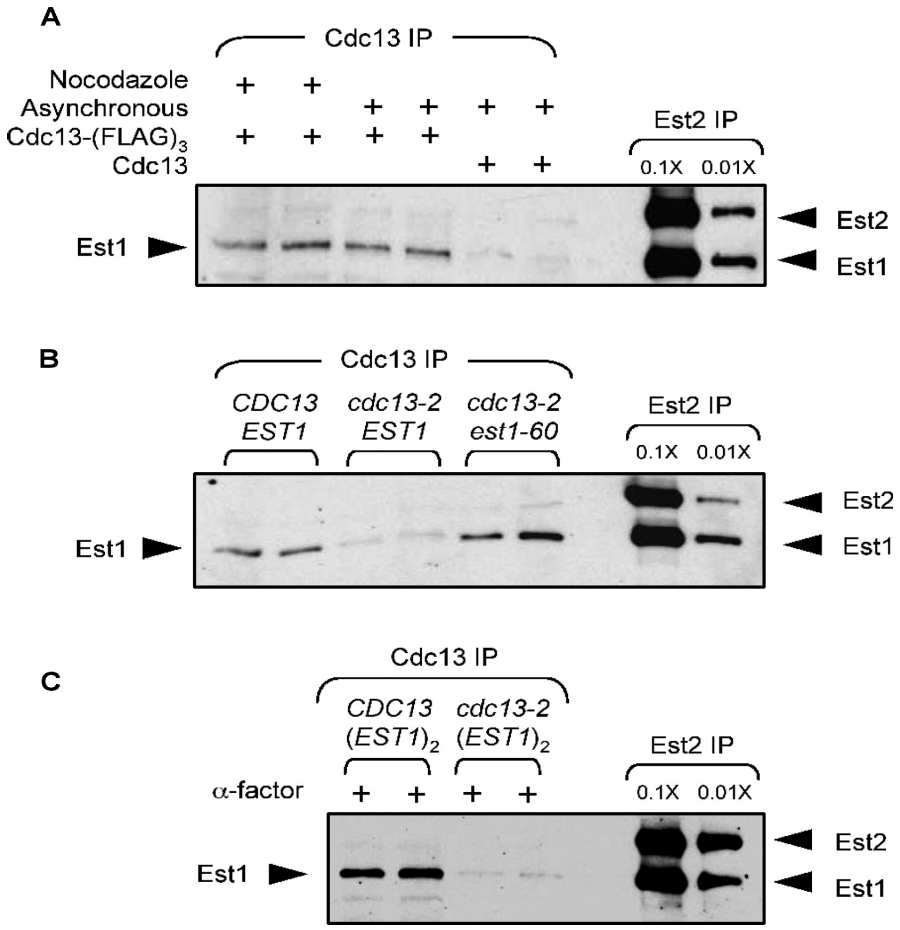

Figure 5.3 Interaction between Est1 and Cdc13. A) Anti-myc Western blots of anti-FLAG IPs prepared from strains expressing Cdc13-$(FLAG)_3$ (lanes 1–4), Cdc13 (lanes 5 and 6), or $(FLAG)_3$-$(myc)_{12}$-Est2 (0.1× and 0.01× indicate the amount of IP relative to the amount loaded in lanes 1–6). B) Same as panel A, but mutations were introduced at the genomic location of the tagged Est1 and Cdc13 proteins. C) Same as panel A, but using *CDC13* and *cdc13*-2 versions of the tandem duplication [Est1-$(myc_{12})]_2$ strain used in Figure 5.2.

This study shows that association of the Est1 protein subunit with the catalytic core is not a regulatory event that contributes to telomere homeostasis. In contrast, binding of Cdc13 to telomeres is highly regulated, with association peaking in the late S phase (Taggart et al., 2002; Takata et al., 2004). This suggests a simple model in which assembly of a recruitment-competent telomerase complex containing both Est1 and Est2 occurs early in the cell cycle. Subsequent binding of chromosome termini by Cdc13 allows recruitment of the telomerase holoenzyme, through a direct interaction between Cdc13 and the Est1 subunit of the telomerase holoenzyme (Figure 5.4). These results, which are also supported by live cell imaging of the telomerase RNA in single cells (Gallardo et al., 2011), argue that a primary regulatory event that initiates telomere elongation during the late S phase is the regulated association of Cdc13 with telomeres.

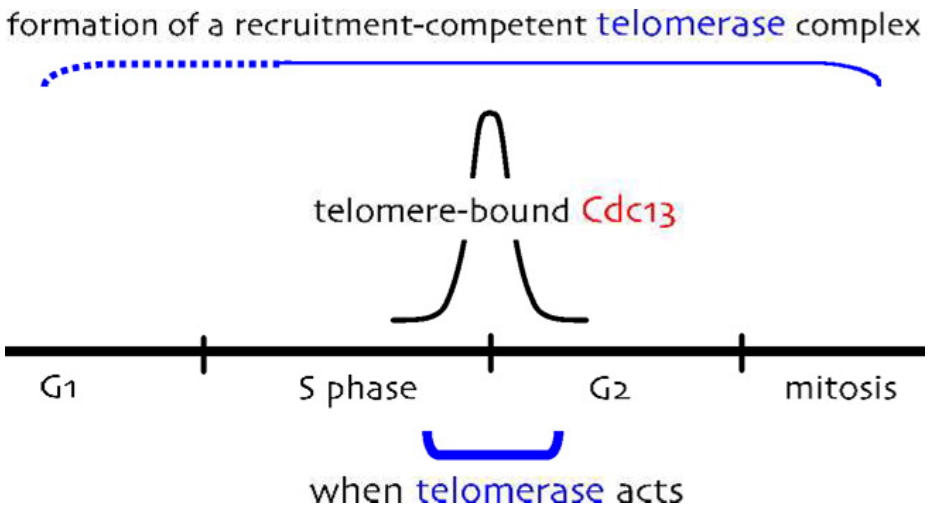

Figure 5.4 A model in which regulated binding of Cdc13 to chromosome termini dictates subsequent interaction of a recruitment-competent telomerase complex with telomeres.

Materials and methods

Genetic methods (telomere length analysis and flow cytometry) were performed as previously described (Lendvay et al., 1996; Paschini et al., 2010). Telomere length in Figures 5.1 and 5.2 was assessed from two single colonies from the relevant strains (which were isogenic in each case), following propagation for ~ 75 generations. For biochemical experiments, YVL3493 (*MAT***a** Est1-$(Gly)_6$-$(myc)_{12}$ $(FLAG)_3$-$(myc)_{12}$-$(Gly)_6$-Est2 *leu2 trp1 ura3-52 prb prc pep4-3*), or isogenic derivatives of YVL3493 constructed using standard yeast strain manipulation techniques, were used (Lubin et al., 2012). For immunoprecipitations, whole cell extracts were prepared from 250 ml cultures grown to O.D. 0.8 – 1.0, with extract preparation and incubation with anti-FLAG M2 beads (Sigma), as described previously (Evans and Lundblad, 2002; Lubin et al., 2012). Both $(FLAG)_3$-$(myc)_{12}$-Est2 and Cdc13-$(FLAG)_3$ could be quantitatively depleted from yeast extracts, as indicated in Figures 3.8 and 5.7. Immunoprecipitates containing Myc- and FLAG-tagged proteins were resolved on 6% SDS-PAGE gels probed with either anti-myc 2272 (Cell Signaling Technology) at 1:1000 or anti-FLAG F7425 (Sigma-Aldrich) at 1:2000 dilution, respectively, followed by anti-rabbit IgG HRP conjugate (Promega) at 1:10,000 and subsequent ECL (enhanced chemiluminescence) detection with pre-flashed film; protein signals were quantitated using FUJIFILM Science Lab Image Gauge. ECL was used rather than alternative options (such as Li-cor Odyssey) because the former protocol had substantially less background, resulting in a significantly higher signal-to-noise ratio. Although the linear detection range is more limited with

ECL, the dilution series in Figure 3.10 (as well as the more restricted dilution series shown in Figure 5.3) demonstrates that even 2-fold differences can be quantitatively observed over a ~10-fold range for a given exposure.

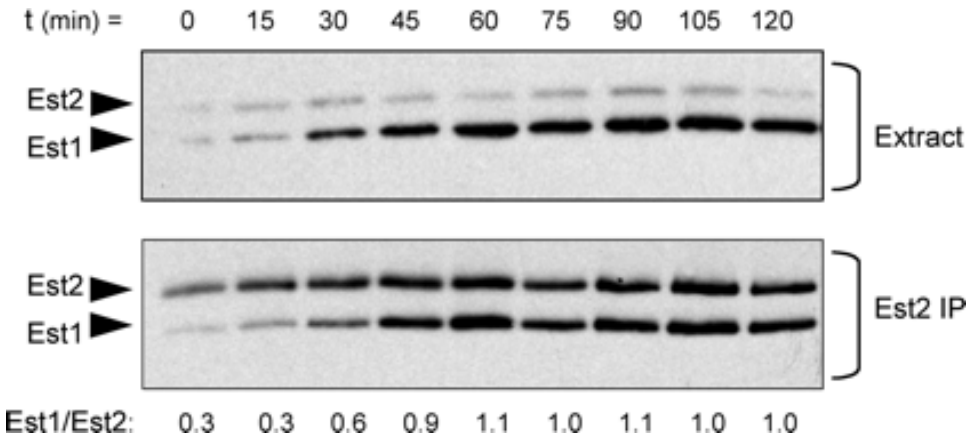

Figure 5.5 Est1:Est2 stoichiometry through the cell cycle (an independent repeat of the experiment shown in Figure 5.1). A culture of the Est1-$(myc)_{12}$ $(FLAG)_3$-$(myc)_{12}$-Est2 strain was released from a G1 arrest (t = 0), and Est1 and Est2 protein levels in extracts (top) and anti-FLAG immunoprecipitates (bottom) were monitored by anti-myc western analysis at the indicated time points. By simultaneously monitoring Est1 and Est2 protein levels in extracts (top panel), this shows that the widely-held assumption that Est1 is present at lower levels than Est2 during early stages of the cell cycle is incorrect.

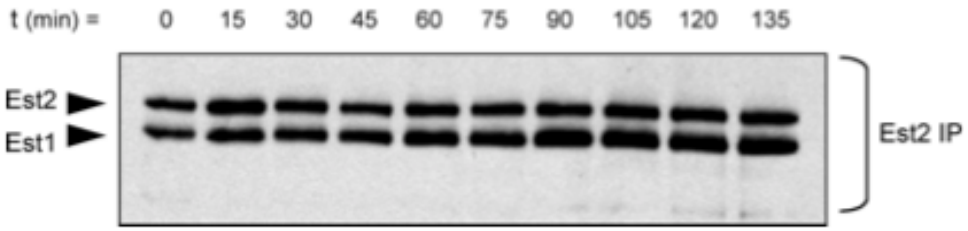

Figure 5.6 Constitutive association of Est1 with telomerase throughout the cell cycle in a strain containing a tandem duplication of Est1-(myc)$_{12}$. Experiment performed as in Figure 5.5.

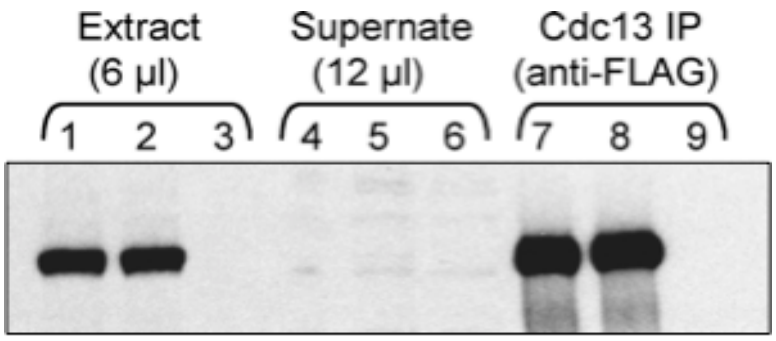

Figure 5.7 Cdc13 is depleted from extracts by anti-FLAG immunoprecipitation. Anti-FLAG western monitoring the Cdc13-$(FLAG)_3$ protein in extracts, immunoprecipitates and supernate, analyzed as in Figure 3.8. In lanes 3, 6 and 9, the genomic copy of *CDC13* lacks the $(FLAG)_3$ epitope.

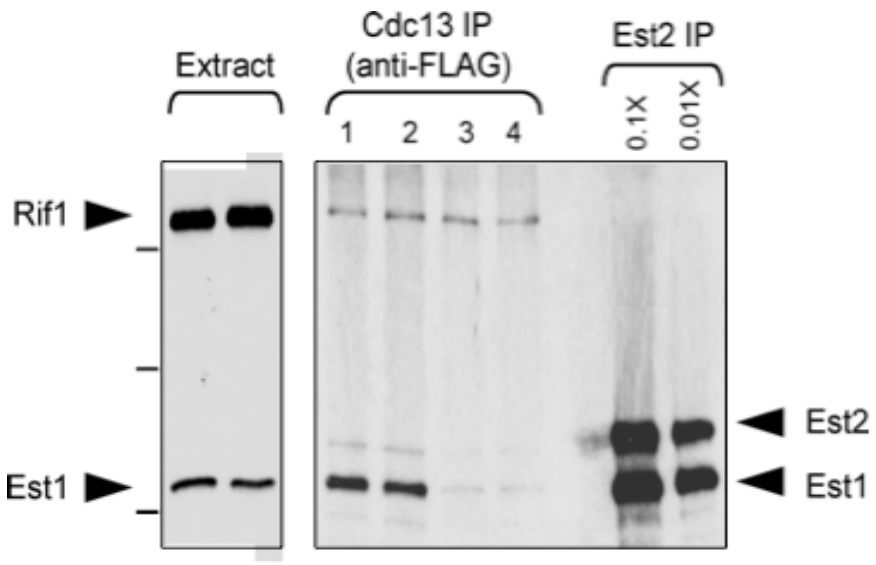

Figure 5.8 The association between Cdc13-(FLAG) and Est1-$(myc)_{12}$ is not an artifact of the $(myc)_{12}$ tag on Est1. Anti-FLAG immunoprecipitates from two strains which both express Est1-$(myc)_{12}$ and Rif1-$(myc)_{13}$ but differ by the presence or absence of a $(FLAG)_3$ epitope on the C-terminus of Cdc13. In contrast to the enrichment of Est1 in the anti-Cdc13 IPs compared to mock IPs, there is no enrichment of Rif1 (lanes 1-2 *vs*. lanes 3-4). Left-hand panel shows relative levels of Rif1-$(myc)_{13}$ and Est1-$(myc)_{12}$ in extracts; both right and left panels are anti-myc westerns. Size markers (indicated by hatch marks) correspond to 250, 150 and 100 kDa, respectively.

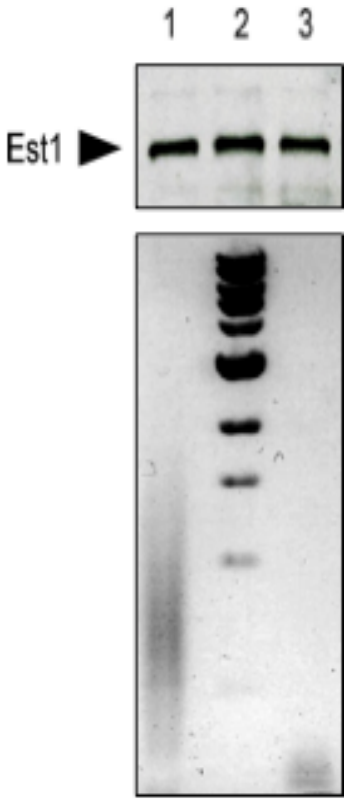

Figure 5.9 The association between Cdc13 and Est1 is not sensitive to DNase I. Anti-FLAG immunoprecipitates prepared from a strain expressing Est1-$(myc)_{12}$ and Cdc13-$(FLAG)_3$ were treated with 10 units of DNase (lanes 1 and 3; independently prepared isolates) or mock treated (lane 2), with 5 μg of 1 kb DNA size ladder added prior to DNase treatment. Upper panel is an anti-myc western monitoring the level of the Est1-$(myc)_{12}$ protein in IPs, lower panel is an EtBr-stained 0.7% agarose gel.

Acknowledgements

Chapter 5 is a formatted reprint of the material as it appears in Tucey, T.M., and Lundblad, V. (2013). A yeast telomerase complex containing the Est1 recruitment protein is assembled early in the cell cycle. Biochemistry *52*, 1131-1133. The dissertation author was the primary researcher of this paper. Reprinted with permission from American Chemical Society, copyright, 2013.

Chapter 6: Identification of four functionally distinct interfaces on Est1

Introduction

The first telomerase subunit, *EST1*, was identified in a screen for genes with defective telomere maintenance (Lundblad and Szostak, 1989). *est1*-Δ cells display the same cellular senescence phenotype as cells lacking either the catalytic protein subunit of telomerase or its template-containing RNA subunit. However, although Est1 is required for telomere maintenance *in vivo*, standard primer extension assays for telomerase activity *in vitro* are not Est1 dependent, suggesting that it performs a telomerase regulatory function (Cohn and Blackburn, 1995). *EST1* encodes for a 699 amino acid protein that originally appeared to lack any obvious structural motifs.

Est1 has been shown to contribute multiple biochemical activities. Est1 binds to the TLC1 RNA, and the bulged stem structure on the RNA that mediates this interaction has been extensively characterized (Seto et al., 2002; Lubin et al., 2012; also see Chapter 4 of this dissertation). Est1 also has weak single-stranded G-rich DNA-binding activity (Virta-Pearlman et al., 1996; Zhang et al., 2010). Furthermore, there is genetic and biochemical evidence that Est1 physically associates with Cdc13, a single-stranded DNA-binding protein involved in telomere capping and maintenance (Nugent et al., 1996; Evans and Lundblad, 1999; Tucey and Lundblad, 2013; also see Chapter 5 of this dissertation). This interaction is direct, because an allele of *CDC13* (*cdc13-2*) that results in telomere shortening can be rescued by a compensatory mutation in *EST1* that restores a putative electrostatic interaction between the two proteins (Pennock et al., 2001). Additional studies have shown that Est1 also contributes to telomere elongation separate from telomerase recruitment, although the

precise nature of this biochemical activity remains unclear (Evans and Lundblad, 2002).

Despite an accumulation of evidence for Est1 providing multiple functions in telomere maintenance, what is lacking from these analyses is a rigorous dissection of the domains on Est1 involved in each of these biochemical activities. There are conflicting reports that Est1's TLC1 RNA binding domain is located at the C-terminus (Zhou et al., 2000) versus the N-terminus (Evans and Lundblad, 2002) and the precise boundaries of either of these proposed RNA binding domains are unclear. Est1's single-stranded G-rich DNA-binding activity resides between amino acids 435 – 565 (Virta-Pearlman et al., 1996), but this is also within the region where the Cdc13 recruitment defective allele, *est1-K444E*, resides. Additional *est1*$^{-}$ alleles involved in the Cdc13 interaction have yet to be identified and the precise boundaries of the Cdc13 interaction domain are unclear, as well as defining whether it constitutes a separate region from the DNA-binding activity. Additional Est1 domains could exist for facilitating Est3 association with the telomerase complex, and potentially, interactions with other factors. This chapter aims to address these issues by combining genetics with biochemistry to rigorously define the domains on Est1 involved in some of these activities.

Est1 homologs have been identified and characterized across the eukaryotic spectrum (Beernink et al., 2003; Fukuhara et al., 2005; Reichenbach et al., 2003; Singh et al., 2002). This has had several important consequences. First, it established that Est1 was not simply a budding yeast-specific telomerase-associated protein,

indicating that observations about the *S. cerevisiae* Est1 protein should extrapolate to other systems, including human cells. Indeed, in other organisms, Est1 homologs similarly associate with telomerase and regulate telomere length and stability, although in some instances their precise contributions to telomere function are still being uncovered. Furthermore, alignment of multiple Est1 homologs revealed several conserved regions that are likely to constitute separate domains. Two domains are located in the N-terminus – domain A and the TPR domain – and there is a third conserved domain in the C-terminus of the protein. This provides a basis for determining which of Est1's reported biochemical activities map to these domains.

The TPR domain contains the region of greatest homology among the Est1 proteins and consists of two tetratricopeptide repeat (TPR) consensus sequences (Clissold and Ponting, 2000). A TPR repeat is a protein-protein interaction module, found in numerous, functionally diverse proteins and usually present in tandem arrays of three or more repeats (D'Andrea and Regan, 2003). Each repeat consists of 34 amino acids with a very weak consensus sequence, defined by a large pattern of large and small amino acids. Each repeat forms two anti-parallel alpha helices, and tandem arrays of repeats pack together to form a right handed helical structure with an amphipathic groove which provides a binding site for the cognate protein. The residues lining the surface of this groove give each TPR structure specificity for its particular binding partner. Given the role of TPR repeats in other proteins, it is likely that the TPR domain in Est1 similarly serves as a protein (or RNA) binding domain, and several mutations have been identified in this domain that affect telomere length

maintenance in a manner that is separate from telomere recruitment (Sealey et al., 2011).

Upstream from the TPR domain is domain A, which is less conserved and poorly understood, but intriguingly, appears to consist of two atypical TPR-like repeats that might similarly be forming a protein-protein or protein-RNA interaction module (Fukuhara et al., 2005). However, given the poor alignment in this region, it is difficult to recognize the particular amino acids responsible for folding into alpha helices, and it is possible that the TPR domain and domain A actually comprise a single module in the N-terminus. The C-terminal domain of Est1 is also weakly conserved, but notably, the Cdc13 interaction residue, K444, as well as other residues in this region, are well-conserved across yeast species. Like with the N-terminus, it is unclear whether the C-terminal domain consists of a single module, or whether there are separate, smaller domains with distinct biochemical functions.

Using a combined genetics and biochemical approach, I have identified four functionally distinct interfaces on Est1, in collaboration with John Lubin in the Lundblad lab. Domain A consists of a ≈70 amino acid RNA-binding domain, and unexpectedly, the association of Est1 with TLC1 appears to be confined to this region. The TPR domain has not been assigned a biochemical function, but critical residues were identified that are not involved in RNA binding and appear to have another yet-to-be-determined binding partner. A cluster of amino acids in the C-terminal domain of Est1 contains a Cdc13-interacting interface, while a separate cluster of amino acids in the C-terminus contains an Est3-associating interface.

Finally, I performed some experiments to investigate the relationship between Est1 and Ebs1. In the *Saccharomyces* clade, Est1 and Ebs1 are paralogs that arose through whole-genome duplication and appear to serve distinct functions in telomere maintenance and nonsense mediated decay (NMD), respectively (Hsu et al., 2012; Luke et al., 2007); whereas other eukaryotes appear to have a single homologue that retains both telomere and NMD regulatory properties. The crystal structure of the human Ebs1 homologue, SMG7, has been solved, and the TPR repeats form a 14-3-3-like domain for binding phosphoserine-containing peptides (Fukuhara et al., 2005). Intriguingly, the TPR repeats in Est1 lack the cleft for binding phosphorylated proteins, suggesting that the TPR domain has a different function in Est1. Based on sequence alignment, many of the critical Est1 residues identified in this chapter also are conserved in Ebs1, and given that Est1 and Ebs1 share a common ancestor, it is possible that they have some functional overlap that would be useful for understanding both proteins, not only in *S. cerevisiae* but also in other species.

Results

Est1 consists of two biochemically distinct halves

The Est1 protein ranges in size from ≈700-800 amino acids in the *Saccharomyces* clade to as small as 491 amino acids in the fission yeast Est1 telomerase subunit. Only two regions of Est1 protein family members share a significant degree of homology: (1) an N-terminal region that includes domain A and a diverged version of the TPR domain; and (2) a C-terminal region that has previously

been shown to bind single-stranded telomeric DNA (Virta-Pearlman et al., 1996) and also contains the conserved residue K444 which is involved in a direct interaction with Cdc13.

Based on alignments of Est1 proteins in the *Saccharomyces* clade, truncated constructs were created to express either the N- or C-terminal halves of Est1, with the boundary of the truncations positioned at amino acid 340, in an region of high divergence that is therefore unlikely to be important for Est1 function (Figure 6.1a). I was able to express and detect the N-terminal (aa1-340) and C-terminal (aa340-699) halves of Est1 from *CEN* plasmids, with each protein containing the same $(myc)_{12}$ tag, and full-length Est1-$(myc)_{12}$ also included for comparison (Figure 6.1b). The ability to express these two halves of Est1 as biochemically discrete proteins suggests that they contain different binding partners.

Association with the telomerase complex was monitored by immunoprecipitation of the Est2 catalytic subunit, which contained a $(FLAG)_3$ epitope in addition to the $(myc)_{12}$ tag (see Chapter 3 for a detailed description of this biochemical assay). When strains expressing the N- and C-terminal halves of Est1 from *CEN* plasmids were examined in this immunoprecipitation assay, only the N-terminal half associated with the complex. No association of the C-terminal half was observed, even though the truncated protein could stably express (Figure 6.1b).

Because the truncated proteins were expressed from plasmids in Figure 6.1b, the wild-type copy of *EST1* was still present in the genome and potentially interfering with the ability of the tagged proteins to associate. Indeed, the stoichiometry of full-

length Est1 in the complex in Figure 6.1b is about half of what is normally observed when using an integrated strain, suggesting that untagged wild-type Est1 is competing for association in the complex. To more directly assess the N- and C-terminal halves of Est1, each was integrated into the genome in place of the full-length Est1 protein, in a strain where $(FLAG)_3$-myc_{12}-Est2 was also integrated. As shown in Figure 6.1c, the result was reproducible when using integrated strains – i.e. the N-terminal half of Est1 could associate with telomerase, but not the C-terminal half. Both strains were also observed to senesce upon further propagation, providing additional confirmation that the N- and C-terminal halves each have critical and distinct functions.

To further increase expression levels of the truncated proteins, the plasmids used in Figure 6.1b were transformed into the integrated strains. In Figure 6.1d, expression levels of the C-terminal half of Est1 were increased to levels comparable to that of full-length Est1, while the N-terminal half expressed about 2-fold lower, suggesting that it might be slightly unstable. However, despite the increased level of expression, the C-terminal half of Est1 was still unable to associate with telomerase. Once again, the N-terminal half of Est1 was observed to associate with telomerase, but to a lower extent than full-length Est1, presumably due to the decreased level of expression. The results from these three separate experiments consistently implicates the N-terminal half of Est1 as containing the domain required for Est2 association, presumably via direct contact with the TLC1 RNA.

The lack of association of the C-terminal half of Est1 with telomerase, despite stable expression, suggested that it is performing a different biochemical activity. In

Chapter 5, I describe a biochemical interaction between the full-length Est1 and Cdc13 proteins that could be observed by co-immunoprecipitation, which was dependent on K444 of Est1, a residue located in the C-terminus. To test whether the C-terminal half of Est1 could also be detected in Cdc13 immunoprecipitates, I integrated the C-terminal construct into a strain expressing Cdc13-$(FLAG)_3$. As shown in Figure 6.1e, a weak but reproducible association of the Est1 C-terminus with Cdc13 could be detected, similar to the detection level of the interaction between full-length Est1 and Cdc13, suggesting that the domain responsible for the Est1-Cdc13 interaction is located within the C-terminal half of Est1.

Figure 6.1 Est1 consists of two biochemically distinct halves. A) Sequence alignment of Est1 proteins from the *Saccharomyces* species clade. Regions of greater conservation are shaded darker, with the three conserved domains of Est1 depicted above the alignment. Positioned below the alignment is the boundary of the N- and C-terminal halves of Est1 that were used for the deletion analysis in panels B through E. B) Anti-myc western of inputs and anti-FLAG IPs from extracts containing the indicated full-length, N- and C-terminal halves of Est1 tagged with $(myc)_{12}$ and expressed from *CEN* plasmids in the strain $(FLAG)_3$-$(myc)_{12}$-Est2. C) Anti-myc western of anti-FLAG IPs from extracts containing the indicated full-length, N- and C-terminal halves of Est1 tagged with $(myc)_{12}$ and genomically integrated in the strain $(FLAG)_3$-$(myc)_{12}$-Est2. D) Anti-myc western of inputs and anti-FLAG IPs from extracts containing the indicated N- and C-terminal halves of Est1 tagged with $(myc)_{12}$ and expressed both from *CEN* plasmids and genomically integrated in the strain $(FLAG)_3$-$(myc)_{12}$-Est2. E) Anti-FLAG and anti-myc westerns of anti-FLAG IPs from extracts containing the C-terminal half of Est1 tagged with $(myc)_{12}$ and integrated in the strain Cdc13-$(FLAG)_3$, compared to the untagged parental strain.

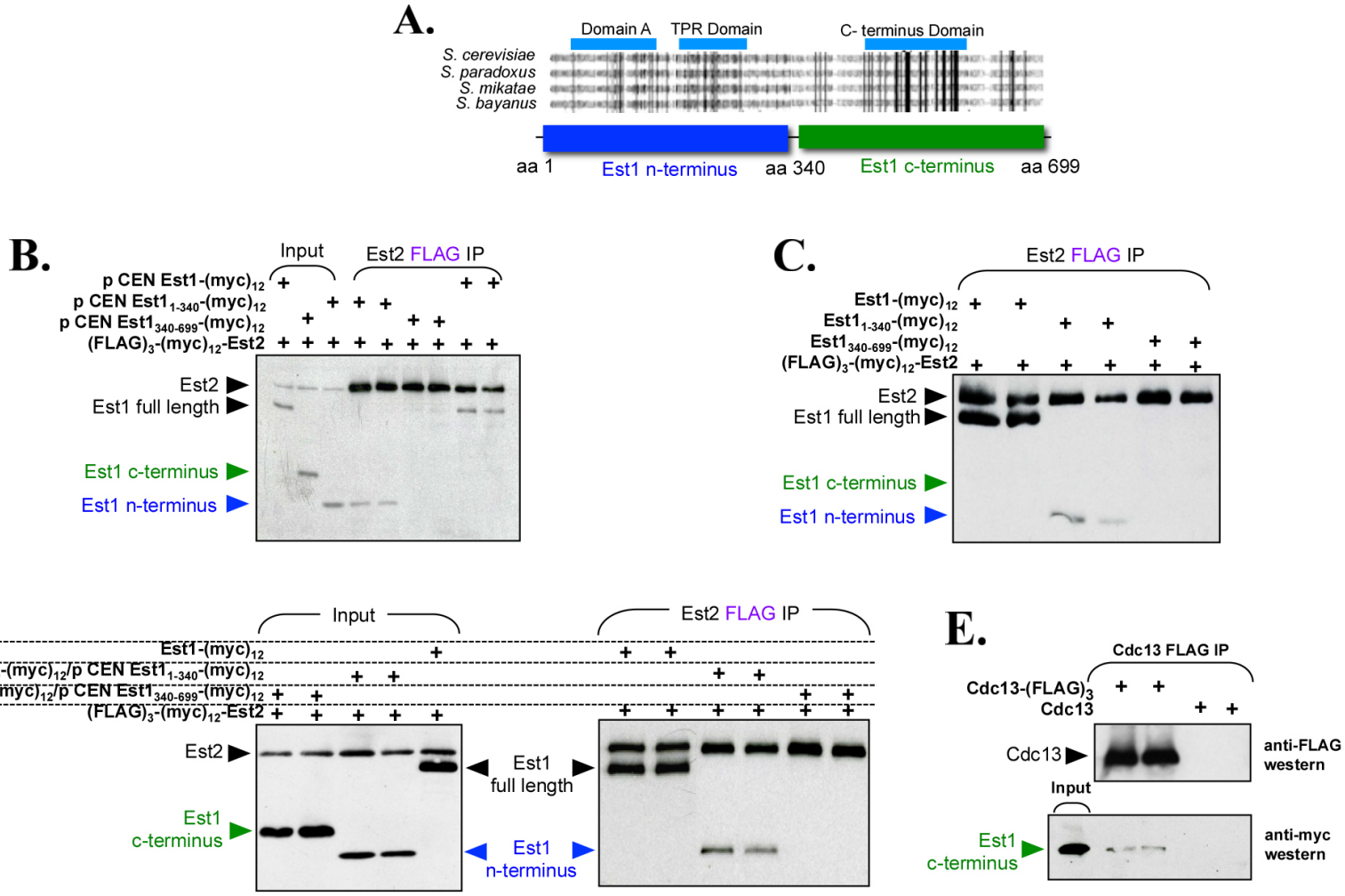
A.
Domain A
TPR Domain
C- terminus Domain
S. cerevisiae
S. paradoxus
S. mikatae
S. bayanus
aa 1
Est1 n-terminus
aa 340
Est1 c-terminus
aa 699
B.
Input
Est2 FLAG IP
p CEN Est1-(myc)12
p CEN Est1 1-340-(myc)12
p CEN Est1 340-699-(myc)12
(FLAG)3-(myc)12-Est2
Est2
Est1 full length
Est1 c-terminus
Est1 n-terminus
C.
Est2 FLAG IP
Est1-(myc)12
Est1 1-340-(myc)12
Est1 340-699-(myc)12
(FLAG)3-(myc)12-Est2
Est2
Est1 full length
Est1 c-terminus
Est1 n-terminus
D.
Input
Est2 FLAG IP
Est1-(myc)12
Est1 1-340-(myc)12/p CEN Est1 1-340-(myc)12
Est1 340-699-(myc)12/p CEN Est1 340-699-(myc)12
(FLAG)3-(myc)12-Est2
Est2
Est1 c-terminus
Est1 full length
Est1 n-terminus
E.
Cdc13 FLAG IP
Cdc13-(FLAG)3
Cdc13
Cdc13
anti-FLAG western
Input
Est1 c-terminus
anti-myc western

Mutational analysis of the N-terminus of Est1 defines the RNA-binding domain

The crude deletion analysis described above suggested that at least one biochemical activity was situated in each of the N- and C-terminal halves of Est1. In collaboration with John Lubin, we employed genetic analyses to uncover separation-of-function mutations that could be used to more precisely define these biochemical activities. Initially, John attempted to obtain dominant negative mutants by using the telomere shortening and *yku80*-Δ synthetic growth assays described in Chapter 2. This was largely successful for identifying alleles in the C-terminus of *EST1* (see next section), but despite extensive mutagenesis in the N-terminus, John was only able to obtain a few alleles that had a significant telomere replication defect when over-expressed. Therefore, we had to take a different approach to identify functionally important residues in the N-terminus.

To identify residues of interest, we used a loss-of-function assay combined with a biochemical assay for protein stability and telomerase complex stoichiometry. The N-terminal half of *EST1* contains two patches of conservation: a moderately conserved region from aa85 to 170 and a second region from 191 to 271. John targeted these two conserved regions, as well as some additional residues in other regions of the N-terminus, in a loss-of-function assay to identify mutants that have a telomere replication defect. Representative southern blots from this analysis are shown in Figures 6.2 – 6.4, and the key residues are highlighted in Figure 6.5.

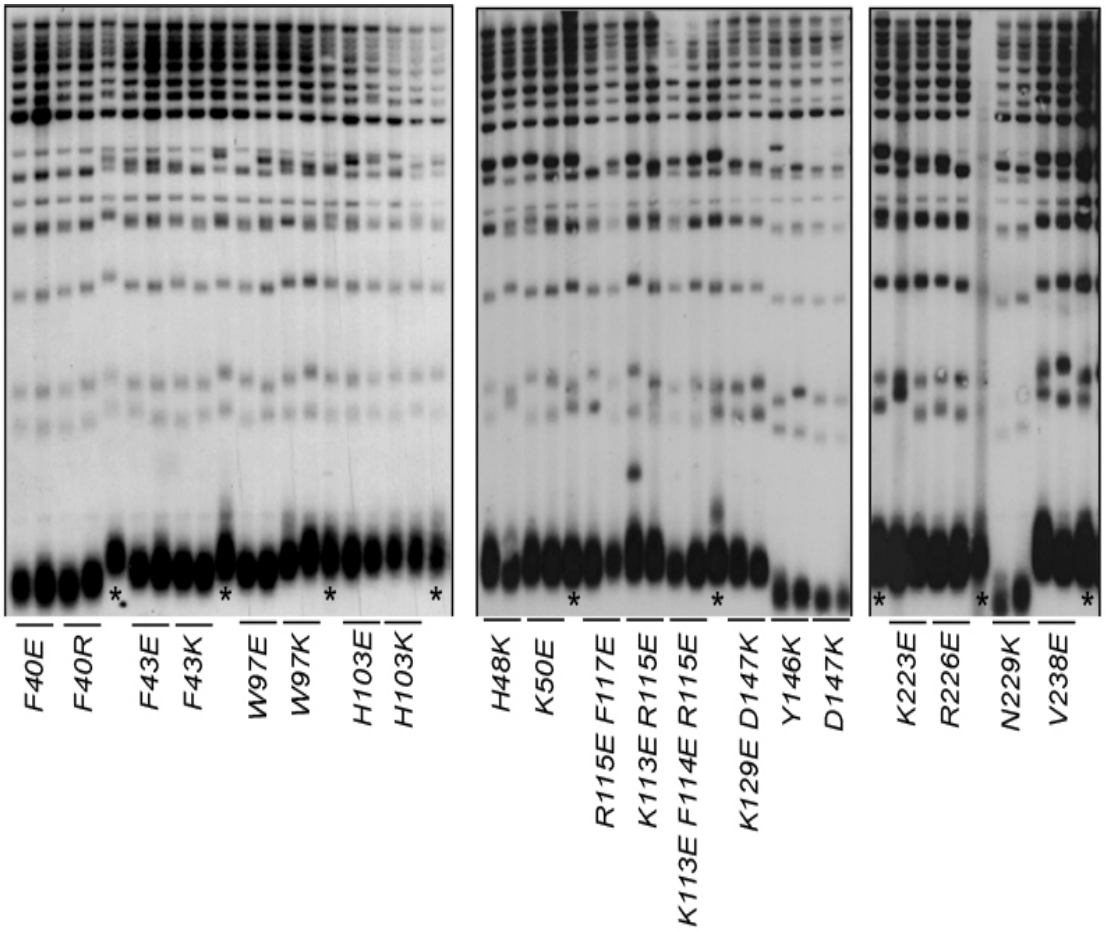

Figure 6.2 Loss-of-function telomere length analysis of *est1*⁻ mutant alleles (1 of 3). An *est1*-Δ strain was transformed with single-copy plasmids expressing either a mutant allele or the wild-type *EST1* gene, propagated for ~80 cell divisions and examined for telomere length. The wild-type *EST1* lanes are marked with asterisks. The southern blots in this figure were completed by John Lubin.

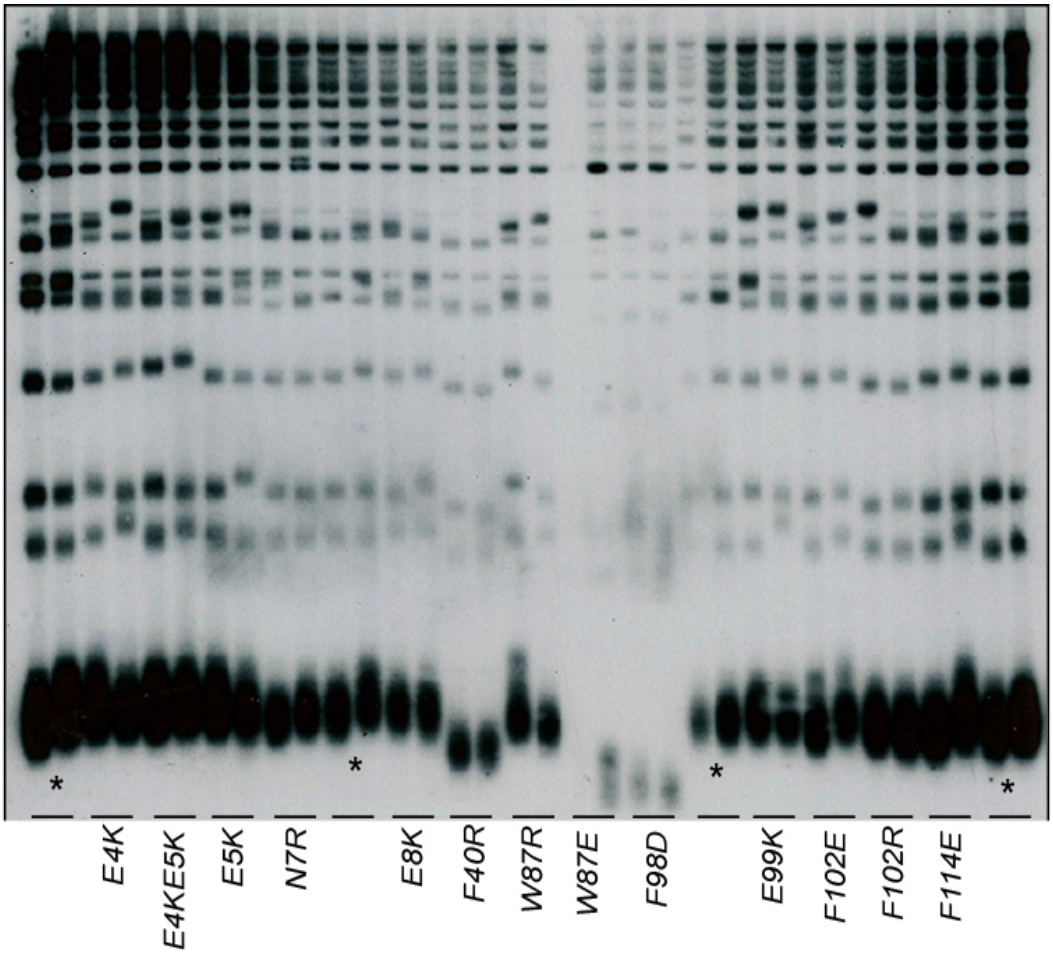

Figure 6.3 Loss-of-function telomere length analysis of *est1*⁻ mutant alleles (2 of 3). An *est1*-Δ strain was transformed with single-copy plasmids expressing either a mutant allele or the wild-type *EST1* gene, propagated for ~80 cell divisions and examined for telomere length. The wild-type *EST1* lanes are marked with asterisks.

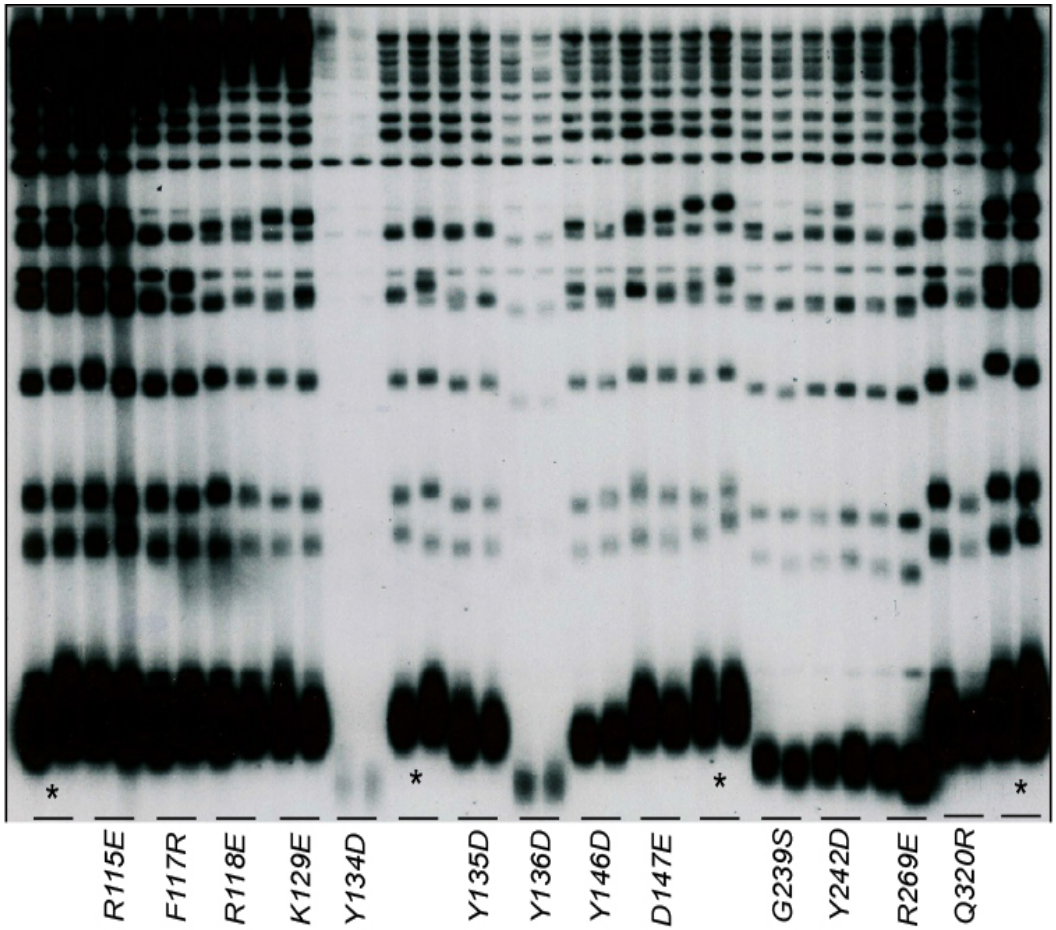

Figure 6.4 Loss-of-function telomere length analysis of *est1*⁻ mutant alleles (3 of 3). An *est1*-Δ strain was transformed with single-copy plasmids expressing either a mutant allele or the wild-type *EST1* gene, propagated for ~80 cell divisions and examined for telomere length. The wild-type *EST1* lanes are marked with asterisks.

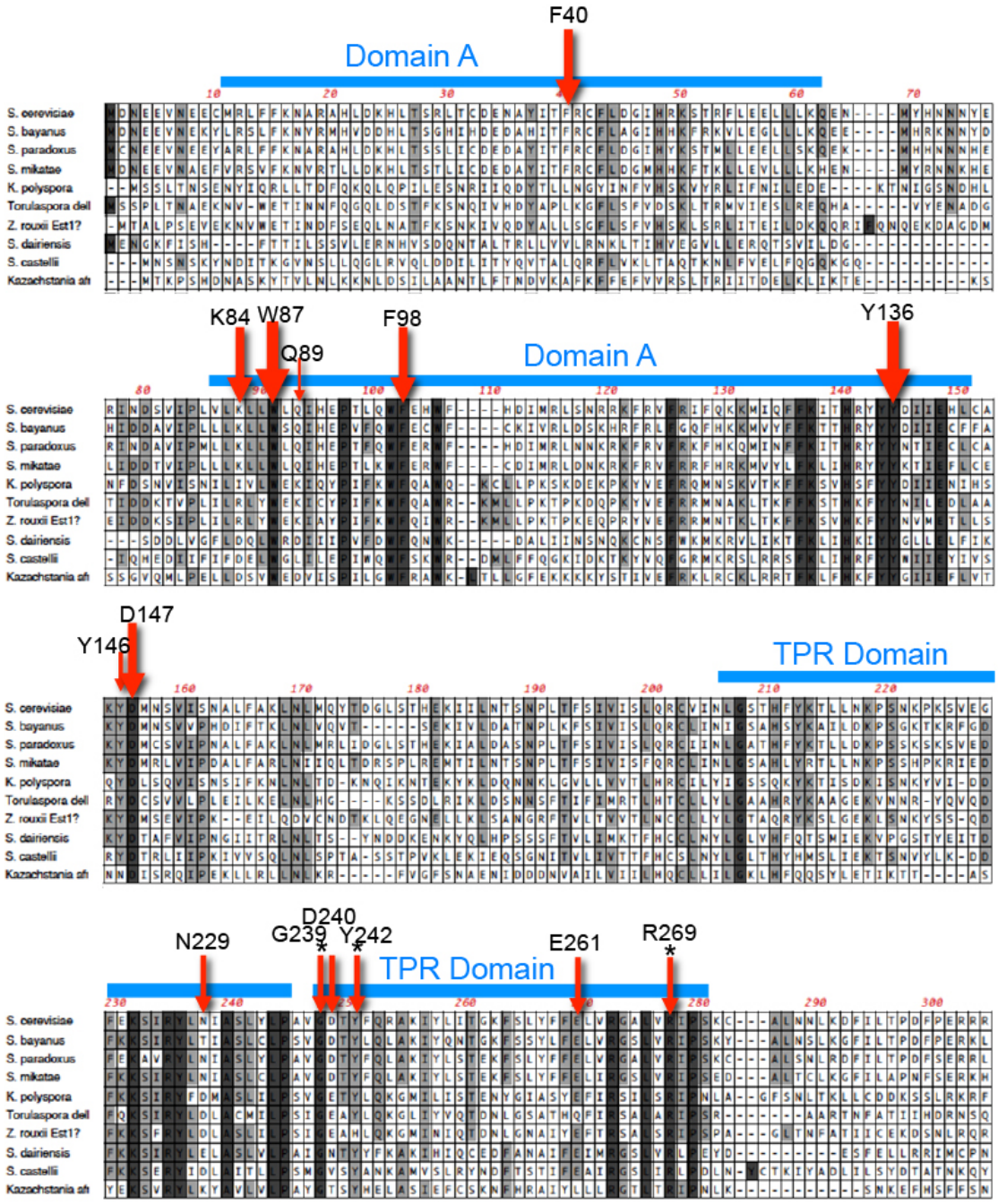

Figure 6.5 Amino acid sequence alignment of the Est1 N-terminus. Size of red arrow represents the relative severity of the loss-of-function phenotype when the indicated residue is mutated. Residues marked with an asterisk also had comparable overexpression dominant negative phenotypes.

Based on the loss-of-function results, I incorporated 26 mutations into a plasmid expressing Est1-$(myc)_{12}$ and introduced them into an *est1-*Δ *$(FLAG)_3$-$(myc)_{12}$-Est2* strain. Mutants were analyzed for protein stability as well as ability to co-immunoprecipitate with Est2. Figure 6.6 highlights the westerns from this analysis, and the corresponding telomere length of the transformant strains is displayed in Figures 6.7 and 6.8. Intriguingly, a large proportion of the mutants had a significant decrease in the ability to associate with telomerase. However, when analyzing telomere length, it became apparent that the parental Est1-$(myc)_{12}$ plasmid was unable to fully complement, and overall, the telomere shortening phenotypes caused by a given mutant were considerably more severe than in the loss-of-function assay.

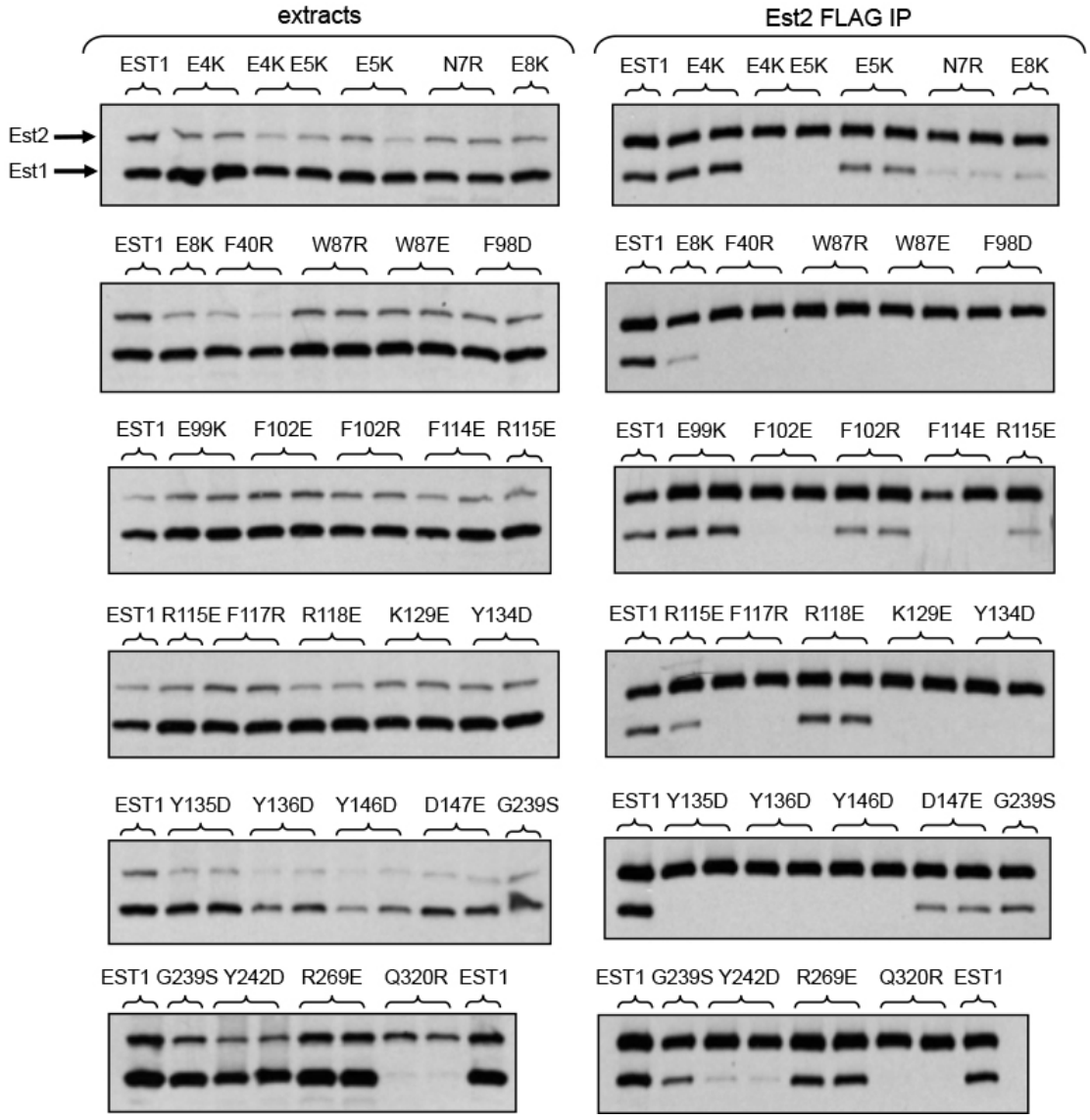

Figure 6.6 Western blot analysis of (myc)$_{12}$ tagged *est1*$^{-}$ mutant alleles when expressed from *CEN* plasmids. Plasmid-borne *EST1-(G)$_6$-(myc)$_{12}$* or mutant allele derivatives were transformed into strain YVL3833 [*est1*-Δ *(FLAG)$_3$-(myc)$_{12}$-(G)$_6$-EST2/*pVL367 (*EST1 URA3 CEN*)*]*, and extracts were prepared from cultures grown immediately following loss of the wild-type *EST1* covering plasmid. Left side depicts anti-myc westerns monitoring the proteins from extracts; right side depicts anti-myc westerns following anti-FLAG immunoprecipitation of Est2.

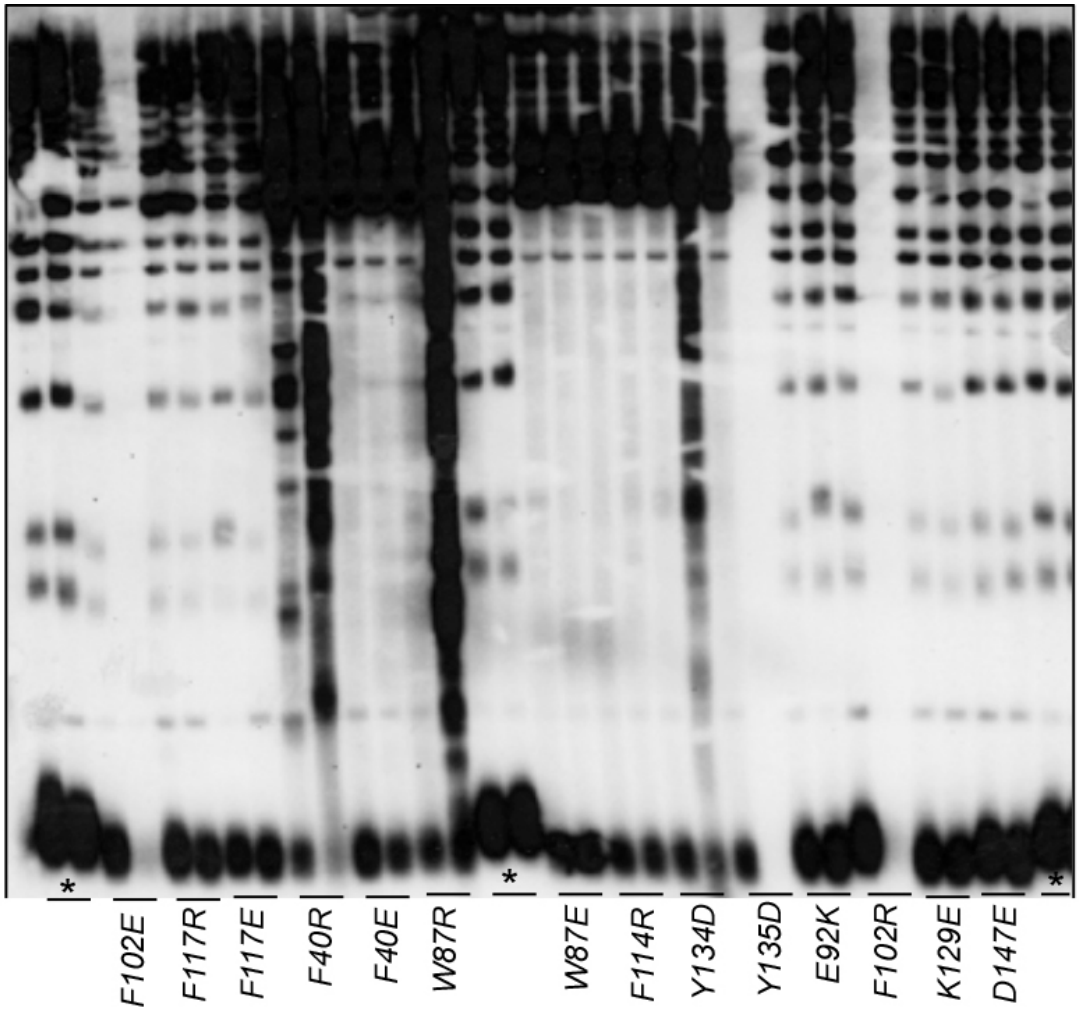

Figure 6.7 Telomere length analysis of $(myc)_{12}$ tagged *est1*$^{-}$ mutant alleles when expressed from *CEN* plasmids (1 of 2). An *est1*-Δ *$(FLAG)_3$-$(myc)_{12}$-$(G)_6$-EST2* strain was transformed with single-copy plasmids expressing *EST1-$(G)_6$-$(myc)_{12}$* or mutant allele derivatives, propagated for ~80 cell divisions and examined for telomere length on a southern blot. The wild-type controls are marked with asterisks.

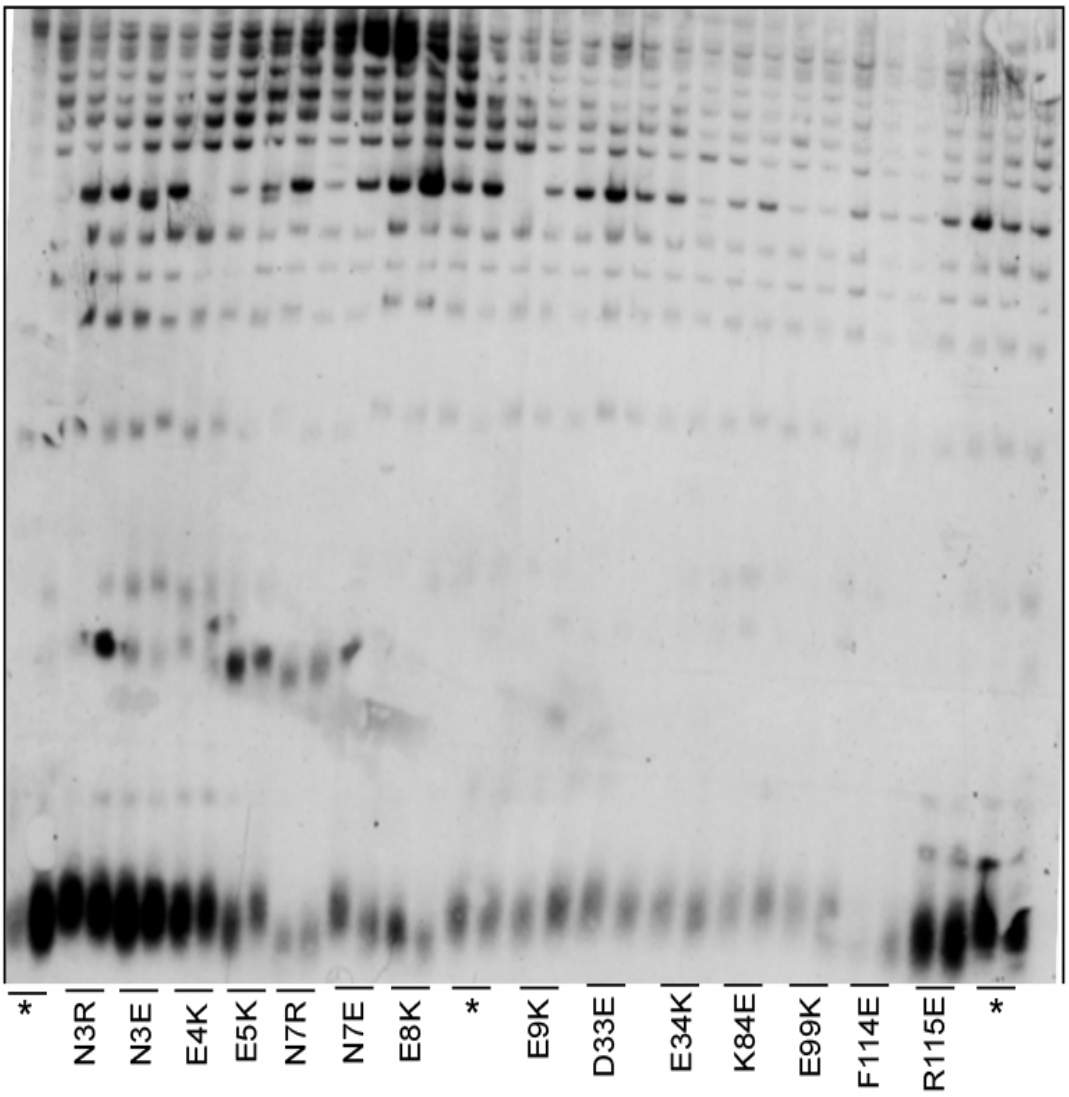

Figure 6.8 Telomere length analysis of $(myc)_{12}$ tagged *est1*⁻ mutant alleles when expressed from *CEN* plasmids (2 of 2). An *est1*-Δ *$(FLAG)_3$-$(myc)_{12}$-$(G)_6$-EST2* strain was transformed with single-copy plasmids expressing *EST1-$(G)_6$-$(myc)_{12}$* or mutant allele derivatives, propagated for ~80 cell divisions and examined for telomere length on a southern blot. The wild-type controls are marked with asterisks.

From this initial dataset, mutations of interest were integrated into the genome in order to more rigorously assess their phenotypic consequences. As Figure 6.9 shows, this analysis identified 4 individual missense mutations that each individually abolished the association of Est1 with the telomerase RNA: W87E, F98D, F114E, and Y136D, as well as 3 other mutations (R118E, K129E, and Y146D) that appeared to have a more moderate reduction in association with telomerase. These integrated strains were also examined for telomere length in Figures 6.10 and 6.11, which revealed that a subset of the mutants – F114E, R118E, K129E – did not have a severe enough *in vivo* telomere replication to qualify as bone fide RNA binding mutants (this was similarly confirmed, in the loss-of-function assay in Figures 6.2 – 6.4, that those three mutants do not significantly perturb telomere replication). Other mutants, like N7R, F40E, F102E, and F117R were eliminated from consideration on the basis that their association with telomerase was to near-completion when integrated (and in the case of F40E and F40R, a reduction in expression levels is a likely explanation for the slightly reduced co-immunoprecipitation signal, as opposed to a defect in RNA binding).

Ultimately, the classification of RNA-binding defective Est1 mutants was based on stringent criteria: significant reduction of co-immunoprecipitation in the biochemical assay, as well as significant telomere shortening in both the plasmid loss-of-function assay as well as when integrated in the genome. Figure 6.12 summarizes the phenotypes of the RNA binding mutants: W87E, F98D, Y136D, and Y146D. These residues define a region of ≈70 amino acids within domain A that mediate

binding to the telomerase RNA. Notably, this region does not bear any of the characteristics of a conventional RNA binding domain, and therefore potentially defines a new RNA binding motif.

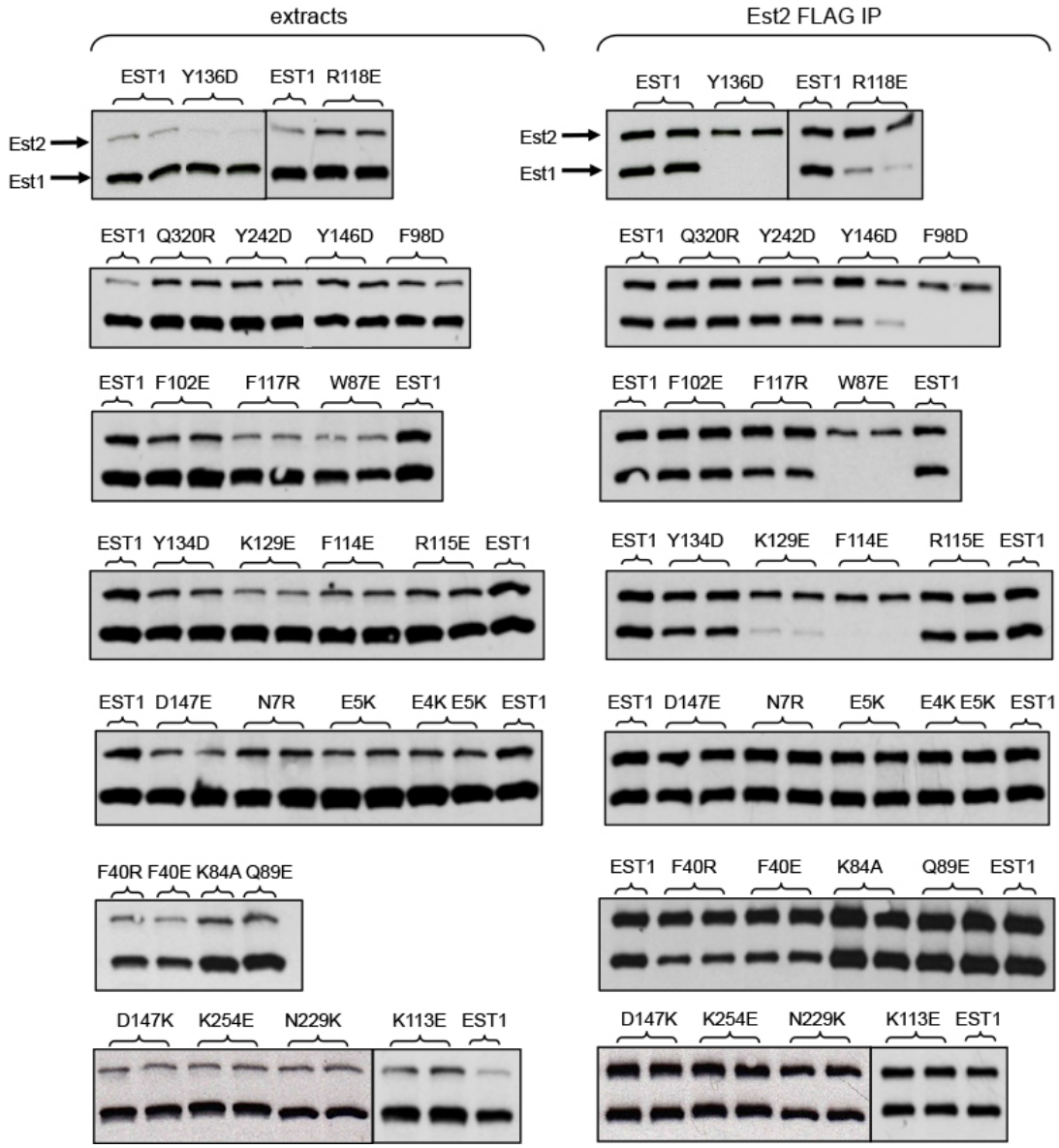

Figure 6.9 Western blot analysis of $(myc)_{12}$ tagged *est1⁻* mutant alleles when integrated in the genome. Pop-in / pop-out allelic replacement was used to integrate *EST1-$(G)_6$-$(myc)_{12}$* or mutant allele derivatives into YVL3802 [*$(FLAG)_3$-$(myc)_{12}$-$(G)_6$-EST2*] and extracts were prepared from cultures grown immediately after pop-out diagnosis. Left side depicts anti-myc westerns monitoring the proteins from extracts; right side depicts anti-myc westerns following anti-FLAG immunoprecipitation of Est2.

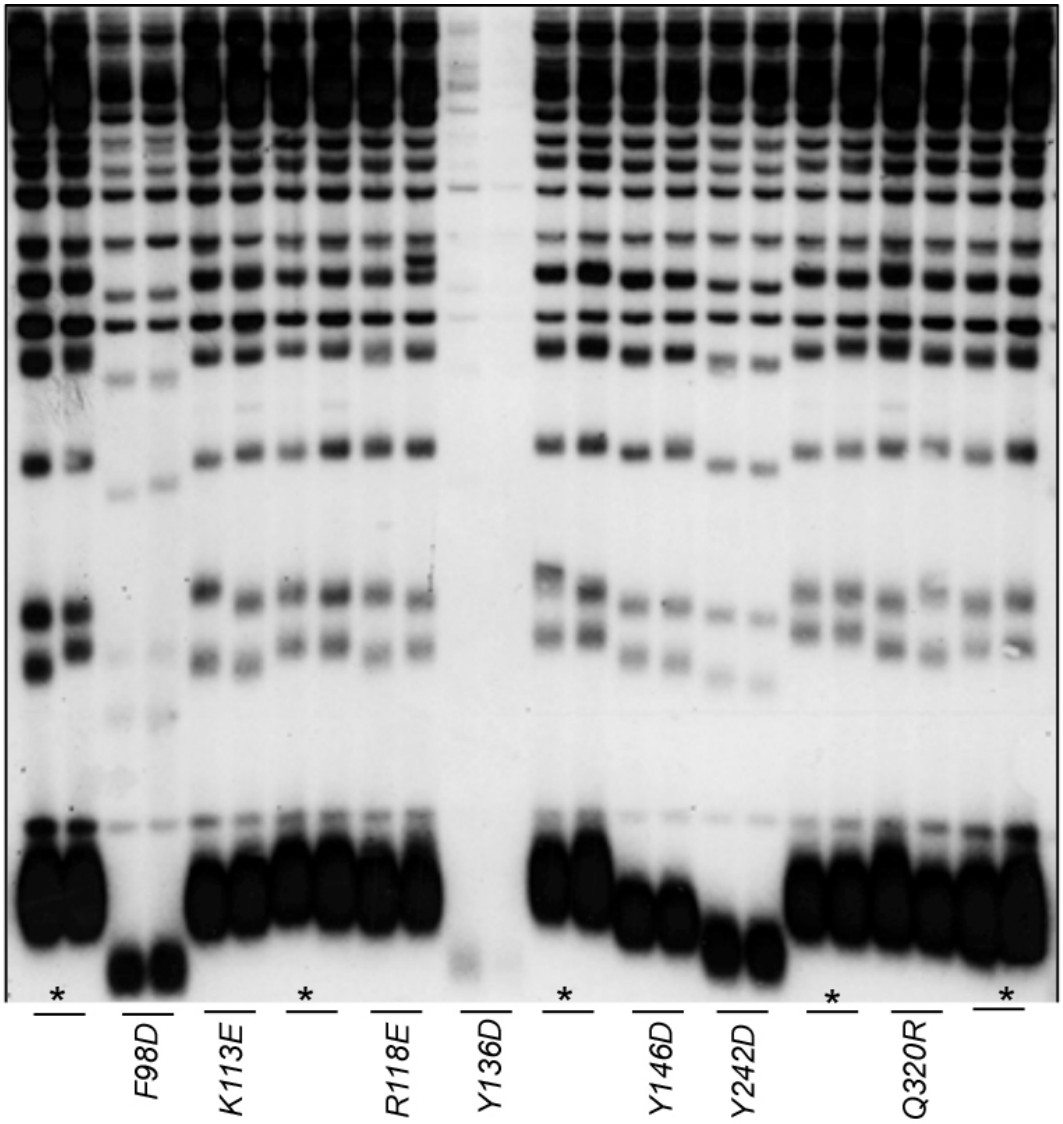

Figure 6.10 Telomere length analysis of $(myc)_{12}$ tagged *est1*$^{-}$ mutant alleles when integrated in the genome (1 of 2). Pop-in / pop-out allelic replacement was used to integrate *EST1-*$(G)_6$*-*$(myc)_{12}$ or mutant allele derivatives into YVL3802 [$(FLAG)_3$*-*$(myc)_{12}$*-*$(G)_6$*-EST2*], and pop-outs were propagated for ~80 cell divisions and examined for telomere length on a southern blot. The parental strain controls are marked with asterisks.

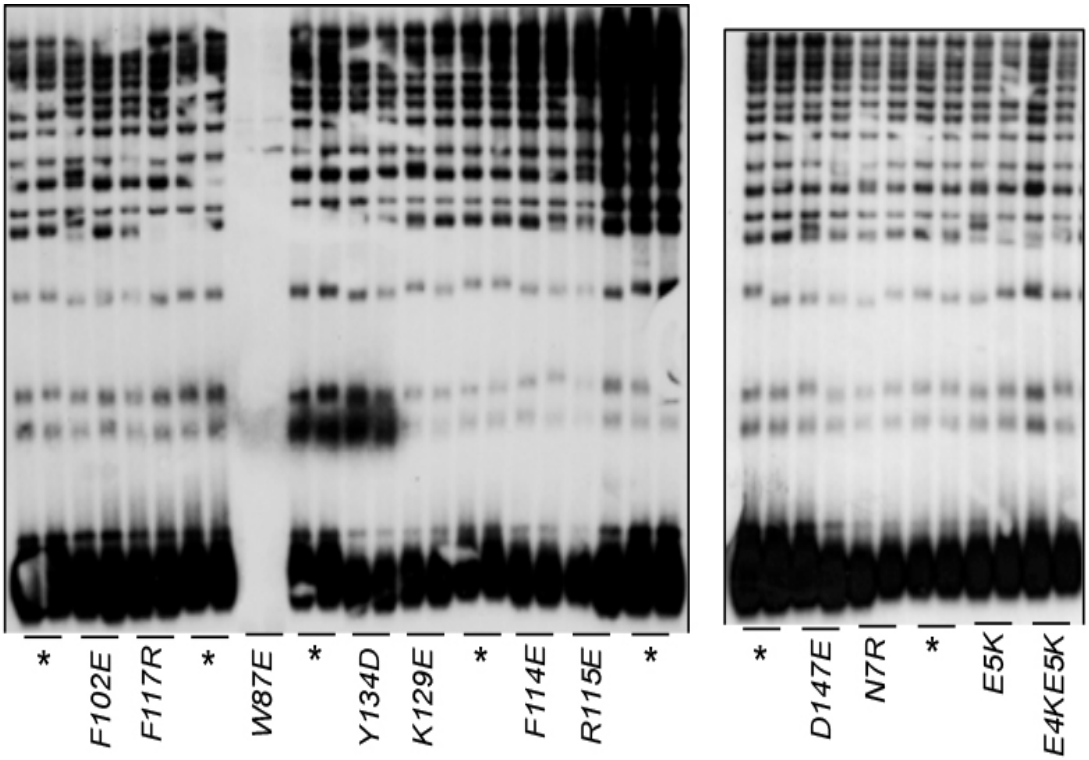

Figure 6.11 Telomere length analysis of (myc)$_{12}$ tagged *est1*$^{-}$ mutant alleles when integrated in the genome (2 of 2). Pop-in / pop-out allelic replacement was used to integrate *EST1-(G)$_6$-(myc)$_{12}$* or mutant allele derivatives into YVL3802 [*(FLAG)$_3$-(myc)$_{12}$-(G)$_6$-EST2*], and pop-outs were propagated for ~80 cell divisions and examined for telomere length on a southern blot. The parental strain controls are marked with asterisks.

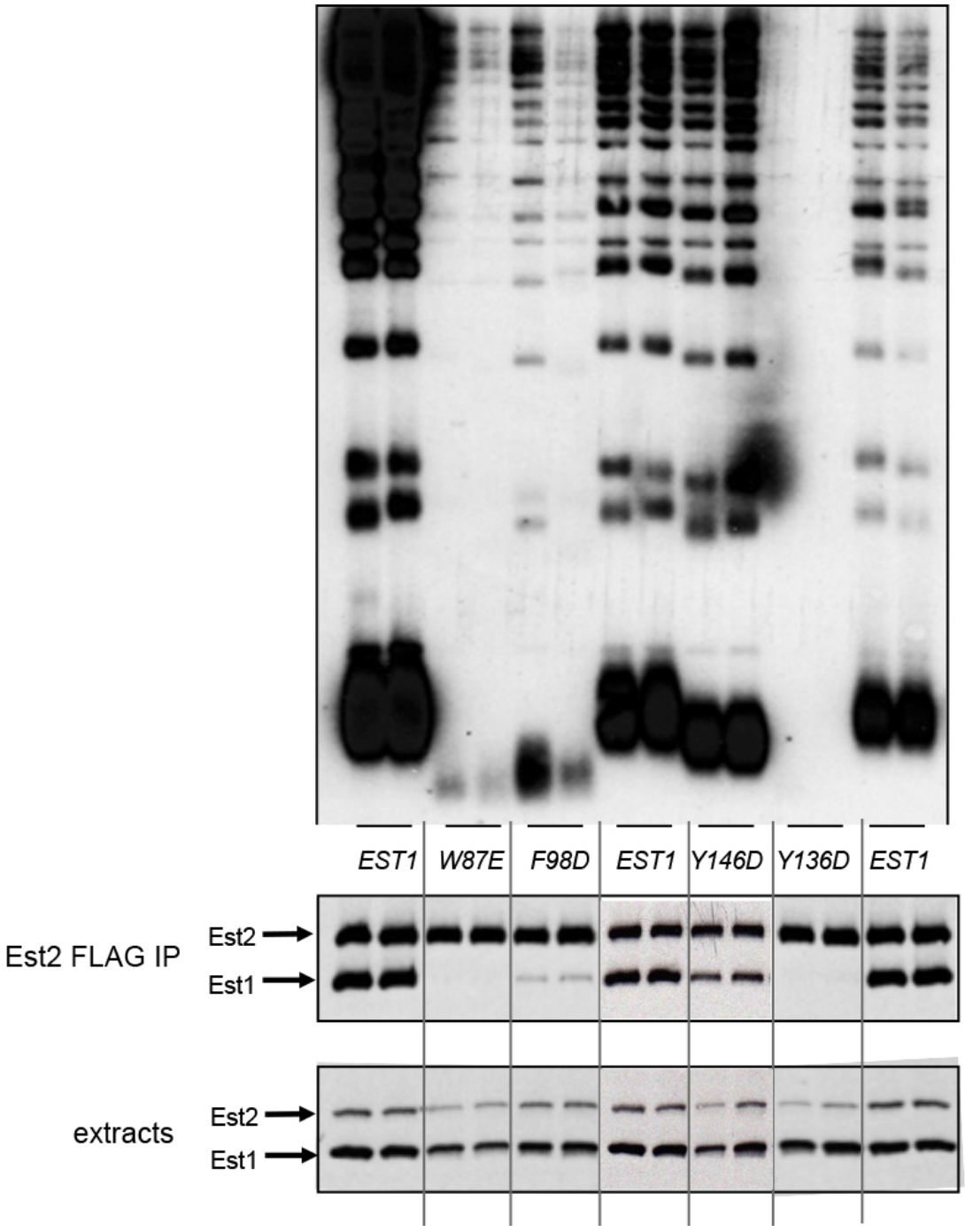

Figure 6.12 Summary of the Est1 RNA-binding mutants identified in this study. All alleles depicted in this figure were integrated into the genome as described in Figure 6.9. The three sets of lanes with a much lower detection of telomeric DNA signal correspond to three Est1 mutant strains that were very senescent (W87E, F98D, and Y136D).

Mutational analysis of the N-terminus of Est1 identifies a second domain

A second region in the N-terminus of the Est1 protein has previously been proposed to consist of two TPR (tetratricopeptide repeat) motifs. The panel of mutations incorporated into the loss-of-function and immunoprecipitation assays described above also included residues in this second region. Strikingly, this TPR domain appears to be dispensable for association of Est1 with telomerase for the mutations that have been tested: N229K, G239S, K254E, Y242D, and R269E (Figures 6.6 and 6.9). However, *in vivo* analysis of telomere length indicates that several mutations in this region have similarly short telomeres in the loss-of-function assay as well as when integrated. Figure 6.13 displays the phenotypes of mutants in this second domain, and Figure 6.14 summarizes the key residues in the N-terminus of Est1 that have been characterized in this chapter.

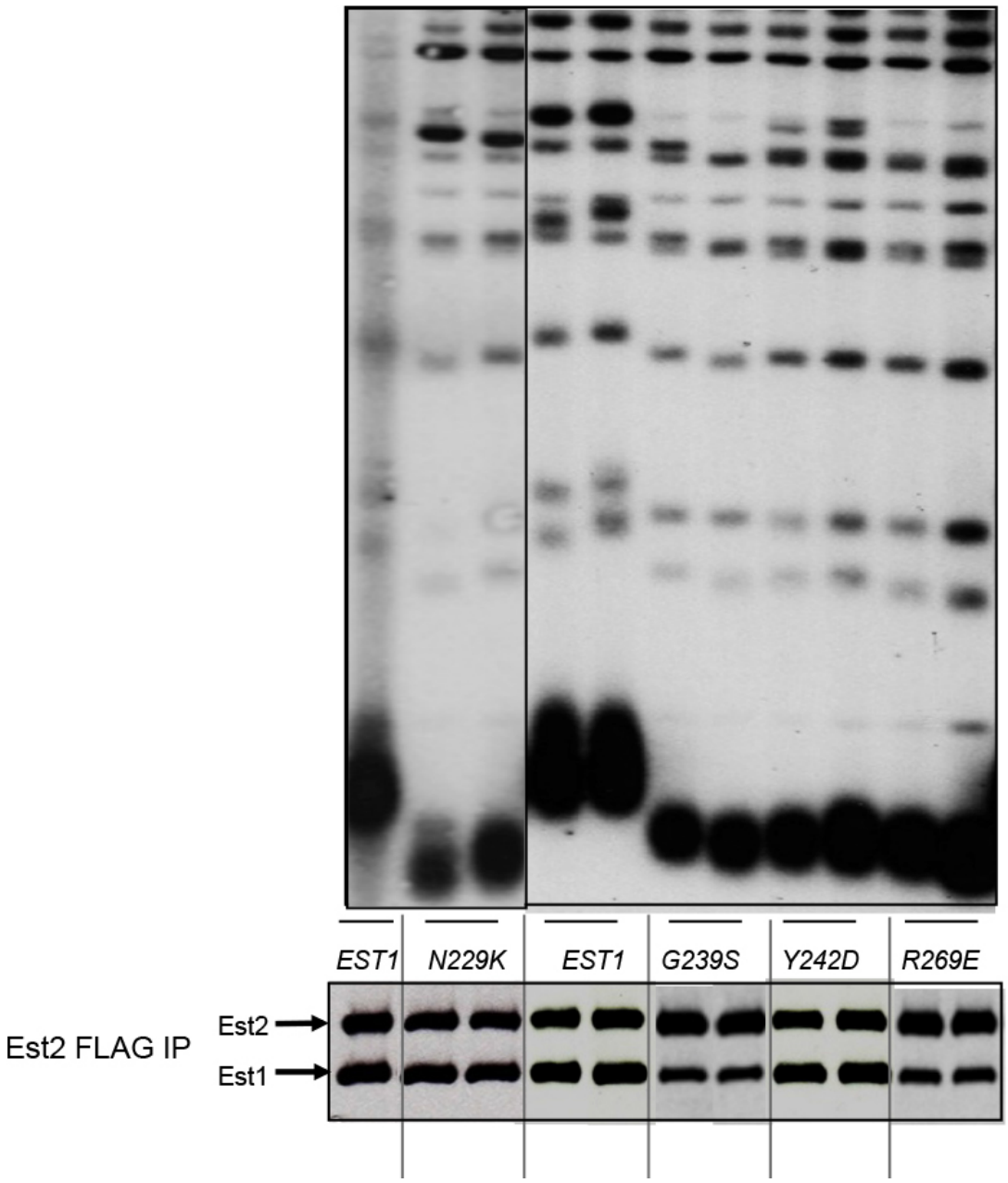

Figure 6.13 Est1 mutants in the TPR domain do not affect TLC1 RNA binding. Southern blots are from the loss-of function assay described in Figure 6.4. For western blot analysis, *est1-G239S* and *est1-R269E* were expressed from *CEN* plasmids as described in Figure 6.6. The rest were integrated into the genome as described in Figure 6.9.

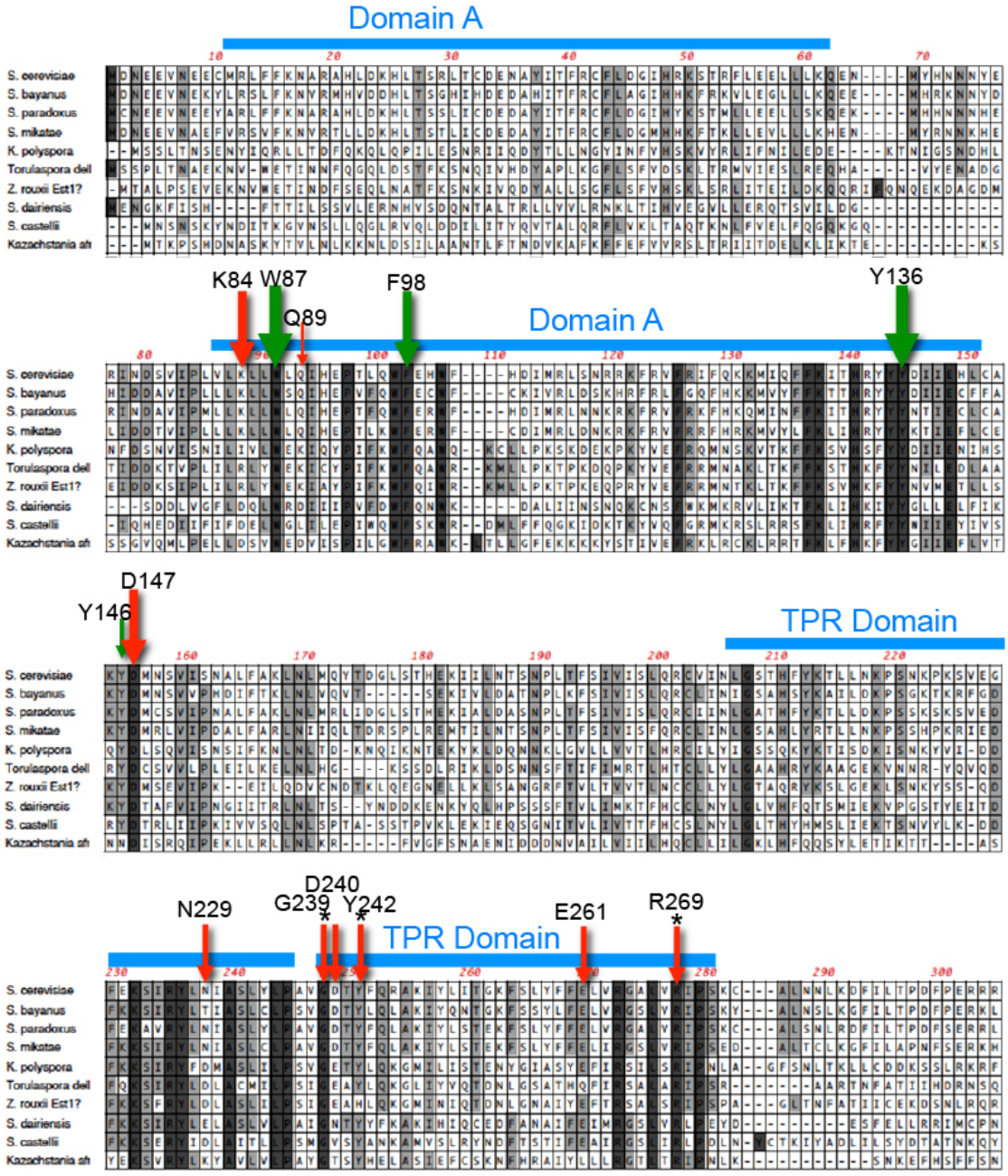

Figure 6.14 Summary of the important amino acid residues identified in the N-terminus of Est1. Size of arrow represents the relative severity of the loss-of-function phenotype when the indicated residue is mutated. Residues marked with an asterisk also had comparable overexpression dominant negative phenotypes. Residues marked with green arrows exhibited a decrease in RNA binding when mutated.

Mutational analysis of the C-terminal domain of Est1

Using the dominant negative strategy described in Chapter 2, John Lubin was able to identify mutations in the C-terminal half of Est1 that had a pronounced telomere replication defect when overexpressed (Figure 6.15). He also examined these mutants in a loss-of-function assay, and Figure 6.16 depicts the 13 residues of interest where mutations were identified that had null, severe or moderate loss-of-function phenotypes with comparable over-expression dominant negative phenotypes. As expected, the recruitment-defective mutant Est1-K444E had a strong over-expression dominant negative phenotype, and this suggests that other nearby residues may also be involved in Cdc13 association.

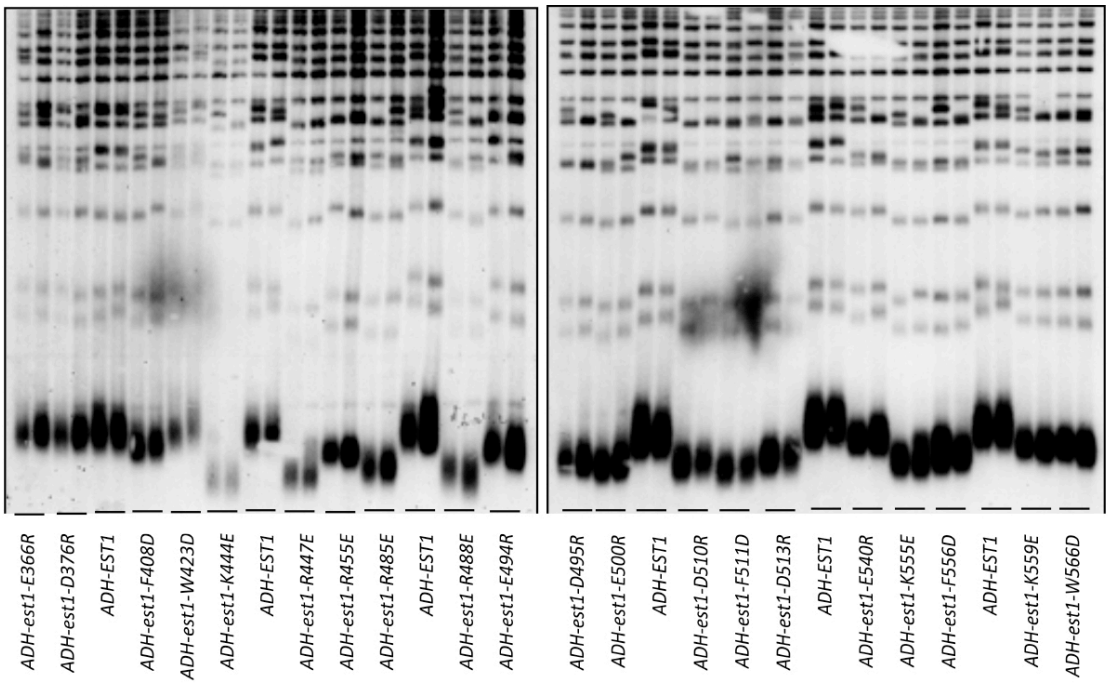

Figure 6.15 The dominant negative effect on telomere length for mutations in the C-terminus of *EST1*. An *EST1* wild-type strain was transformed with 2μ plasmids over-expressing either wild-type or mutant alleles of *EST1* and examined for telomere length after ~75 generations of propagation. The southern blots in this figure were completed by John Lubin.

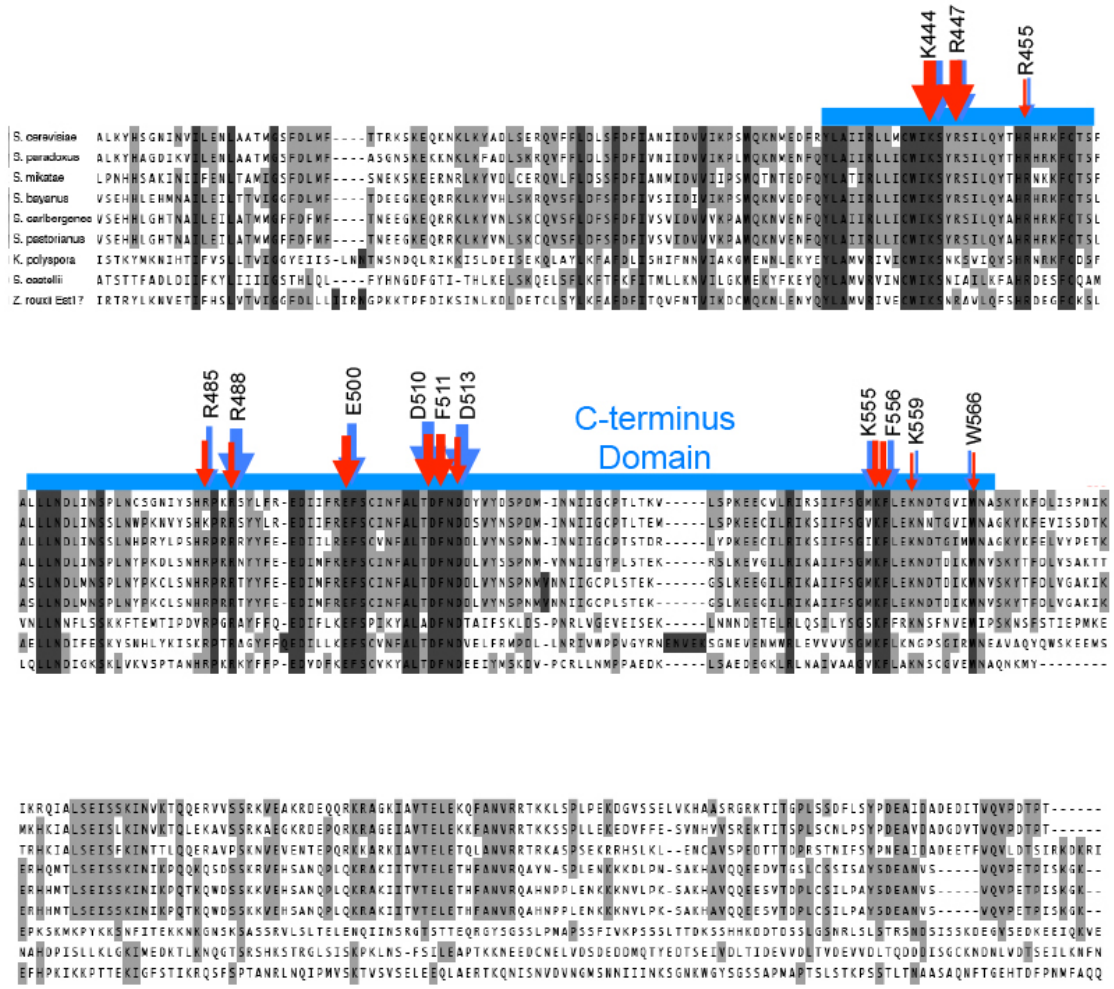

Figure 6.16 Amino acid sequence alignment of the Est1 C-terminus. Size of blue arrow represents the relative severity of the loss-of-function phenotype when the indicated residue is mutated, while size of red arrow represents the relative severity of the same mutation in the overexpression dominant negative assay.

Some of the C-terminus mutants were integrated into the genome and tested biochemically for association with Cdc13. Given that the immunoprecipitation assay is barely sensitive enough to detect the Cdc13-Est1 interaction, only the most severe mutants were included – i.e. the mutants that were severely defective in the loss-of-function assay and similarly had a strong dominant negative phenotype when over-expressed: K444E, R447E, R488E, D500R, D510R, F511D – as well as the moderately severe K555E. Figure 6.17 shows the western blot analysis. As expected, Est1-K444E displays a decreased interaction with Cdc13 that is restored by the compensatory *cdc13-2* mutation. R447E similarly has a reduced association with Cdc13, while R488E, D500R, D510R, and F511D retain normal levels of association and K555E appears slightly reduced. This indicates that a subset of residues in the C-terminus of Est1 define a site of interaction with Cdc13. However, due to detection level limitations of the biochemical assay, the precise boundaries of this domain have yet to be identified.

The integrated Est1 C-terminus mutants were also examined biochemically for association with Est3. *CEN EST3-(FLAG)$_3$* plasmids were introduced into strains expressing (myc)$_{12}$-Est2 and mutant Est1-(myc)$_{12}$. In the wild-type control, Est2 and Est1 are detected in the anti-FLAG immunoprecipitate, with Est1 at a much higher stoichiometry than Est2 (see Chapter 7 for a detailed discussion of this observation). For three of the Est1 C-terminal mutants, E500R, F511D, and D510R, there was a decrease in Est3 association, suggesting that these residues are contributing either directly or indirectly to Est3 association with the telomerase complex (Figure 6.18).

Interestingly, these three residues had normal levels of interaction with Cdc13, indicating that a separate interface on the C-terminus of Est1 defines a site of association for Est3. Figure 6.19 summarizes the key residues in the C-terminus that have been identified in this study.

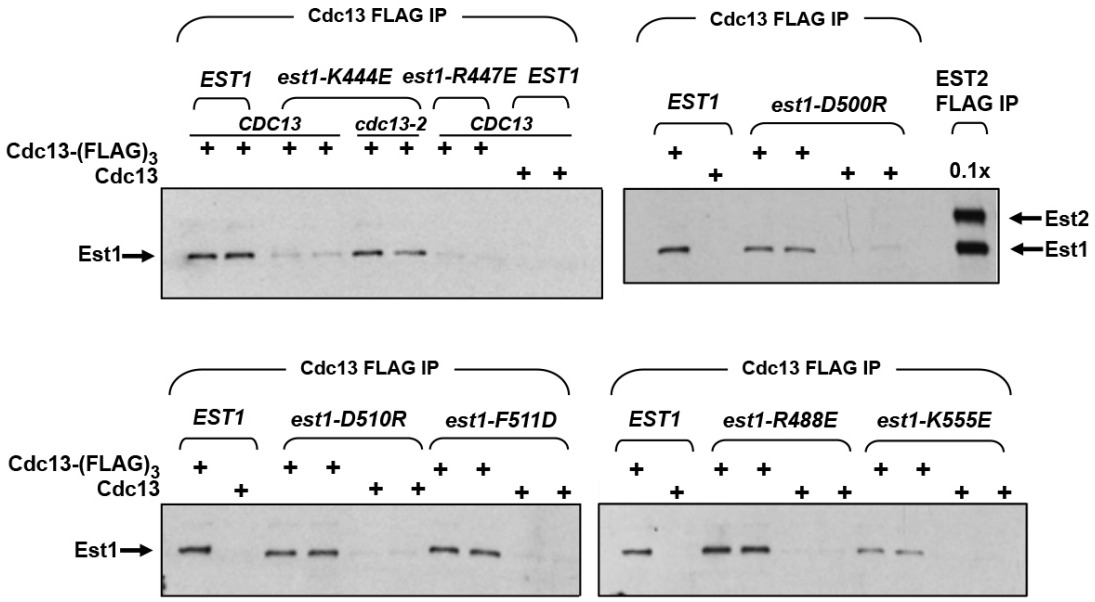

Figure 6.17 Examining the biochemical interaction of C-terminal Est1 mutants with Cdc13. Anti-myc western blots of anti-FLAG IPs prepared from strains expressing Cdc13-$(FLAG)_3$ and Est1-$(myc)_{12}$, with mutations introduced at the genomic location of the tagged Est1 and Cdc13 proteins as indicated. Top right lane is an anti-FLAG IP prepared from a strain expressing $(FLAG)_3$-$(myc)_{12}$-Est2 and Est1-$(myc)_{12}$ (0.1X indicates the amount of IP relative to the amount loaded in the other lanes).

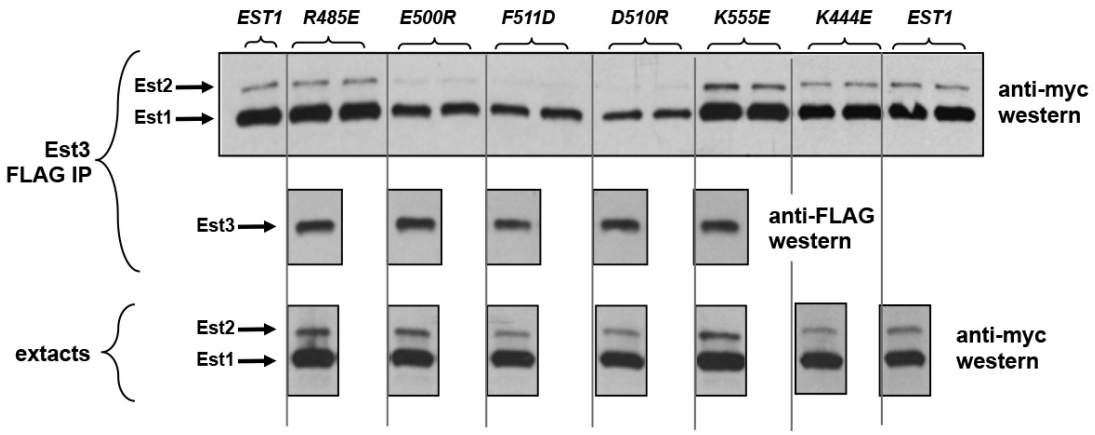

Figure 6.18 A subset of mutants in the C-terminus of Est1 affect Est3 association. Anti-FLAG and anti-myc western blots of anti-FLAG IPs prepared from strains expressing Est3-$(FLAG)_3$, from a *CEN* plasmid, and Est2-$(myc)_{12}$ and Est1-$(myc)_{12}$ integrated in the genome, with *est1*$^-$ mutations as indicated. For each mutation, two independent isolates were prepared for the anti-myc IP western, and one isolate was checked on the anti-myc input and anti-FLAG IP westerns to confirm similar levels of protein expression and Est3 immunoprecipitation, respectively.

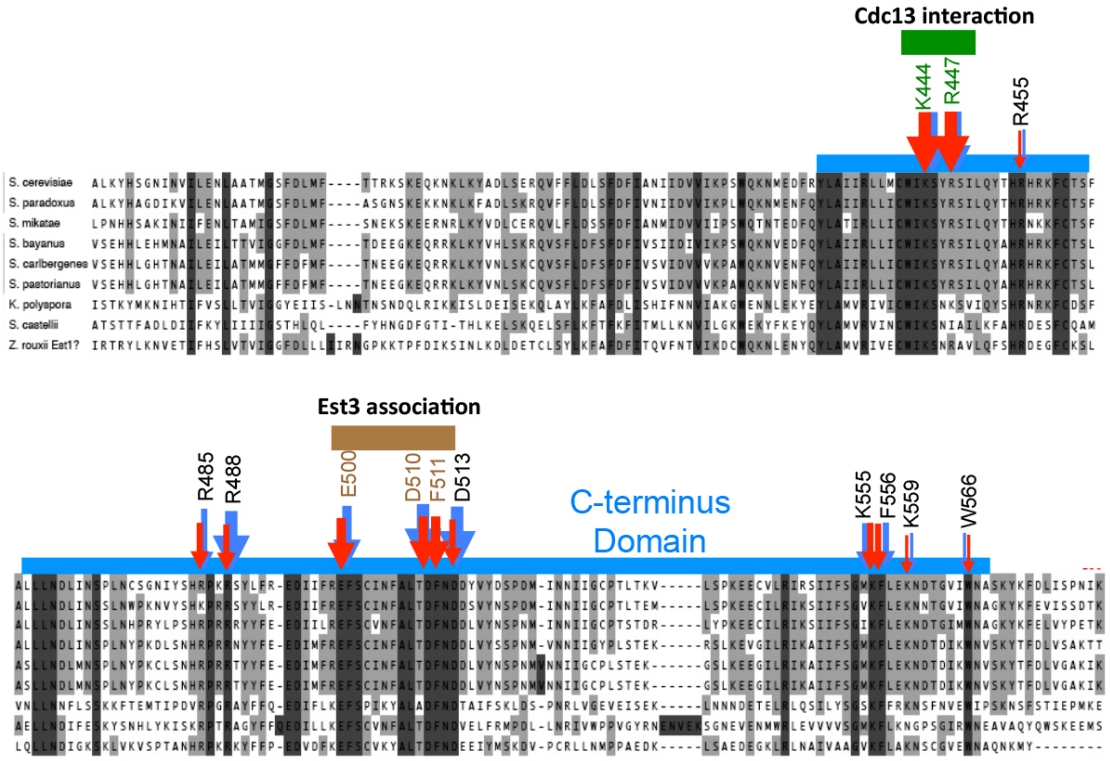

	LOF	ODN	Cdc13	Est3
K444E	short	short	reduced	normal
R447E	short	short	reduced	not tested
R485E	short	(med) short	normal	normal
R488E	null	short	normal	not tested
E500R	short	short	normal	reduced
D510R	null	short	normal	reduced
F511D	null	short	normal	reduced
K555E	med short	med short	normal	normal

Figure 6.19 Summary of the important amino acid residues identified in the C-terminus of Est1. Size of blue arrow represents the relative severity of the loss-of-function phenotype when the indicated residue is mutated, while size of red arrow represents the relative severity of the same mutation in the overexpression dominant negative assay. Residues labeled in green interact with Cdc13, and residues labeled in brown are involved in Est3 association.

Multiple subunits of Est1 do not associate at the same telomerase complex

Given that the TPR domain at the N-terminus of Est1 has an unknown function, and that immunoprecipitations using an HA-tagged version of Est2 suggested that Est1 could associate at a higher level of stoichiometry (see Chapter 3), I asked whether multiple molecules of Est1 could assemble in a single telomerase complex.

To investigate this, I created a version of Est1 that is tagged with $(FLAG)_6$-$(myc)_{12}$ so that Est1 could be immunoprecipitated using anti-FLAG beads. This FLAG tagged version of Est1 could be quantitatively depleted from extracts, and both Est3 (Figure 6.20a) and Est2 (data not shown) associate as expected, indicating that this tagged version of Est1 is functional in immunoprecipitating a telomerase complex that is similar to the complex immunoprecipitated by Est2.

To test whether Est1 could associate with itself, I created a strain with a tandem duplication at the *EST1* locus, consisting of *EST1-*$(myc)_{12}$ and *EST1-*$(FLAG)_6$-$(myc)_{12}$. Using this strain, both tagged versions of Est1 can be detected from extracts at comparable levels (Figure 6.20b, lane 3). However, when the FLAG-tagged version of Est1 is immunoprecipitated, there is no indication of the other version of Est1 being present in this complex. This suggests that multiple molecules of Est1 do not bind to the same complex.

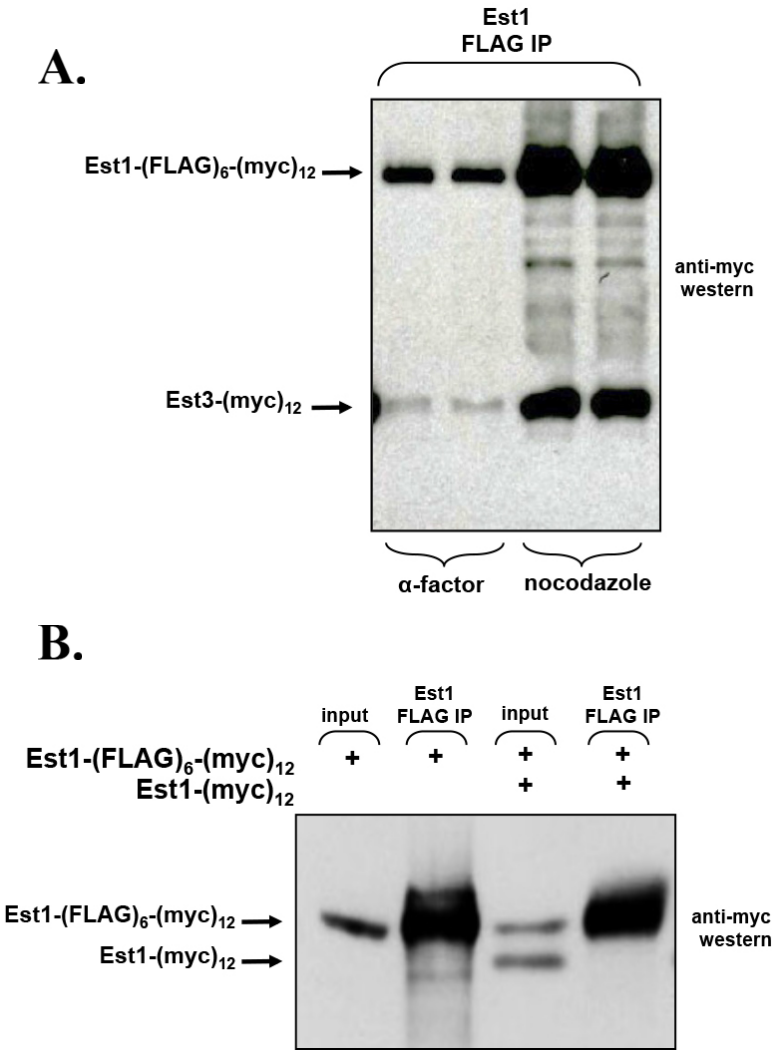

Figure 6.20 Analysis of the telomerase complex when Est1 is immunoprecipitated. A) Anti-myc western blot of anti-FLAG IPs prepared from a strain expressing Est1-$(FLAG)_6$-$(myc)_{12}$ and Est3-$(myc)_{12}$, both integrated in the genome. B) Anti-myc western of inputs and anti-FLAG IPs comparing a strain containing a single copy of Est1-$(FLAG)_6$-$(myc)_{12}$ with a strain containing tandem copies of Est1 integrated in the genome: Est1-$(FLAG)_6$-$(myc)_{12}$ / Est1-$(myc)_{12}$.

Investigating the relationship between Est1 and Ebs1

Est1 and Ebs1 are paralogs that arose from a whole genome duplication event prior to the *Saccharomyces* clade (Figure 6.21). The degree of similarity between the two proteins suggests that Ebs1 might be capable of associating with telomerase directly or performing an analogous subset of biochemical activities in similarly discrete domains. Intriguingly, many of the important N- and C-terminal residues identified in this chapter are conserved in Ebs1.

To examine this relationship, Ebs1 was tagged with $(FLAG)_3$ in a strain expressing $(myc)_{12}$-tagged versions of Est1 and Est2, and anti-FLAG immunoprecipitates were examined for association of Ebs1 with the telomerase complex. Although Ebs1 could be quantitatively depleted from extracts by IP, no association with Est1 and Est2 was detected (Figure 6.22a). I also considered the possibility that Ebs1 and Est1 might be able to compete for association with the complex; however, I also failed to detect an interaction between Ebs1 and Est2 in a strain that contained the *est1-Y136D* mutation that eliminates Est1 binding to the complex.

Nevertheless, the similarities between Est1 and Ebs1 were such that like Est1, Ebs1 could be expressed as two biochemically discrete domains (aa 1-365 and aa 366-384) (Figure 6.22d). I created a construct that replaces the N-terminus of Est1 with Ebs1 aa1-365, to test whether this chimeric protein, containing Ebs1 aa1-365 fused with Est1 aa340-699, could associate with telomerase. Although the chimera

expressed at a similar level to full-length Est1, it was unable to associate with the telomerase complex at any appreciable level (Figure 6.22b).

Upf1 has previously been shown to interact with Ebs1 (Luke et al., 2007). Consistent with these prior observations, I also noticed that full-length Ebs1 could efficiently immunoprecipitate Upf1 (Figure 6.22c, left side). To test whether this interaction can be impacted by a single missense mutation, similar to the Cdc13-Est1 interaction, I generated *ebs1-K452E*, which is equivalent to *est1-K444E* based on sequence alignment. However, when the FLAG-tagged Ebs1-K452E protein was immunoprecipitated, Upf1 retains association at a level comparable to wild-type Ebs1 (Figure 6.22c, right side). Additionally, I tested whether the N- or C-terminal halves of Ebs1 could retain association with Upf1 in a manner similar to the Est1-TLC1 or Est1-Cdc13 interactions. However, I detected a much weaker level of association of Upf1 with both the N- and C-terminal truncations of Ebs1 (Figure 6.22d). At least for Ebs1-Upf1, this suggests that the nature of the interaction is not analogous to two of the domains defined on Est1.

Finally, I tested whether Est1 or Est3 could directly interact with Upf1. Est1 and Est3 were tagged with $(FLAG)_3$ in a strain expressing a $(myc)_{13}$-tagged version of Upf1. However, no interaction was detected between Upf1 and either Est1 or Est3 (Figure 6.22e). Given that Ebs1 has been reported to interact with several other partners, including Dcp1 and Cdc33, there could be other yet-to-be-determined protein-protein interactions that overlap between Est1 and Ebs1.

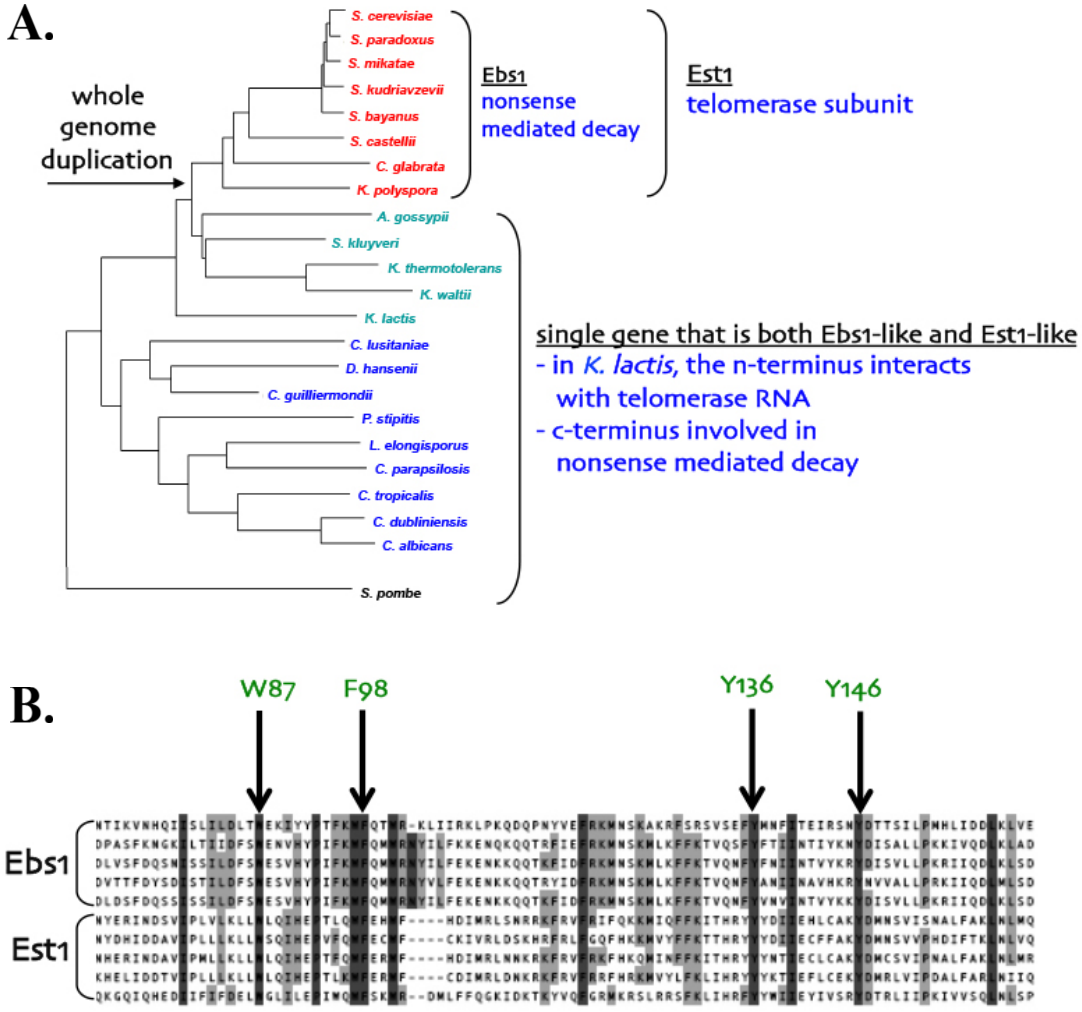

Figure 6.21 Ebs1 and Est1 are paralogs that arose through whole genome duplication. A) Phylogenetic analysis of Est1 / Ebs1 homologues in budding yeast species and *S. pombe*. A whole genome duplication event occurred prior to speciation of the *Saccharomyces* clade, giving rise to paralogs with separate functions. B) Amino acid sequence alignment of *Saccharomyces* Ebs1 and Est1 homologues. The four *S. cerevisiae* RNA-binding residues described in this chapter are also conserved in Ebs1 homologues.

Figure 6.22 Comparison of Est1 and Ebs1 biochemical properties. A) Anti-FLAG and anti-myc westerns of anti-FLAG IPs comparing a strain expressing Ebs1-$(FLAG)_3$ (myc)12-Est2 Est1-$(myc)_{12}$ with a strain expressing Ebs1-$(FLAG)_3$ (myc)12-Est2 est1-Y136D-$(myc)_{12}$, all integrated in the genome. Last two lanes are anti-FLAG IPs prepared from a strain expressing $(FLAG)_3$-$(myc)_{12}$-Est2 and Est1-$(myc)_{12}$ (0.1X and 0.01X indicate the amount of IP relative to the amount loaded in the other lanes). B) Anti-myc western of inputs and anti-FLAG IPs prepared from plasmid-borne Est1-$(myc)_{12}$ or $Ebs1_{1\text{-}355}$-$Est1_{340\text{-}699}$-$(myc)_{12}$ (behind *EST1* promoter) transformed into YVL3802 [*(FLAG)3-(myc)12-EST2*]. C) Anti-FLAG and anti-myc westerns of inputs and anti-FLAG IPs comparing a strain expressing Upf1-$(myc)_{13}$ with a strain expressing Ebs1-$(FLAG)_3$ Upf1-$(myc)_{13}$ (left side), and a strain expressing ebs1-K542E-$(FLAG)_3$ Upf1-$(myc)_{13}$ (right side), all integrated in the genome. D) Anti-FLAG and anti-myc westerns of inputs and anti-FLAG IPs comparing a strain expressing $Ebs1_{1\text{-}365}$-$(FLAG)_3$ Upf1-$(myc)_{13}$ with a strain expressing $Ebs1_{366\text{-}884}$-$(FLAG)_3$ Upf1-$(myc)_{13}$. Note that the Ebs1 truncations were integrated as pop-ins, so the untagged wild-type genomic copy of *EBS1* is also present in tandem. E) Anti-FLAG and anti-myc westerns of inputs and anti-FLAG IPs comparing a strain expressing Est1-$(FLAG)_3$ Upf1-$(myc)_{13}$ with a strain expressing Est3-$(FLAG)_3$ Upf1-$(myc)_{13}$, all integrated in the genome.

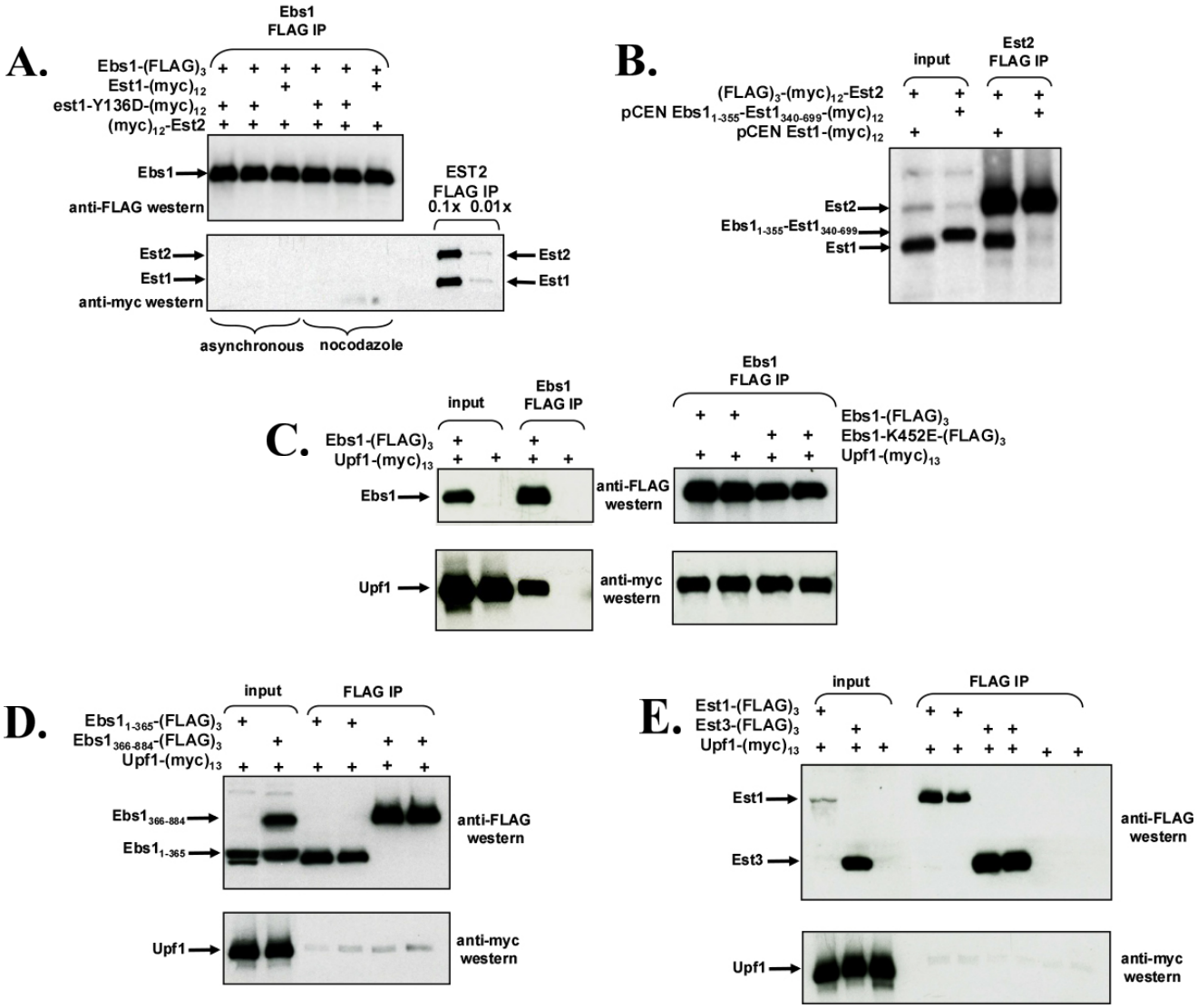
A.
Ebs1 FLAG IP
Ebs1-(FLAG)3
Est1-(myc)12
est1-Y136D-(myc)12
(myc)12-Est2
Ebs1
anti-FLAG western
EST2 FLAG IP 0.1x 0.01x
Est2
Est1
anti-myc western
asynchronous
nocodazole
B.
input
Est2 FLAG IP
(FLAG)3-(myc)12-Est2
pCEN Ebs1 1-355-Est1 340-699-(myc)12
pCEN Est1-(myc)12
Est2
Ebs1 1-355-Est1 340-699
Est1
C.
input
Ebs1 FLAG IP
Ebs1-(FLAG)3
Upf1-(myc)13
Ebs1
Upf1
anti-FLAG western
anti-myc western
Ebs1-(FLAG)3
Ebs1-K452E-(FLAG)3
Upf1-(myc)13
D.
input
FLAG IP
Ebs1 1-365-(FLAG)3
Ebs1 366-884-(FLAG)3
Upf1-(myc)13
Ebs1 366-884
Ebs1 1-365
Upf1
anti-FLAG western
anti-myc western
E.
input
FLAG IP
Est1-(FLAG)3
Est3-(FLAG)3
Upf1-(myc)13
Est1
Est3
Upf1
anti-FLAG western
anti-myc western

Discussion

This study identified four functionally distinct interfaces on Est1: RNA binding, which maps to Domain A, an unknown activity that maps to the TPR domain, and Cdc13 and Est3 interaction surfaces which map to adjacent regions in the C-terminal half of Est1.

Domain A consists of atypical TPR-like repeats and functions to interact with the TLC1 RNA. Four mutants (W87E, F98D, Y136D, and Y146D) were identified that have a clear defect in association with the telomerase complex, and interestingly, all four are aromatic amino acid residues. Aromatic residues are known to be important for protein-nucleic acid recognition, and tryptophan is especially involved in the interaction with RNAs (Baker and Grant, 2007; Hall, 2002). Therefore, these four residues could be making a critical contact with TLC1, while other residues in this domain are probably also involved but make less of an individual contribution to RNA binding to cause a detectable phenotype from a single missense mutation. Several other mutants (F40E, F114E, R118E, and K129E) appeared to have more modest reductions in telomerase complex association in some of the biochemical assays, so these residues could also be in direct RNA contact.

The TPR domain is located downstream from Domain A, and although several mutants (N229K, G239S, Y242D, and R239E) were identified with a clear telomere replication defect – with three of the mutants also having a comparable overexpression dominant negative phenotype – a specific function has yet to be assigned to this domain. The mutants in this domain do not affect RNA binding and preliminary

evidence also indicates that they are not involved in Est3 association (data not shown), suggesting that this domain is making an additional contribution to telomerase function.

In the C-terminus of Est1, two functionally distinct activities were identified. Residues K444 and R447 are directly involved in an interaction with Cdc13, and these two residues also had a severe overexpression dominant negative phenotype when mutated, suggesting that the Cdc13 interaction via these two residues is critical for proper recruitment of telomerase to the telomere. Given the large number of dominant negative alleles isolated in this region, it is likely that other residues are also involved in the Cdc13 interaction. One other mutant (K555E) displayed a slight decrease in Cdc13 interaction, but given the detection limits of this biochemical interaction, it is unclear whether this is a biologically significant result. This mutant also had a weaker dominant negative phenotype. As with the RNA-binding mutants, I chose to classify mutants with the most clear and reproducible phenotypes in multiple assays.

Another functionally distinct activity was identified in the C-terminus that consists of mutants with severe dominant negative phenotypes, normal interaction with Cdc13, and reduced association with Est3. I have named this an Est3-associating activity, rather than Est3-interacting, because unlike Cdc13, it is unclear whether this is attributable to a direct protein-protein interaction between Est1 and Est3. Other results from this thesis suggest that Est3 association with telomerase involves a more complex combination of residues on Est1, Est2, and potentially nucleotides on the TLC1 RNA as well (see Chapter 7 and Appendix B).

For each of these activities, the precise boundaries are still unclear. The results from the loss-of-function and dominant negative mutagenesis, along with the conserved residues identified from alignments, suggest that there are two separate domains in the N-terminus. The C-terminus is a bit more confusing, given the low detection level of the Cdc13-Est1 interaction, which limits the amount of residues that can be directly tested in this assay. To further complicate the analysis in the C-terminus, the single-stranded G-rich DNA binding region (amino acids 435 – 565) is also located within a region that spans both the Cdc13 interaction and Est3 association residues, so it is unclear whether there is some kind of connection between these three biochemical activities and whether it constitutes a single domain in the C-terminus. In addition, there could be other yet-to-be-identified biochemical activities in Est1 at the C-terminus, as well as in the N-terminus.

Surprisingly, no alleles with a strong dominant negative phenotype were able to be isolated in Domain A, the RNA-binding domain. This suggests that the dominant negative alleles in the other Est1 domains are due to titration of the RNA away from the endogenous telomerase complex. For example, the dominant negative phenotype for Est1-K444E might be due to binding most of the limited amount of RNA molecules when it is over-expressed, thereby preventing the RNA from getting recruited to the telomere. However, when a severe RNA-binding mutant like Est1-W87E is overexpressed, it presumably does not interfere with the RNA, and the higher expression levels of Cdc13 and Est3, and/or weaker or more transient interactions of those proteins with Est1, precludes a significant amount of Cdc13 and Est3 from

getting displaced from their endogenous complexes to cause a significant defect in telomere maintenance.

So far, based on the experiments shown in Figure 6.22, there does not appear to be any connection between the biochemical properties of Est1 and Ebs1, even though the critical Est1 residues are conserved in Ebs1. Like with Est1, Ebs1 is reported to have numerous biochemical activities and interacting partners, so it is possible that Ebs1 is involved in other protein-protein and protein-RNA interactions that involve these conserved residues.

Materials and methods

Strains and plasmids

The parental strain used for the loss-of-function and dominant negative assays was YVL2967 (*MAT***a** *ura3-52 lys2-801 trp1-*Δ*1 his3-*Δ*200 leu2-*Δ*1*).

The parental strain for generating the tagged strains for biochemical analysis was AVL78 (*MAT***a** *leu2 trp1 ura3-52 prb1 prc1 pep4-3*). Strains were constructed in five different ways: (1) plasmid transformation, (2) pop-in / pop-out two step allele replacement, (3) pop-in tandem gene duplication, (4) C-terminal tagging via one step gene replacement (Longtine et al., 1998), (5) deletion via one step gene replacement (Longtine et al., 1998).

Tables 6.1 and 6.2 list the strains used in this chapter and the corresponding figure(s) in which they appear. Tables 6.3 – 6.7 list the plasmids used in this chapter and the corresponding figure(s) in which they appear.

Table 6.1 Strains used in this chapter (1 of 2).

Figure	Strain	Genotype
6-1b, 6-22b	YVL3487	$(FLAG)_3$-$(myc)_{12}$-$(G)_6$-Est2
6-1c, 6-d	YVL3528	Est1-$(G)_6$-$(myc)_{12}$ $(FLAG)_3$-$(myc)_{12}$-$(G)_6$-Est2 *bar1-Δ::KAN*
	YVL3692	$Est1_{1-340}$-$(G)_6$-$(myc)_{12}$ $(FLAG)_3$-$(myc)_{12}$-$(G)_6$-Est2 *bar1-Δ::KAN/*p *CEN URA ADH-EST1*
	YVL3830	$Est1_{340-699}$-$(G)_6$-$(myc)_{12}$ $(FLAG)_3$-$(myc)_{12}$-$(G)_6$-Est2 *bar1-Δ::KAN/*p *CEN URA ADH-EST1*
6-1e, 6-17	YVL3803	Est1-$(G)_6$-$(myc)_{12}$ $(myc)_{12}$-$(G)_6$-Est2 *bar1-Δ::NAT*
	YVL3992	Cdc13-(FLAG)3*::TRP1* $Est1_{340-699}$-$(G)_6$-$(myc)_{12}$/p *CEN URA ADH-EST1*
6-2 – 6-4, 6-13	YVL3814	*MAT***a** *est1-Δ::KAN ura3-52 lys2-801 trp-Δ1 his3-Δ200 leu2-Δ1/*p *CEN URA ADH-EST1*
6-6 – 6-8, 6-13	YVL3833	*est1-Δ::KAN* $(FLAG)_3$-$(myc)_{12}$-$(G)_6$-Est2 *bar1-Δ::KAN/* p *CEN URA EST1*
6-9 – 6-13	YVL3802	$(FLAG)_3$-$(myc)_{12}$-$(G)_6$-Est2 *bar1-Δ::NAT*
	YVL4234	est1-E4K E5K-$(G)_6$-$(myc)_{12}$ $(FLAG)_3$-$(myc)_{12}$-$(G)_6$-Est2 *bar1-Δ::NAT*
	YVL4232	est1-E5K-$(G)_6$-$(myc)_{12}$ $(FLAG)_3$-$(myc)_{12}$-$(G)_6$-Est2 *bar1-Δ::NAT*
	YVL4228	est1-N7R-$(G)_6$-$(myc)_{12}$ $(FLAG)_3$-$(myc)_{12}$-$(G)_6$-Est2 *bar1-Δ::NAT*
	YVL4311	est1-F40R-$(G)_6$-$(myc)_{12}$ $(FLAG)_3$-$(myc)_{12}$-$(G)_6$-Est2 *bar1-Δ::NAT*
	YVL4327	est1-F40E-$(G)_6$-$(myc)_{12}$ $(FLAG)_3$-$(myc)_{12}$-$(G)_6$-Est2 *bar1-Δ::NAT*
	YVL4331	est1-K84A-$(G)_6$-$(myc)_{12}$ $(FLAG)_3$-$(myc)_{12}$-$(G)_6$-Est2 *bar1-Δ::NAT*
	YVL4222	est1-W87E-$(G)_6$-$(myc)_{12}$ $(FLAG)_3$-$(myc)_{12}$-$(G)_6$-Est2 *bar1-Δ::NAT*
	YVL4333	est1-Q89E-$(G)_6$-$(myc)_{12}$ $(FLAG)_3$-$(myc)_{12}$-$(G)_6$-Est2 *bar1-Δ::NAT*
	YVL4132	est1-F98D-$(G)_6$-$(myc)_{12}$ $(FLAG)_3$-$(myc)_{12}$-$(G)_6$-Est2 *bar1-Δ::NAT*
	YVL4216	est1-F102E-$(G)_6$-$(myc)_{12}$ $(FLAG)_3$-$(myc)_{12}$-$(G)_6$-Est2 *bar1-Δ::NAT*
	YVL4137	est1-K113E-$(G)_6$-$(myc)_{12}$ $(FLAG)_3$-$(myc)_{12}$-$(G)_6$-Est2 *bar1-Δ::NAT*
	YVL4230	est1-F114E-$(G)_6$-$(myc)_{12}$ $(FLAG)_3$-$(myc)_{12}$-$(G)_6$-Est2 *bar1-Δ::NAT*
	YVL4236	est1-R115E-$(G)_6$-$(myc)_{12}$ $(FLAG)_3$-$(myc)_{12}$-$(G)_6$-Est2 *bar1-Δ::NAT*
	YVL4218	est1-F117R-$(G)_6$-$(myc)_{12}$ $(FLAG)_3$-$(myc)_{12}$-$(G)_6$-Est2 *bar1-Δ::NAT*
	YVL4134	est1-R118E-$(G)_6$-$(myc)_{12}$ $(FLAG)_3$-$(myc)_{12}$-$(G)_6$-Est2 *bar1-Δ::NAT*
	YVL4226	est1-K129E-$(G)_6$-$(myc)_{12}$ $(FLAG)_3$-$(myc)_{12}$-$(G)_6$-Est2 *bar1-Δ::NAT*
	YVL4224	est1-Y134D-$(G)_6$-$(myc)_{12}$ $(FLAG)_3$-$(myc)_{12}$-$(G)_6$-Est2 *bar1-Δ::NAT*
	YVL3896	est1-Y136D-$(G)_6$-$(myc)_{12}$ $(FLAG)_3$-$(myc)_{12}$-$(G)_6$-Est2 *bar1-Δ::NAT*
	YVL3898	est1-Y146D-$(G)_6$-$(myc)_{12}$ $(FLAG)_3$-$(myc)_{12}$-$(G)_6$-Est2 *bar1-Δ::NAT*
	YVL4238	est1-D147E-$(G)_6$-$(myc)_{12}$ $(FLAG)_3$-$(myc)_{12}$-$(G)_6$-Est2 *bar1-Δ::NAT*
	YVL4356	est1-D147K-$(G)_6$-$(myc)_{12}$ $(FLAG)_3$-$(myc)_{12}$-$(G)_6$-Est2 *bar1-Δ::NAT*
	YVL4352	est1-N229K-$(G)_6$-$(myc)_{12}$ $(FLAG)_3$-$(myc)_{12}$-$(G)_6$-Est2 *bar1-Δ::NAT*
	YVL3900	est1-Y242D-$(G)_6$-$(myc)_{12}$ $(FLAG)_3$-$(myc)_{12}$-$(G)_6$-Est2 *bar1-Δ::NAT*
	YVL4354	est1-K254E-$(G)_6$-$(myc)_{12}$ $(FLAG)_3$-$(myc)_{12}$-$(G)_6$-Est2 *bar1-Δ::NAT*
	YVL3902	est1-Q320R-$(G)_6$-$(myc)_{12}$ $(FLAG)_3$-$(myc)_{12}$-$(G)_6$-Est2 *bar1-Δ::NAT*

Table 6.2 Strains used in this chapter (2 of 2).

Figure	Strain	Genotype
6-15	YVL2967	*MAT***a** *ura3-52 lys2-801 trp1-Δ1 his3-Δ200 leu2-Δ1*
6-17, 6-18	YVL3979	Cdc13-(FLAG)3*::TRP1* Est1-$(G)_6$-$(myc)_{12}$ $(myc)_{12}$-$(G)_6$-Est2 *bar1-Δ::NAT*
	YVL4301	Cdc13-(FLAG)3*::TRP1* est1-K444E-$(G)_6$-$(myc)_{12}$ $(myc)_{12}$-$(G)_6$-Est2 *bar1-Δ::NAT*
	YVL4329	est1-K444E-$(G)_6$-$(myc)_{12}$ $(myc)_{12}$-$(G)_6$-Est2 *bar1-Δ::NAT*
	YVL3994	cdc13-E252K-(FLAG)3*::TRP1* est1-K444E-$(G)_6$-$(myc)_{12}$ $(myc)_{12}$-$(G)_6$-Est2 *bar1-Δ::NAT*
	YVL4340	Cdc13-(FLAG)3*::TRP1* est1-R447E-$(G)_6$-$(myc)_{12}$ $(myc)_{12}$-$(G)_6$-Est2 *bar1-Δ::NAT*
	YVL4313	est1-R485E-$(G)_6$-$(myc)_{12}$ $(myc)_{12}$-$(G)_6$-Est2 *bar1-Δ::NAT*
	YVL4325	Cdc13-(FLAG)3*::TRP1* est1-R488E-$(G)_6$-$(myc)_{12}$ $(myc)_{12}$-$(G)_6$-Est2 *bar1-Δ::NAT*
	YVL4315	est1-R488E-$(G)_6$-$(myc)_{12}$ $(myc)_{12}$-$(G)_6$-Est2 *bar1-Δ::NAT*
	YVL4305	Cdc13-(FLAG)3*::TRP1* est1-E500R-$(G)_6$-$(myc)_{12}$ $(myc)_{12}$-$(G)_6$-Est2 *bar1-Δ::NAT*
	YVL4317	est1-E500R-$(G)_6$-$(myc)_{12}$ $(myc)_{12}$-$(G)_6$-Est2 *bar1-Δ::NAT*
	YVL4307	Cdc13-(FLAG)3*::TRP1* est1-D510R-$(G)_6$-$(myc)_{12}$ $(myc)_{12}$-$(G)_6$-Est2 *bar1-Δ::NAT*
	YVL4321	est1-D510R-$(G)_6$-$(myc)_{12}$ $(myc)_{12}$-$(G)_6$-Est2 *bar1-Δ::NAT*
	YVL4344	Cdc13-(FLAG)3*::TRP1* est1-F511D-$(G)_6$-$(myc)_{12}$ $(myc)_{12}$-$(G)_6$-Est2 *bar1-Δ::NAT*
	YVL4319	est1-F511D-$(G)_6$-$(myc)_{12}$ $(myc)_{12}$-$(G)_6$-Est2 *bar1-Δ::NAT*
	YVL4309	Cdc13-(FLAG)3*::TRP1* est1-K555E-$(G)_6$-$(myc)_{12}$ $(myc)_{12}$-$(G)_6$-Est2 *bar1-Δ::NAT*
	YVL4323	est1-K555E-$(G)_6$-$(myc)_{12}$ $(myc)_{12}$-$(G)_6$-Est2 *bar1-Δ::NAT*
6-20	YVL4032	Est1-$(G)_6$-$(FLAG)_6$-$(myc)_{12}$ $(myc)_{12}$-$(G)_6$-Est2 Est3-$(G)_6$-$(myc)_{12}$ *bar1-Δ::KAN*
	YVL3616	Est1-$(G)_6$-$(FLAG)_6$-$(myc)_{12}$/Est1-$(G)_6$-$(myc)_{12}$ $(myc)_{12}$-$(G)_6$-Est2 Est3-$(G)_6$-$(myc)_{12}$
6-22a	YVL3905	Est1-$(G)_6$-$(myc)_{12}$ $(myc)_{12}$-$(G)_6$-Est2 Ebs1-$(FLAG)_3$*::TRP bar1-Δ::NAT*
	YVL3983	est1-Y136D-$(G)_6$-$(myc)_{12}$ $(myc)_{12}$-$(G)_6$-Est2 Ebs1-$(FLAG)_3$*::TRP bar1-Δ::NAT*
6-22c, e	YVL4127	Upf1-$(myc)_{13}$*::KAN*
	YVL4128	Est1-$(G)_6$-$(myc)_{12}$ $(myc)_{12}$-$(G)_6$-Est2 Ebs1-$(FLAG)_3$::TRP Upf1-$(myc)_{13}$*::KAN bar1-Δ::NAT*
	YVL4144	Est1-$(G)_6$-$(myc)_{12}$ $(myc)_{12}$-$(G)_6$-Est2 ebs1-K452E-$(FLAG)_3$*::TRP* Upf1-$(myc)_{13}$*::KAN bar1-Δ::NAT*
6-22e	YVL4145	Est1-$(FLAG)_3$*::TRP* Upf1-$(myc)_{13}$*::KAN*

Table 6.3 Plasmids used in this chapter (1 of 5).

Figure	Plasmid name	Type	Marker	Promoter	Gene
6-1b	pVL5613	*CEN*	*TRP1*	native	$EST1_{340\text{-}699}$-$(G)_6$-$(myc)_{12}$
	pVL5572	*CEN*	*TRP1*	native	$EST1_{1\text{-}340}$-$(G)_6$-$(myc)_{12}$
	pVL5573	*CEN*	*TRP1*	native	*EST1*-$(G)_6$-$(myc)_{12}$
6-1b, c	pVL5894	*CEN*	*URA3*	*ADH*	*EST1*
	pVL5570	integrating	*URA3*	native	$EST1_{1\text{-}340}$-$(G)_6$-$(myc)_{12}$
	pVL5608	integrating	*URA3*	native	$EST1_{340\text{-}699}$-$(G)_6$-$(myc)_{12}$
6-1d	pVL5575	*CEN*	*LEU2*	native	$EST1_{1\text{-}340}$-$(G)_6$-$(myc)_{12}$
	pVL5614	*CEN*	*LEU2*	native	$EST1_{340\text{-}699}$-$(G)_6$-$(myc)_{12}$
6-2 – 6-4	pVL367	*CEN*	*URA3*	native	*EST1*
	pVL6811	*CEN*	*URA3*	native	*est1-E4K*
	pVL6812	*CEN*	*URA3*	native	*est1-E4KE5K*
	pVL6813	*CEN*	*URA3*	native	*est1-E5K*
	pVL6789	*CEN*	*URA3*	native	*est1-N7R*
	pVL6814	*CEN*	*URA3*	native	*est1-E8K*
	pVL6791	*CEN*	*URA3*	native	*est1-F40E*
	pVL6790	*CEN*	*URA3*	native	*est1-F40R*
	pVL6872	*CEN*	*URA3*	native	*est1-F43E*
	pVL6871	*CEN*	*URA3*	native	*est1-F43K*
	pVL6911	*CEN*	*URA3*	native	*est1-H48K*
	pVL6912	*CEN*	*URA3*	native	*est1-K50E*
	pVL6793	*CEN*	*URA3*	native	*est1-W87E*
	pVL6792	*CEN*	*URA3*	native	*est1-W87R*
	pVL6858	*CEN*	*URA3*	native	*est1-W97E*
	pVL6873	*CEN*	*URA3*	native	*est1-W97K*
	pVL6794	*CEN*	*URA3*	native	*est1-F98D*
	pVL6815	*CEN*	*URA3*	native	*est1-E99K*
	pVL6795	*CEN*	*URA3*	native	*est1-F102E*
	pVL6816	*CEN*	*URA3*	native	*est1-F102R*
	pVL6875	*CEN*	*URA3*	native	*est1-H103E*
	pVL6874	*CEN*	*URA3*	native	*est1-H103K*
	pVL6914	*CEN*	*URA3*	native	*est1-K113E R115E*
	pVL6915	*CEN*	*URA3*	native	*est1-K113E F114E R115E*
	pVL6796	*CEN*	*URA3*	native	*est1-F114E*

Table 6.4 Plasmids used in this chapter (2 of 5).

Figure	Plasmid name	Type	Marker	Promoter	Gene
6-2 – 6-4	pVL6797	*CEN*	*URA3*	native	*est1-R115E*
	pVL6913	*CEN*	*URA3*	native	*est1-R115E F117E*
	pVL6798	*CEN*	*URA3*	native	*est1-F117R*
	pVL6817	*CEN*	*URA3*	native	*est1-R118E*
	pVL6800	*CEN*	*URA3*	native	*est1-K129E*
	pVL6917	*CEN*	*URA3*	native	*est1-K129E D147K*
	pVL6878	*CEN*	*URA3*	native	*est1-Y134D*
	pVL6802	*CEN*	*URA3*	native	*est1-Y135D*
	pVL6803	*CEN*	*URA3*	native	*est1-Y136D*
	pVL6804	*CEN*	*URA3*	native	*est1-Y146D*
	pVL6818	*CEN*	*URA3*	native	*est1-D147E*
	pVL6917	*CEN*	*URA3*	native	*est1-D147K*
	pVL6933	*CEN*	*URA3*	native	*est1-K223E*
	pVL6934	*CEN*	*URA3*	native	*est1-R226E*
	pVL6935	*CEN*	*URA3*	native	*est1-N229K*
	pVL6936	*CEN*	*URA3*	native	*est1-V238E*
	pVL6819	*CEN*	*URA3*	native	*est1-G239S*
	pVL6805	*CEN*	*URA3*	native	*est1-Y242D*
	pVL6820	*CEN*	*URA3*	native	*est1-R269E*
	pVL6806	*CEN*	*URA3*	native	*est1-Q320R*
6-6 – 6-8	pVL5576	*CEN*	*LEU2*	native	*EST1-$(G)_6$-$(myc)_{12}$*
	pVL6523	*CEN*	*LEU2*	native	*est1-N3R-$(G)_6$-$(myc)_{12}$*
	pVL6524	*CEN*	*LEU2*	native	*est1-N3E-$(G)_6$-$(myc)_{12}$*
	pVL6525	*CEN*	*LEU2*	native	*est1-E4K-$(G)_6$-$(myc)_{12}$*
	pVL6809	*CEN*	*LEU2*	native	*est1-E4K E5K-$(G)_6$-$(myc)_{12}$*
	pVL6526	*CEN*	*LEU2*	native	*est1-E5K-$(G)_6$-$(myc)_{12}$*
	pVL6528	*CEN*	*LEU2*	native	*est1-N7E-$(G)_6$-$(myc)_{12}$*
	pVL6527	*CEN*	*LEU2*	native	*est1-N7R-$(G)_6$-$(myc)_{12}$*
	pVL6529	*CEN*	*LEU2*	native	*est1-E8K-$(G)_6$-$(myc)_{12}$*
	pVL6531	*CEN*	*LEU2*	native	*est1-D33E-$(G)_6$-$(myc)_{12}$*
	pVL6532	*CEN*	*LEU2*	native	*est1-E34K-$(G)_6$-$(myc)_{12}$*
	pVL6534	*CEN*	*LEU2*	native	*est1-F40E-$(G)_6$-$(myc)_{12}$*
	pVL6533	*CEN*	*LEU2*	native	*est1-F40R-$(G)_6$-$(myc)_{12}$*

Table 6.5 Plasmids used in this chapter (3 of 5).

Figure	Plasmid name	Type	Marker	Promoter	Gene
6-6 – 6-8	pVL6535	*CEN*	*LEU2*	native	*est1-K84E-(G)$_6$-(myc)$_{12}$*
	pVL6536	*CEN*	*LEU2*	native	*est1-W87R-(G)$_6$-(myc)$_{12}$*
	pVL6537	*CEN*	*LEU2*	native	*est1-W87E-(G)$_6$-(myc)$_{12}$*
	pVL6538	*CEN*	*LEU2*	native	*est1-E92K-(G)$_6$-(myc)$_{12}$*
	pVL6050	*CEN*	*LEU2*	native	*est1-F98D-(G)$_6$-(myc)$_{12}$*
	pVL6539	*CEN*	*LEU2*	native	*est1-E99K-(G)$_6$-(myc)$_{12}$*
	pVL6541	*CEN*	*LEU2*	native	*est1-F102E-(G)$_6$-(myc)$_{12}$*
	pVL6540	*CEN*	*LEU2*	native	*est1-F102R-(G)$_6$-(myc)$_{12}$*
	pVL6543	*CEN*	*LEU2*	native	*est1-F114E-(G)$_6$-(myc)$_{12}$*
	pVL6542	*CEN*	*LEU2*	native	*est1-F114R-(G)$_6$-(myc)$_{12}$*
	pVL6544	*CEN*	*LEU2*	native	*est1-R115E-(G)$_6$-(myc)$_{12}$*
	pVL6546	*CEN*	*LEU2*	native	*est1-F117E-(G)$_6$-(myc)$_{12}$*
	pVL6545	*CEN*	*LEU2*	native	*est1-F117R-(G)$_6$-(myc)$_{12}$*
	pVL6810	*CEN*	*LEU2*	native	*est1-R118E-(G)$_6$-(myc)$_{12}$*
	pVL6547	*CEN*	*LEU2*	native	*est1-K129E-(G)$_6$-(myc)$_{12}$*
	pVL6548	*CEN*	*LEU2*	native	*est1-Y134D-(G)$_6$-(myc)$_{12}$*
	pVL6549	*CEN*	*LEU2*	native	*est1-Y135D-(G)$_6$-(myc)$_{12}$*
	pVL6051	*CEN*	*LEU2*	native	*est1-Y136D-(G)$_6$-(myc)$_{12}$*
	pVL6052	*CEN*	*LEU2*	native	*est1-Y146D-(G)$_6$-(myc)$_{12}$*
	pVL6550	*CEN*	*LEU2*	native	*est1-D147E-(G)$_6$-(myc)$_{12}$*
	pVL6053	*CEN*	*LEU2*	native	*est1-G239S-(G)$_6$-(myc)$_{12}$*
	pVL6054	*CEN*	*LEU2*	native	*est1-Y242D-(G)$_6$-(myc)$_{12}$*
	pVL6055	*CEN*	*LEU2*	native	*est1-R269E-(G)$_6$-(myc)$_{12}$*
	pVL6056	*CEN*	*LEU2*	native	*est1-Q320R-(G)$_6$-(myc)$_{12}$*
6-9 – 6-13	pVL6643	integrating	*URA3*	native	*est1-E4K E5K-(G)$_6$-(myc)$_{12}$*
	pVL6642	integrating	*URA3*	native	*est1-E5K-(G)$_6$-(myc)$_{12}$*
	pVL6639	integrating	*URA3*	native	*est1-N7R-(G)$_6$-(myc)$_{12}$*
	pVL6888	integrating	*URA3*	native	*est1-F40R-(G)$_6$-(myc)$_{12}$*
	pVL6889	integrating	*URA3*	native	*est1-F40E-(G)$_6$-(myc)$_{12}$*
	pVL6896	integrating	*URA3*	native	*est1-K84A-(G)$_6$-(myc)$_{12}$*
	pVL6636	integrating	*URA3*	native	*est1-W87E-(G)$_6$-(myc)$_{12}$*
	pVL6897	integrating	*URA3*	native	*est1-Q89E-(G)$_6$-(myc)$_{12}$*
	pVL6071	integrating	*URA3*	native	*est1-F98D-(G)$_6$-(myc)$_{12}$*
	pVL6633	integrating	*URA3*	native	*est1-F102E-(G)$_6$-(myc)$_{12}$*

Table 6.6 Plasmids used in this chapter (4 of 5).

Figure	Plasmid name	Type	Marker	Promoter	Gene
6-9 – 6-13	pVL6413	integrating	*URA3*	native	*est1-K113E-$(G)_6$-$(myc)_{12}$*
	pVL6640	integrating	*URA3*	native	*est1-F114E-$(G)_6$-$(myc)_{12}$*
	pVL6644	integrating	*URA3*	native	*est1-R115E-$(G)_6$-$(myc)_{12}$*
	pVL6634	integrating	*URA3*	native	*est1-F117R-$(G)_6$-$(myc)_{12}$*
	pVL6414	integrating	*URA3*	native	*est1-R118E-$(G)_6$-$(myc)_{12}$*
	pVL6638	integrating	*URA3*	native	*est1-K129E-$(G)_6$-$(myc)_{12}$*
	pVL6637	integrating	*URA3*	native	*est1-Y134D-$(G)_6$-$(myc)_{12}$*
	pVL6072	integrating	*URA3*	native	*est1-Y136D-$(G)_6$-$(myc)_{12}$*
	pVL6073	integrating	*URA3*	native	*est1-Y146D-$(G)_6$-$(myc)_{12}$*
	pVL6646	integrating	*URA3*	native	*est1-D147E-$(G)_6$-$(myc)_{12}$*
	pVL6985	integrating	*URA3*	native	*est1-D147K-$(G)_6$-$(myc)_{12}$*
	pVL6986	integrating	*URA3*	native	*est1-N229K-$(G)_6$-$(myc)_{12}$*
	pVL6074	integrating	*URA3*	native	*est1-Y242D-$(G)_6$-$(myc)_{12}$*
	pVL6987	integrating	*URA3*	native	*est1-K254E-$(G)_6$-$(myc)_{12}$*
	pVL6075	integrating	*URA3*	native	*est1-Q320R-$(G)_6$-$(myc)_{12}$*
6-15	pVL809	2μ	*HIS3*	*ADH*	*EST1*
	pVL4733	2μ	*HIS3*	*ADH*	*est1-E366R*
	pVL4734	2μ	*HIS3*	*ADH*	*est1-D376R*
	pVL4692	2μ	*HIS3*	*ADH*	*est1-F408D*
	pVL4802	2μ	*HIS3*	*ADH*	*est1-W423D*
	pVL4534	2μ	*HIS3*	*ADH*	*est1-K444E*
	pVL4512	2μ	*HIS3*	*ADH*	*est1-R447E*
	pVL4513	2μ	*HIS3*	*ADH*	*est1-R455E*
	pVL4695	2μ	*HIS3*	*ADH*	*est1-W566D*
	pVL4517	2μ	*HIS3*	*ADH*	*est1-R485E*
	pVL4519	2μ	*HIS3*	*ADH*	*est1-R488E*
	pVL4823	2μ	*HIS3*	*ADH*	*est1-E494R*
	pVL4824	2μ	*HIS3*	*ADH*	*est1-D495R*
	pVL4826	2μ	*HIS3*	*ADH*	*est1-E500R*
	pVL4827	2μ	*HIS3*	*ADH*	*est1-D510R*
	pVL6473	2μ	*HIS3*	*ADH*	*est1-F511D*
	pVL4526	2μ	*HIS3*	*ADH*	*est1-D513R*
	pVL4530	2μ	*HIS3*	*ADH*	*est1-E540R*
	pVL4612	2μ	*HIS3*	*ADH*	*est1-K555E*

Table 6.7 Plasmids used in this chapter (5 of 5).

Figure	Plasmid name	Type	Marker	Promoter	Gene
6-15	pVL4694	2μ	*HIS3*	*ADH*	*est1-F556D*
	pVL4614	2μ	*HIS3*	*ADH*	*est1-K559E*
6-17 – 6-18	pVL5236	integrating	*URA3*	native	*est1-K444E-$(G)_6$-$(myc)_{12}$*
	pVL6686	integrating	*URA3*	native	*est1-R447E-$(G)_6$-$(myc)_{12}$*
	pVL6687	integrating	*URA3*	native	*est1-R485E-$(G)_6$-$(myc)_{12}$*
	pVL6688	integrating	*URA3*	native	*est1-R488E-$(G)_6$-$(myc)_{12}$*
	pVL6689	integrating	*URA3*	native	*est1-E500R-$(G)_6$-$(myc)_{12}$*
	pVL6691	integrating	*URA3*	native	*est1-D510R-$(G)_6$-$(myc)_{12}$*
	pVL6690	integrating	*URA3*	native	*est1-F511D-$(G)_6$-$(myc)_{12}$*
	pVL6692	integrating	*URA3*	native	*est1-K555E-$(G)_6$-$(myc)_{12}$*
6-18	pVL2076	CEN	*LEU2*	native	*EST3-$(FLAG)_3$*
6-20	pVL5577	integrating	*URA3*	native	*EST1-$(G)_6$-$(FLAG)_6$-$(myc)_{12}$*
6-22b	pVL6058	CEN	*LEU2*	native *EST1*	*$EBS1_{1-355}$-$EST1_{340-699}$-$(G)_6$-$(myc)_{12}$*

Site-directed mutation by Quickchange

For the loss-of-function assay, all untagged mutants were derived from pVL367 (p *CEN URA3 EST1*). For the dominant negative assay, all untagged mutants were derived from pVL809 (2μ *HIS3 ADH-EST1*). For plasmid-based biochemistry, all tagged mutants were derived from pVL5576 [(p *CEN LEU2 EST1-*$(G)_6$*-*$(myc)_{12}$)]. For integration, all tagged mutants were derived from pVL5187 [(*URA3 EST1-*$(G)_6$*-*$(myc)_{12}$)].

Oligos were designed so that the forward and reverse primers had ~40bp of overlap with one another, and 8-10bp of 5' non-overlapping sequence. PCR was carried out using the polymerase pfu Turbo (Stratagene) and the accompanying buffer. PCR conditions were as follows: 95˚ for 30s, followed by 18 cycles of 95˚ for 30s, 60˚ for 1min, and 68˚ for 15min. Resulting DNA was digested by DpnI, then amplified in *E. coli*, purified, and sent for sequencing of the mutated region (Eton Bioscience).

Loss of function assay

Standard genetic methods were used to transform p *CEN est1*$^-$ mutations (derived from pVL367) into YVL3814 [*est1*-Δ*::KAN* $(FLAG)_3$-$(myc)_{12}$-$(G)_6$-Est2 *bar1*-Δ*::KAN/* p *CEN URA EST1*] following 5-FOA eviction of the *EST1* covering plasmid. Transformants were propagated for ~80 cell divisions and examined for telomere length on southern blots as described in Chapter 2.

Dominant negative assay

Standard genetic methods were used to transform 2μ *est1*$^{-}$ mutations (derived from pVL809) into YVL2967. Transformants were propagated for ~80 cell divisions and examined for telomere length on southern blots as described in Chapter 2.

Biochemistry

Extract preparation, anti-FLAG immunoprecipitation, anti-FLAG and anti-myc western blots, and α-factor and nocodazole arrest were all performed as described in Chapter 3.

Acknowledgements

Chapter 6 contains material from a manuscript that is being prepared for publication: Tucey, T.M., Lubin, J.W., and Lundblad, V. (2013). Identification of four functionally distinct interfaces on Est1.

I am grateful to my collaborator, John Lubin, for providing an extensive genetic analysis of *EST1*.

Chapter 7: Yeast telomerase exists in two complexes

Introduction

The stoichiometry of the yeast telomerase complex is largely unknown. The prevailing assumption in the field has been that the three protein subunits are all in 1:1 stoichiometry with the RNA subunit, but there could be higher levels of association, as well as separate sub-complexes with distinct regulatory roles. There is also conflicting evidence for dimerization of telomerase subunits in yeast, as well as in other species (Alves et al., 2008; Bryan et al., 2003; Sauerwald et al., 2013; Shcherbakova et al., 2009; Yang et al., 2006). In budding yeast, it has been difficult to detect TLC1 and the Est proteins using *in vitro* and cytological techniques due to their low expression levels (Mozdy and Cech, 2006), and this has precluded a rigorous assessment of complex stoichiometry.

The pathways for biogenesis of the mature telomerase RNA vary from species to species, as well as the cellular processes involved in assembly of a biologically functional telomerase holoenzyme. In budding yeast, the proteins involved in RNA biogenesis have been identified but the mechanistic details are largely unclear. After *TLC1* is transcribed, it exists primarily as a nonpolyadenylated form (Chapon et al., 1997), with the 5' end modified as a TMG cap in the nucleolus. This processed form of TLC1 is exported to the cytoplasm and then re-imported to the nucleus (Gallardo et al., 2008). However, it is unknown when and in what cellular location Est1, Est2, and Est3 associate with the RNA, if all three proteins must be in a complex with TLC1 in order for it get imported to the nucleus, and subsequently, the composition of the nuclear complex that engages at the telomere.

With regard to the yeast telomerase subunit interactions, it has been well-established that the TLC1 RNA contains separate binding sites for Est1 and Est2 (Chappell and Lundblad, 2004; Seto et al., 2002), and that Est1 and Est2 can each form a stable complex with TLC1 in the absence of the other protein (Hughes et al., 2000). However, it is unclear how efficiently the limiting RNA subunit is in a complex with Est1 and Est2, and whether both proteins are fully bound to every RNA molecule throughout the cell cycle. In contrast to Est1 and Est2, Est3 does not appear to directly bind the RNA, but rather, its association requires an intact catalytic core and it is unclear exactly how it associates with telomerase, with conflicting evidence that Est3 associates via the N-terminus of Est2 (Hughes et al., 2000; Talley et al., 2011) or via Est1 (Tuzon et al., 2011). Furthermore, although individual protein-protein and protein-RNA interactions have been described, it is unclear how these interactions come together to form an active complex, and if there are intermediates or sub-complexes with different compositions.

Development of the biochemical assay described in Chapter 3 has allowed for a more rigorous assessment of complex stoichiometry through the cell cycle, and in this chapter, I provide evidence that yeast telomerase consists of at least two different complexes.

Results

Examining complex stoichiometry when Est3 is immunoprecipitated

In the process of developing a telomerase co-immunoprecipitation assay, multiple iterations of strains were constructed. As discussed in Chapters 3 and 5, when different tagged strains were subjected to Est2 immunoprecipitation, a general pattern emerged. Est1 was detected in a complex with Est2 throughout the cell cycle – with Est1 initially at a lower level of association in G1, and then fully associating with the complex in S phase and remaining fully associated for the remainder of the cell cycle. In contrast, association of the Est3 protein was barely detectable in G1 cells, and did not exhibit appreciable levels of association with telomerase until much later in the cell cycle (see Figure 3.4). Given that Est3 is the most abundantly expressed of the telomerase subunits, this suggests that Est3 association with telomerase is highly regulated and that it may be part of a separate sub-complex containing Est1 or other regulatory proteins.

To examine the Est3 complex directly, several different tagged strains were available for immunoprecipitating Est3. Figure 7.1 summarizes the biochemical properties of two different strains that allow for either Est2 or Est3 to be immunoprecipitated so that the two complexes can be directly compared from the exact same strain. The strain in Figure 7.1a has all tagged modifications integrated in the three *EST* genes, with the epitopes for immunoprecipitation highlighted in bold:

Est1-$(myc)_{13}$::TRP1 $(myc)_{12}$-**$(HA)_3$**-Est2 Est3-$(G)_8$-$(myc)_9$-**$(FLAG)_3$**

When doing an anti-FLAG immunoprecipitation from this strain, which quantitatively depletes Est3 from extracts, it is apparent that the ratio of Est1:Est2 is greater compared to the anti-HA immunoprecipitation of Est2. This same overall trend was observed in a different strain that has the tags for immunoprecipitation switched (Figure 7.1b). In this strain, the tags on Est1 and Est2 were integrated in the genome, and the tagged Est3 protein is expressed from a plasmid:

Est1-$(G)_6$-$(myc)_{12}$ **$(FLAG)_3$**-$(myc)_{12}$-$(G)_6$-Est2 pCEN Est3-$(G)_6$-$(myc)_6$-**$(HA)_3$**

From this strain, an anti-HA immunoprecipitation depletes the tagged Est3 protein from extracts, while anti-FLAG can be used to immunoprecipitate Est2. Using this strain, the Est3 complex also contains a greater ratio of Est1:Est2 compared to the Est2 complex (Figure 7.1b), although the overall amount of Est1 in either complex is less compared the strain shown in Figure 7.1a. Combined together, the results from Figure 7.1 suggest one of two possibilities: (1) there is a single telomerase complex containing multiple subunits of Est1, or (2) there are at least two different complexes.

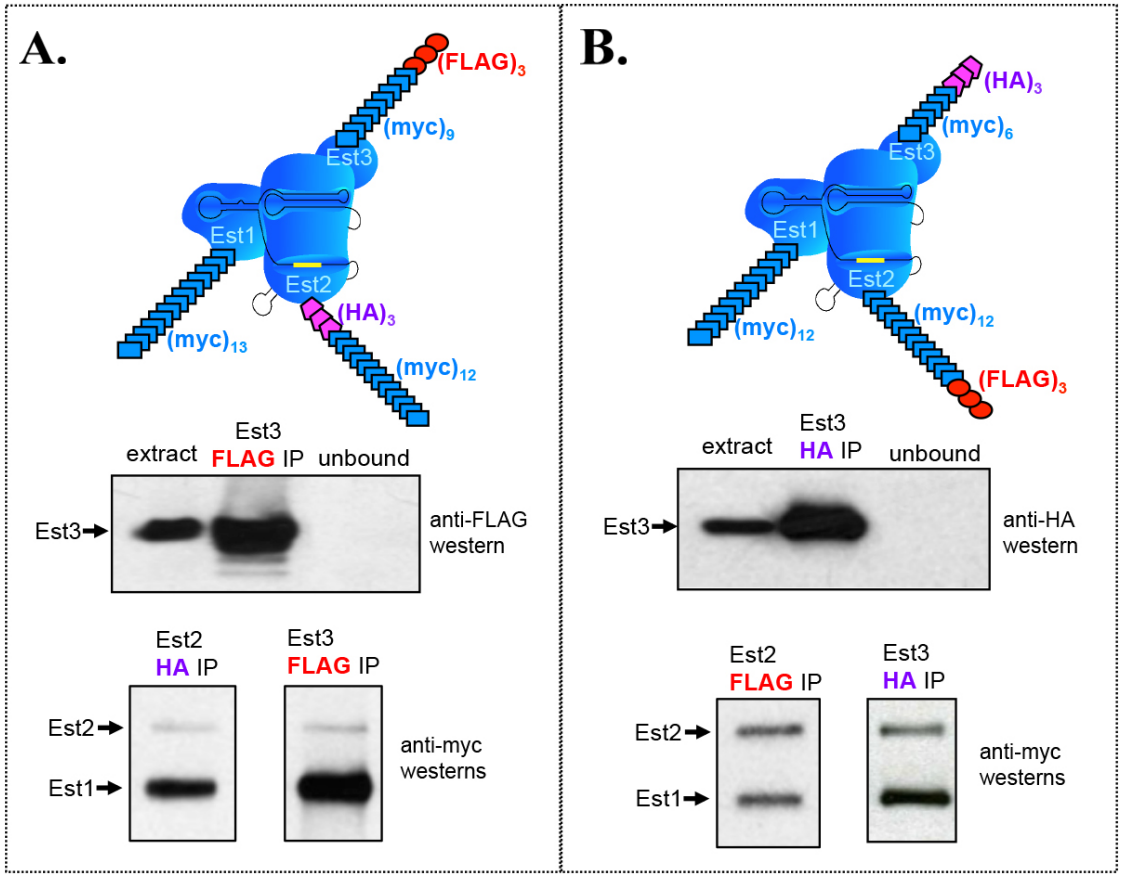

Figure 7.1 Comparison of Est2 and Est3 immunoprecipitation complexes from two different tagged strains. A) Biochemical analysis of a strain containing genomic integrations of Est1(myc)$_{13}$::TRP (myc)$_{12}$-(HA)$_3$-Est2 Est3-(myc)$_9$-(FLAG)$_3$: top panel illustrates the tag placement for this strain; middle panel is an anti-FLAG western monitoring the Est3-(myc)$_9$-(FLAG)$_3$ protein in extracts, Est3 immunoprecipitates, and the supernate recovered from the IP (two-fold more supernate than extract was loaded); bottom panel contains anti-myc westerns comparing the Est2 and Est3 immunoprecipitation complexes from this strain. B) Biochemical analysis of a strain containing genomic integrations of Est1-(myc)$_{12}$ (FLAG)$_3$-(myc)$_{12}$-Est2 and transformed with p *CEN* Est3-(myc)$_6$-(HA)$_3$: top panel illustrates the tag placement for this strain; middle panel is an anti-HA western monitoring the Est3-(myc)$_6$-(HA)$_3$ protein in extracts, Est3 immunoprecipitates, and the supernate recovered from the IP (two-fold more supernate than extract was loaded); bottom panel contains anti-myc westerns comparing the Est2 and Est3 immunoprecipitation complexes from this strain.

Because the strains in Figure 7.1 utilize different epitopes for immunoprecipitating Est2 or Est3, each epitope could be influencing the co-immunoprecipitated complex in subtle ways. To compare immunoprecipitations of Est2 and Est3 using the same epitope, two different strains were constructed (with all modifications integrated in the genome) that differed only in whether the $(FLAG)_3$ tag is positioned on Est2 or Est3:

Strain A: Est1-$(G)_6$-$(myc)_{12}$ **$(FLAG)_3$**-$(myc)_{12}$-$(G)_6$-Est2

Strain B: Est1-$(G)_6$-$(myc)_{12}$ $(myc)_{12}$-$(G)_6$-Est2 Est3-**$(FLAG)_3$**

As shown in Figure 7.2, the difference between the Est2 and Est3 complexes is even more dramatic, with greater than twice the ratio of Est1:Est2 in the Est3 complex compared to the Est2 complex. Furthermore, when the Est3-$(FLAG)_3$ protein was expressed form a plasmid rather than integrated, the same complex stoichiometry was observed. In all situations tested, the Est3 complex appears to contain a different stoichiometry than the Est2 complex.

The Est3 complex was also compared in G1 and G2/M arrested cells using α-factor and nocodazole, respectively. Figure 7.3 summarizes the observations from two different strains. As expected, the Est3 complex contains a barely detectable level of Est2 in G1 arrested cells, in agreement with the observation that Est2 immunoprecipitations contain a low detection of Est3 in this stage of the cell cycle. However, longer exposures reveal that the Est3 complex has the same stoichiometry in α-factor as the complex observed in nocodazole and asynchronous cells. Therefore, the stoichiometry of the Est3 complex appears to be consistent throughout the cell

cycle, but the overall amount of this complex is greater at later stages of the cell cycle. In contrast, the stoichiometry of the Est2 complex changes, with an increase in Est1 stoichiometry occurring during S phase at the time when Est1 expression levels increase, and a separate increase in Est3 stoichiometry later in the cell cycle. An α-factor arrest and release experiment has not yet been performed for the Est3 complex, but given that Est3 shows a delayed association with the Est2 complex (relative to Est1), it is expected that the increased presence of the Est3 complex will have a similarly delayed timing.

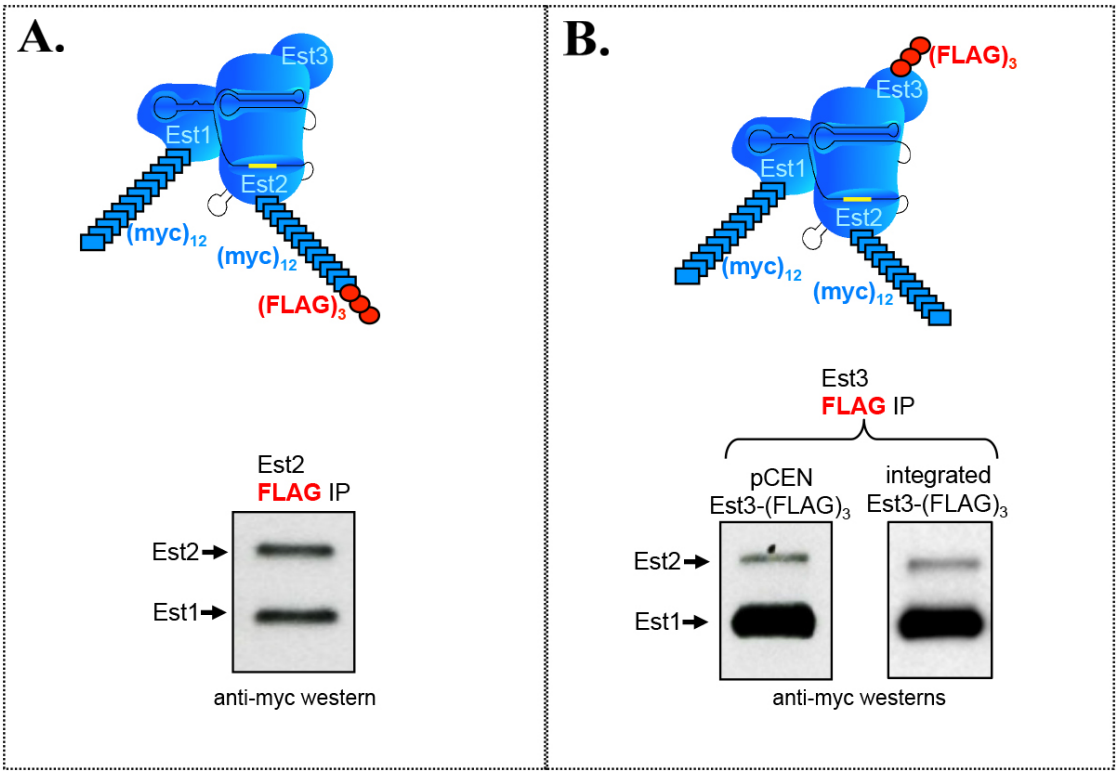

Figure 7.2 Comparison of Est2 and Est3 complexes when the same epitope is used for immunoprecipitation. A) Biochemical analysis of a strain containing genomic integrations of Est1(myc)$_{12}$ (FLAG)$_3$-(myc)$_{12}$-Est2: top panel illustrates the tag placement for this strain; bottom panel contains an anti-myc western of the Est2 immunoprecipitation complex from this strain. B) Biochemical analysis of strains containing genomic integrations of Est1(myc)$_{12}$ (myc)$_{12}$-Est2, and with Est3-(FLAG)$_3$ either integrated or expressed from a *CEN* plasmid: top panel illustrates the tag placement for these strains; bottom panel contains anti-myc westerns of the Est3 immunoprecipitation complexes from the strains.

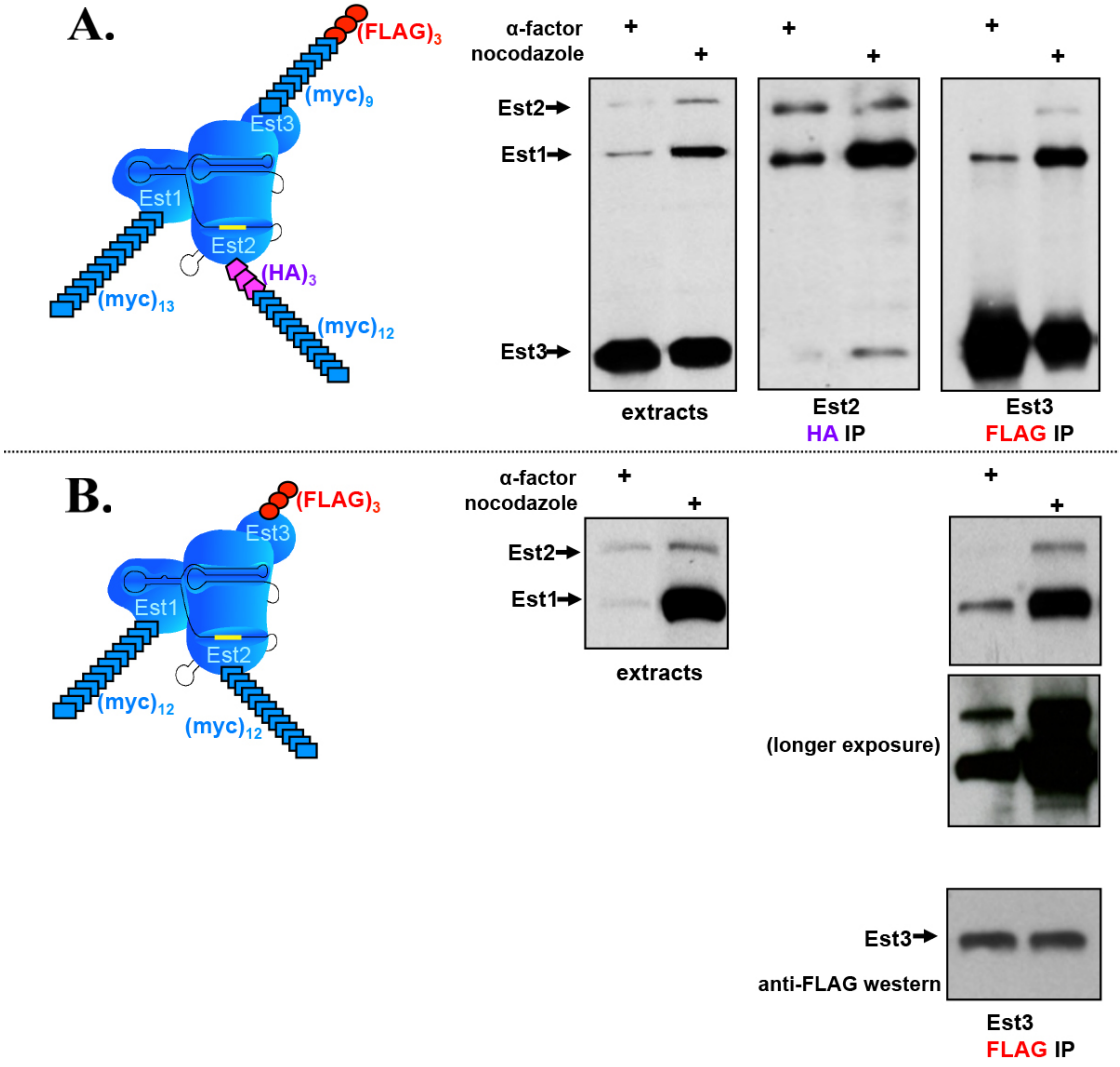

Figure 7.3 Examination of the Est3 immunoprecipitation complex from G1 and G2/M arrested cells. A) Biochemical analysis of a strain containing genomic integrations of Est1(myc)$_{13}$::TRP (myc)$_{12}$-(HA)$_3$-Est2 Est3-(myc)$_9$-(FLAG)$_3$: left panel illustrates the tag placement for this strain; right panel contains anti-myc westerns from extracts, Est2, and Est3 immunoprecipitations, from cells arrested in α-factor or nocodazole as indicated. B) Biochemical analysis of a strain containing genomic integrations of Est1(myc)$_{12}$ (myc)$_{12}$-Est2 Est3-(FLAG)$_3$: left panel illustrates the tag placement for this strain; middle panel contains an anti-myc western from extracts, from cells arrested in α-factor or nocodazole as indicated; right panel contains anti-myc and anti-FLAG westerns monitoring the Est3 immunoprecipitation complex from this strain.

A separate Est3-Est1 complex is detected in extracts depleted of Est2

The above observations suggest that multiple telomerase complexes could exist, but they do not rule out the possibility of a single Est1:Est2:Est3 complex that simply increases in abundance as the cell cycle progresses, but always retains the same stoichiometry. In order to directly look for separate complexes from the same extracts of the same strain, Est2 was depleted from extracts and then immunoprecipitated for Est3 to see if an Est3-Est1 complex could be detected. As shown in Figure 7.4, anti-FLAG immunoprecipitation could quantitatively deplete Est2 from extracts, and as expected, this Est2 complex was in 1:1 stoichiometry with Est1. When the supernatant was subsequently immunoprecipitated for Est3 using anti-HA beads, a separate Est1:Est3 complex could be detected that lacked any appreciable level of Est2. In contrast, when the same starting extract was directly immunoprecipitated for Est3, both Est2 and Est1 could be detected at the expected stoichiometry levels (about twice as much Est1 as Est2 in the complex). This provides direct evidence for a separate Est3-Est1 complex, although the levels of association with the Est3 complex were extremely modest: in both of the anti-HA immunoprecipitations, only a trace amount of Est2 and Est1 disappeared from the extract when examining the supernatant fractions.

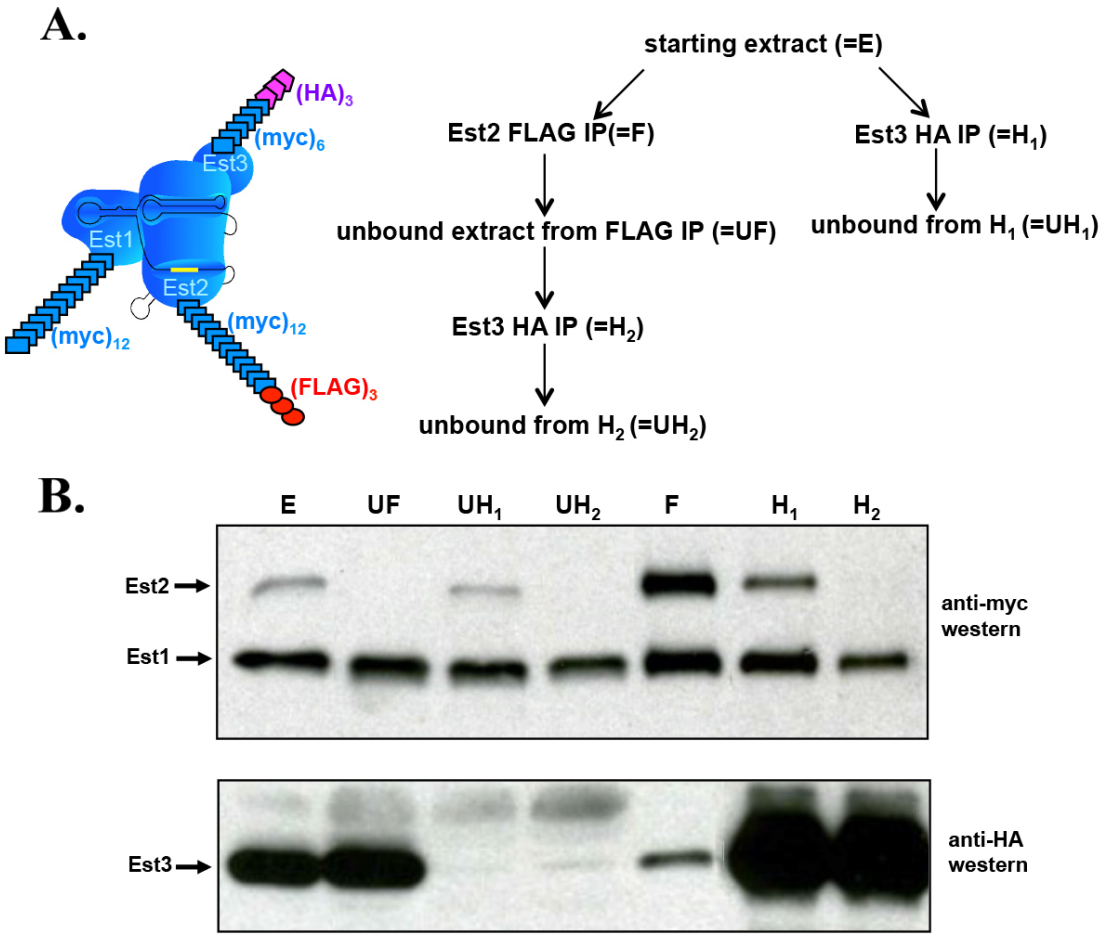

Figure 7.4 Detection of a separate Est3-Est1 complex from extracts depleted of Est2. A) Flow chart of the extract and immunoprecipitation samples collected from a strain containing genomic integrations of Est1-$(myc)_{12}$ $(FLAG)_3$-$(myc)_{12}$-Est2 and transformed with p *CEN* Est3-$(myc)_6$-$(HA)_3$. 1mL of starting extract was divided into equal 500µL aliquots for the anti-HA or anti-FLAG immunoprecipitations. B) anti-myc and anti-HA westerns monitoring Est1, Est2, and Est3 from the extract and immunoprecipitation samples. For the unbound lanes (UF, UH_1 and UH_2), the same volume was loaded as the volume loaded from the starting extract (E).

An Est1-TLC1-Est2 complex is required for Est3 association

The detection of a separate Est3-Est1 complex raises the possibility that Est3 might play a regulatory role in assembling or stabilizing a complex containing Est1, Est2, and TLC1, or that Est1 could be regulating Est3's association with the catalytic core. To test these possibilities, I investigated the Est2 and Est3 complexes under several genetic conditions, as shown in Figure 7.5. First, in a tagged stain where *EST3* is deleted, I found that I could still detect a complete association of Est1 with Est2 immunoprecipitates from asynchronous cells (Figure 7.5a), as well as in G1- and G2/M-arrested cells (data not shown). Thus, Est3 is not required for assembly of the complex containing Est1-TLC1-Est2.

Next, I examined the Est3 complex in three different mutations that have been shown to disrupt formation of the Est1-TLC1-Est2 complex: *tlc1-47* disrupts the binding site for Est1, *est1-Y136D* is an RNA-binding mutant (see Chapter 6), and *tlc1-59* disrupts the binding site for Est2. In all three genetic conditions, immunoprecipitation of Est2 has been shown to contain significantly reduced association of Est1. Similarly, when I examined the Est3 complex by anti-FLAG immunoprecipitation of Est3-$(FLAG)_3$, I found that the association of Est2 and Est1 were significantly reduced (Figures 7.5b – 7.5e). In all, the results from Figure 7.5 implicate two separate steps in the assembly of a telomerase complex containing Est1, Est2, and Est3: first, an Est1-TLC1-Est2 complex forms (which is not dependent on Est3), then a separate step occurs for Est3 association (which is completely dependent on the presence of an Est1-TLC1-Est2 complex).

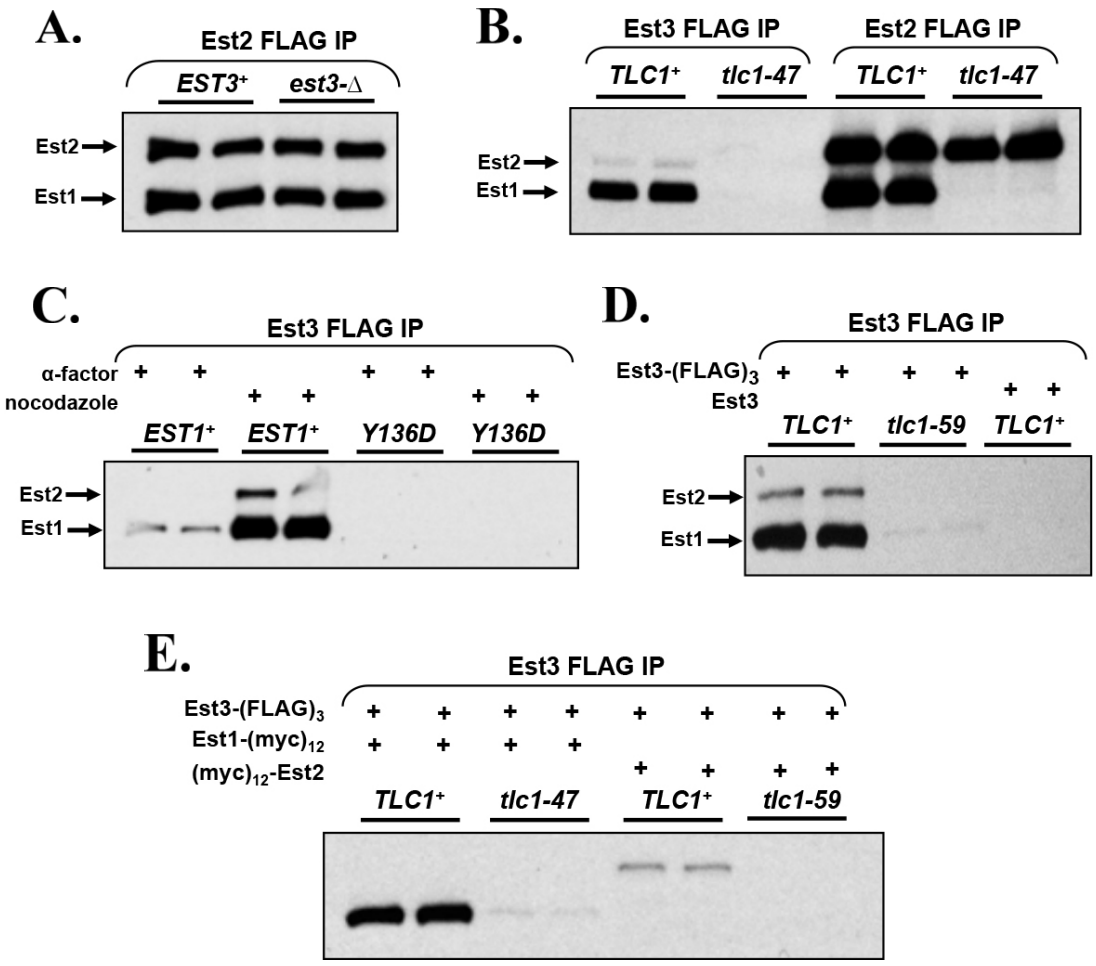

Figure 7.5 Loss of Est3 does not affect the formation of an Est1-TLC-Est2 complex, but the Est1-TLC1-Est2 complex is required for Est3 assembly. A) Anti-myc western comparing Est2 immunoprecipitates from strains expressing $(FLAG)_3$-$(myc)_{12}$-Est2 Est1-$(myc)_{12}$ with or without *est3*-Δ, all integrated in the genome. B) anti-myc western comparing Est3 immunoprecipitates from strains expressing Est1-$(myc)_{12}$ $(myc)_{12}$-Est2 p *CEN* Est3-$(FLAG)_3$ with or without the *tlc1-47* mutation, and Est2 immunoprecipitates from strains expressing Est1-$(myc)_{12}$ $(FLAG)_3$-$(myc)_{12}$-Est2 with or without the *tlc1-47* mutation. C) anti-myc western comparing Est3 immunoprecipitates from a strain expressing Est1-$(myc)_{12}$ $(myc)_{12}$-Est2 Est3-$(FLAG)_3$ with a strain expressing est1-Y136D-$(myc)_{12}$ $(myc)_{12}$-Est2 Est3-$(FLAG)_3$, all integrated in the genome. Cells were arrested in α-factor or nocodazole as indicated. D) anti-myc western comparing Est3 immunoprecipitates from strains expressing Est1-$(myc)_{12}$ $(myc)_{12}$-Est2 Est3-$(FLAG)_3$ all integrated in the genome, with or without the *tlc1-59* mutation. E) anti-myc western comparing Est3 immunoprecipitates from strains expressing Est1-$(myc)_{12}$ Est3-$(FLAG)_3$ or $(myc)_{12}$-Est2 Est3-$(FLAG)_3$, with or without an additional mutation in *tlc1-47* or *tlc1-59* as indicated.

The C-terminal half of Est1 associates with the Est3 complex, but only in the presence of full-length Est1

As discussed in Chapter 6, both the N- and C-terminal halves of Est1 could be detected from extracts, when expressed from plasmids as well as when integrated at the *EST1* locus. The N-terminus was shown to associate with the Est2 complex, suggesting that this half of the protein is involved in binding to the TLC1 RNA. However, the C-terminal half of Est1 did not associate with the Est2 complex, and mutants were identified in the C-terminus that reduced Est3 association, suggesting that the C-terminus of Est1 could be involved in the formation of a telomerase complex (or sub-complex) containing Est3.

To investigate this further, I expressed from plasmids the tagged versions of full-length Est1 and the N- and C-terminal halves, to see whether they co-immunoprecipitate with Est3. As shown in figure 7.6a, both halves of Est1 were detected in Est3 immunoprecipitates (left side), whereas only the N-terminal half of Est1 was detected in Est2 immunoprecipitates (right side). Furthermore, the stoichiometry of the Est1 fragments (as well as full-length Est1) were all greater in the Est3 complex compared to the Est2 complex, in agreement with previous results comparing the relative levels of Est1 in the Est2 versus Est3 complexes. However, since the truncations were expressed from plasmids, wild-type Est1 is also being expressed from the genomic locus, and presumably, a stable complex consisting of Est2, full-length untagged Est1, and TLC1, is also present.

To more directly examine the association of the Est1 truncations, the experiment was repeated using a strain where the tagged Est1 C-terminal half is integrated so that there is no untagged full-length Est1 interfering with the analysis. Surprisingly, when Est3 is immunoprecipitated from this strain, there is no detection of Est2 or the Est1 C-terminus in the Est3 complex (Figure 7.6b). This suggests that association of the Est1 C-terminus with the Est3 complex is dependent on full-length Est1 also being present, and that if full-length Est1 is present, the Est1 C-terminus can form a separate complex with Est3 that does not contain Est2. Combined with the results from Figure 7.5, the assembly of an Est1-TLC1-Est2 complex appears to subsequently allow the formation of a separate Est3-Est1 complex that involves the C-terminus of Est1.

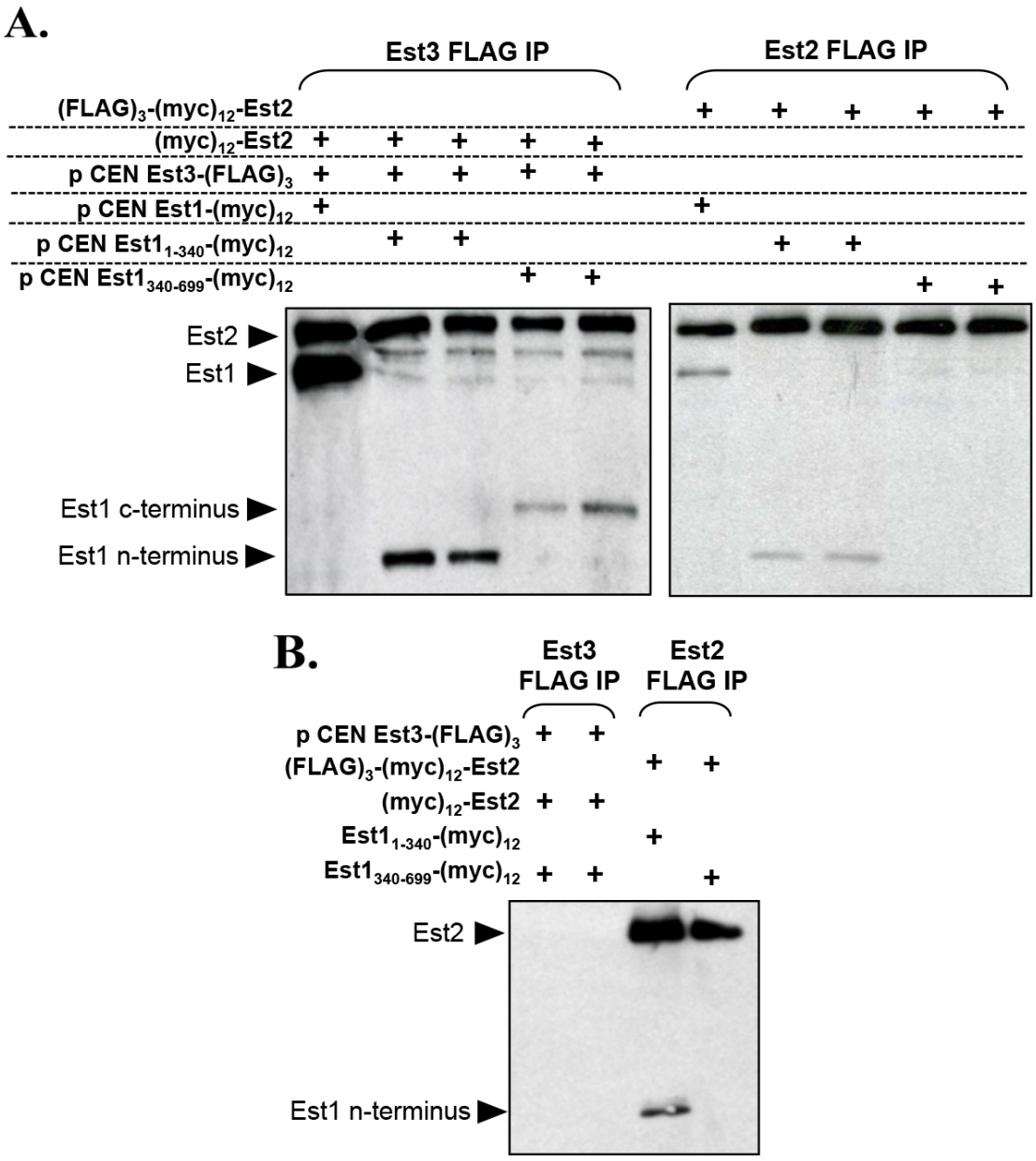

Figure 7.6 The C-terminal half of Est1 associates with the Est3 complex in the presence of full-length Est1. A) Anti-myc westerns: left side contains Est3 immunoprecipitations from strains containing $(myc)_{12}$-Est2 integrated in the genome and *CEN* plasmids introduced as indicated; right side contains Est2 immunoprecipitations from strains containing $(FLAG)_3$-$(myc)_{12}$-Est2 integrated in the genome and *CEN* plasmids introduced as indicated. B) anti-myc western comparing Est2 and Est3 immunoprecipitates from strains expressing Est3-$(FLAG)_3$ from a CEN plasmid, and $(FLAG)_3$-$(myc)_{12}$-Est2, $(myc)_{12}$-Est2, $Est1_{1-340}$-$(myc)_{12}$, and $Est1_{340-699}$-$(myc)_{12}$ integrated as indicated.

Mutations in all three Est protein subunits affect the stability of the Est3 complex

It is unclear exactly how Est3 associates with the telomerase complex, with conflicting reports of a direct interaction with Est1 (Tuzon et al., 2011) or Est2 (Talley et al., 2011). However, given the evidence in Figures 7.4 and 7.6 that telomerase exists in two separate complexes, it is possible that multiple protein-protein and/or protein-RNA interactions exist in order for Est3 to stably associate in two separate complexes.

The tagged strains described in Chapter 3, as well as the tagged Est3 constructs described in this chapter, provided multiple options for introducing mutations in *EST1*, *EST2*, and *EST3* to see whether any mutations affect the formation of the Est3 complex, in terms of the relative stoichiometry of Est1 and Est2 in the complex, as well as the overall levels of the Est3-containing complex compared to the parental strain controls. As shown in Figure 6.18, three mutations in the C-terminus of *EST1* (*est1-E500R*, *D510R*, and *F511D)* showed reduced levels of the Est3-containing complex despite similar protein expression from extracts. However, the stoichiometry of Est1/Est2 in these Est3-containing complexes appeared to be the same as the parental control strain. Similarly, 13 mutations in the N-terminus of *EST2* were also identified that resulted in a reduction of the Est3-containing complex but no change in Est1/Est2 stoichiometry (see Appendix B). Several of the Est2 mutants were especially pronounced for the reduction of the Est3 complex, suggesting that each individual residue is making a substantial contribution to Est3 association.

To examine Est3, mutations were generated in the p *CEN EST3-(FLAG)$_3$* plasmid, with particular emphasis on the classes of mutants from the dominant negative assays (see Chapter 2) that retained versus lost association with telomerase based on co-immunoprecipitation of TLC1. Unexpectedly, two mutations (*est3-N108R* and *est3-R110A*) resulted in strikingly increased amounts of the Est3-containing complex, to the extent where the detection in G1-arrested cells looked similar to the wild-type control nocodazole arrested cells (Figure 7.7a). However, other mutations resulted in significantly decreased levels of detection. This was consistent with the TLC1 co-immunoprecipitation results: mutations in E114A, N117K, D166R, and V168D all showed reduced levels of TLC1 co-immunoprecipitation as well as reduced association of Est2/Est1, while mutations in K71E and R110A retained association in both assays (and with R110A showing increased association in the western blot analysis). Similar to the Est1 and Est2 mutants, the overall stoichiometry of Est1/Est2 was consistent, but rather, the overall amounts of the complex changed. So far, no mutations have been isolated that change the stoichiometry of the Est3-containing complex.

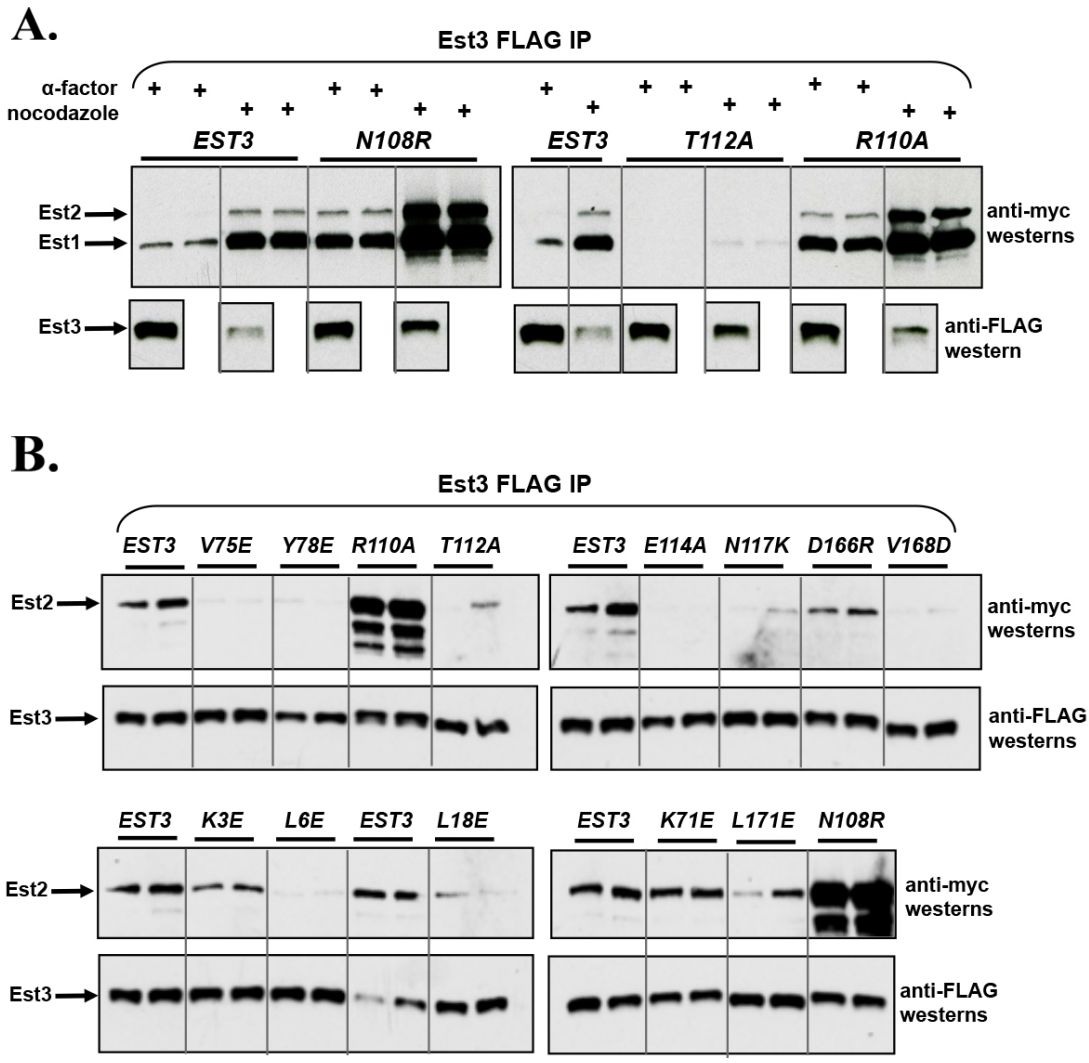

Figure 7.7 Mutations in *EST3* result in an increase or decrease in complex abundance. A) Anti-FLAG and anti-myc western blots of anti-FLAG IPs prepared from strains expressing est3-(FLAG)$_3$ mutants from a *CEN* plasmid, and Est1-(myc)$_{12}$ and Est2-(myc)$_{12}$ integrated in the genome, in α-factor and nocodazole-arrested cells as indicated. For each condition, two independent isolates were prepared for the anti-myc western, and one isolate was checked on an anti-FLAG western for Est3 immunoprecipitation levels. B) Anti-FLAG and anti-myc western blots of anti-FLAG IPs prepared from strains expressing est3-(FLAG)3 mutants from a *CEN* plasmid, and Est2-(myc)12 integrated in the genome. For each mutation, immunoprecipitates were prepared for two independent isolates and both isolates were examined on anti-myc and anti-FLAG western blots.

Discussion

Using the biochemical assay described in this thesis, I have made two different observations about Est3 that create a paradox. In contrast to Est1, Est3 does not fully associate with the Est2-containing complex (i.e. the catalytic core) until much later in the cell cycle. Since Est3 is in excess by ≈4-fold relative to the other subunits, this implies that there is a distinct regulatory mechanism that dictates Est3 association with the complex. However, when Est3 is immunoprecipitated, a different picture emerges. The Est3 immunoprecipitation brings down Est1 early in the cell cycle, but with a greater stoichiometry of Est1 than Est2 in the complex, and this stoichiometry remains unchanged throughout the cell cycle while the overall amount of this complex increases. Curiously, however, the ability of Est1 AND Est2 to associate with the RNA is absolutely required for the association of Est3. This paradox is not consistent with current models about telomerase and suggests that I have uncovered a potential key regulatory step.

There are three possibilities for explaining the different complex stoichiometries observed when Est3 versus Est2 is immunoprecipitated: (1) in the Est2 immunoprecipitates, only a portion of the Est2 subunits are actually in a complex with Est1 (in a stoichiometry that is the same as the Est3 complex), while the remaining Est2 subunits contain no Est1 and are obscuring the analysis; (2) the tagged Est2 and Est3 proteins are behaving differently, in terms of how they are immunoprecipitated or detected on western blots, or there is a functional consequence from the tags

(particularly for Est3) that changes how the complex is forming; (3) the stoichiometry differences actually reflect distinct complexes of telomerase.

With regard to possibility 1, given the low expression levels of TLC1 and Est2 in the cell, I am inclined to believe that there is a tight regulation of telomerase biogenesis that results in the majority of RNA molecules being bound with both Est2 as well as Est1. In G1 of the cell cycle, when Est2 and Est1 are expressed at the same levels, roughly half of the Est1 molecules are present in the Est2-containing complex. Furthermore, by late S phase, Est1 appears to be fully associated in the Est2-containing complex, and if Est1 is over-expressed, no further increase in association is observed, suggesting that the complex is fully saturated. Also, I did not see evidence for multiple Est1 subunits being present in a single complex when two different tagged versions of Est1 were expressed in the same strain (see Figure 6.20). Therefore, I believe that most, if not all, of the Est2 molecules are in a complex with TLC1 and Est1 by early S phase of the cell cycle. In contrast, Est3 is clearly in excess with only a small portion existing in a complex with Est2 and Est1, arguing that its association with telomerase is not tightly coupled with biogenesis.

Possibility 2 is a significant issue in terms of how the placement of different epitope tags could be affecting the biochemical analysis. Indeed, I noticed some striking differences in complex stoichiometry when different epitopes were used for the immunoprecipitations. Another caveat is that every integrated strain with a tag on Est3 resulted in a noticeable decrease in telomere length. Thus, it is possible that Est3 would normally display a stronger association with telomerase and potentially form a

complex with even Est1:Est2 stoichiometry if, for example, the tag on Est3 is impeding an association with Est2. However, I created so many different combinations of strains that all highlight the same general trend: that Est1 and Est3 have different patterns of association with the catalytic core of telomerase, with Est1 at a higher stoichiometry in the Est3 complex compared to the Est2 complex. This trend is consistent when the tagged proteins are expressed from plasmids as well as when integrated in the genome, and there does not appear to be a significant change in this trend when using different tagged Est3 proteins that cause different degrees of telomere shortening. It is also notable that I have yet to find any mutations in any of the *EST* genes that change the stoichiometry of the Est3-containing complex for a given strain – only the overall levels of the complex appear to change – arguing that any functional consequence from the tag on Est3 is not affecting the complex stoichiometry, but potentially is affecting the total amount of the complex that forms.

I believe that possibility 3 is the most likely explanation for the stoichiometry differences. Two experiments shown in this chapter directly implicate a separate Est3-Est1 complex. After Est2 was depleted from extracts, an Est3-Est1 complex was detected that lacked any appreciable level of Est2 (Figure 7.4). Also, it was shown that the C-terminal half of Est1 is incapable of associating with the Est2 complex in the presence of full-length untagged Est1. In contrast, the C-terminal half of Est1 was clearly detected in the Est3 complex in the presence of full-length Est1 (Figure 7.6), and since this complex also contained Est2, then by default, the Est2 complex should have also contained the C-terminal half of Est1 unless it is in a separate complex.

Somewhat surprisingly, in *tlc1-59*, an Est3-Est1 complex was not detected, suggesting that the stem loop defined by that mutation is required for a separate Est3-Est1 complex, or that a separate Est3-Est1 complex is only present after formation of an Est1-TLC1-Est2 complex. If so, this separate Est3-Est1 complex could potentially have a key regulatory role, or it could serve as an intermediate for subsequent placement of Est3 onto the Est1-TLC1-Est2 complex, resulting in a more stable Est1-TLC1-Est2-Est3 complex. This is supported by the observation that mutations in the C-terminus of Est1 affected Est3 association, but to a lesser extent than mutations in the N-terminus of Est2.

Given that the Est1-TLC1-Est2 complex can stably associate in the absence of Est3, I believe that Est3 association is occurring as a downstream step following Est1-TLC1-Est2 complex formation. Since Est3 is in excess, it should readily associate with the telomerase complex unless there is some kind of negative regulation that is delaying its association. Furthermore, the observation that different mutations in Est3 significantly increase or decrease the amount of the Est3-containing complex, with both classes of mutants having severe dominant negative phenotypes, suggests that there is an additional level of regulation involving Est3.

Most of the results from this chapter were obtained towards the end of my graduate studies, and some additional experiments should be performed to examine the biological significance of separate telomerase complexes. An α-factor arrest and release analysis should be done on the Est3 complex to look for any stoichiometry changes at specific stages in the cell cycle, as well as to determine whether the timing

of Est3 complex formation corresponds with the timing of the Est1 or Est3 association observed in the Est2 complex. I expect that the Est3 complex stoichiometry will be consistent throughout the cell cycle, with the levels of the complex increasing later in the cell cycle (around late S phase or G2) compared to when Est1 fully assembles with the Est2 complex (in early S phase). This could be further confirmed by examining the Est3 complex in a strain containing tandem copies of Est1-$(myc)_{12}$, to see whether there is any change in the levels of the Est3 complex when Est1 is fully assembled with the Est2 complex throughout the cell cycle. In this situation, if Est3 still exhibits delayed association, with the Est3 complex increasing in abundance during the later stages of the cell cycle, then that would implicate a distinct regulatory mechanism for Est3 association with telomerase that is independent of Est1 association with the complex.

Further experiments should also be done to examine the residues on Est1, Est2, and Est3 that are involved in stable complex formation. This thesis has identified residues in the C-terminus of Est1, the N-terminus of Est2, as well as a cluster of residues on the structurally determined surface of Est3, that all affect the levels of Est3 complex formation. Combinations of mutations should be examined for inter- and intragenic suppression. Furthermore, the Est3 mutants should be examined for association with the Est2 complex, to see if there is similarly an increase or decrease in association that is similar to what was observed when the Est3 mutants were immunoprecipitated.

Finally, additional experiments should be done to confirm the presence and biological relevance of separate Est1-Est3 and Est1-Est2-Est3 complexes. Similar to the Est1 analysis shown in Figure 6.20, different tagged versions of Est2 and Est3 should also be used to confirm that multiple subunits of Est2 or Est3 do not exist in the same complex. Also, Est2, the limiting protein, should be overexpressed to see whether a separate Est1-Est3 complex can still be detected. If so, it would suggest that this separate Est1-Est3 complex is not simply due to a limited availability of Est2 to fully associate with all the complexes, but rather, it could be a sub-complex that performs a regulatory role in telomere homeostasis distinct from the intact holoenzyme.

Materials and methods

Strains and plasmids

The parental strain for generating the tagged strains for biochemical analysis was AVL78 (*MAT***a** *leu2 trp1 ura3-52 prb1 prc1 pep4-3*). Strains were constructed in four different ways: (1) plasmid transformation, (2) pop-in / pop-out two step allele replacement, (3) C-terminal tagging via one step gene replacement (Longtine et al., 1998), (4) deletion via one step gene replacement (Longtine et al., 1998). See Chapter 3 for more details, including pedigrees that outline the derivations of tagged strain constructions.

For strains containing covering plasmids, 5-fluoroorotic acid (5-FOA) was used for eviction as described in previous chapters.

Table 7.1 lists the strains used in this chapter and the corresponding figure(s) in which they appear. Table 7.2 lists the plasmids used in this chapter and the corresponding figure(s) in which they appear.

Table 7.1 Strains used in this chapter.

Figure	Strain	Genotype
7.1a, 7.3a	YVL3437	Est1-$(myc)_{13}$::TRP1 $(myc)_{12}$-$(HA)_3$-Est2 Est3-$(G)_8$-$(myc)_9$-$(FLAG)_3$
7.1b, 7.2a, 7.4, 7.5	YVL3528	Est1-$(G)_6$-$(myc)_{12}$ $(FLAG)_3$-$(myc)_{12}$-$(G)_6$-Est2 *bar1-Δ::KAN*
7.2b, 7.5d	YVL3803	Est1-$(G)_6$-$(myc)_{12}$ $(myc)_{12}$-$(G)_6$-Est2 *bar1-Δ::NAT*
7.2b, 7.3a, 7.5	YVL3813	Est1-$(G)_6$-$(myc)_{12}$ $(myc)_{12}$-$(G)_6$-Est2 Est3-$(FLAG)_3$ *bar1-Δ::NAT*
7.5a	YVL3978	Est1-(G)6-(myc)12 (FLAG)3-(myc)12-(G)6-Est2 est3-Δ::NAT bar1-Δ::KAN/p *CEN URA EST3*
7.5b	YVL3828	Est1-$(G)_6$-$(myc)_{12}$ $(myc)_{12}$-$(G)_6$-Est2 *tlc1-47 bar1-Δ::NAT/* p *CEN URA TLC1*
	YVL3781	Est1-$(G)_6$-$(myc)_{12}$ $(FLAG)_3$-$(myc)_{12}$-$(G)_6$-Est2 *tlc1-47/* p *CEN URA TLC1*
7.5c	YVL4025	est1-Y136D-$(G)_6$-$(myc)_{12}$ $(myc)_{12}$-$(G)_6$-Est2 Est3-$(FLAG)_3$ *bar1-Δ::NAT/* p *CEN URA EST1*
7.5d	YVL4048	Est1-$(G)_6$-$(myc)_{12}$ $(myc)_{12}$-$(G)_6$-Est2 Est3-$(FLAG)_3$ *tlc1-59 bar1-Δ::NAT/* p *CEN URA TLC1*
7.5e	YVL4348	Est1-$(G)_6$-$(myc)_{12}$ Est3-$(FLAG)_3$ *bar1-Δ::NAT*
	YVL4358	Est1-$(G)_6$-$(myc)_{12}$ Est3-$(FLAG)_3$ *tlc1-47 bar1-Δ::NAT/*p *CEN URA TLC1*
	YVL4350	$(myc)_{12}$-$(G)_6$-Est2 Est3-$(FLAG)_3$ *bar1-Δ::NAT*
	YVL4360	$(myc)_{12}$-$(G)_6$-Est2 Est3-$(FLAG)_3$ *tlc1-59 bar1-Δ::NAT/*p *CEN URA TLC1*
7.6a	YVL3485	$(myc)_{12}$-$(G)_6$-Est2
	YVL3487	$(FLAG)_3$-$(myc)_{12}$-$(G)_6$-Est2
7.6b	YVL3692	$Est1_{1-340}$-$(G)_6$-$(myc)_{12}$ $(FLAG)_3$-$(myc)_{12}$-$(G)_6$-Est2 *bar1-Δ::KAN/* p *CEN URA EST1*
	YVL3830	$Est1_{340-699}$-$(G)_6$-$(myc)_{12}$ $(FLAG)_3$-$(myc)_{12}$-$(G)_6$-Est2 *bar1-Δ::KAN/* p *CEN URA EST1*
	YVL3832	$Est1_{340-699}$-$(G)_6$-$(myc)_{12}$ $(myc)_{12}$-$(G)_6$-Est2 *bar1-Δ::NAT/* p *CEN URA EST1*

Table 7.2 Plasmids used in this chapter.

Figure	Plasmid name	Type	Marker	Promoter	Gene
7.1b, 7.4	pVL6314	*CEN*	*LEU2*	native	*EST3-$(G)_6$-$(myc)_6$-$(HA)_3$*
7.2b, 7.6	pVL2076	*CEN*	*LEU2*	native	*EST3-$(FLAG)_3$*
7.5	pSD120	*CEN*	*URA3*	native	*TLC1*
7.5a	pVL2535	*CEN*	*URA3*	native	*EST3*
7.5c, 7.6	pVL5894	*CEN*	*URA3*	ADH	*EST1*
7.6a	pVL5573	*CEN*	*TRP1*	native	*EST1-$(G)_6$-$(myc)_{12}$*
	pVL5572	*CEN*	*TRP1*	native	*$EST1_{1-340}$-$(G)_6$-$(myc)_{12}$*
	pVL5613	*CEN*	*TRP1*	native	*$EST1_{340-699}$-$(G)_6$-$(myc)_{12}$*
7.7	pVL3506	*CEN*	*LEU2*	native	*est3-K3E-$(FLAG)_3$*
	pVL3505	*CEN*	*LEU2*	native	*est3-L6E-$(FLAG)_3$*
		CEN	*LEU2*	native	*est3-L18E-$(FLAG)_3$*
	pVL3454	*CEN*	*LEU2*	native	*est3-K71E-$(FLAG)_3$*
		CEN	*LEU2*	native	*est3-V75E-$(FLAG)_3$*
		CEN	*LEU2*	native	*est3-Y78E-$(FLAG)_3$*
		CEN	*LEU2*	native	*est3-N108R-$(FLAG)_3$*
		CEN	*LEU2*	native	*est3-R110A-$(FLAG)_3$*
		CEN	*LEU2*	native	*est3-T112A-$(FLAG)_3$*
		CEN	*LEU2*	native	*est3-E114A-$(FLAG)_3$*
	pVL3472	*CEN*	*LEU2*	native	*est3-N117K-$(FLAG)_3$*
	pVL3404	*CEN*	*LEU2*	native	*est3-D166R-$(FLAG)_3$*
	pVL3464	*CEN*	*LEU2*	native	*est3-V168D-$(FLAG)_3$*
		CEN	*LEU2*	native	*est3-L171E-$(FLAG)_3$*

Biochemical methods

Cell cycle arrests, extract preparation, HA and FLAG immunoprecipitations, and anti-FLAG and anti-myc westerns were performed as described in Chapter 3. Anti-HA westerns were probed with HA-11 16B12 (Covance) at 1:1000, followed by anti-mouse HRP (Cell signalling Technology) at 1:5000 and subsequent ECL detection as described in Chapter 3.

Site-directed mutation by Quickchange

For expressing tagged Est3 mutants, all plasmids were derived from pVL2076 [p *CEN URA3 EST3-(FLAG)$_3$*]. Quickchange mutagenesis was performed as described in Chapter 6.

Appendix A: Examination of candidate proteins for telomerase association

Testing proteins implicated in telomere homeostasis for association with yeast telomerase

In addition to examining the assembly and regulation of the known telomerase subunits, I was interested in finding novel proteins that interact with the complex. To the biochemical system described in Chapter 3, I introduced $(myc)_{13}$ or $(FLAG)_3$ tags onto a set of candidate proteins to determine whether each candidate associates with the telomerase complex. Candidates were chosen based on a selected subset of genes that have been reported to change telomere length when deleted (Askree et al., 2004). One class of candidates consists of proteins with well-characterized roles in telomere length regulation, but the biochemical function of the protein in question has not been determined (ex. Rif1, Rif2, Pif1, Sit4). The other class of candidates consists of novel ORFs which have a telomere length defect when deleted but otherwise have not been characterized at all. Two additional candidates, Rgi1 and Rgi2, were hits from a *C. albicans* Est3 yeast two hybrid screen.

The following candidates were tagged at the C-terminus with $(myc)_{13}$ via one-step gene modification (Longtine et al., 1998): Pif1, Pol12, Rif1, Rif2, Rgi1, Rgi2, Rtc1, Sit4, Tel1, Tpd3, Ygr042w. These candidates were tested for association with Est2 anti-FLAG immunoprecipitates, and a subset were also tested for association with Est3 anti-FLAG immunoprecipitates.

The following candidates were tagged at the C-terminus with $(FLAG)_3$ via one-step gene modification (Longtine et al., 1998): Ebs1, Mps3, Pif1, Pol1, Pol2,

Pol3, Pol30, Sir4, Yku80. These candidates were immunoprecipitated and then examined for Est1/Est2 co-immunoprecipitation.

All of the candidates I tested were inconclusive and/or did not display a significant association with telomerase, although I cannot rule out sub-stoichiometric or cell-cycle specific associations.

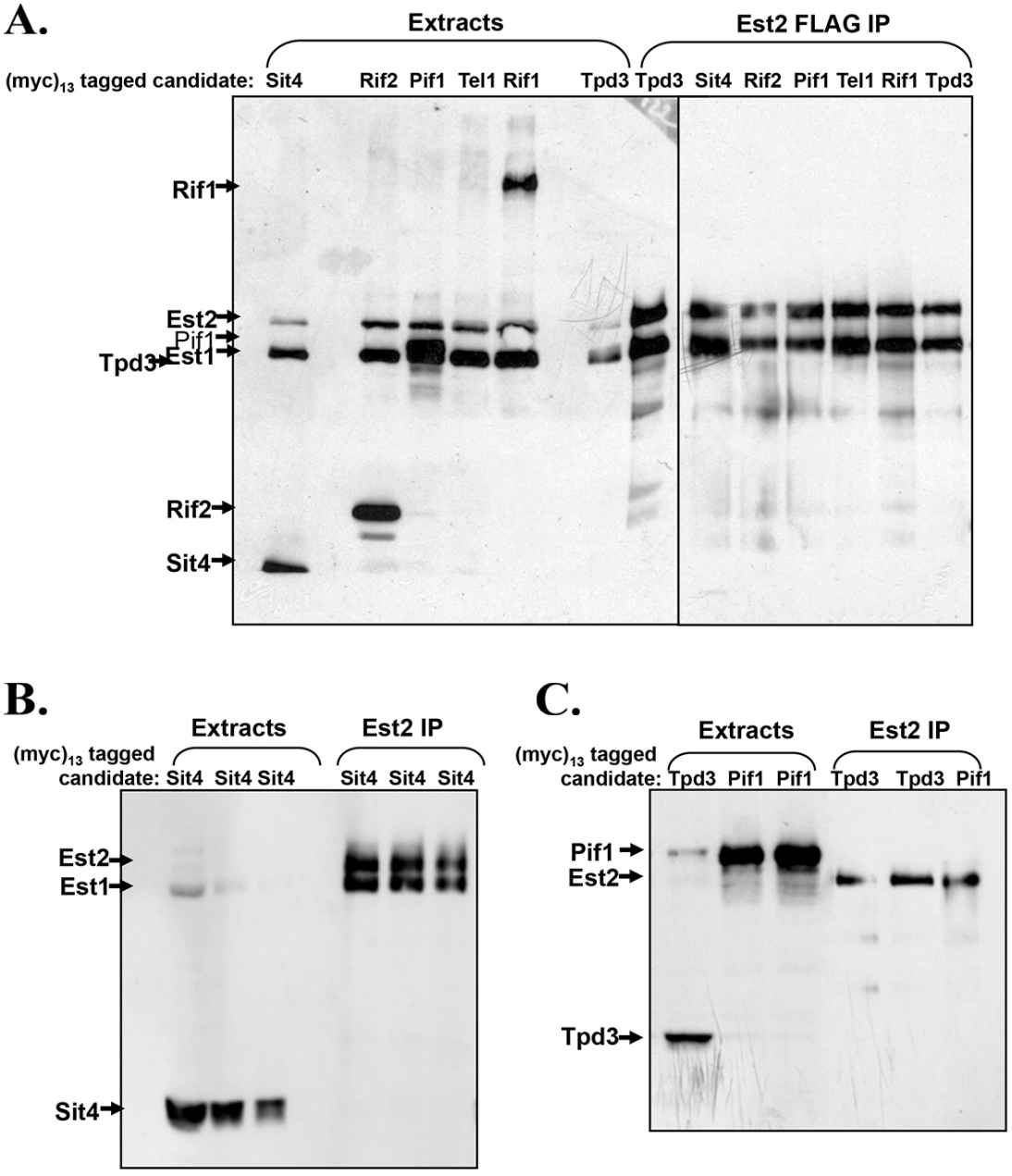

Figure A.1 Pif1, Rif1, Rif2, Sit4, and Tpd3 do not significantly associate with telomerase. A) Anti-myc western blots of extracts (left side) and anti-FLAG IPs (right side) prepared from stains expressing Est1-$(myc)_{12}$ $(FLAG)_3$-$(myc)_{12}$-Est2, with the candidate proteins tagged at the C-terminus with $(myc)_{13}$::TRP1 as indicated. Note that Tel1 was unable to be detected because the protein size is too large to be resolved on these 6% SDS-PAGE gels. B) anti-myc western blot prepared from the same Sit4 tagged strain in panel A, resolved on a higher percentage gel for better Sit4 detection. C) anti-myc western blot prepared from strains expressing $(FLAG)_3$-$(myc)_{12}$-Est2, with Tpd3 or Pif1 tagged at the C-terminus with $(myc)_{13}$::TRP1, as indicated.

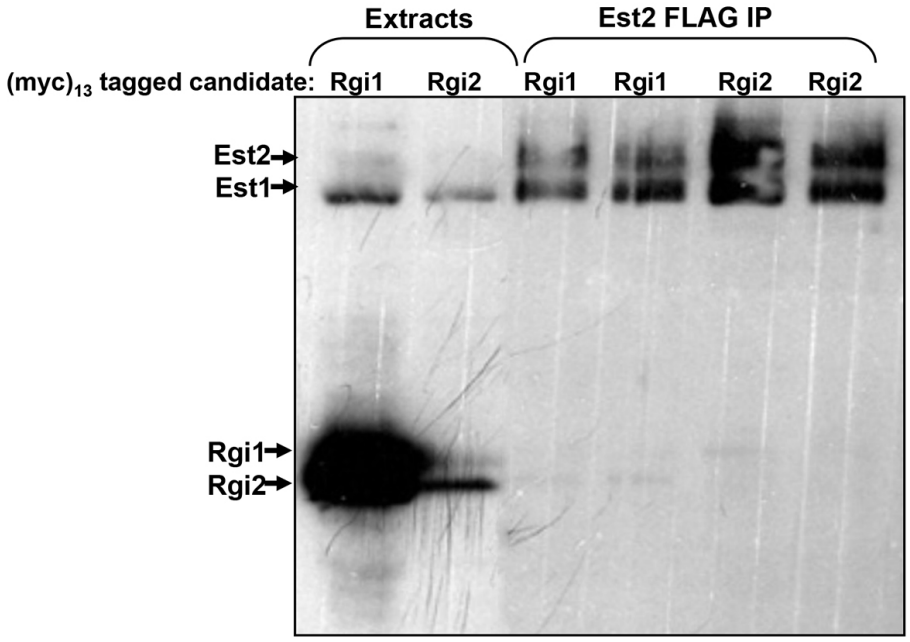

Figure A.2 Rgi1 and Rgi2 do not significantly associate with telomerase. Anti-myc western blot of extracts and anti-FLAG IPs prepared from stains expressing Est1-$(myc)_{12}$ $(FLAG)_3$-$(myc)_{12}$-Est2, with Rgi1 or Rgi2 tagged at the C-terminus with $(myc)_{13}$::TRP1 as indicated.

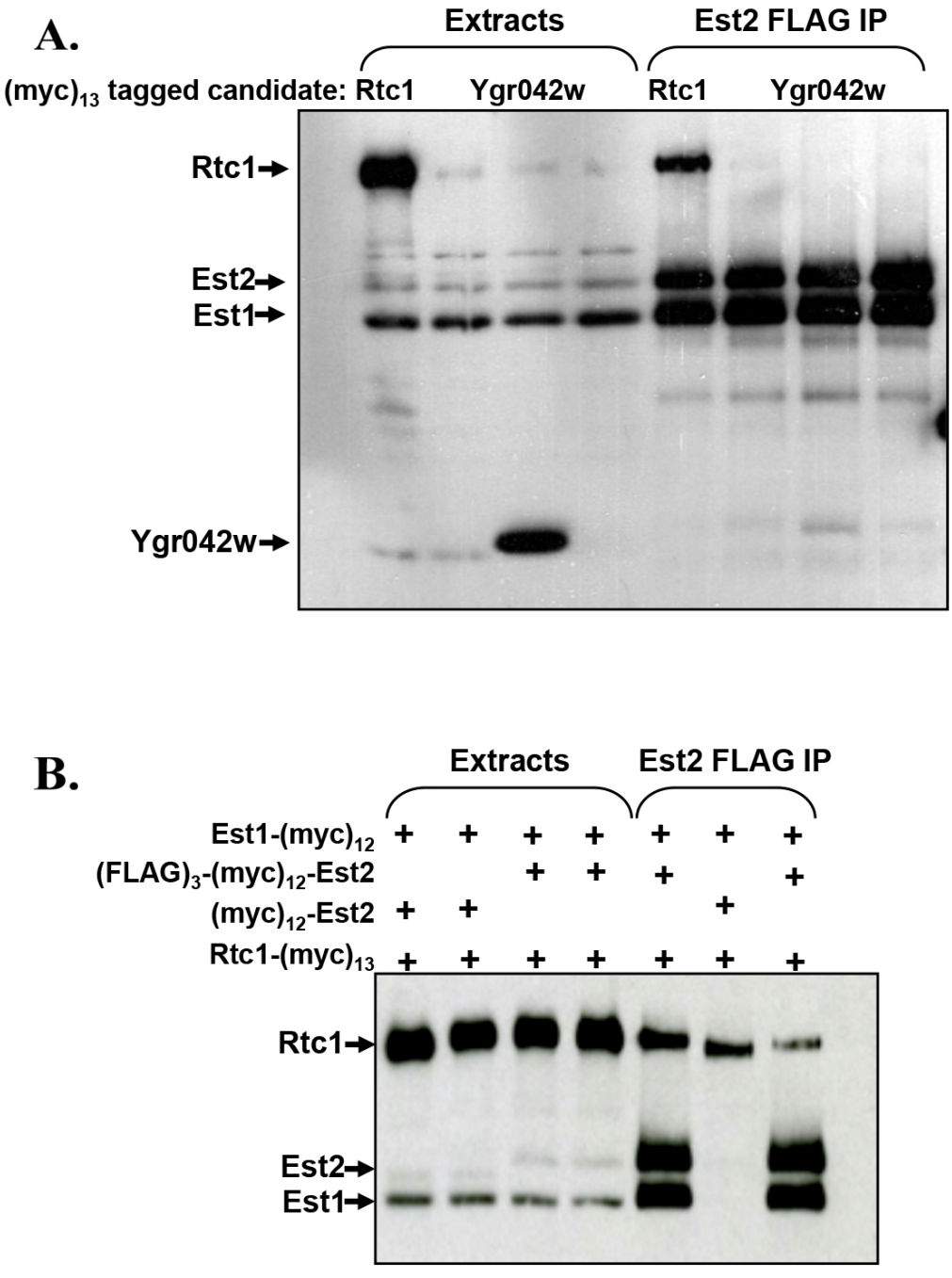

Figure A.3 Rtc1 and Ygr042w do not significantly associate with telomerase. A) Anti-myc western blot of extracts and anti-FLAG IPs prepared from stains expressing Est1-$(myc)_{12}$ $(FLAG)_3$-$(myc)_{12}$-Est2, with Rtc1 or Ygr042w tagged at the C-terminus with $(myc)_{13}$::TRP1 as indicated. Rtc1 appears to associate, but this is refuted by the untagged control in panel B. B) Anti-myc western blot of extracts and anti-FLAG IPs prepared from strains expressing Est1-$(myc)_{12}$ Rtc1-$(myc)_{13}$::TRP1 $(FLAG)_3$-$(myc)_{12}$-Est2, or $(myc)_{12}$-Est2 as an untagged control.

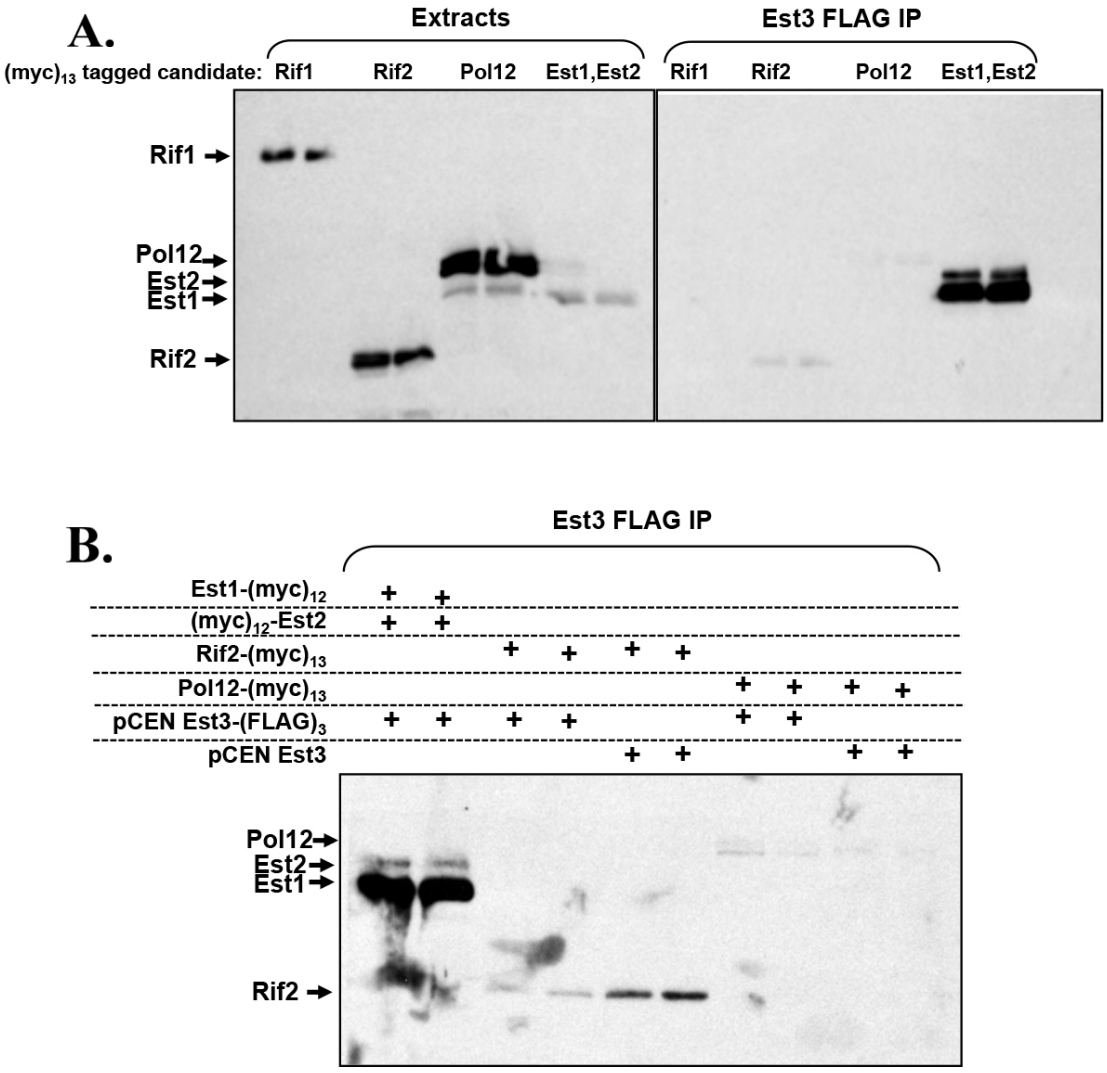

Figure A.4 Pol12, Rif1, or Rif2 do not significantly associate with Est3. A) Anti-myc western blots of extracts (left side) and anti-FLAG IPs (right side) prepared from stains expressing Est3-$(FLAG)_3$ from a *CEN* plasmid and candidates tagged at the C-terminus with $(myc)_{13}$::TRP1 as indicated. Pol12 and Rif2 appear to weakly associate, but this is refuted by the untagged controls in panel B. B) Anti-myc western blot of anti-FLAG IPs prepared from tagged strains expressing Est3-$(FLAG)_3$ or untagged Est3 from a *CEN* plasmid, as indicated.

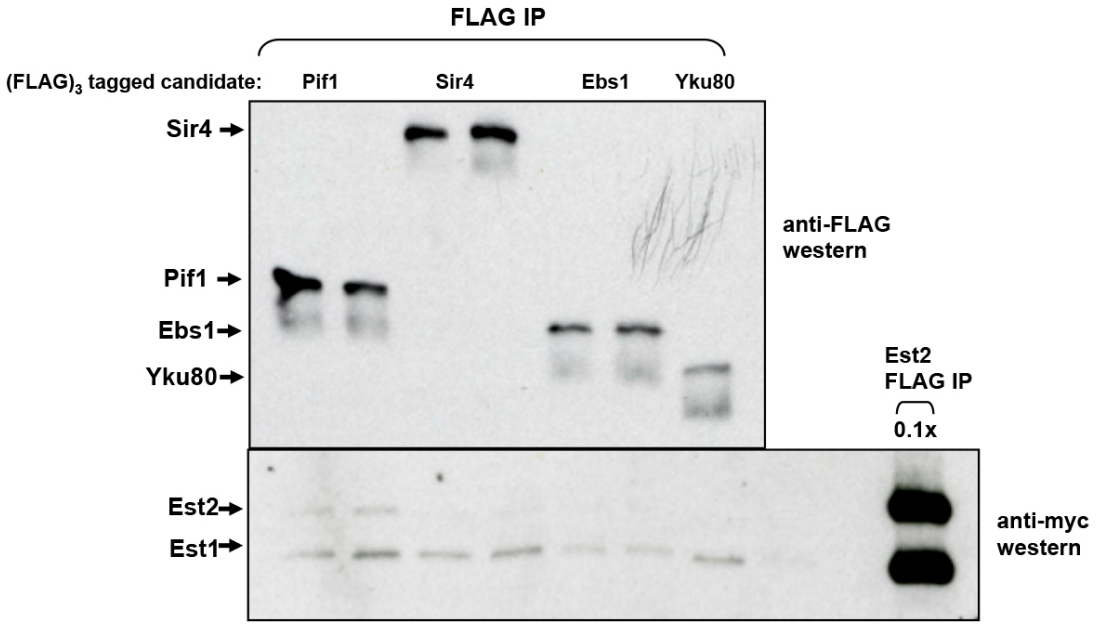

Figure A.5 Telomerase does not significantly associate with Ebs1, Pif1, Sir4, or Yku80. Anti-FLAG (top) and anti-myc (bottom) western blots of anti-FLAG IPs prepared from strains expressing Est1-$(myc)_{12}$ $(myc)_{12}$-Est2 and candidates tagged at the C-terminus with $(FLAG)_3$::TRP1 as indicated. The far right lane is an anti-FLAG IP prepared from a strain expressing $(FLAG)_3$-$(myc)_{12}$-Est2 and Est1-$(myc)_{12}$ (0.1X indicates the amount of IP relative to the amount loaded in the other lanes).

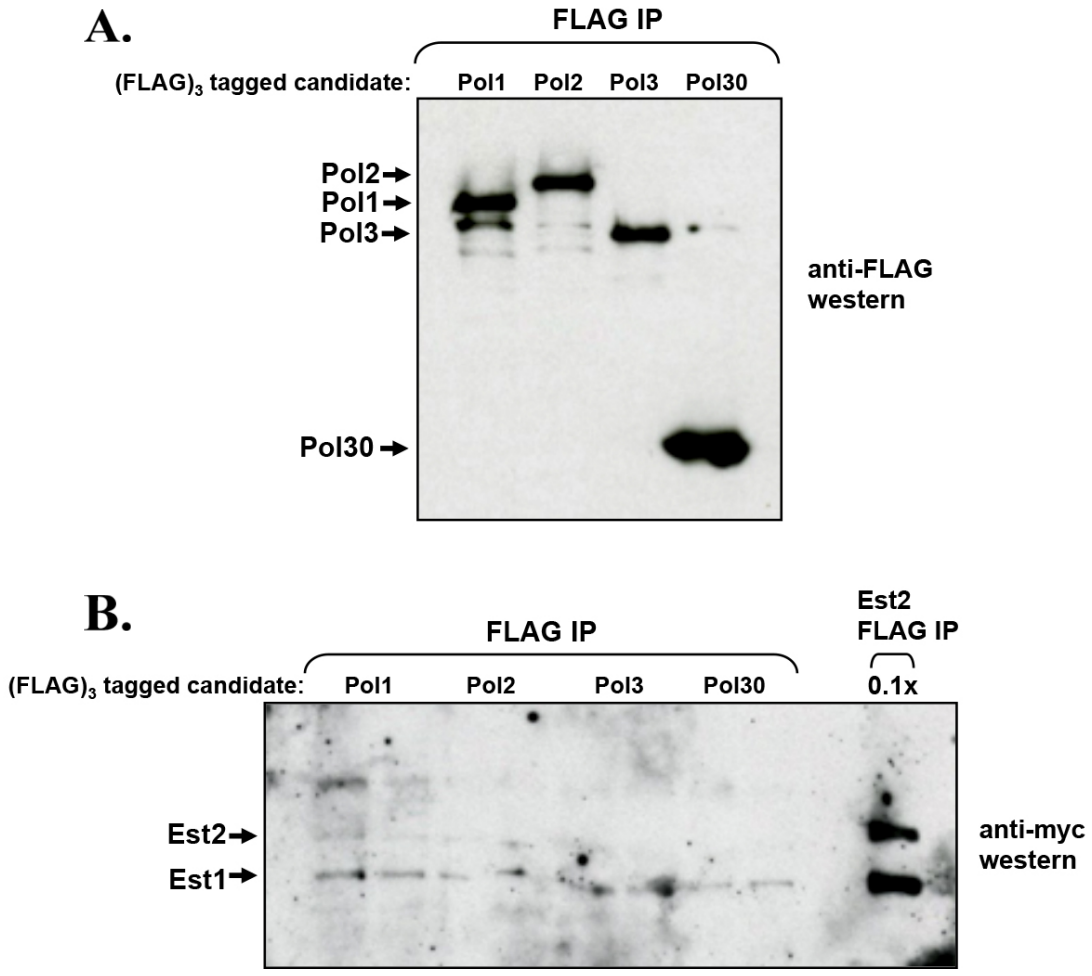

Figure A.6 Telomerase does not significantly associate with Pol1, Pol2, Pol3, or Pol30. A) Anti-FLAG western blot of anti-FLAG IPs prepared from strains expressing Est1-$(myc)_{12}$ $(myc)_{12}$-Est2 and candidates tagged at the C-terminus with $(FLAG)_3$::TRP1 as indicated. B) Anti-myc western blot of the same anti-FLAG IPs from panel A. The far right lane is an anti-FLAG IP prepared from a strain expressing $(FLAG)_3$-$(myc)_{12}$-Est2 and Est1-$(myc)_{12}$ (0.1X indicates the amount of IP relative to the amount loaded in the other lanes).

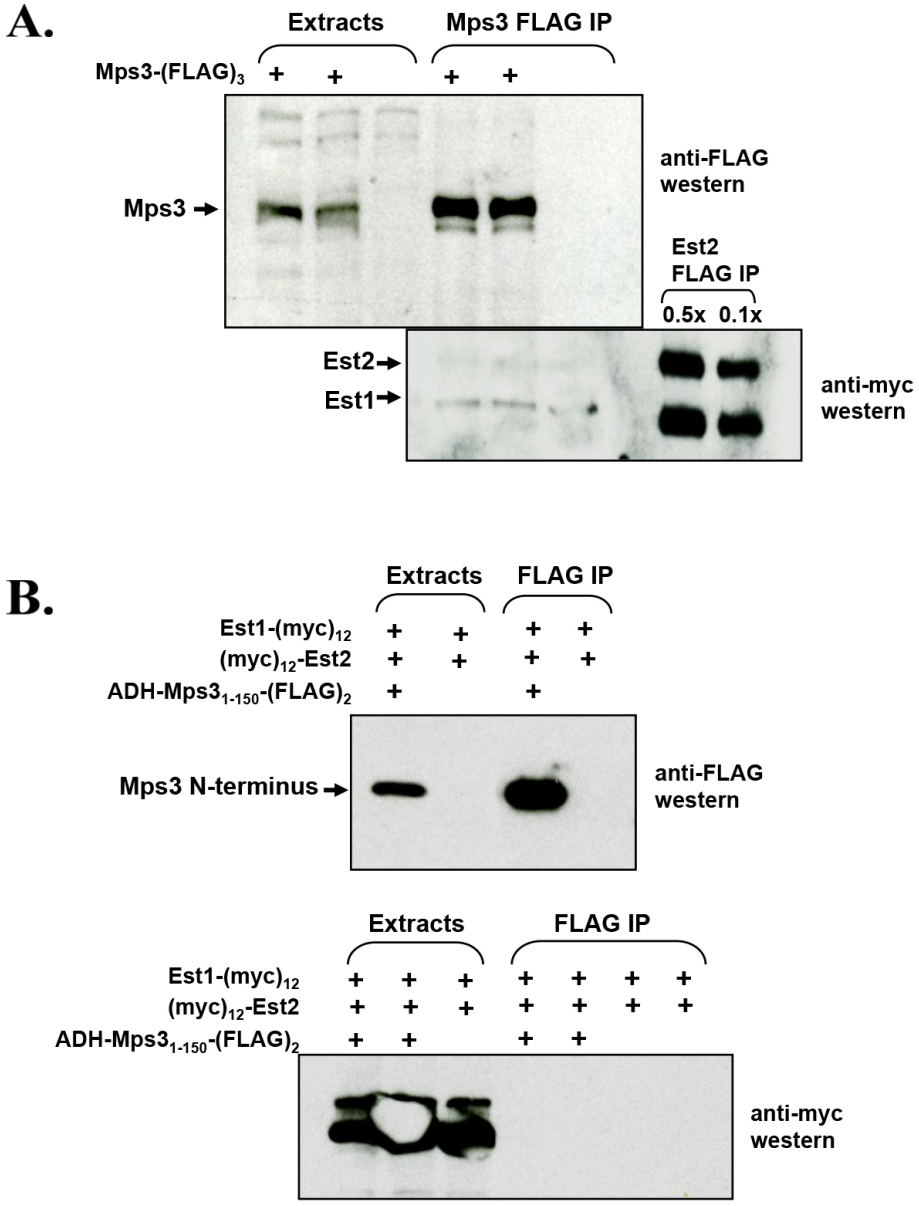

Figure A.7 Telomerase does not significantly associate with Mps3. A) Anti-FLAG (top) and anti-myc (bottom) western blots of extracts and anti-FLAG IPs prepared from strains expressing Est1-$(myc)_{12}$ $(myc)_{12}$-Est2 and Mps3 tagged at the C-terminus with $(FLAG)_3$::TRP1 as indicated. B) Anti-FLAG (top) and anti-myc (bottom) western blots of extracts and anti-FLAG IPs prepared from strains expressing Est1-$(myc)_{12}$ $(myc)_{12}$-Est2, with $Mps3_{1-150}$-$(FLAG)_2$ over-expressed from a 2μ plasmid behind the *ADH* promoter, as indicated.

Appendix B: Preliminary biochemistry data for Est2

Biochemical analysis of Est2

The catalytic protein subunit Est2 is involved in RNA binding and reverse transcriptase catalysis, but there are other functions yet to be determined based on the identification of several domains with unassigned functions. In collaboration with Lisa Nguyen in the Lundblad lab, we have approached the analysis of Est2 through an extensive collection of separation-of-function mutations predicted to reside on the surface of the protein. The mutations were isolated by Lisa according to the reverse genetics method described in Chapter 2 (Nguyen, 2013).

Initially, I conducted a deletion analysis on Est2 similar to the method used for Est1 as described in Chapter 6 (see Figure 6.1). I found that the 884 amino acid Est2 protein could be truncated at C-terminus (resulting in a protein with amino acids 1-757), or at both the N-and C-terminal ends (resulting in a protein with amino acids 180-757) and still retain association with Est1, although the latter construct showed a decrease in association. Based on this crude deletion analysis, the C-terminus (from amino acids 757-884) is dispensable for RNA binding, while the N-terminus (from amino acids 1-180) appears to be making a modest contribution to RNA binding. The results from this deletion analysis are displayed in Figures B.1 – B.3.

I performed biochemical analyses on a subset of the *EST2* alleles using the stoichiometry assay described in Chapter 3. Est2 mutants were tagged with $(FLAG)_3$-$(myc)_{12}$ and expressed from a *CEN* plasmid and/or integrated in the genome by pop-in / pop-out two step gene replacement by Lisa Nguyen. Unexpectedly, missense mutations in three different domains of Est2 affect RNA binding, which contradicts

with a long-standing assumption that a single domain on Est2 affects RNA binding. Furthermore, some of these mutations are conserved from yeast to human telomerase. The results are displayed from Figures B.4 – B.7.

I also examined a subset of the *EST2* alleles for the ability to associate with the Est3 complex, as determined by FLAG immunoprecipitation of Est3-$(FLAG)_3$. The results from this analysis are displayed in Figures B.8 and B.9. Unexpectedly, mutations in the N-terminus of *EST2* result in a significant reduction of the Est3-containing complex but no change in the Est1/Est2 stoichiometry, while mutations in other regions of *EST2* do not affect the Est3 association. This suggests that the N-terminus of Est2 contains an interface for Est3 association. Several alleles of *EST3* were tested for genetic suppression with *est2-R151E*, which would implicate a direct interaction between the two proteins, but so far, no suppression has been observed.

Finally, I did some initial work to develop a system for expressing the telomerase subunits from a related yeast species, *Saccharomyces castellii*, in *Saccharomyces cerevisiae*. If the *S. castellii* proteins express and are able to form a telomerase complex, with no interference from the *S. cerevisiae* cellular environment, then it would serve as a convenient system for directly testing subunit interactions. I was able to epitope tag, express, and immunoprecipitate full-length and truncated versions of *S. castellii* telomerase subunits. However, I did not observe any substantial evidence for direct protein-protein interactions (Figures B.10 and B.11).

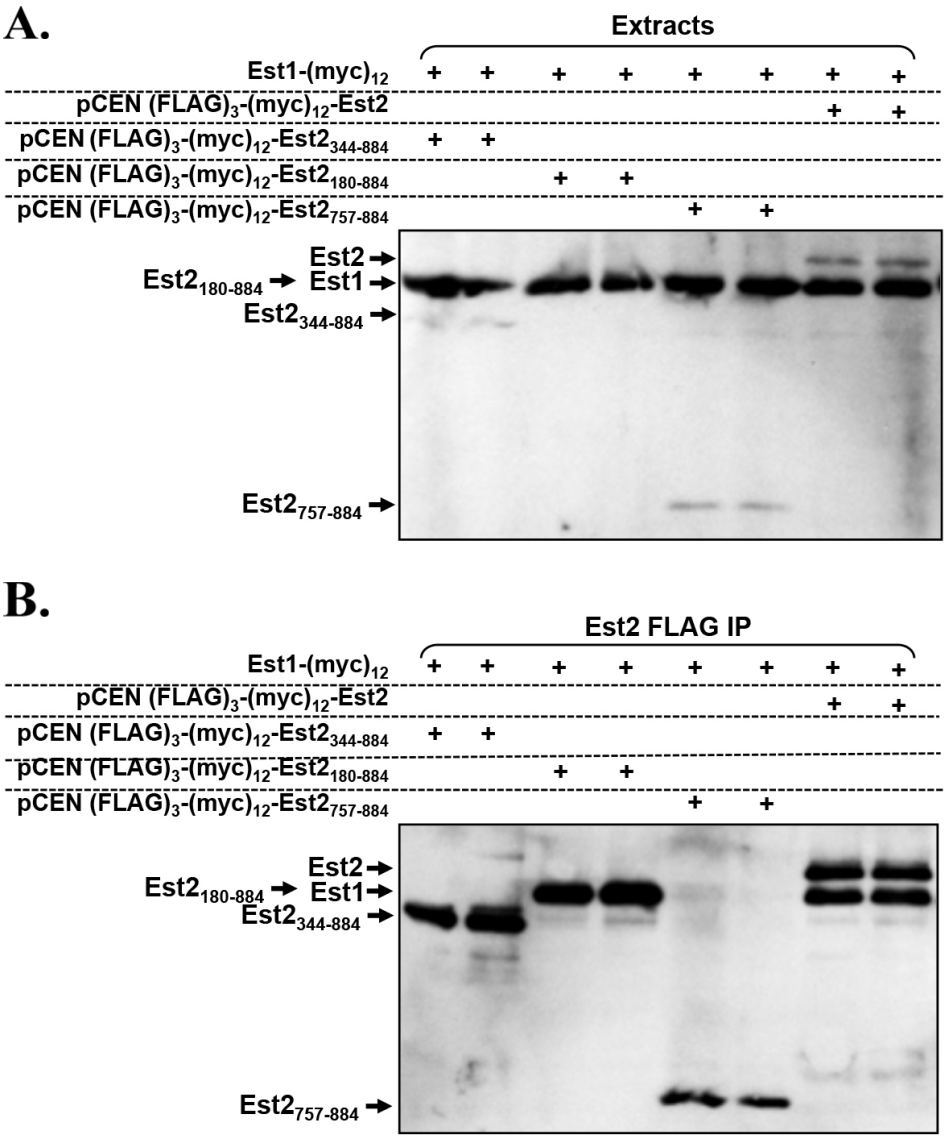

Figure B.1 Deletion analysis of Est2 N-terminal truncations. A) Anti-myc western blot of extracts prepared from strains with Est1-$(myc)_{12}$ integrated in the genome and expressing truncations of $(FLAG)_3$-$(myc)_{12}$-Est2 from *CEN* plasmids, as indicated. B) Anti-myc western blot of anti-FLAG IPs prepared from strains with Est1-$(myc)_{12}$ integrated in the genome and expressing truncations of $(FLAG)_3$-$(myc)_{12}$-Est2 from *CEN* plasmids, as indicated. Note that $Est2_{180-884}$ migrates at the same size as Est1, so it is inconclusive as to whether Est1 associates with that truncation.

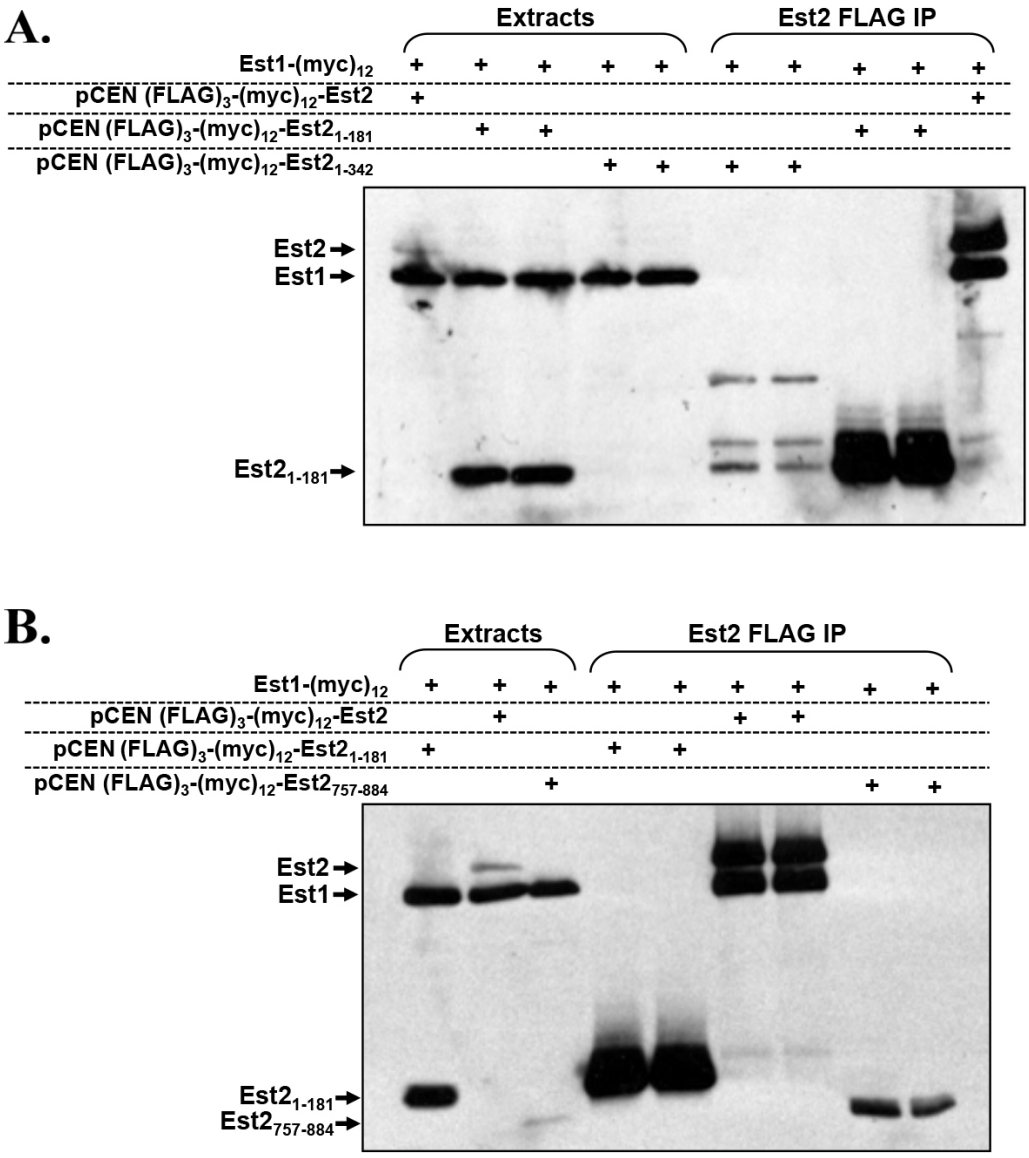

Figure B.2 Deletion analysis of Est2 C-terminal truncations. Two different anti-myc western blots containing extracts and anti-FLAG IPs prepared from strains with Est1-$(myc)_{12}$ integrated in the genome and expressing truncations of $(FLAG)_3$-$(myc)_{12}$-Est2 from *CEN* plasmids, as indicated.

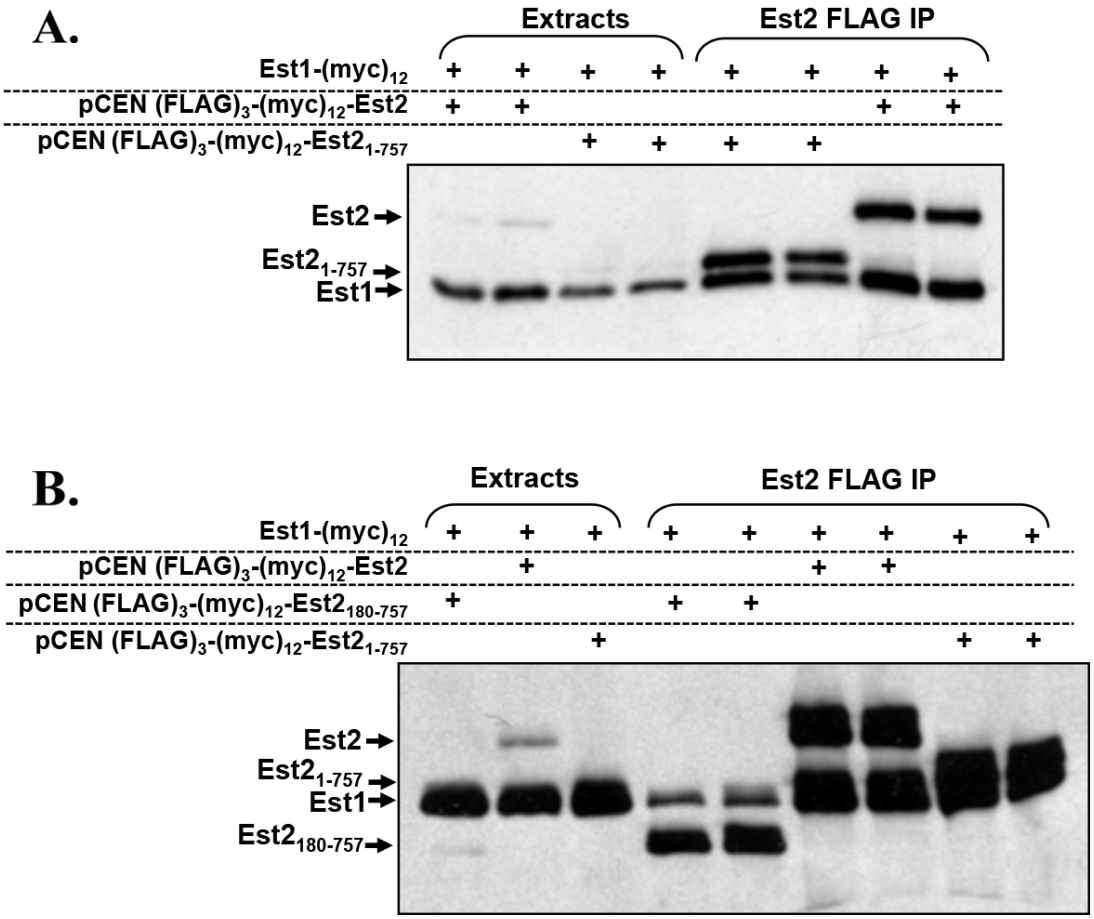

Figure B.3 Truncated versions of Est2 (expressing amino acids 1-757 or 180-757) are proficient for RNA binding. A) Anti-myc western blot of extracts and anti-FLAG IPs prepared from strains with Est1-$(myc)_{12}$ integrated in the genome and expressing truncations of $(FLAG)_3$-$(myc)_{12}$-Est2 from *CEN* plasmids, as indicated. Note that Est1 fully associates with the $Est2_{1-757}$ truncation. B) Anti-myc western blot of extracts and anti-FLAG IPs prepared from strains with Est1-$(myc)_{12}$ integrated in the genome and expressing truncations of $(FLAG)_3$-$(myc)_{12}$-Est2 from *CEN* plasmids, as indicated. Note that Est1 fully associates with the $Est2_{1-757}$ truncation, and partially associates with the $Est2_{180-757}$ truncation.

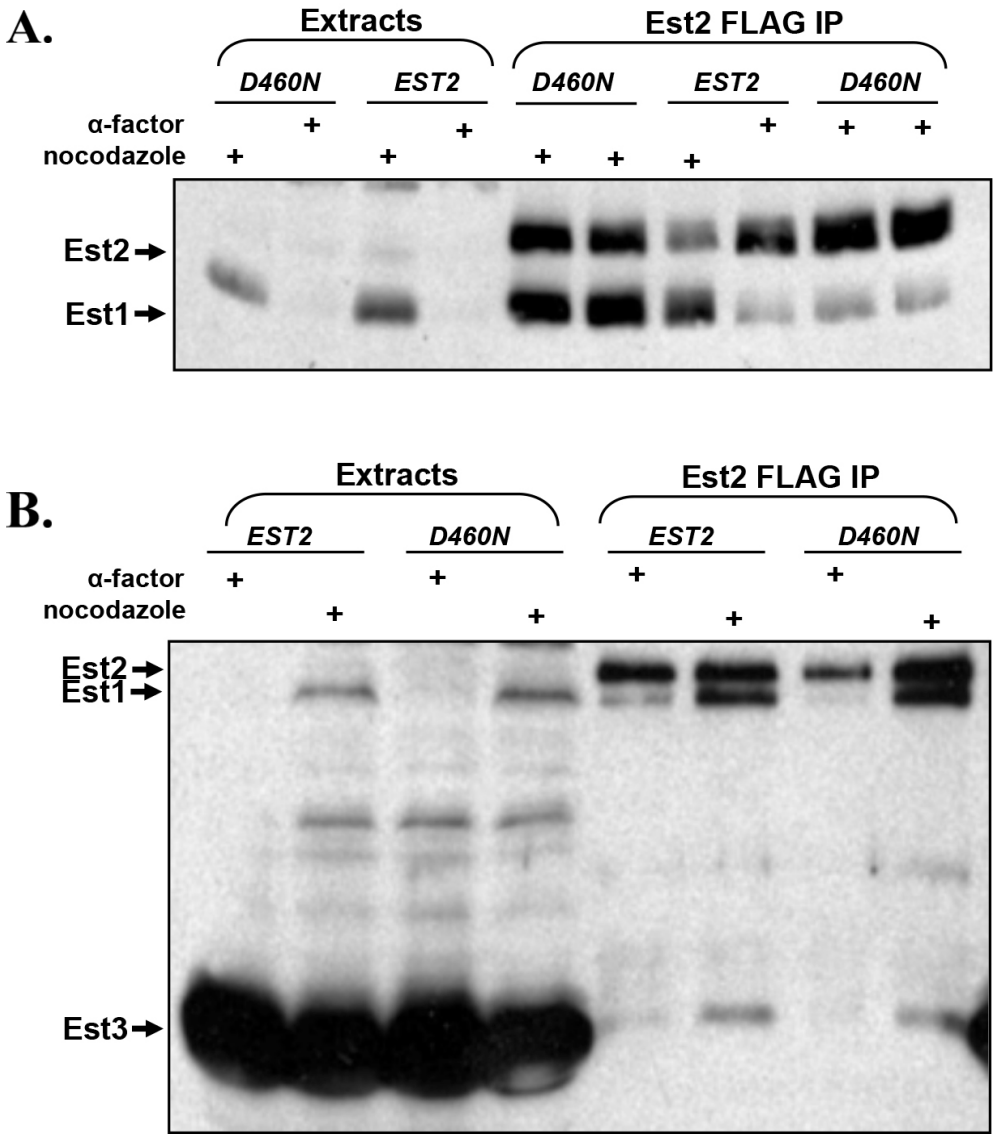

Figure B.4 Western blot analysis of *est2-D460N* when integrated in the genome. A) Anti-myc western blot from extracts and anti-FLAG IPs. Pop-in / pop-out allelic replacement was used to integrate *est2-D460N* into a strain containing *(FLAG)$_3$-(myc)$_{12}$-EST2 EST1-(myc)$_{12}$ EST3-(myc)$_{12}$*, and extracts were prepared from cultures grown immediately after pop-out diagnosis to identify isolates that retained both the epitope tag and mutation. Cells were arrested with α-factor or nocodazole as indicated. B) Anti-myc western blot from extracts and anti-FLAG IPs, from the same samples in panel A, but run on a higher percentage SDS-PAGE gel for detection of Est3.

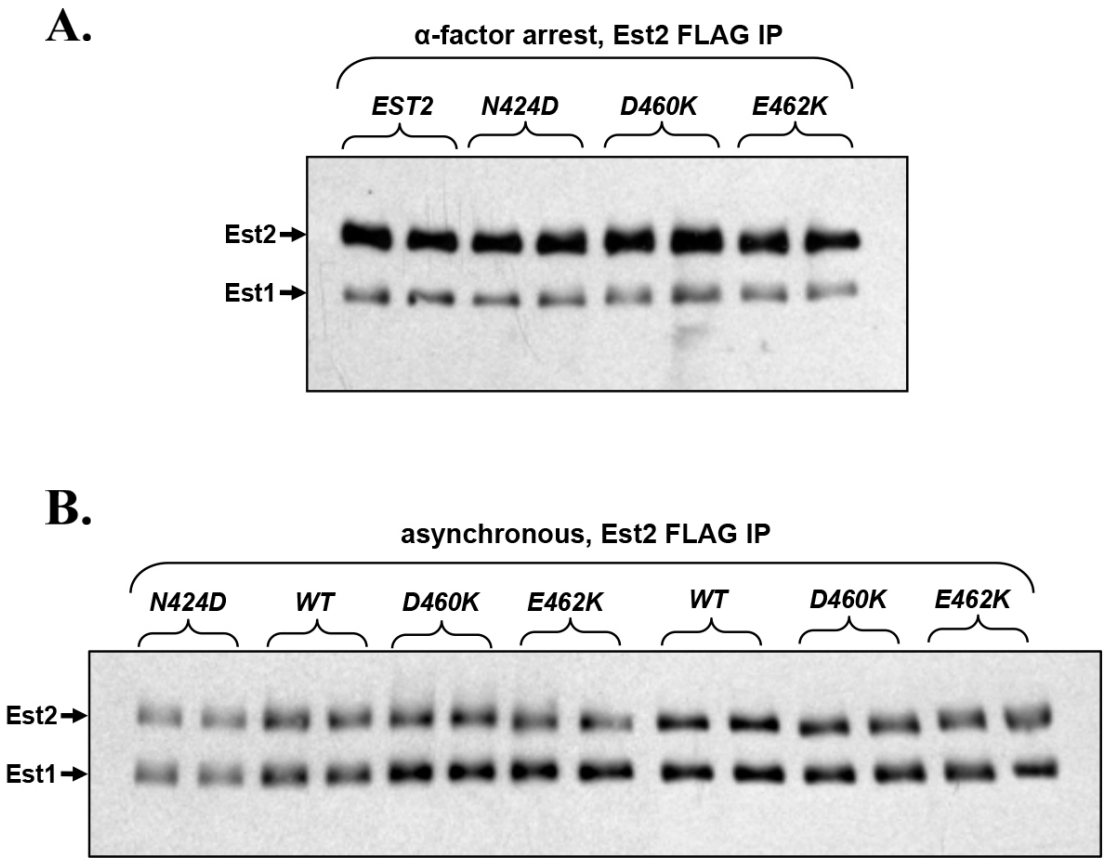

Figure B.5 Western blot analysis of *est2-N424D, D460K, and E462K* when expressed from *CEN* plasmids. A) Anti-myc western blot from anti-FLAG IPs of a strain expressing Est1-$(myc)_{12}$ and transformed with *CEN* $(FLAG)_3$-$(myc)_{12}$-*EST2* or mutant allele derivatives. Cells were arrested with α-factor. B) Anti-myc western blot from anti-FLAG IPs using asynchronous cultures of the same transformants as in panel A.

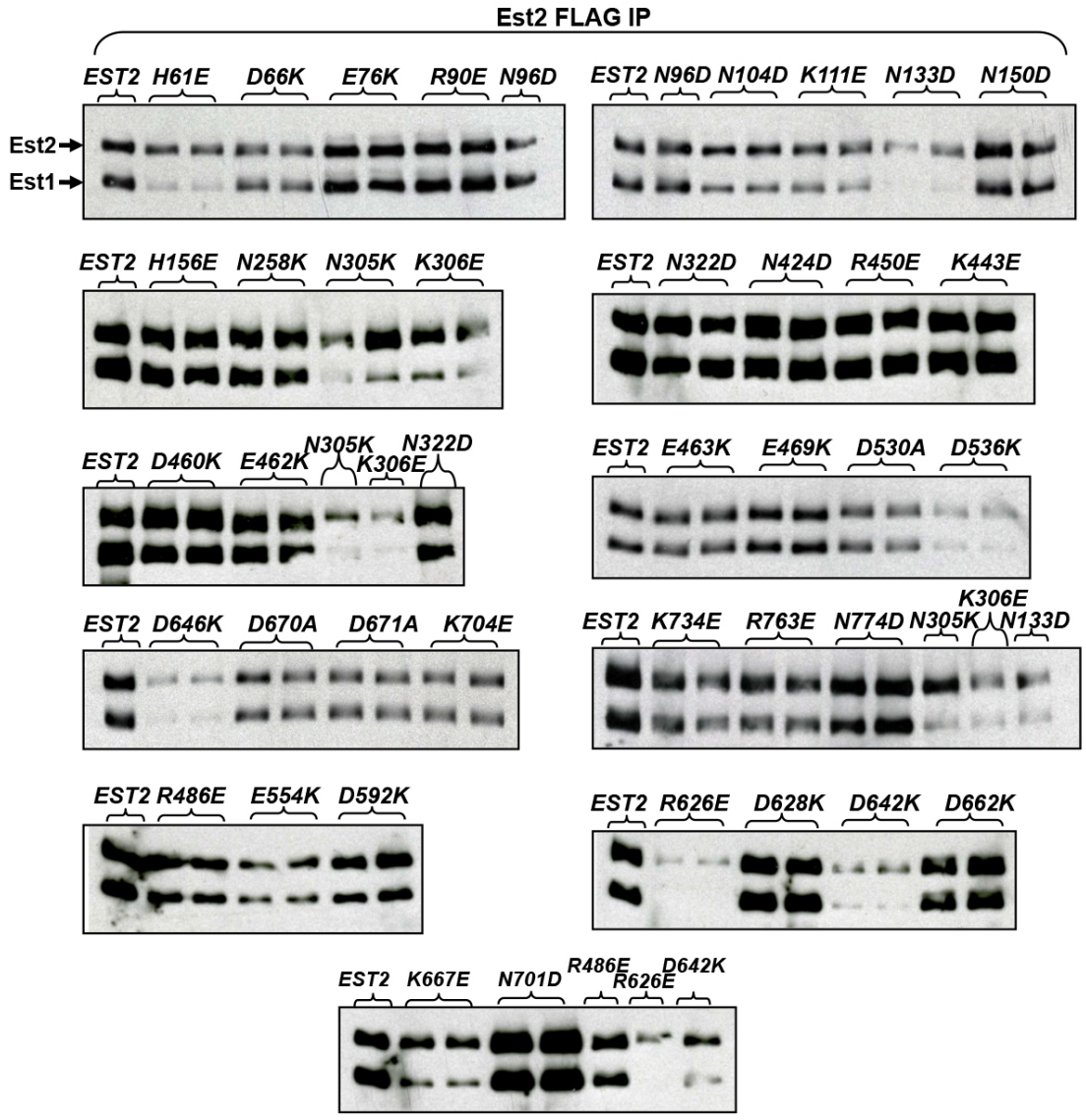

Figure B.6 Western blot analysis of additional $(FLAG)_3$-$(myc)_{12}$ tagged *est2*⁻ alleles expressed from *CEN* plasmids. Anti-myc western blots from anti-FLAG IPs of a strain expressing Est1-$(myc)_{12}$ and transformed with *CEN* $(FLAG)_3$-$(myc)_{12}$-*EST2* or mutant allele derivatives.

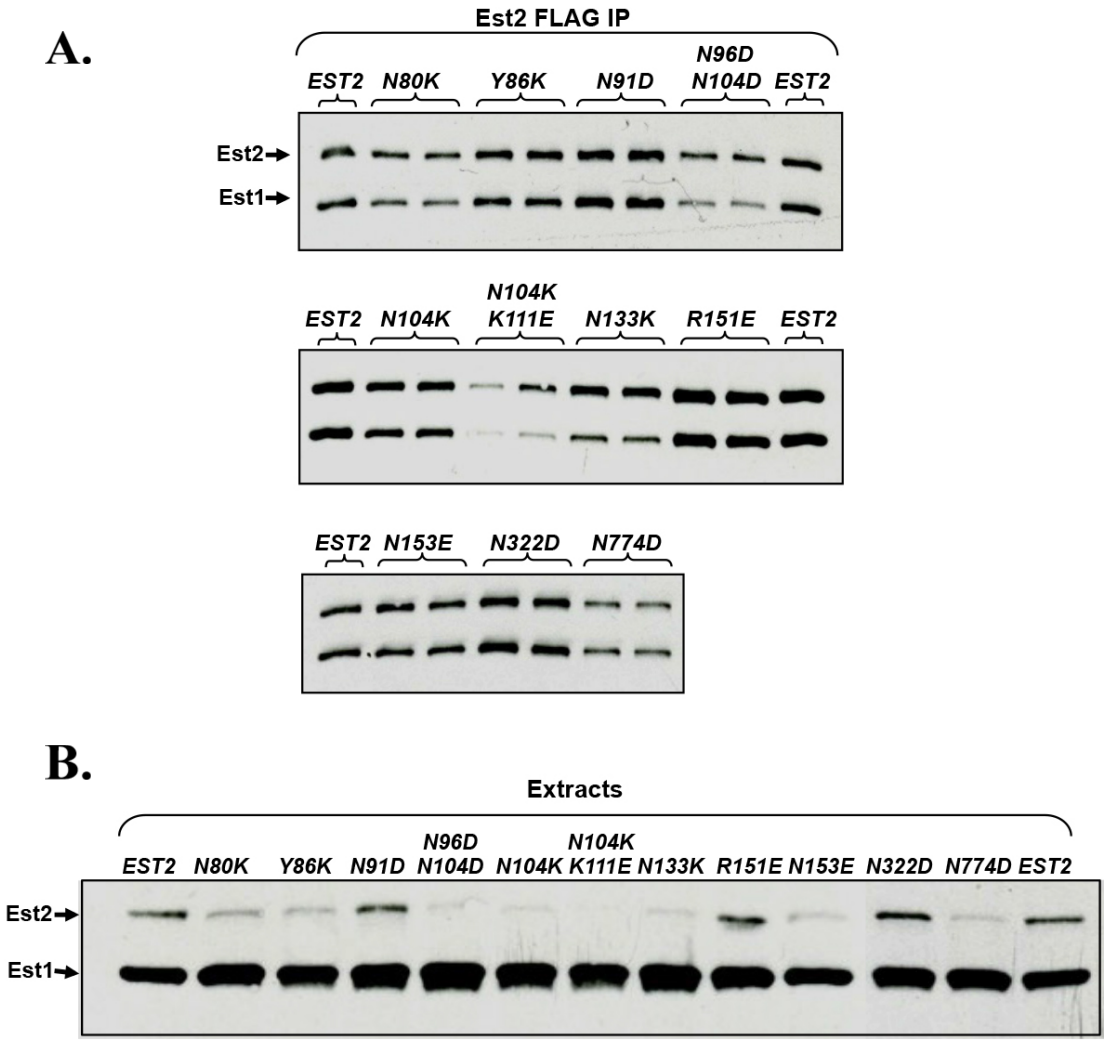

Figure B.7 Western blot analysis of $(FLAG)_3$-$(myc)_{12}$ tagged *est2*⁻ alleles when integrated in the genome. A) Anti-myc western blots from anti-FLAG IPs. Pop-in / pop-out allelic replacement (done by Lisa Nguyen in the Lundblad lab) was used to integrate mutant allele derivatives of *$(FLAG)_3$-$(myc)_{12}$-EST2* into a strain expressing Est1-$(myc)_{12}$. B) Anti-myc western blots of extracts from the same strains as in panel A. One isolate was examined for each strain.

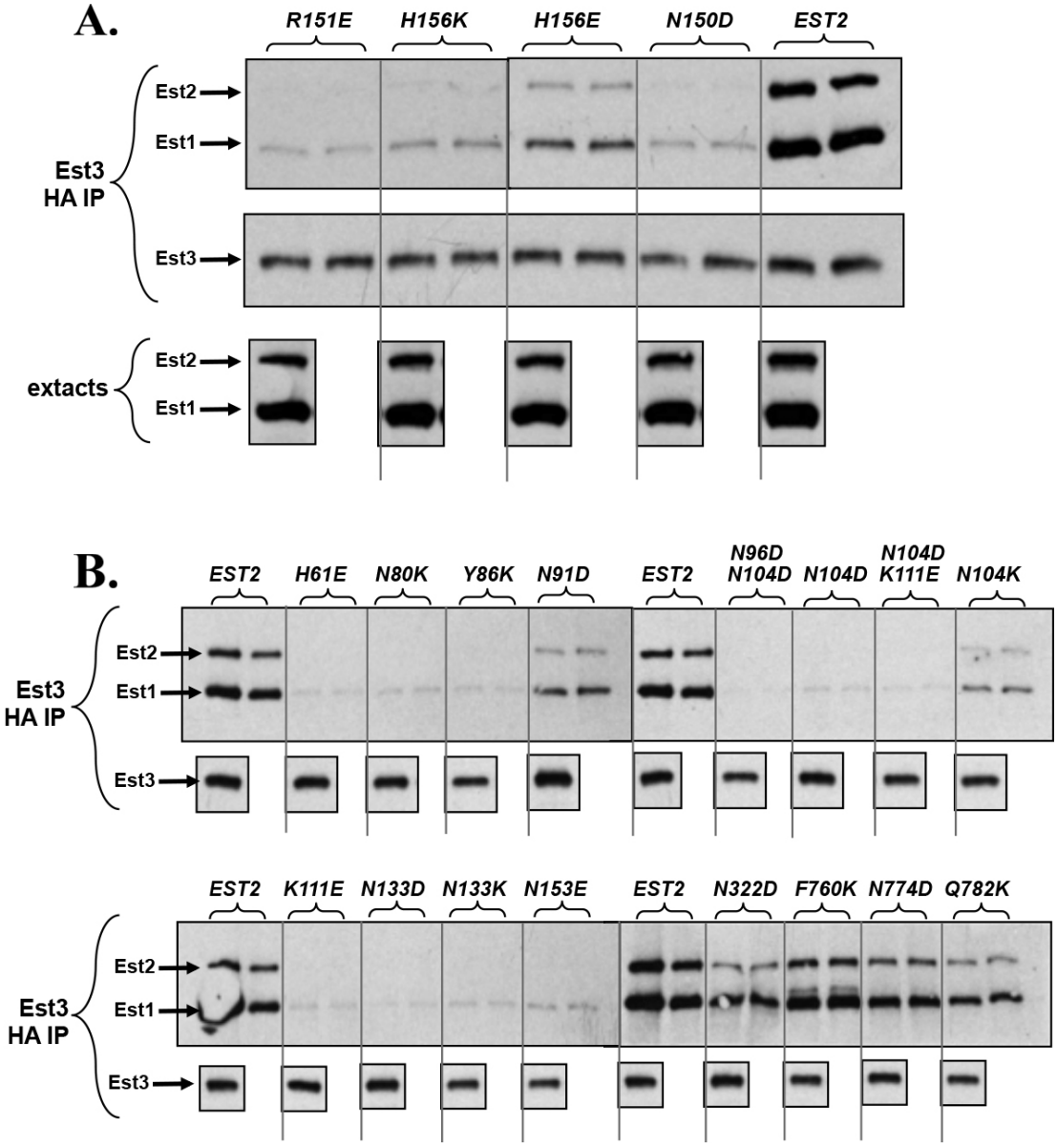

Figure B.8 Mutants in the N-terminus of Est2 affect Est3 association. A) Anti-myc western blots of extracts and anti-HA IPs prepared from strains expressing Est3-$(myc)_6$-$(HA)_3$ from a *CEN* plasmid and $(myc)_{12}$-Est2 and Est1-$(myc)_{12}$ integrated in the genome, with *est2*$^-$ mutations as indicated. *est2*$^-$ mutations were integrated by pop-in / pop-out allelic replacement (done by Lisa Nguyen in the Lundblad lab). For each mutation, two independent isolates were prepared for anti-HA immunoprecipitation, and protein expression levels were also checked for one of the two isolates. B) Anti-myc western blots of an additional set of Est2 mutants, prepared in the similar manner as described in panel A.

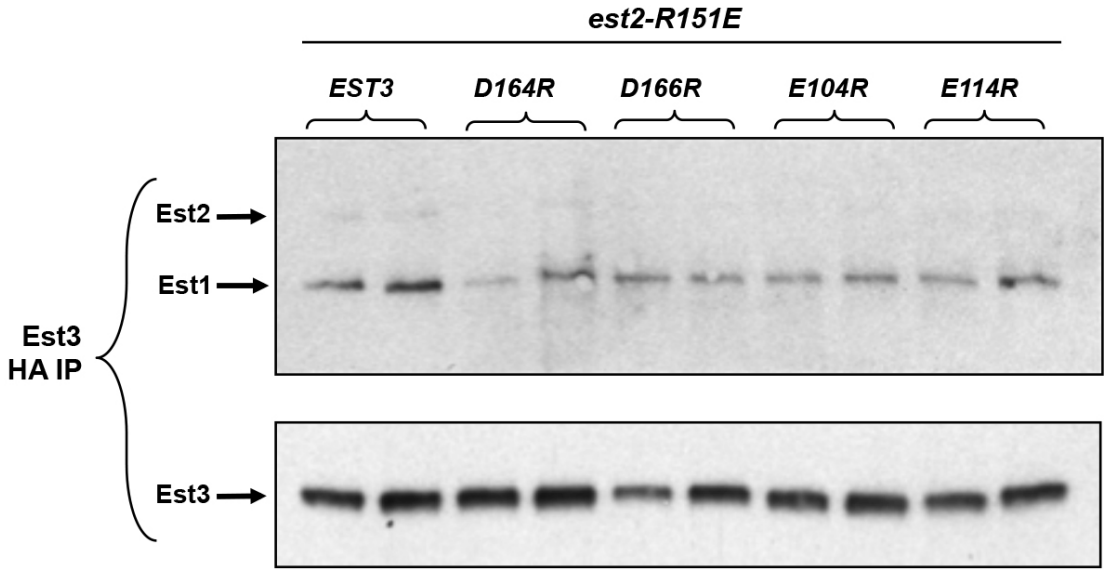

Figure B.9 The decreased association of Est2-R151E with Est3 is not suppressed by Est3 mutants. Anti-myc western blots of anti-HA IPs prepared from strains containing $(myc)_{12}$-est2-R151E and Est1-$(myc)_{12}$ integrated in the genome, and Est3-$(myc)_6$-$(HA)_3$, or mutant allele derivatives, expressed from *CEN* plasmids as indicated.

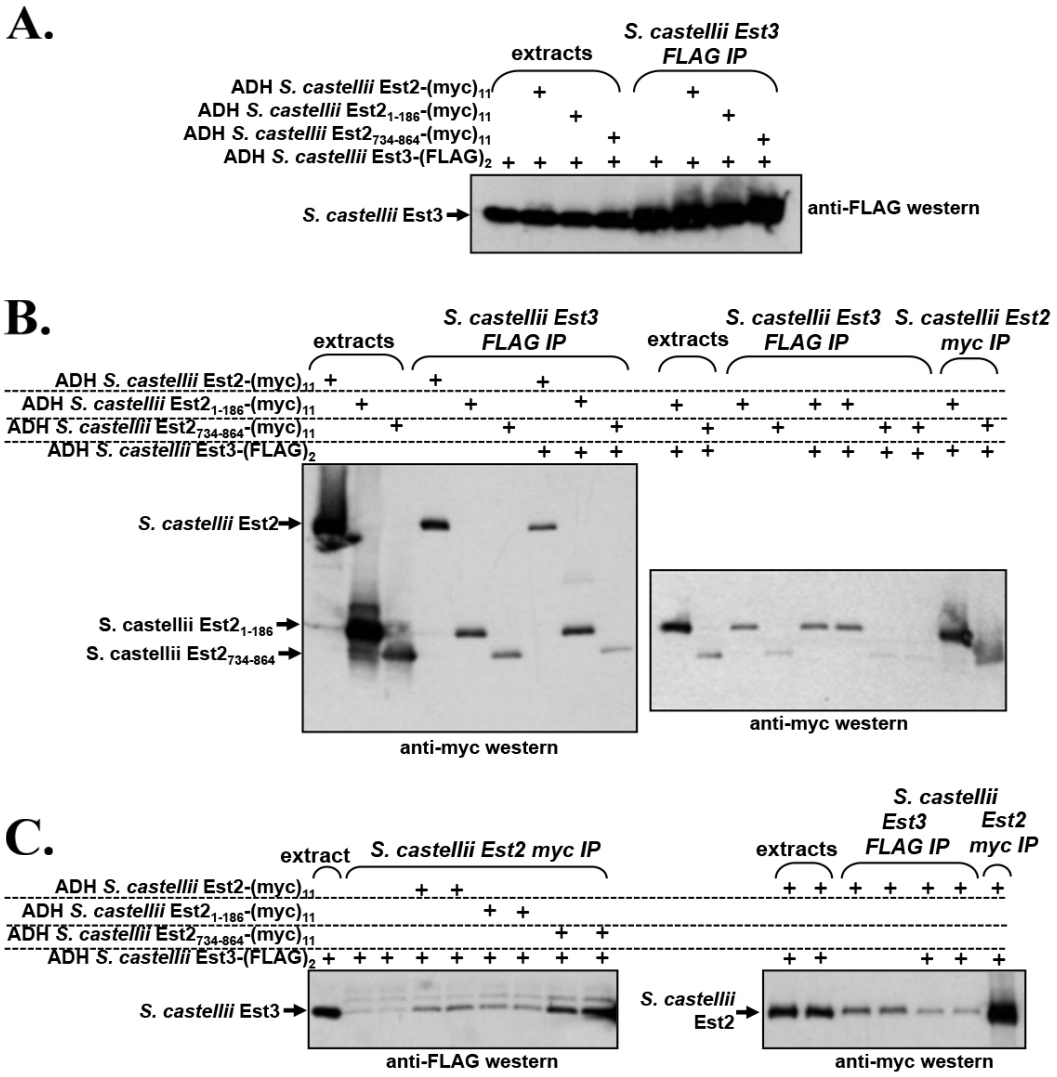

Figure B.10 Western blot analysis of *S. castellii* Est2 and Est3 proteins expressed in *S. cerevisiae*. A) Anti-FLAG western blot of extracts and anti-FLAG IPs from *S. cerevisiae* strain AVL78 (*MAT***a** *leu2 trp1 ura3-52 prb1 prc1 pep4-3*) transformed with 2μ plasmids over-expressing epitope-tagged *S. castellii* proteins as indicated. This western blot is examining expression levels and immunoprecipitation of *S. castellii* Est3. B) Anti-myc western blots of the same transformants described in panel A, examining whether *S. castellii* Est2 (full-length or truncations) associates when *S. castellii* Est3 is IP'd. C) Anti-FLAG and anti-myc western blots of the same transformants described in panel A, examining whether *S. castellii* Est3 associates when *S. castellii* Est2 (full-length or truncations) is IP'd.

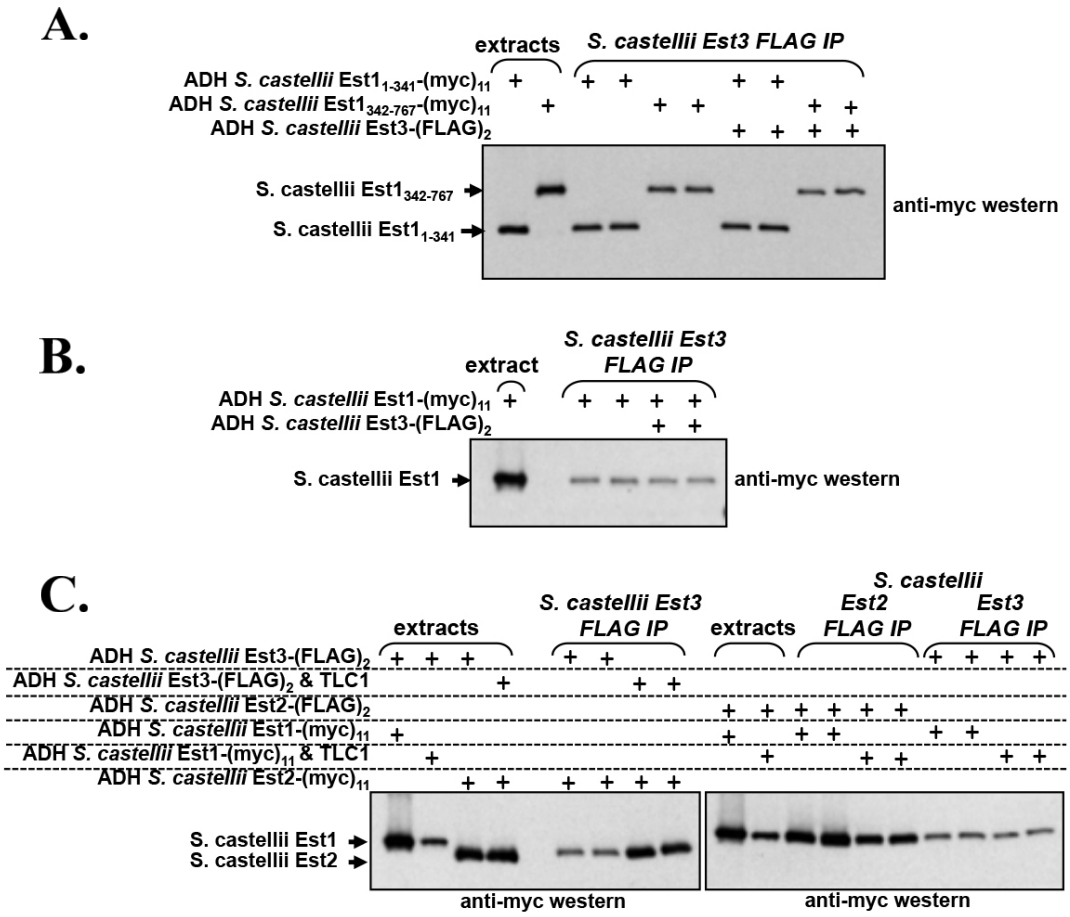

Figure B.11 Western blot analysis of *S. castellii* Est1, Est2, and Est3 proteins expressed in *S. cerevisiae* in the presence or absence of *S. castellii* TLC1. A) Anti-myc western blot of extracts and anti-FLAG IPs from *S. cerevisiae* strain AVL78 (*MAT***a** *leu2 trp1 ura3-52 prb1 prc1 pep4-3*) transformed with 2μ plasmids over-expressing epitope-tagged *S. castellii* proteins as indicated. This western blot is examining whether *S. castellii* Est1 N- and C-terminal truncations associate when *S. castellii* Est3 is IP'd. B) Anti-myc western blot of additional AVL78 transformants as indicated, detecting expression of *S. castellii* full-length Est1 and examining whether it associates when *S. castellii* Est3 is immunoprecipitated. C) anti-myc western blots of extracts and FLAG IPs from additional AVL78 transformants, over-expressing the indicated *S. castellii* proteins in the presence or absence of *S. castellii* TLC1 (note that TLC1 is expressed from the same 2μ plasmid but behind the *S. cerevisiae* TLC1 promoter).

References

Alber, T. (1989). Mutational effects on protein stability. Annu Rev Biochem *58*, 765-798.

Alves, D., Li, H., Codrington, R., Orte, A., Ren, X., Klenerman, D., and Balasubramanian, S. (2008). Single-molecule analysis of human telomerase monomer. Nat Chem Biol *4*, 287-289.

Anderson, E.M., Halsey, W.A., and Wuttke, D.S. (2002). Delineation of the high-affinity single-stranded telomeric DNA-binding domain of Saccharomyces cerevisiae Cdc13. Nucleic Acids Res *30*, 4305-4313.

Armanios, M. (2009). Syndromes of telomere shortening. Annual review of genomics and human genetics *10*, 45-61.

Askree, S.H., Yehuda, T., Smolikov, S., Gurevich, R., Hawk, J., Coker, C., Krauskopf, A., Kupiec, M., and McEachern, M.J. (2004). A genome-wide screen for Saccharomyces cerevisiae deletion mutants that affect telomere length. Proceedings of the National Academy of Sciences of the United States of America *101*, 8658-8663.

Baker, C.M., and Grant, G.H. (2007). Role of aromatic amino acids in protein-nucleic acid recognition. Biopolymers *85*, 456-470.

Baumann, P., and Cech, T.R. (2001). Pot1, the putative telomere end-binding protein in fission yeast and humans. Science *292*, 1171-1175.

Beernink, H.T., Miller, K., Deshpande, A., Bucher, P., and Cooper, J.P. (2003). Telomere maintenance in fission yeast requires an Est1 ortholog. Curr Biol *13*, 575-580.

Bianchi, A., Negrini, S., and Shore, D. (2004). Delivery of yeast telomerase to a DNA break depends on the recruitment functions of Cdc13 and Est1. Mol Cell *16*, 139-146.

Blackburn, E.H. (2000). Telomere states and cell fates. Nature *408*, 53-56.

Blackburn, E.H., and Collins, K. (2011). Telomerase: an RNP enzyme synthesizes DNA. Cold Spring Harb Perspect Biol *3*.

Blackburn, E.H., and Gall, J.G. (1978). A tandemly repeated sequence at the termini of the extrachromosomal ribosomal RNA genes in Tetrahymena. J Mol Biol *120*, 33-53.

Blasco, M.A., Lee, H.W., Hande, M.P., Samper, E., Lansdorp, P.M., DePinho, R.A., and Greider, C.W. (1997). Telomere shortening and tumor formation by mouse cells lacking telomerase RNA. Cell *91*, 25-34.

Boulton, S.J., and Jackson, S.P. (1996). Identification of a Saccharomyces cerevisiae Ku80 homologue: roles in DNA double strand break rejoining and in telomeric maintenance. Nucleic Acids Res *24*, 4639-4648.

Broccoli, D., Smogorzewska, A., Chong, L., and de Lange, T. (1997). Human telomeres contain two distinct Myb-related proteins, TRF1 and TRF2. Nat Genet *17*, 231-235.

Bryan, T.M., Goodrich, K.J., and Cech, T.R. (2003). Tetrahymena telomerase is active as a monomer. Mol Biol Cell *14*, 4794-4804.

Chakrabarti, K., Pearson, M., Grate, L., Sterne-Weiler, T., Deans, J., Donohue, J.P., and Ares, M., Jr. (2007). Structural RNAs of known and unknown function identified in malaria parasites by comparative genomics and RNA analysis. RNA *13*, 1923-1939.

Chan, A., Boule, J.B., and Zakian, V.A. (2008). Two pathways recruit telomerase to Saccharomyces cerevisiae telomeres. PLoS Genet *4*, 24.

Chang, M., Arneric, M., and Lingner, J. (2007). Telomerase repeat addition processivity is increased at critically short telomeres in a Tel1-dependent manner in Saccharomyces cerevisiae. Genes Dev *21*, 2485-2494.

Chapon, C., Cech, T.R., and Zaug, A.J. (1997). Polyadenylation of telomerase RNA in budding yeast. RNA *3*, 1337-1351.

Chappell, A.S., and Lundblad, V. (2004). Structural elements required for association of the Saccharomyces cerevisiae telomerase RNA with the Est2 reverse transcriptase. Mol Cell Biol *24*, 7720-7736.

Chen, J.L., Blasco, M.A., and Greider, C.W. (2000). Secondary structure of vertebrate telomerase RNA. Cell *100*, 503-514.

Clissold, P.M., and Ponting, C.P. (2000). PIN domains in nonsense-mediated mRNA decay and RNAi. Curr Biol *10*, 888-890.

Cohen, S.B., Graham, M.E., Lovrecz, G.O., Bache, N., Robinson, P.J., and Reddel, R.R. (2007). Protein composition of catalytically active human telomerase from immortal cells. Science *315*, 1850-1853.

Cohn, M., and Blackburn, E.H. (1995). Telomerase in yeast. Science *269*, 396-400.

Collins, K. (2006). The biogenesis and regulation of telomerase holoenzymes. Nat Rev Mol Cell Biol *7*, 484-494.

Conrad, M.N., Wright, J.H., Wolf, A.J., and Zakian, V.A. (1990). RAP1 protein interacts with yeast telomeres in vivo: overproduction alters telomere structure and decreases chromosome stability. Cell *63*, 739-750.

Cooper, J.P., Nimmo, E.R., Allshire, R.C., and Cech, T.R. (1997). Regulation of telomere length and function by a Myb-domain protein in fission yeast. Nature *385*, 744-747.

D'Andrea, L.D., and Regan, L. (2003). TPR proteins: the versatile helix. Trends Biochem Sci *28*, 655-662.

Dandjinou, A.T., Levesque, N., Larose, S., Lucier, J.F., Abou Elela, S., and Wellinger, R.J. (2004). A phylogenetically based secondary structure for the yeast telomerase RNA. Curr Biol *14*, 1148-1158.

de Bruin, D., Zaman, Z., Liberatore, R.A., and Ptashne, M. (2001). Telomere looping permits gene activation by a downstream UAS in yeast. Nature *409*, 109-113.

Eugster, A., Lanzuolo, C., Bonneton, M., Luciano, P., Pollice, A., Pulitzer, J.F., Stegberg, E., Berthiau, A.S., Forstemann, K., Corda, Y.*, et al.* (2006). The finger subdomain of yeast telomerase cooperates with Pif1p to limit telomere elongation. Nat Struct Mol Biol *13*, 734-739.

Evans, S.K., and Lundblad, V. (1999). Est1 and Cdc13 as comediators of telomerase access. Science *286*, 117-120.

Evans, S.K., and Lundblad, V. (2002). The Est1 subunit of Saccharomyces cerevisiae telomerase makes multiple contributions to telomere length maintenance. Genetics *162*, 1101-1115.

Ferrezuelo, F., Steiner, B., Aldea, M., and Futcher, B. (2002). Biogenesis of yeast telomerase depends on the importin mtr10. Mol Cell Biol *22*, 6046-6055.

Fisher, T.S., Taggart, A.K., and Zakian, V.A. (2004). Cell cycle-dependent regulation of yeast telomerase by Ku. Nat Struct Mol Biol *11*, 1198-1205.

Fukuhara, N., Ebert, J., Unterholzner, L., Lindner, D., Izaurralde, E., and Conti, E. (2005). SMG7 is a 14-3-3-like adaptor in the nonsense-mediated mRNA decay pathway. Mol Cell *17*, 537-547.

Gallardo, F., Laterreur, N., Cusanelli, E., Ouenzar, F., Querido, E., Wellinger, R.J., and Chartrand, P. (2011). Live cell imaging of telomerase RNA dynamics reveals cell cycle-dependent clustering of telomerase at elongating telomeres. Mol Cell *44*, 819-827.

Gallardo, F., Olivier, C., Dandjinou, A.T., Wellinger, R.J., and Chartrand, P. (2008). TLC1 RNA nucleo-cytoplasmic trafficking links telomerase biogenesis to its recruitment to telomeres. Embo J *27*, 748-757.

Gao, H., Cervantes, R.B., Mandell, E.K., Otero, J.H., and Lundblad, V. (2007). RPA-like proteins mediate yeast telomere function. Nat Struct Mol Biol *14*, 208-214.

Garcia, C.K. (2011). Idiopathic pulmonary fibrosis: update on genetic discoveries. Proc Am Thorac Soc *8*, 158-162.

Garvik, B., Carson, M., and Hartwell, L. (1995). Single-stranded DNA arising at telomeres in cdc13 mutants may constitute a specific signal for the RAD9 checkpoint. Mol Cell Biol *15*, 6128-6138.

Gottschling, D.E., and Zakian, V.A. (1986). Telomere proteins: specific recognition and protection of the natural termini of Oxytricha macronuclear DNA. Cell *47*, 195-205.

Greider, C.W., and Blackburn, E.H. (1985). Identification of a specific telomere terminal transferase activity in Tetrahymena extracts. Cell *43*, 405-413.

Griffith, J.D., Comeau, L., Rosenfield, S., Stansel, R.M., Bianchi, A., Moss, H., and de Lange, T. (1999). Mammalian telomeres end in a large duplex loop. Cell *97*, 503-514.

Gu, B., Bessler, M., and Mason, P.J. (2009). Dyskerin, telomerase and the DNA damage response. Cell Cycle *8*, 6-10.

Gunisova, S., Elboher, E., Nosek, J., Gorkovoy, V., Brown, Y., Lucier, J.F., Laterreur, N., Wellinger, R.J., Tzfati, Y., and Tomaska, L. (2009). Identification and comparative analysis of telomerase RNAs from Candida species reveal conservation of functional elements. RNA *15*, 546-559.

Guo, N., Parry, E.M., Li, L.S., Kembou, F., Lauder, N., Hussain, M.A., Berggren, P.O., and Armanios, M. (2011). Short telomeres compromise beta-cell signaling and survival. PloS one *6*, 0017858.

Hall, K.B. (2002). RNA-protein interactions. Curr Opin Struct Biol *12*, 283-288.

Harley, C.B., Futcher, A.B., and Greider, C.W. (1990). Telomeres shorten during ageing of human fibroblasts. Nature *345*, 458-460.

Hastie, N.D., Dempster, M., Dunlop, M.G., Thompson, A.M., Green, D.K., and Allshire, R.C. (1990). Telomere reduction in human colorectal carcinoma and with ageing. Nature *346*, 866-868.

Hayflick, L., and Moorhead, P.S. (1961). The serial cultivation of human diploid cell strains. Exp Cell Res *25*, 585-621.

Heiss, N.S., Knight, S.W., Vulliamy, T.J., Klauck, S.M., Wiemann, S., Mason, P.J., Poustka, A., and Dokal, I. (1998). X-linked dyskeratosis congenita is caused by mutations in a highly conserved gene with putative nucleolar functions. Nat Genet *19*, 32-38.

Hemann, M.T., Strong, M.A., Hao, L.Y., and Greider, C.W. (2001). The shortest telomere, not average telomere length, is critical for cell viability and chromosome stability. Cell *107*, 67-77.

Holt, S.E., Aisner, D.L., Baur, J., Tesmer, V.M., Dy, M., Ouellette, M., Trager, J.B., Morin, G.B., Toft, D.O., Shay, J.W.*, et al.* (1999). Functional requirement of p23 and Hsp90 in telomerase complexes. Genes Dev *13*, 817-826.

Hsu, M., Yu, E.Y., Sprusansky, O., McEachern, M.J., and Lue, N.F. (2012). Functional analysis of the single Est1/Ebs1 homologue in Kluyveromyces lactis reveals roles in both telomere maintenance and rapamycin resistance. Eukaryot Cell *11*, 932-942.

Hughes, T.R., Evans, S.K., Weilbaecher, R.G., and Lundblad, V. (2000). The Est3 protein is a subunit of yeast telomerase. Curr Biol *10*, 809-812.

Jacobs, S.A., Podell, E.R., and Cech, T.R. (2006). Crystal structure of the essential N-terminal domain of telomerase reverse transcriptase. Nat Struct Mol Biol *13*, 218-225.

Ji, H., Adkins, C.J., Cartwright, B.R., and Friedman, K.L. (2008). Yeast Est2p affects telomere length by influencing association of Rap1p with telomeric chromatin. Mol Cell Biol *28*, 2380-2390.

Kachouri-Lafond, R., Dujon, B., Gilson, E., Westhof, E., Fairhead, C., and Teixeira, M.T. (2009). Large telomerase RNA, telomere length heterogeneity and escape from senescence in Candida glabrata. FEBS Lett *583*, 3605-3610.

Kim, J.H., Park, S.M., Kang, M.R., Oh, S.Y., Lee, T.H., Muller, M.T., and Chung, I.K. (2005). Ubiquitin ligase MKRN1 modulates telomere length homeostasis through a proteolysis of hTERT. Genes Dev *19*, 776-781.

Kim, N.W., Piatyszek, M.A., Prowse, K.R., Harley, C.B., West, M.D., Ho, P.L., Coviello, G.M., Wright, W.E., Weinrich, S.L., and Shay, J.W. (1994). Specific association of human telomerase activity with immortal cells and cancer. Science *266*, 2011-2015.

Laroche, T., Martin, S.G., Tsai-Pflugfelder, M., and Gasser, S.M. (2000). The dynamics of yeast telomeres and silencing proteins through the cell cycle. J Struct Biol *129*, 159-174.

Larrivee, M., LeBel, C., and Wellinger, R.J. (2004). The generation of proper constitutive G-tails on yeast telomeres is dependent on the MRX complex. Genes Dev *18*, 1391-1396.

Lee, J., Mandell, E.K., Tucey, T.M., Morris, D.K., and Lundblad, V. (2008). The Est3 protein associates with yeast telomerase through an OB-fold domain. Nat Struct Mol Biol *15*, 990-997.

Lendvay, T.S., Morris, D.K., Sah, J., Balasubramanian, B., and Lundblad, V. (1996). Senescence mutants of Saccharomyces cerevisiae with a defect in telomere replication identify three additional EST genes. Genetics *144*, 1399-1412.

Leonardi, J., Box, J.A., Bunch, J.T., and Baumann, P. (2008). TER1, the RNA subunit of fission yeast telomerase. Nat Struct Mol Biol *15*, 26-33.

Li, S., Makovets, S., Matsuguchi, T., Blethrow, J.D., Shokat, K.M., and Blackburn, E.H. (2009). Cdk1-dependent phosphorylation of Cdc13 coordinates telomere elongation during cell-cycle progression. Cell *136*, 50-61.

Lin, J., and Blackburn, E.H. (2004). Nucleolar protein PinX1p regulates telomerase by sequestering its protein catalytic subunit in an inactive complex lacking telomerase RNA. Genes Dev *18*, 387-396.

Lingner, J., and Cech, T.R. (1996). Purification of telomerase from Euplotes aediculatus: requirement of a primer 3' overhang. Proceedings of the National Academy of Sciences of the United States of America *93*, 10712-10717.

Lingner, J., Cech, T.R., Hughes, T.R., and Lundblad, V. (1997a). Three Ever Shorter Telomere (EST) genes are dispensable for in vitro yeast telomerase activity. Proceedings of the National Academy of Sciences of the United States of America *94*, 11190-11195.

Lingner, J., Hughes, T.R., Shevchenko, A., Mann, M., Lundblad, V., and Cech, T.R. (1997b). Reverse transcriptase motifs in the catalytic subunit of telomerase. Science *276*, 561-567.

Livengood, A.J., Zaug, A.J., and Cech, T.R. (2002). Essential regions of Saccharomyces cerevisiae telomerase RNA: separate elements for Est1p and Est2p interaction. Mol Cell Biol *22*, 2366-2374.

Longtine, M.S., McKenzie, A., 3rd, Demarini, D.J., Shah, N.G., Wach, A., Brachat, A., Philippsen, P., and Pringle, J.R. (1998). Additional modules for versatile and

economical PCR-based gene deletion and modification in Saccharomyces cerevisiae. Yeast *14*, 953-961.

Lubin, J.W., Rao, T., Mandell, E.K., Wuttke, D.S., and Lundblad, V. (2013). Dissecting protein function: an efficient protocol for identifying separation-of-function mutations that encode structurally stable proteins. Genetics *193*, 715-725.

Lubin, J.W., Tucey, T.M., and Lundblad, V. (2012). The interaction between the yeast telomerase RNA and the Est1 protein requires three structural elements. RNA *18*, 1597-1604.

Luke, B., Azzalin, C.M., Hug, N., Deplazes, A., Peter, M., and Lingner, J. (2007). Saccharomyces cerevisiae Ebs1p is a putative ortholog of human Smg7 and promotes nonsense-mediated mRNA decay. Nucleic Acids Res *35*, 7688-7697.

Lundblad, V., and Blackburn, E.H. (1993). An alternative pathway for yeast telomere maintenance rescues est1- senescence. Cell *73*, 347-360.

Lundblad, V., and Szostak, J.W. (1989). A mutant with a defect in telomere elongation leads to senescence in yeast. Cell *57*, 633-643.

Maizels, N. (2006). Dynamic roles for G4 DNA in the biology of eukaryotic cells. Nat Struct Mol Biol *13*, 1055-1059.

Marcand, S., Brevet, V., Mann, C., and Gilson, E. (2000). Cell cycle restriction of telomere elongation. Curr Biol *10*, 487-490.

Mason, J.M., and Biessmann, H. (1995). The unusual telomeres of Drosophila. Trends Genet *11*, 58-62.

McClintock, B. (1941). The Stability of Broken Ends of Chromosomes in Zea Mays. Genetics *26*, 234-282.

McClintock, B. (1942). The Fusion of Broken Ends of Chromosomes Following Nuclear Fusion. Proceedings of the National Academy of Sciences of the United States of America *28*, 458-463.

Mitchell, J.R., Wood, E., and Collins, K. (1999). A telomerase component is defective in the human disease dyskeratosis congenita. Nature *402*, 551-555.

Morris, D.K. (2000). Investigating the role of Est3 in yeast telomere replication. PhD Dissertation, Baylor College of Medicine, Houston, Texas.

Morris, D.K., and Lundblad, V. (1997). Programmed translational frameshifting in a gene required for yeast telomere replication. Curr Biol *7*, 969-976.

Mozdy, A.D., and Cech, T.R. (2006). Low abundance of telomerase in yeast: implications for telomerase haploinsufficiency. RNA *12*, 1721-1737.

Muller, H.J. (1938). The remaking of chromosomes. The Collecting Net *8*, 182-195.

Nakamura, T.M., Cooper, J.P., and Cech, T.R. (1998). Two modes of survival of fission yeast without telomerase. Science *282*, 493-496.

Nakamura, T.M., Morin, G.B., Chapman, K.B., Weinrich, S.L., Andrews, W.H., Lingner, J., Harley, C.B., and Cech, T.R. (1997). Telomerase catalytic subunit homologs from fission yeast and human. Science *277*, 955-959.

Nandakumar, J., and Cech, T.R. (2013). Finding the end: recruitment of telomerase to telomeres. Nat Rev Mol Cell Biol *14*, 69-82.

Nguyen, L. (2013). Defining the functional surface of the Est2 catalytic subunit of yeast telomerse. MS thesis, University of California, San Diego, California.

Nugent, C.I., Hughes, T.R., Lue, N.F., and Lundblad, V. (1996). Cdc13p: a single-strand telomeric DNA-binding protein with a dual role in yeast telomere maintenance. Science *274*, 249-252.

Olovnikov, A.M. (1971). Principle of marginotomy in template synthesis of polynucleotides. Dokl Akad Nauk SSSR *201*, 1496-1499.

Osterhage, J.L., Talley, J.M., and Friedman, K.L. (2006). Proteasome-dependent degradation of Est1p regulates the cell cycle-restricted assembly of telomerase in Saccharomyces cerevisiae. Nat Struct Mol Biol *13*, 720-728.

Paeschke, K., Juranek, S., Simonsson, T., Hempel, A., Rhodes, D., and Lipps, H.J. (2008). Telomerase recruitment by the telomere end binding protein-beta facilitates G-quadruplex DNA unfolding in ciliates. Nat Struct Mol Biol *15*, 598-604.

Paeschke, K., Simonsson, T., Postberg, J., Rhodes, D., and Lipps, H.J. (2005). Telomere end-binding proteins control the formation of G-quadruplex DNA structures in vivo. Nat Struct Mol Biol *12*, 847-854.

Palm, W., and de Lange, T. (2008). How shelterin protects mammalian telomeres. Annu Rev Genet *42*, 301-334.

Paschini, M., Mandell, E.K., and Lundblad, V. (2010). Structure prediction-driven genetics in Saccharomyces cerevisiae identifies an interface between the t-RPA proteins Stn1 and Ten1. Genetics *185*, 11-21.

Peng, Y., Mian, I.S., and Lue, N.F. (2001). Analysis of telomerase processivity: mechanistic similarity to HIV-1 reverse transcriptase and role in telomere maintenance. Mol Cell *7*, 1201-1211.

Pennock, E., Buckley, K., and Lundblad, V. (2001). Cdc13 delivers separate complexes to the telomere for end protection and replication. Cell *104*, 387-396.

Prescott, J., and Blackburn, E.H. (1997). Telomerase RNA mutations in Saccharomyces cerevisiae alter telomerase action and reveal nonprocessivity in vivo and in vitro. Genes Dev *11*, 528-540.

Qi, H., and Zakian, V.A. (2000). The Saccharomyces telomere-binding protein Cdc13p interacts with both the catalytic subunit of DNA polymerase alpha and the telomerase-associated est1 protein. Genes Dev *14*, 1777-1788.

Reichenbach, P., Hoss, M., Azzalin, C.M., Nabholz, M., Bucher, P., and Lingner, J. (2003). A human homolog of yeast Est1 associates with telomerase and uncaps chromosome ends when overexpressed. Curr Biol *13*, 568-574.

Romanos, M.A., Scorer, C.A., and Clare, J.J. (1992). Foreign gene expression in yeast: a review. Yeast *8*, 423-488.

Sabourin, M., Tuzon, C.T., Fisher, T.S., and Zakian, V.A. (2007). A flexible protein linker improves the function of epitope-tagged proteins in Saccharomyces cerevisiae. Yeast *24*, 39-45.

Sauerwald, A., Sandin, S., Cristofari, G., Scheres, S.H., Lingner, J., and Rhodes, D. (2013). Structure of active dimeric human telomerase. Nat Struct Mol Biol *20*, 454-460.

Savage, S.A., and Alter, B.P. (2008). The role of telomere biology in bone marrow failure and other disorders. Mechanisms of ageing and development *129*, 35-47.

Scherer, S., and Davis, R.W. (1979). Replacement of chromosome segments with altered DNA sequences constructed in vitro. Proceedings of the National Academy of Sciences of the United States of America *76*, 4951-4955.

Sealey, D.C., Kostic, A.D., LeBel, C., Pryde, F., and Harrington, L. (2011). The TPR-containing domain within Est1 homologs exhibits species-specific roles in telomerase interaction and telomere length homeostasis. BMC Mol Biol *12*, 1471-2199.

Seimiya, H., Sawada, H., Muramatsu, Y., Shimizu, M., Ohko, K., Yamane, K., and Tsuruo, T. (2000). Involvement of 14-3-3 proteins in nuclear localization of telomerase. Embo J *19*, 2652-2661.

Seto, A.G., Livengood, A.J., Tzfati, Y., Blackburn, E.H., and Cech, T.R. (2002). A bulged stem tethers Est1p to telomerase RNA in budding yeast. Genes Dev *16*, 2800-2812.

Seto, A.G., Zaug, A.J., Sobel, S.G., Wolin, S.L., and Cech, T.R. (1999). Saccharomyces cerevisiae telomerase is an Sm small nuclear ribonucleoprotein particle. Nature *401*, 177-180.

Shakirov, E.V., Surovtseva, Y.V., Osbun, N., and Shippen, D.E. (2005). The Arabidopsis Pot1 and Pot2 proteins function in telomere length homeostasis and chromosome end protection. Mol Cell Biol *25*, 7725-7733.

Shay, J.W., and Wright, W.E. (2002). Telomerase: a target for cancer therapeutics. Cancer Cell *2*, 257-265.

Shay, J.W., and Wright, W.E. (2005). Senescence and immortalization: role of telomeres and telomerase. Carcinogenesis *26*, 867-874.

Shcherbakova, D.M., Sokolov, K.A., Zvereva, M.I., and Dontsova, O.A. (2009). Telomerase from yeast Saccharomyces cerevisiae is active in vitro as a monomer. Biochemistry *74*, 749-755.

Singer, M.S., and Gottschling, D.E. (1994). TLC1: template RNA component of Saccharomyces cerevisiae telomerase. Science *266*, 404-409.

Singh, S.M., Steinberg-Neifach, O., Mian, I.S., and Lue, N.F. (2002). Analysis of telomerase in Candida albicans: potential role in telomere end protection. Eukaryot Cell *1*, 967-977.

Szostak, J.W., and Blackburn, E.H. (1982). Cloning yeast telomeres on linear plasmid vectors. Cell *29*, 245-255.

Taggart, A.K., Teng, S.C., and Zakian, V.A. (2002). Est1p as a cell cycle-regulated activator of telomere-bound telomerase. Science *297*, 1023-1026.

Takata, H., Kanoh, Y., Gunge, N., Shirahige, K., and Matsuura, A. (2004). Reciprocal association of the budding yeast ATM-related proteins Tel1 and Mec1 with telomeres in vivo. Mol Cell *14*, 515-522.

Talley, J.M., DeZwaan, D.C., Maness, L.D., Freeman, B.C., and Friedman, K.L. (2011). Stimulation of yeast telomerase activity by the ever shorter telomere 3 (Est3) subunit is dependent on direct interaction with the catalytic protein Est2. The Journal of biological chemistry *286*, 26431-26439.

Teixeira, M.T., Arneric, M., Sperisen, P., and Lingner, J. (2004). Telomere length homeostasis is achieved via a switch between telomerase- extendible and -nonextendible states. Cell *117*, 323-335.

Teixeira, M.T., Forstemann, K., Gasser, S.M., and Lingner, J. (2002). Intracellular trafficking of yeast telomerase components. EMBO Rep *3*, 652-659.

Teng, S.C., and Zakian, V.A. (1999). Telomere-telomere recombination is an efficient bypass pathway for telomere maintenance in Saccharomyces cerevisiae. Mol Cell Biol *19*, 8083-8093.

Theimer, C.A., and Feigon, J. (2006). Structure and function of telomerase RNA. Curr Opin Struct Biol *16*, 307-318.

Theobald, D.L., Mitton-Fry, R.M., and Wuttke, D.S. (2003). Nucleic acid recognition by OB-fold proteins. Annu Rev Biophys Biomol Struct *32*, 115-133.

Toogun, O.A., Zeiger, W., and Freeman, B.C. (2007). The p23 molecular chaperone promotes functional telomerase complexes through DNA dissociation. Proceedings of the National Academy of Sciences of the United States of America *104*, 5765-5770.

Tucey, T.M., and Lundblad, V. (2013). A yeast telomerase complex containing the Est1 recruitment protein is assembled early in the cell cycle. Biochemistry *52*, 1131-1133.

Tuzon, C.T., Wu, Y., Chan, A., and Zakian, V.A. (2011). The Saccharomyces cerevisiae telomerase subunit Est3 binds telomeres in a cell cycle- and Est1-dependent manner and interacts directly with Est1 in vitro. PLoS Genet *7*, 5.

Virta-Pearlman, V., Morris, D.K., and Lundblad, V. (1996). Est1 has the properties of a single-stranded telomere end-binding protein. Genes Dev *10*, 3094-3104.

von Figura, G., Wagner, M., Nalapareddy, K., Hartmann, D., Kleger, A., Guachalla, L.M., Rolyan, H., Adler, G., and Rudolph, K.L. (2011). Regeneration of the exocrine pancreas is delayed in telomere-dysfunctional mice. PloS one *6*, 0017122.

Watson, J.D. (1972). Origin of concatemeric T7 DNA. Nat New Biol *239*, 197-201.

Webb, C.J., and Zakian, V.A. (2008). Identification and characterization of the Schizosaccharomyces pombe TER1 telomerase RNA. Nat Struct Mol Biol *15*, 34-42.

Webb, C.J., and Zakian, V.A. (2012). Schizosaccharomyces pombe Ccq1 and TER1 bind the 14-3-3-like domain of Est1, which promotes and stabilizes telomerase-telomere association. Genes Dev *26*, 82-91.

Witkin, K.L., and Collins, K. (2004). Holoenzyme proteins required for the physiological assembly and activity of telomerase. Genes Dev *18*, 1107-1118.

Witkin, K.L., Prathapam, R., and Collins, K. (2007). Positive and negative regulation of Tetrahymena telomerase holoenzyme. Mol Cell Biol *27*, 2074-2083.

Wu, Y., and Zakian, V.A. (2011). The telomeric Cdc13 protein interacts directly with the telomerase subunit Est1 to bring it to telomeric DNA ends in vitro. Proceedings of the National Academy of Sciences of the United States of America *108*, 20362-20369.

Yang, C.P., Chen, Y.B., Meng, F.L., and Zhou, J.Q. (2006). Saccharomyces cerevisiae Est3p dimerizes in vitro and dimerization contributes to efficient telomere replication in vivo. Nucleic Acids Res *34*, 407-416.

Ye, A.J., and Romero, D.P. (2002). Phylogenetic relationships amongst tetrahymenine ciliates inferred by a comparison of telomerase RNAs. Int J Syst Evol Microbiol *52*, 2297-2302.

Yu, E.Y., Steinberg-Neifach, O., Dandjinou, A.T., Kang, F., Morrison, A.J., Shen, X., and Lue, N.F. (2007). Regulation of telomere structure and functions by subunits of the INO80 chromatin remodeling complex. Mol Cell Biol *27*, 5639-5649.

Zappulla, D.C., and Cech, T.R. (2004). Yeast telomerase RNA: a flexible scaffold for protein subunits. Proceedings of the National Academy of Sciences of the United States of America *101*, 10024-10029.

Zhang, M.L., Tong, X.J., Fu, X.H., Zhou, B.O., Wang, J., Liao, X.H., Li, Q.J., Shen, N., Ding, J., and Zhou, J.Q. (2010). Yeast telomerase subunit Est1p has guanine quadruplex-promoting activity that is required for telomere elongation. Nat Struct Mol Biol *17*, 202-209.

Zhou, J., Hidaka, K., and Futcher, B. (2000). The Est1 subunit of yeast telomerase binds the Tlc1 telomerase RNA. Mol Cell Biol *20*, 1947-1955.

Zijlmans, J.M., Martens, U.M., Poon, S.S., Raap, A.K., Tanke, H.J., Ward, R.K., and Lansdorp, P.M. (1997). Telomeres in the mouse have large inter-chromosomal variations in the number of T2AG3 repeats. Proceedings of the National Academy of Sciences of the United States of America *94*, 7423-7428.